CR 73132

Spectrolab

12484 GLADSTONE AVENUE, SYLMAR, CALIFORNIA
EMPIRE 5-4683 TWX: 213-764-5983

Final Report FR 6002

Analytical, Experimental & Developmental Work

for a

Radiative Heating System

Volume I of III

Contract No.: NAS2-1620

Prepared by

Spectrolab, Div. of Textron Electronics, Inc.
12484 Gladstone Avenue
Sylmar, California

for

National Aeronautics and Space Administration

Ames Research Center

Moffett Field, California

FACILITY FORM 602

N67-36736 (ACCESSION NUMBER)

237 (PAGES)

CR-73132 (NASA CR OR TMX OR AD NUMBER)

1 (THRU)

(CODE)

33 (CATEGORY)

FR 6002

Final Report

Analytical, Experimental & Developmental Work

for a

Radiative Heating System

Volume I of III

Contract No.: NAS2-1620

Prepared by

Spectrolab, Div. of Textron Electronics, Inc.
12484 Gladstone Avenue
Sylmar, California

for

National Aeronautics and Space Administration
Ames Research Center
Moffett Field, California

This report has been divided into three volumes.

Volume I entitled "System Development" covers the work performed in the optical system concept study, optical and thermal design, and the fabrication and evaluation of the prototype optical system.

Volume II entitled "Source Development" describes the development program on the radiation source, including the work performed under subcontract and covers all test runs in the operation of the final prototype radiation source.

Volume III entitled "Facility Design" covers the detailed design of the radiative heating system facility.

TABLE OF CONTENTS

Volume I

Para.	Title	Page
1.	Summary	1 - 1
2.	Introduction	2 - 1
3.	System Requirements	3 - 1
3.1	Intensity	3 - 1
3.2	Rate of Intensity Variation	3 - 1
3.3	Intensity Uniformity	3 - 1
3.4	Power Outside Heating Zone	3 - 2
3.5	Spectral Distribution	3 - 2
3.6	Operating Characteristics	3 - 2
3.7	Radiation Source Requirements	3 - 2
3.7.1	Spectral Distribution	3 - 3
3.7.2	Energy Conversion Efficiency	3 - 3
3.7.3	Solid Angle of Irradiation	3 - 3
3.7.4	Average Radiance	3 - 3
3.7.5	Operational Life	3 - 3
3.7.6	Output Power Variation	3 - 3
3.8	Priority of Design and Performance Goals	3 - 4
4.	Summary - Volume I	4 - 1
5.	Introduction - Volume I	5 - 1
6.	Theoretical Considerations	6 - 1
6.1	Radiometric Considerations	6 - 1

Continued

TABLE OF CONTENTS

Volume I (Continued)

Para.	Title	Page
6.2	System Efficiency	6 - 5
6.2.1	Optical Efficiency	6 - 5
6.2.2	Collection Efficiency	6 - 6
6.2.3	Energy Conversion	6 - 6
6.2.4	Geometrical Efficiency	6 - 6
7.	Systems Concept Study	7 - 1
7.1	Performance Criteria	7 - 1
7.2	Systems Selected for Analysis	7 - 1
7.3	Recommended System Approach	7 - 2
7.4	System Approach Selection	7 - 2
8.	Optical Design Development	8 - 1
8.1	Optical Design Evolution	8 - 1
8.2	Optical System Sizing	8 - 7
8.2.1	Effective Solid Angle of Irradiation	8 - 7
8.2.2	Projection Lens Packing	8 - 9
8.2.3	Geometrical Relationships	8 - 10
8.2.4	System Parameter Selection	8 - 11
8.3	Optical Lens Analysis	8 - 12
8.3.1	Spherical Lenses	8 - 12
8.3.2	Aspheric Projection Lens	8 - 15
8.3.3	Tilted Projection Lens	8 - 16
8.3.4	Summary	8 - 17
8.4	Mask Analysis	8 - 17

Continued

TABLE OF CONTENTS

Volume I (Continued)

Para.	Title	Page
8.5	Collection Optics	8 - 19
8.5.1	Compatibility with Radiation Sources	8 - 20
8.5.2	Basic Collector Sizing	8 - 20
8.5.3	General Method of Evaluation	8 - 21
8.5.4	Trade-off Study	8 - 22
9.	Thermal Loading Analysis	9 - 1
9.1	Thermal Load Distribution	9 - 1
9.2	Lens Absorption Analysis	9 - 3
9.3	Lens Temperature Analysis	9 - 3
10.	Projection Lens Vacuum Seal Development Work	10 - 1
11.	Spectral Filter Studies	11 - 1
11.1	Cold Mirror Development Work	11 - 2
11.2	Filter Thermal Degradation Test	11 - 3
11.3	Water Cell Filter	11 - 3
12.	Prototype Optical System Components	12 - 1
12.1	Prototype Requirements	12 - 1
12.2	Quartz Selection	12 - 1
12.3	Optical Tooling and Fabrication	12 - 2
12.3.1	Lenses	12 - 2
12.3.2	Collector Mirror	12 - 2
12.3.3	Folding Mirror	12 - 3

Continued

TABLE OF CONTENTS

Volume I (Continued)

Para.	Title	Page
12.4	Mechanical Components	12 - 3
12.4.1	Douser	12 - 3
12.4.2	Water-cooled Apertures and Mask	12 - 4
12.4.3	Backstop Calorimeter	12 - 4
12.4.4	Collector-Source Mount	12 - 4
12.4.5	Lens Holders	12 - 5
13.	Instrumentation	13 - 1
13.1	Sensors	13 - 1
13.2	Optical Viewing Instrumentation	13 - 2
13.3	Mechanical Instrumentation	13 - 2
13.4	Spectral Distribution Measurement Instrumentation	13 - 3
14.	Prototype Testing	14 - 1
14.1	Test Site Description	14 - 1
14.2	Alignment	14 - 2
14.2.1	Initial Positioning	14 - 2
14.2.2	Optical Bench	14 - 3
14.2.3	Folding Mirror	14 - 3
14.2.4	Source-Collector Axis	14 - 3
14.2.5	Alignment Check	14 - 3
14.2.6	Field Lens Alignment	14 - 3
14.2.7	Projection Lens Centering Error Compensation	14 - 4

Continued

TABLE OF CONTENTS

Volume I (Continued)

Para.	Title	Page
14.2.8	Collector Alignment	14 - 4
14.2.9	Final Alignment with Source Operating	14 - 5
14.3	Combined Radiation Source - Optical System Testing	14 - 5
14.3.1	Water Cell Transmission Test	14 - 8
14.3.2	Field Lens Intensity Distribution	14 - 8
14.3.3	Target Intensity as a Function of Gas Flow	14 - 9
14.3.4	Target Edge Intensities at Reduced Diameters	14 - 9
14.3.5	Collector Focus Sensitivity	14 - 9
14.3.6	Uniformity Filter Tests	14 - 9
14.3.7	Collector Damage Due to Envelope Failure	14 - 10
14.4	Target Edge Intensity - 14-Lamp System	14 - 10

Volume II

1.	Summary	1
2.	Introduction	2
3.	60 KW Prototype Radiation Source	3
3.1	Description of the Source Design	3
3.2	Test Facility	4
3.2.1	Starter	4
3.2.2	Power Supply	4

Continued

TABLE OF CONTENTS

Volume II (Continued)

Para.	Title	Page
3.2.3	Control Console	4
3.2.4	Enclosure	4
3.3	Instrumentation	4
3.3.1	Electrical Instrumentation	4
3.3.2	Gas Flow and Pressure	4
3.3.3	Water Flow and Temperature	5
3.3.4	Arc Image	5
3.4	Major Development Effort on Components	5
3.4.1	Electrode Development	5
3.4.2	Envelopes	6
3.4.3	Tierods	6
3.5	Tests Performed	7
3.5.1	Evaluation Tests Performed at Giannini Scientific Corporation	7
3.5.2	Tests Performed at Spectrolab	8
3.6	Data Evaluation	9
3.7	Conclusions	10
3.8	Recirculator Development	10
4.	Experimental Radiation Source	11
4.1	Scope	11
4.2	Source Design	12

Continued

TABLE OF CONTENTS

Volume II (Continued)

Para.	Title	Page
4.3	Test Facility	12
4.3.1	Starter	12
4.3.2	Power Supplies	12
4.3.3	Control Console	12
4.3.4	Enclosure	12
4.4	Instrumentation	13
4.5	Development Effort	13
4.5.1	Bore Type Anode	13
4.5.2	Solid Anode	15
4.5.3	Envelopes	17
4.6	Analytical Work	18
4.7	Tests Performed	18
4.7.1	Performance Testing	19
4.7.2	Temperature Measurements in the Bore Type Anode	19
4.8	Data Evaluation	21
4.8.1	Bore Type Anode	21
4.8.2	Solid Anode	21
4.9	System Development	22
4.10	Conclusions	23
5.	Final 150 KW Radiation Source	23
5.1	Design Concept	23
5.2	Completion of the Final Source	26
5.3	Analytical Work	26

Continued

TABLE OF CONTENTS

Volume II (Continued)

Para.	Title	Page
5.4	Testing	27
5.5	Conclusions	31

Volume III

1.	Summary	1
1.1	Scope	1
1.2	Completion	2
2.	Introduction	3
3.	Design	3
3.1	Site Restraints	3
3.2	Interfaces	3
3.3	Design Methods	4
3.4	Utility Design	4
3.5	Optical Components	5
3.6	Design Testing	5
4.	Drawings	6
5.	Specifications and Manuals	6

LIST OF ILLUSTRATIONS

Volume I

Sec.	Figure No.	Title
6	6.2	Model Face Inclined from Optical Axis
	6.3	Model Face on Axis Viewing Circular Mirror Circumscribing Nozzle
7	7.1	Single Lamp Projection System - Frontal Approach
	7.2	Facet Mirror Projection System
	7.3	Searchlight System
8	8.1	Geometrical Configuration of Projection Lens, Target and Nozzle
	8.2	Target Normal to Axis, Lens with Spherical Aberration
	8.3	Inclined Target, Lens with Spherical Aberration
	8.4	Target Normal to Axis, No Spherical Aberration
	8.5	Inclined Target, No Spherical Aberration
	8.6	Postulated Intensity Distribution Across Field Lens Clear Aperture
	8.7	Intensity Distribution Across Inclined Target Using Aspherized Projection Lens
	8.8	Intensity Distribution Across Inclined Target Using Spherical Projection Lens
	8.9	Superposition of Intensity Distribution from Diametrically Opposite Optical Channels
	8.10	Tilted Projection Lens
	8.11	Mask Analysis

Continued

LIST OF ILLUSTRATIONS

Volume I (Continued)

Sec.	Figure No.	Title
	8.12	Arc Image Micro-radiance Contours (60 KW Radiation Source)
	8.13	Polar Distribution of 60 KW Plasma Source
	8.14	Predicted Intensity - Relative Aconic Collector vs Ellipsoidal Collector 24" Dia.
	8.15	Relative Intensity - Aconic Collector 10" Dia.
	8.16	Predicted Intensity - Relative Aconic Collector vs Ellipsoidal Collector 10" Dia.
11	11.1	Specified Spectral Distribution
	11.2	Spectral Distribution of Plasmadyne Source with Partial Filtering to Approximate Specification with Reduced Energy Rejection
	11.3	Derived Filter Transmittances (for minimum, complete and maximum filtering)
	11.4	Transmission of two 1/8 GE 101 Quartz Discs Separated by 1/2 cm Distilled Water
	11.5	Transmission of two 1/8 GE 101 Quartz Discs Separated by 1 cm Distilled Water
12	12.1	Source-Collector Mounting System
13	13.1	Block Diagram of Spectral Measurement and Data Reduction System
14	14.1	Photograph Viewing Control Console and Input Water Distribution System Outside Test Enclosure
	14.2	Photograph Viewing Installed Projection Lens, Target Area and Conical Backstop Calorimeter Outside Test Enclosure
	14.3	View of Target Area with Protective Covers in Place for Target Intensity Scans

Continued

LIST OF ILLUSTRATIONS

Volume I (Continued)

Sec.	Figure No.	Title
	14.4	View of Installed Folding Mirror Inside Test Enclosure
	14.5	Installed Collector in Test Enclosure Showing Monitoring Optics
	14.6	Installed Radiation Source-Collector Assembly in Enclosure Showing Remote Alignment Provisions
	14.7	View of Portion of Prototype Optical System from Within Test Enclosure
	14.8	Closeup of Installed Field Lens Assembly
	14.9	View of Installed Field Lens-Water Cell Assembly and Douser
	14.10	Rear View of Installed Folding Mirror Showing Alignment Provisions
	14.11	Intensity Scanner Positioned for Target Intensity Scans
	14.12	Collector Alignment Disc Attached to Collector
	14.13	Filament Images Obtained at Field Lens Using Alignment Lamp in Collector
	14.14	Telescope Mounted in Projection Lens Holder

Continued

LIST OF ILLUSTRATIONS

Volume II

Figure No.	Title
1	60 KW Prototype Radiation Source
2	Relative Spectral Power 21.4 KW Argon VSRS 16.2 ATM - 60 KW Prototype Source
3	Relative Spectral Power 60.3 KW Argon VSRS 19.7 ATM - 60 KW Prototype Source
4	.425μ Intensity VS. Power and Pressure - 60 KW Prototype Source
5	Arc Image Micro-radiance Contours - 60 KW Prototype Source
6	Polar Distribution of Intensity and Energy - 60 KW Prototype Source
7	Spectral Intensity Distribution - 60 KW Prototype Source
8	150 KW Experimental Radiation Source - 43 mm O.D. Inner Tube Assembly - 8 mm Bore Type Anode
9	150 KW Experimental Radiation Source - 84 mm O.D. Inner Tube Assembly - Solid Anode Assembly
10a	Instrumentation - Schematic - 150 KW Experimental Unit
10b	Instrumentation - Listing of the Instruments - 150 KW Experimental Unit
11	Correlation Between Radiation, Current, Bore Size Bore Type Anode - 150 KW Experimental Unit
12	Volume Flow VS. Voltage Bore Type Anode - 150 KW Experimental Unit
13	Correlation Between Efficiency, Current, Bore Size Bore Type Anode - 150 KW Experimental Unit

Continued

LIST OF ILLUSTRATIONS

Volume II (Continued)

Figure No.	Title
14	Axial Temperature Distribution in the Anode - 150 KW Experimental Unit
15	Heat Input to the Anode - Bore Type Anode - 150 KW Experimental Unit
16	Anode Temperature VS. Cooling Rate - 150 KW Experimental Unit
17	Solid Anode Performance - 150 KW Experimental Unit
18	Solid Anode Performance - 150 KW Experimental Unit
19	150 KW Final Radiation Source
20	Quartz Envelope in Final Radiation Source
21	Diffusion of the Arc Foot

Volume III

1	Radiative Heating System Model with 6-ft. Man Superimposed in Proper Perspective

APPENDICES

Volume I

Number	Description
DM 272-9	Vacuum Seal Development Work
DM 272-12	Projection Lens Vacuum Seal Development Work
DM 272-13	Thermopile Calibration
DM 272-15	Comparison of Sensors (Test Run No. 10)
DM 272-18	Prototype Evaluation Testing, Runs 5 through 9
DM 272-19	Vacuum Seal Development Work
DM 272-21	Comparison of Sensors
DM 272-26	Water Cell Absorption Test
DM 272-31	Sensor Comparison in Projection Plane
DM 272-32	Field Lens Scan - Runs 24 and 25
DM 272-33	Comparison of NASA/Ames Slug Calorimeter with Spectrolab
DM 272-35	Damage to 24 Inch Collector Due to Mechanical Failure of Source Outer Envelope
DM 272-39	Target Edge Intensity and Sensor Comparison
DM 272-40	Effect of Gas Flow Rate Variation on Target Intensity
DM 272-41	Target Edge Intensities at Reduced Diameters
DM 272-42	Target Edge Intensities
DM 272-46	Comparison of Sensors
DM 272-47	Elliptical Mask for Radiative Heating System Field Lens
DM 272-49	Uniformity Filter Test
DM 272-95	Lens Absorption Analysis for the Radiative Heating System

Continued

APPENDICES

Volume I (Continued)

Number	Description
DM 272-96	Thermal Analysis for the Field and Projection Lens
DM 272-97	Filtering Study - NAS2-1620

Volume II

	Data Summary Sheet - Model L-60 Light Source
DM 272-1	Brazing Test Results
DM 272-2	Energy Absorption in the Envelope of a Plasma Radiation Source
DM 272-3	Determination of the Heat Transfer Coefficient from the Envelope to the Cooling Medium
DM 272-4	Radial Temperature Distribution in the Envelope of a Plasma Radiation Source
DM 272-5	Simplified Stress Analysis of a Radiation Source Envelope
DM 272-6	Transient Heat Transfer in the Envelope of a Plasma Radiation Source
DM 272-7	Heat Transfer in a Composite Diffuser
DM 272-8	Recirculator Testing
DM 272-10	DC Electrical System Calibration
DM 272-11	Recirculator Testing
DM 272-14	Radiation Source Evaluation Testing (Runs 1-4)
DM 272-16	Radiation Source Performance During Prototype Testing

Continued

APPENDICES

Volume II (Continued)

Number	Description
DM 272-17	Documentation of Source Performance in Test Run 10
DM 272-22	Polar Distribution and Total Energy Runs 13.1, 13.2 and 13.3
DM 272-23	Documentation of Source Performance in Test Runs 11, 12 and 13
DM 272-24	Radiation Source Life Tests (Runs 14 Through 19 and 22)
DM 272-25	Documentation of Source Operation During Spectral Tests (Runs 20 and 21)
DM 272-27	Spectral Distribution of 150 KW Radiation Source
DM 272-28	Spectral Distribution of 150 KW Vortex Stabilized Argon Plasma Arc Source
DM 272-29	Micro-radiance Distribution in Final Radiation Source
DM 272-30	Source Documentation - Runs 23 through 30
DM 272-34	Recalibration of Prototype DC Electrical System
DM 272-36	Documentation of Source Performance in Test Runs 33, 34 and 35
DM 272-37	Source Documentation in Test Runs 36 through 39, Including $2\frac{1}{2}$ Hour Continuous Run
DM 272-38	Documentation of Source Performance in Runs 40 and 41, Including Failure of Outer Envelope
DM 272-43	Source Documentation - Test Runs 42 through 49
DM 272-48	Micro-radiance Plot Calibration
DM 272-52	Recirculator Evaluation
DM 272-61	Heat Transfer in the Cathode
DM 272-62	Total Reflection in the Plasma Radiation Source
DM 272-63	Radial Heat Flux and Thermal Stresses in a Sleeve

Continued

APPENDICES
(Continued)

Volume III

Number	Description
	List of Drawings
DM 272-51	Douser Mockup Test
DM 272-54	Intensity Monitor Report

1. SUMMARY

The material testing associated with the design of thermal protection systems for vehicles entering the earth's atmosphere at escape velocities require facilities capable of subjecting materials to both radiative and convective heating fluxes of large magnitude. The basic needs for equipment to satisfy the radiative flux requirements resulted in the program reported on here. It was the primary objective of this program to perform the necessary analytical, experimental and development work to provide the information for a recommended design of a radiative heating system.

This work, performed under Contract NAS 2-1620 for the National Aeronautics and Space Administration, Ames Research Center, was initiated on 1 June 1963 and continued into 1965. In January 1965, the scope of the work was extended to include the detailed design of the radiative heating system which would be fabricated and installed as a component in a new wind tunnel in the Mass Transfer Cooling and Aerodynamics Facility at NASA/Ames Research Center, Moffett Field, California.

One of the major tasks in this program was to develop a high powered plasma radiation source which would allow satisfying the radiative heating system performance goals. To accomplish this end, those firms experienced in the development of plasma arc sources were surveyed. As a result of this survey and technical evaluation, a CPFF subcontract was let to Giannini Scientific for the development of a 150 KW plasma radiation source.

The initial radiation source developed at Giannini Scientific was a 60 KW rated lamp which was thought to represent the prototype of the final radiation source. This lamp used a double concentric envelope design with a tungsten cathode and a hollow bore anode.

An experimental radiation source unit was constructed in order to permit an orderly upgrading to the 150 KW rated power level. This experimental unit was designed to accommodate three different size inner quartz envelopes and four different size electrodes. During initial tests, hollow bore type anode configurations were utilized. Subsequently a solid anode configuration was conceived and upon test proved to be superior to the bore type anode previously employed.

With the development data obtained from the testing of the experimental radiation source and from supporting analyses, the final

radiation source design was conceived and detailed. This design, based upon the vortex stabilized arc concept, contained a solid anode and employed a cantilevered self-supporting outer quartz envelope. The final manufacture, assembly and testing of this radiation source was performed at Spectrolab after termination of the subcontract. The radiation source using argon gas was operated at current levels up to 1600 amps and satisfactorily performed for a period of two hours continuous operation, as well as approximately 25 intermittent test runs of 15 minutes duration..

Concurrent with the radiation source development work, a prototype optical system was conceived and developed for integration with the final radiation source.

A Systems Concept Study was conducted in order to analyze and evaluate the more promising system approaches. The relative merits of the systems evaluated were made based upon operating and performance characteristics and also potential upgrading capability. As a result of this study, a system concept was selected by NASA/Ames personnel which provided a starting point for detailed study and development work. The system concept selected consisted of multiple single lamp projection channels using simple relay optics which would penetrate the vacuum chamber around the periphery of the nozzle in a frontal approach to the model.

The original intensity goals for the radiative heating system included a low intensity mode for a 6" diameter model and a high intensity mode for a 2" diameter model. Upon evaluation of the Systems Concept Report and reevaluation of system performance requirements, the performance goals were revised. The major change limited system performance to a single model size of 4 inches in diameter with an intensity goal of 1088 BTU/ft^2-sec.

The final prototype optical channel design, which was utilized in the demonstration testing, evolved from the initial design concept. Fourteen (14) such optical channels were selected for use in the radiative heating system. With each optical channel system, a collector mirror projects a purposely distorted image of the arc onto the clear aperture of a field lens. A projection lens is utilized to project the radiation intensity distribution at the field lens onto the target which is inclined to the optical axis. A mirror is utilized to fold the beam for packaging considerations. The final spectral filtering was limited to the use of a water cell to reject the long wavelength radiation.

A pneumatic actuated douser and projection lens vacuum seal provisions were developed for use with the radiative heating system. The design and fabrication of the radiation source collector represented the major development task associated with the prototype optical system. Based upon scheduling considerations, the development of the collector was optimization using the radiation source data from the 60 KW prototype radiation source unit.

The development work on the final radiation source was curtailed prior to completion. Testing of the final radiation source indicated that it fell short of satisfying the input power of 150 KW although subsequent improvements on the radiation source diffuser at Ames Research Center indicates that this goal has now been achieved. The final arc size of approximately $15\frac{1}{2}$ mm by 10 mm is significantly larger than the design goal of 8 mm by 6 mm. Hence, the average source radiance, measured to be on the order of 3200 Watts/cm^2-str. fell short of satisfying the initial goal of 7000 Watts/cm^2-str. Even with these shortcomings, the final radiation source represented a significant advancement in the state-of-the-art of high powered radiation sources.

A comprehensive test program was conducted with the combined final radiation source and prototype optical system. The results of this testing indicated that the minimum unfiltered target edge intensity for a 14-lamp radiative heating system would be on the order of 546 BTU/ft^{-2}-sec. over the 4" diameter target. Tests utilizing an aluminum dot pattern filter at the water cell indicated that a uniformity filter could be designed for the radiative heating system which would allow satisfying the $\pm$ 5% system intensity uniformity goal.

Upon evaluation of the performance of the prototype system, the scope of the program was extended to include the detailed design of the radiative heating system. Necessary drawings and specifications were prepared to allow for competitive, fixed-price procurement of the radiative heating system hardware fabrication, installation and system checkouts. The detailed design and specifications associated with the electrical system design, including the control system and DC power rectification, were accomplished by NASA/Ames personnel. Maintenance manuals and an alignment manual for the radiative heating system were also prepared.

Because of the long leadtime required for fabrication of the optical components, specifications for the individual components were prepared separately to allow NASA/Ames to initiate procurement for these components prior to awarding the main fabrication and installation contract.

Based upon competitive fixed-price bidding, NASA/Ames awarded S & Q Construction Company the main contract to fabricate and install the radiative heating system. This work is currently in progress and scheduled to be completed during 1967.

2. INTRODUCTION

The initial objectives of this program were to perform the necessary analytical, experimental and development work to provide information for a recommended design of a radiative heating system. Near the completion of this work, the objectives were extended to include the detailed design of the radiative heating system, including the preparation of detailed specifications for competitive fixed-price bidding for the hardware fabrication, installation and system checkout.

The final report has been prepared in three separate volumes. That work associated with the development of the prototype optical system and the combined testing of the final radiation source-optical system is presented in Volume I, titled "System Development."

Volume II, titled "Source Development," describes the development program on the radiation source, including the work performed under the source development subcontract, and all test runs on the operation of the final radiation source.

Volume III, titled "Facility Design," covers the detailed design of the radiative heating system.

Certain documents prepared in this program have not been reproduced for inclusion in this final report. These documents include the following:

a. The Systems Concept Report: This report was prepared and transmitted under separate cover on 1 October 1963. This report contains the results of the analysis and evaluation of those promising system approaches which allowed the selection of the system concept for further development work.

b. Specification A-10960: A draft of this specification was prepared and transmitted to NASA/Ames in June of 1965. Specification covered services and materials necessary for the fabrication and testing of collector assemblies for the radiative heating facility and was used for procurement of the collector assemblies prior to award of the main fabrication and assembly contract.

c. Specification A-11091(D8-8): This specification covers the services and materials necessary for the fabrication and testing of flat circular folding mirror assemblies of the radiative heating system facility and was prepared and submitted in draft form in June 1965 to NASA/Ames.

d. Specification A-10745: This specification was prepared and submitted to NASA/Ames in draft form in May 1965 to allow for NASA/Ames procurement of the projection lenses, field lenses, and uniformity filter plates.

e. Alignment Manual A-11054(RP-39): This manual was prepared and transmitted to NASA/Ames in December 1965 and provides instructions for alignment of the optical channels of the radiative heating system.

f. Maintenance Manual for the Radiative Heating System: This manual was transmitted to NASA/Ames in September 1966 and covers the maintenance requirements of the radiation source, optics, and utilities.

g. Portions of Specification A-11054: Portions of this specification which covers the overall radiative heating system hardware fabrication, installation and checkout were submitted to NASA/Ames in numerous transmittals during 1965. The completed specification was utilized in the final fixed-price competitive bidding for the radiative heating system.

3. SYSTEM REQUIREMENTS

The scope of the work under this contract consisted of analytical, experimental, and development work to provide information for a recommended design of a radiative heating system. The scope was later changed to include the detailed design of the radiative heating system facility. This system was to be incorporated as a component in a new wind tunnel to be installed in the Mass Transfer Cooling and Aerodynamics Facility at Ames Research Center, Moffett Field, California.

One of the basic requirements of this development work was that the resulting recommended design of the radiative heating system should be practical to construct within an allotted budget. Thus, as the development work progressed and additional information became available, a number of the original performance goals of the system were modified in order to insure that this fixed budget would be adequate to complete the facility.

The original desired performance and operating characteristics of the radiative heating system, including later changes in these desired characteristics, are reviewed below.

3.1 INTENSITY

The original intensity goals for the radiative heating system included a low intensity mode for a 6" diameter model and a high intensity mode for a 2" diameter model. The intensity goal for the low intensity mode called for a continuously variable flux intensity from 0 to 500 BTU/ft^2-sec. For the high intensity mode, the flux intensity of 0 to 3000 BTU/ft^2-sec. was specified. On 8 November 1963, the desired intensity performance and target size goals were reviewed to an intensity level of 1088 BTU/ft^2-sec., on a 4" diameter model.

3.2 RATE OF INTENSITY VARIATION

The maximum rate of intensity variation for the radiative heating system required the capability of performing a step function and/or 700 BTU/ft^2-sec^2 for programmed flux control.

3.3 INTENSITY UNIFORMITY

The goal for intensity uniformity across the heating zone was $\pm$ 5 percent.

3.4 POWER OUTSIDE HEATING ZONE

Minimum irradiation outside of the heating zone was specified as a desired performance characteristic of the radiative heating system.

3.5 SPECTRAL DISTRIBUTION

The original desired spectral distribution characteristic of the radiative heating system is illustrated in Figure 11.1. In NASA/Ames letter dated 8 November 1963, the requirements for the spectral distribution were changed. The new specification required complete cutoff of all radiation above 6,000 Å. In NASA/Ames letter on 24 April 1964, the spectral distribution requirements were further modified. The new specification required that 60% of the radiation should fall in the wavelength range of 2,000 Å and 6,000 Å.

3.6 OPERATING CHARACTERISTICS

The desired operating characteristics of the radiative heating system included the following:

a. Independent controls to allow the radiative heating system to heat the model independently or concurrently with the convective heating system.

b. Flux control for setting and automatically maintaining intensity levels within $\pm$ 3% of the desired value of intensity.

c. Chopping for instrumentation purposes was an original system operating characteristic desired but was deleted from the specification on 8 November 1963.

d. Operating Period: The initial requirements for the radiative heating system required that the system be capable of continuous operation at maximum intensity for runs as long as one hour with a maximum of one-half hour between runs. This requirement was later changed per Change Order Number 2 dated 15 February 1965 to limit the length of operation at maximum intensity to 15 minutes with 5 minutes between runs.

3.7 RADIATION SOURCE REQUIREMENTS

This program required the design, development and test of a plasma radiation source suitable for integration into an optical system with the following performance and operating characteristics.

3.7.1 Spectral Distribution

The spectral distribution requirement for the radiation source specified a close match of the emitted flux to the desired spectral distribution depicted in Figure 4 of the Statement of Work, which is reproduced as Figure 11.1 of this report.

3.7.2 Energy Conversion Efficiency

Energy conversion efficiency of at least 30 percent was the design goal for the development of the radiation source.

3.7.3 Solid Angle of Irradiation

The development of the radiation source was restrained by the requirement that it irradiate irradiation to a solid angle of approximately 10 steradians.

3.7.4 Average Radiance

To satisfy the radiative heating system intensity goals, a radiance of 7,000 Watts/cm^2-str. was set for the radiation source.

3.7.5 Operational Life

The requirement for minimum operating life was set equal to that of the radiative heating system; that is, one hour at maximum rated power level with a maximum of one-half hour between runs. As indicated above, this requirement was changed to 15 minutes of maximum power run with 5 minute intervals between runs.

3.7.6 Output Power Variation

Per NASA/Ames letter dated 8 November 1963, the requirement that the radiant power output of the radiation source be continuously variable from 100 percent to 25 percent or lower was added.

3.8 PRIORITY OF DESIGN AND PERFORMANCE GOALS

To govern the proper weighing of performance characteristics of the radiative heating system, priority of performance goals was set forth to be used in the event that system performance compromises were required in order to complete the program within the allowable time or funds. At the initiation of the program, the priority for performance characteristics was listed in decreasing importance as follows:

a. Intensity - 500 BTU/ft^2-sec.

b. Intensity - 3,000 BTU/ft^2-sec.

c. Flux Distribution

d. 6" Diameter Model Size

e. Rate of Intensity Variation

f. Spectral Match

Changes in this priority list were made in order to accommodate other design changes. With the change to only one intensity mode and target size, the first priority became that of intensity. The 6" diameter target became 4". Spectral match was placed ahead of rate of intensity variation. The priority list of operating characteristics did not change throughout the program with the exception of the chopping requirement being deleted. The order of priority as set forth was as follows:

a. Intensity Variation with Time

b. $\pm$ 3% Control of Intensity

c. Minimization of Back Radiation from Optical System

d. One Hour Continuous Operation

4. SUMMARY - VOLUME I

The development of the prototype optical system and the test results of the combined final radiation source-prototype optical system are described. At the initiation of this program, a Systems Concept Study was performed to analyze the various possible system approaches. An evaluation and comparison trade-off study was made between the most promising design approaches weighing the various operating and performance characteristics and potential upgrading capability. As a result of this study and subsequent evaluation by NASA/Ames personnel, a system concept was selected for further detailed development work. The basic system approach selected consisted of multiple single lamp projection channels using simple relay optics in a frontal approach. The last element of each optical channel is the projection lens which acts as the vacuum interface of the test chamber. These projection lenses are mounted in a great circle around the center line of the nozzle. The center line on each optical channel intersects the model and nozzle center line with an inclination angle of approximately 53°.

The final prototype optical channel design, which was utilized in the demonstration testing, evolved from the initial design concept. With each optical channel system, a collector mirror projects a purposely distorted image of the arc onto the clear aperture of the field lens. The projection lens is utilized to project the radiation intensity distribution at the field lens onto the target which is inclined to the optical axis. A folding mirror is utilized in each optical channel for packaging convenience.

In the detailed design of this prototype optical system, it was found that the only important aberration existing in the system was that of spherical aberration of the projection lens. Correction of this aberration by aspherizing the projection lens was evaluated with the results indicating that this approach would adversely affect the intensity uniformity distribution across the target which is inclined to each optical channel. Also, correction of this spherical aberration by tilting the projection lens in order to maintain symmetry was found to be undesirable because of the significant amount of astigmatism introduced. It was determined that this astigmatism would result in a considerable loss of target power. It was thus concluded for the present optical system concept being developed, which requires a radiation of an inclined target, the use of spherical surfaces were warranted since alternate corrective measures did not seem to improve the overall performance or had a negative effect.

Analyses were performed to determine the severity of the thermal loading problem. As a result of these analyses, the radiation source collector was water-cooled as well as the aluminum folding mirror. Water-cooling was also provided for the field and projection lens mounts.

The thermal loading conditions at the projection lens, which represents the vacuum interface with the test chamber, required use of a high temperature vacuum seal. Difficulties were experienced in obtaining a satisfactory seal at the projection lens-mount interface. Several approaches were attempted with varying degrees of success. The final approach selected for this vacuum seal utilized a metal thin walled O-ring that is compressed against the periphery of the lens during installation.

The spectral requirements for the radiative heating system were modified during this program. The final output radiation spectral distribution requirements allowed the use of a water cell filter. Prior to this specification change, development work had been directed to obtaining a reflective type filter which would reject all radiation above 6000 Å.

The design and fabrication of the radiation source collector represented possibly the major development task associated with the prototype optical system. Since the design of this collector had to be finalized concurrent with the early stages of the radiation source development work, radiation source data associated with the 60 KW prototype radiation source was utilized for the necessary optimization of the collector contour. The electro-forming technique was selected as the means to produce the prototype collector. This required the fabrication of an electroforming mandrel. Prior to initiating this fabrication, various mandrel materials were evaluated regarding ease of polishing and compatibility with electroforming. As a result of this study, stainless steel 304 was selected for the basic mandrel material.

Studies were conducted to determine instrumentation required for the radiation source measurements and target intensity distribution measurements of the prototype optical system. Eppley thermopile radiometers and a photo diode sensor were the primary sensors utilized in the radiation source measurements. Hy-Cal radiometers and a NASA/Ames slug calorimeter were utilized for prototype target intensity measurements. A Spectrolab developed spectral radiometer system was utilized to determine the output spectral radiation distribution from the radiation source and prototype optical system. Sensor comparison tests were performed to obtain some measure of confidence between the various factory calibration factors associated with the sensors used. Difficulties were experienced in obtaining good agreement in these comparison tests.

A comprehensive test program was conducted with the combined final radiation source-prototype optical system. The power intensity distribution across the field lens aperture was measured. Transmission measurements of the water cell were also conducted, which indicated a filter transmission factor of approximately .67. Target intensity scans were conducted at various times during the test program under varying radiation source operating parameters. Evaluation of these results indicates that the minimum unfiltered target edge intensity for a 14-lamp radiative heating system would be on the order of 546 BTU/ft^2-sec. over a 4" diameter target. Tests utilizing an aluminum dot filter deposited on a water cell plate indicated that uniformity filtering could be designed for the radiative heating system which would allow satisfying the $\pm$ 5% system intensity uniformity goal.

5. INTRODUCTION - VOLUME I

The following contents of Volume I of this final report cover the work performed in the optical system concept study, optical and thermal design development work, and the fabrication and test evaluation of the prototype optical system.

Those theoretical considerations which were applied to the performance goals of the radiative heating system to establish certain restraints and requirements on the system design and radiation source parameters are presented in Section 6. This includes discussions on radiometric considerations as well as the various overall system efficiency factors.

The system concept study is reported on in Section 7. The objective of this study was to provide a recommended design concept for the radiative heating system. As a result of this work, a system approach concept was selected by NASA/Ames allowing initiation of more detailed study and development work.

The development of the optical system design is presented in Section 8. A brief summary of the history of the evolution of the prototype optical system, including the many system requirement changes and design modifications that transpired during the course of the contract, is included.

The results of the thermal loading analysis are reported on in Section 9. The analysis of the field lens and projection lens absorption coefficient is also reported on as well as the analysis predicting the estimated operating temperatures of the respective lenses. In Section 10, the development test program leading to the recommended vacuum seal design is reported on.

The initial spectral distribution requirement for the radiative heating system required a close spectral match to the desired spectral distribution depicted in Figure 4 of the Statement of Work. Prior to changes in this specification, design work on reflecting type filters was performed in the attempt to satisfy the spectral distribution requirement. The results of this development work are reported on in Section 11 as well as the work performed on the water cell filter which represents the final design of the system's spectral filtering.

In Section 12, the various prototype system components are described. Those development programs and/or studies associated with the development of the individual prototype components are also reported on in this section.

Instrumentation, as required in this program to measure and monitor the radiation source characteristics, and instrumentation required for the measurement of the output intensity distribution of the prototype optical system are reported on in Section 13. Also included is a description of Spectrolab's spectroradiometer measuring equipment used to measure the spectral output radiation distribution from the radiation source and the prototype optical system. In Section 14, the combined final radiation source-prototype optical system testing is reported on. Included in this section is a description of the test site and prototype optical system. Alignment methods and problems experienced in obtaining adequate alignment are presented. The estimated 14-lamp system target edge intensity, without water cell losses, as reported on during the period of the test program, are tabulated.

6. THEORETICAL CONSIDERATIONS

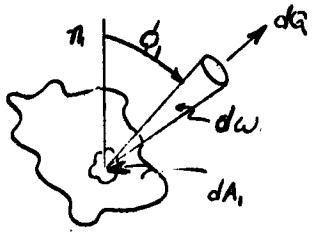
In the selection of an optical system and in the determination of the minimum radiation source requirements for a radiation power transfer system, it is necessary to correctly appraise the performance requirements and the demands they make on the system. This section covers those theoretical considerations which were applied to the performance goals of the radiative heating system to establish certain restraints and requirements on the system design and radiation source parameters.

6.1 RADIOMETRIC CONSIDERATIONS

The relationships between the intrinsic source radiance and the minimum solid angle required to irradiate a target with an intensity E are governed by fundamental radiometric considerations. This limiting performance effect, so to speak, is established by the conservation of radiance, discussed in most optical textbooks.* (e.g. Hardy and Perrin, Principles of Optics, Ch. XIX)

By definition, the radiance R in a given direction ϕ at any point on an extended source is equal to the flux Q per unit solid angle emanating from the surface in the direction ϕ divided by the area of the element projected in a plane perpendicular to the given direction. In mathematical symbols

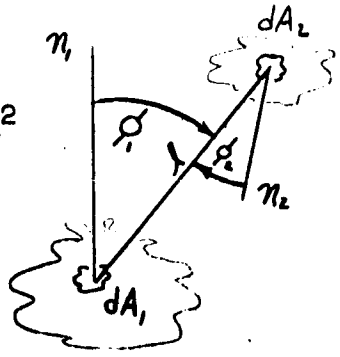
$$R = \frac{dQ}{d\omega_1 dA_1 \cos\phi_1} \qquad (6.1)$$



The radiation from dA_1 incident on a differential area dA_2 can be therefore expressed as

$$dQ_{1\rightarrow 2} = R\, dA_1 \cos\phi_1\, d\omega_1 \qquad (6.2)$$

where the solid angle $d\omega_1 = dA_2 \cos\phi_2 / \ell^2$ (6.3)



Substituting 6.3 into 6.2, the flux intensity dE on dA_2 by dA_1 is obtained:

$$dE = \frac{dQ_{1\rightarrow 2}}{dA_2} = \frac{R dA_1 \cos \phi_1 \cos \phi_2}{\ell^2} \qquad (6.4)$$

For relatively simple shapes of extended Lambertion sources, the relationship can be expressed analytically. For an example, consider a disk shaped source illustrated in Figure 6.1 where θ is the half angle subtended by the disk to the area dA_2 irradiated.

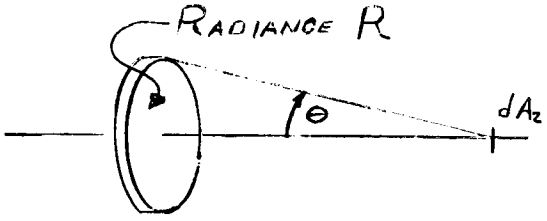


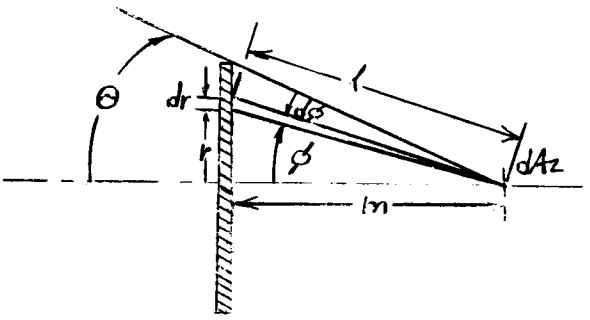
Figure 6.1
Disk Shaped Source
Irradiating Area dA_2

Using polar coordinates, the differential area dA_1 on the source A_1 can be expressed as

$$dA_1 = 2\pi r dr$$

Also, where dA_2 is parallel to A_1

$$\cos \phi_1 = \cos \phi_2 = \cos \phi$$



Substituting these expressions into Equation 6.4 results in

$$dE = \frac{R 2\pi r dr \cos^2 \phi}{\ell^2} \qquad (6.5)$$

Utilizing the following substitutions $\ell = m \sec \phi$ and $r = m \tan \phi$ in Equation 6.5, an expression in terms of ϕ is obtained.

$$dE = 2\pi R \sin \phi \cos \phi \, d\phi \tag{6.6}$$

Integrating over the range of $\phi = 0$ to $\phi = \theta$ for the entire disk gives

$$E = \int_{\phi = 0}^{\phi = \theta} 2\pi R \sin \phi \cos \phi \, d\phi \tag{6.7}$$

$$E = \pi R \sin^2 \theta \tag{6.8}$$

This equation is of considerable utility in the analysis and evaluation of system approaches since it relates the intensity produced at any point on the axis of an aplanatic system by an extended circular shaped source emitting, transmitting, or reflecting according to Lambert's law within the field of view of the point. For this application, Equation 6.8 describes the performance of an optical system which transmits without losses due to absorption, interface reflection, and other causes. To take into account these losses, R should be written kR where the coefficient k expresses the optical efficiency of the system. The optical efficiency factor k is defined as the product of those efficiency factors which act to attenuate the source radiance as viewed from the point of irradiation.

In the problem of providing combined convective and radiative heating on a model face in re-entry simulation, a convective heating nozzle is located directly in front of the model face. Because of the geometrical location of the nozzle relative to the model, all radiation incident upon the model face from a radiative heating system must strike the model at some angle inclined to the model axis. In general, either the model will be inclined to the optical axis of many optical systems or the model will view a large optical element appearing as a circular disk with the center portion occluded by the nozzle.

For the case where the model face is inclined to the optical axis of an optical system as illustrated in Figure 6.2, the flux will be spread over a larger area than the projected area viewed from the optical element. Thus, the intensity or flux per unit area will be diminished by a factor approximately equal to the ratio of the projected area to actual area or the cosine of the inclination. Hence, Equation 6.8 becomes

$$E = \pi k R \, \mathrm{Sin}^2 \theta \, \mathrm{Cos}\alpha \tag{6.9}$$

Where n identical optical systems irradiate the model face at the same inclination angle, the resulting intensity is a result of the contribution from each irradiating system and hence Equation 6.9 becomes

$$E = n \pi kR \, \mathrm{Sin}^2 \theta \, \mathrm{Cos}\alpha \tag{6.10}$$

For the case where the model is irradiated by a large mirror circumscribing the nozzle as illustrated in Figure 6.3, the mirror appears as a circular disk with the center portion occluded when viewed from the model face. If the mirror exhibits a radiance kR within the field of view of the model, then the integration of Equation 6.6 over the range of $\phi_1 = \theta_1$ to $\phi_2 = \theta_2$ gives the applicable radiometric equation for this case.

$$E = \int_{\theta_1}^{\theta_2} 2\pi R \, \mathrm{Sin}\phi \, \mathrm{Cos}\phi \, d\phi \tag{6.11}$$

$$E = 2\pi kR \left(\mathrm{Sin}^2\theta_2 - \mathrm{Sin}^2\theta_1\right) \tag{6.12}$$

It is, therefore, apparent that the required relationships between the source radiance and the solid angle of irradiation places a theoretical limit on the intensity levels achievable upon a model face. It is noted that this limit is independent upon the number of radiation sources utilized and the total output power of the radiation sources.

The above radiometric equations were derived for the irradiation upon a differential area located on-axis of an optical system. For off-axis points on a finite model, a higher radiance would be required to achieve the same intensity level since the solid angle that the last optical elements subtend to that off-axis point is less than the solid angle subtending to the on-axis point.

The determination of the total system power required to irradiate a finite target size with a given intensity level is obtained by knowledge of the system efficiency which is covered in Section 6.2.

6.2 SYSTEM EFFICIENCY

In this section, the various factors which contribute to an overall system efficiency are described. The importance of the efficiency considerations cannot be overemphasized due to their relationship to the number and size of radiation sources required and hence to the total system cost. The overall system efficiency can be expressed as the product of all system efficiency factors. For convenience, these efficiency factors are grouped into four main categories consisting of the following:

(1) Optical Efficiency

(2) Collection Efficiency

(3) Energy Conversion Efficiency

(4) Geometrical Efficiency

It is important to note the difference between the overall system efficiency and the optical efficiency of a system. The overall system efficiency is defined as the ratio of the total radiant power delivered to target to the total electrical power input. The optical efficiency is defined as a product of only those efficiency factors which have the effect of attentuating the source radiance as seen by the target. An accounting of all efficiency factors is presented in the following paragraphs.

6.2.1 Optical Efficiency

As defined above, the optical efficiency indicates the effectiveness of the optical system in reproducing the source radiance as seen from the model. Those factors which act to reduce the optical efficiency are listed below:

a. Degradation: This results from deposition of dust and other materials on optical surfaces, deterioration of reflecting surfaces and source envelopes.

b. Reflection Losses: Some energy is absorbed and scattered by any mirror surface.

c. Spectral Filtering: The desired spectral distribution of radiation can be attained only by rejecting undesired energy from the source radiation.

d. Uniformity Filtering: To obtain uniformity of energy distribution at the target, some energy must be rejected.

e. Lens Transmission: Energy is absorbed in passing through any lens and is reflected at each lens surface.

f. Chopping Factor: The requirement for chopping results in additional energy loss equivalent to a reduction in source radiance.

6.2.2 Collection Efficiency

Collection efficiency describes the effectiveness of the geometrical design in collecting energy emitted by the source and projected into the transfer optics. It includes the following:

a. Flux Capture: Flux capture is defined as the percentage of radiation emitted from the radiation source which is incident upon the collecting optics.

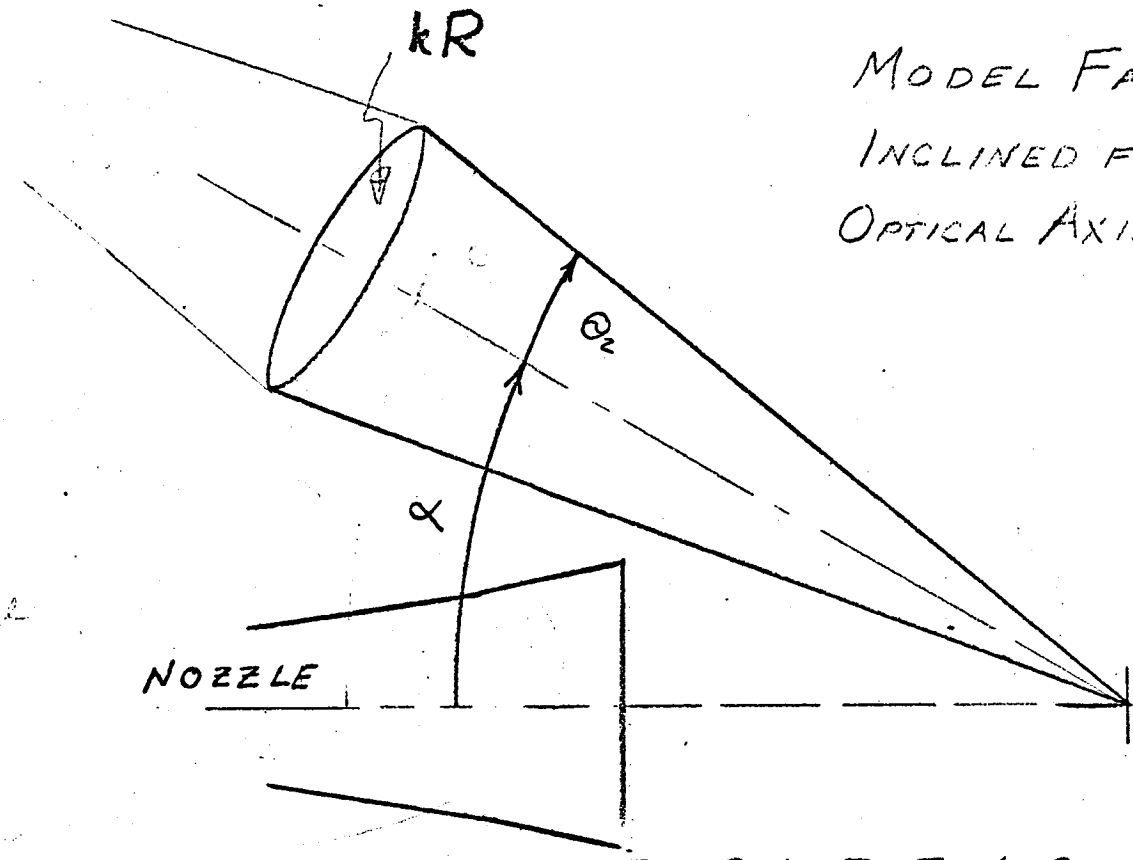
b. Arc Utilization: The degree to which an optical system can utilize the arc of a radiation source is referred to as arc utilization. This efficiency factor is defined as the percentage of the total radiation reflected from the collecting optics which is incident upon the transfer optics.

6.2.3 Energy Conversion

An important efficiency factor which must be considered is the source conversion factor. This conversion factor is defined as the ratio of arc emission transmitted through the quartz envelope to the total electrical power input.

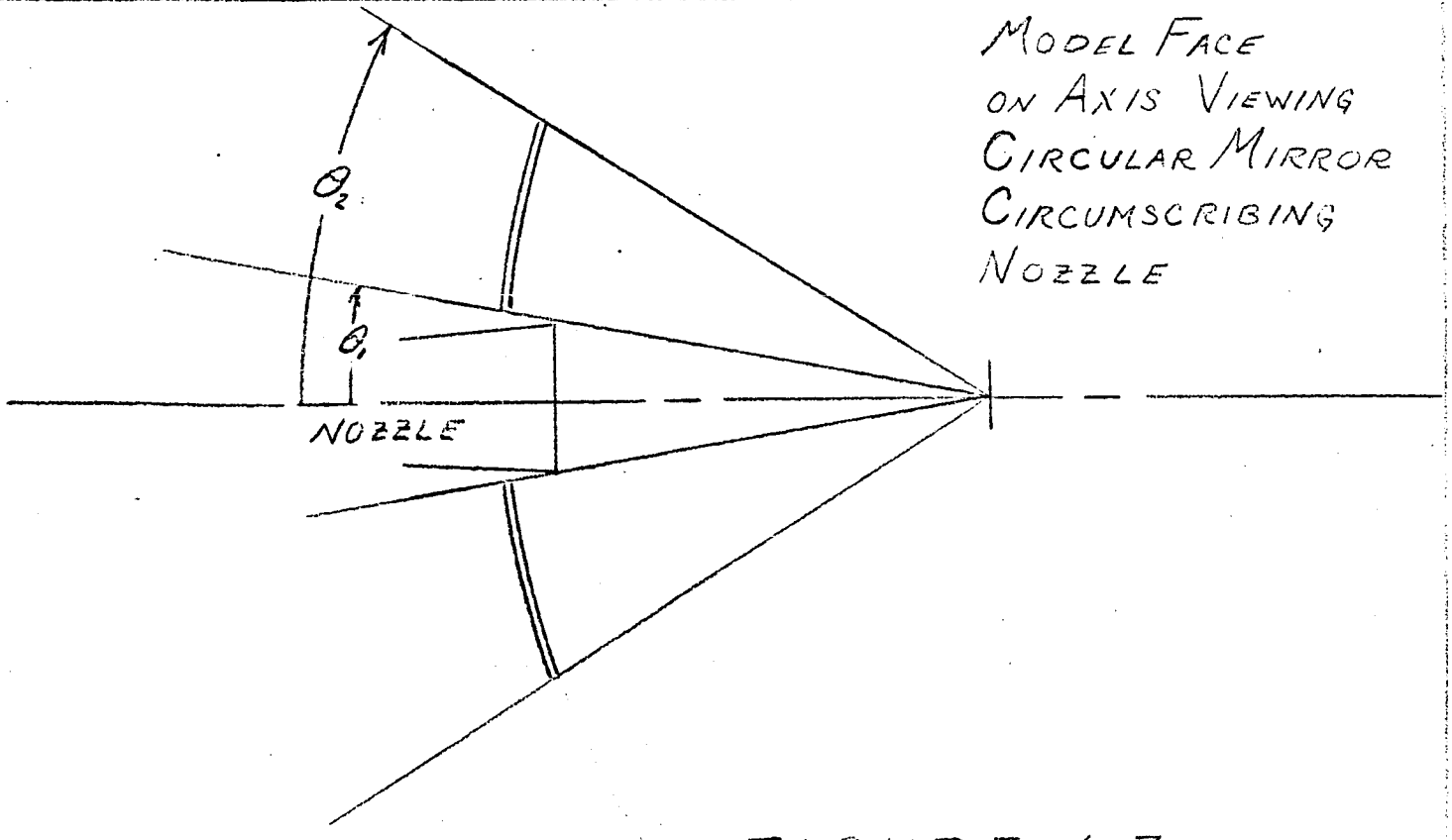
6.2.4 Geometrical Efficiency

There are some losses peculiar to specific optical systems and are included under this heading. In general, this efficiency factor would take into consideration the spillover losses encountered at the model due to the target being inclined to the optical axis. It would also include those losses associated with the penumbral regions of collimated or nearly collimated beams and losses resulting from interstices of a mirror array.



MODEL FACE INCLINED FROM OPTICAL AXIS

FIGURE 6.2



MODEL FACE ON AXIS VIEWING CIRCULAR MIRROR CIRCUMSCRIBING NOZZLE

FIGURE 6.3

7. SYSTEMS CONCEPT STUDY

A systems concept study was performed in order to analyze those promising system approaches. This work included a trade-off study between the more promising design approaches taking into consideration various operating and performance characteristics and upgrading capability.

The objective of this study was to provide a recommended design concept for the radiative heating system. As a result of this work, a system approach concept was selected by NASA/Ames allowing initiation of more detailed study and development work.

7.1 PERFORMANCE CRITERIA

The criteria for system performance evaluation in the Systems Concept Study were specified by NASA/Ames by listing the priorities of the desired performance characteristics of the radiative heating system in Paragraph 1.2.2 of the Statement of Work. These priorities, as modified on 3 September 1963, are here listed in order of decreasing importance.

a. Intensity-500 BTU/ft^2-sec. (6" diameter target)

b. 6" diameter model size

c. Flux distribution

d. Intensity-3,000 BTU/ft^2-sec. (3" diameter target)

e. Spectral match

f. Rate of intensity variation

Upon applying these criteria, only those systems giving expectation of being capable of delivering power to the 6" diameter target with an intensity of 500 BTU/ft^2-sec. or more, with at least fair uniformity, were considered for detailed analysis.

7.2 SYSTEMS SELECTED FOR ANALYSIS

Three basic types of systems were selected for detailed analysis. These consisted of searchlight systems, frontal projection type systems and facet mirror array systems. Minor variations of each type system brought the total number of systems considered to 16. These systems are described in detail in the Systems Concept Study report.

7.3 RECOMMENDED SYSTEM APPROACH

The system approach recommended as a result of this study was multiple single lamp projection systems utilizing simple relay optics in a frontal approach to the model. Figure 7.1 depicts this basic approach. Three of the variations of this system included the use of multiple rows of the single lamp projection systems requiring the use of up to 30 sources and optical systems. It was recognized that the cost of the multiple row system would exceed the available funds and hence the recommended system utilized only 15 radiation sources and optical systems which could be built with the necessary provisions for upgrading at a later date. It was predicted that the performance of the recommended system without spectral and uniformity filtering would satisfy the low intensity mode requirements. The chief advantages of this system approach over other systems considered were (a) good uniformity over the entire target; (b) high intensity mode capabilities; (c) capable of masking waste energy that would otherwise irradiate the model outside of the heating zone; (d) comparable with the implementation of radiation chopping mechanisms.

The other promising approaches which were analyzed in detail were a facet mirror array approach illustrated in Figure 7.2 and a searchlight system approach illustrated in Figure 7.3. The attractiveness of the facet mirror array approach was somewhat dimmed by the difficulty of obtaining an adequate effective solid angle and hence reasonable intensities on a 6" diameter target. The searchlight system utilizing "aconic" type collectors represented the most economical system considered but had many unfavorable system characteristics. The chief disadvantages noted with this system approach was the inability of masking the beams to reduce the large amount of energy missing the heating zone. Also, the degree of uniformity obtainable with that approach was strictly dependent upon the collector design.

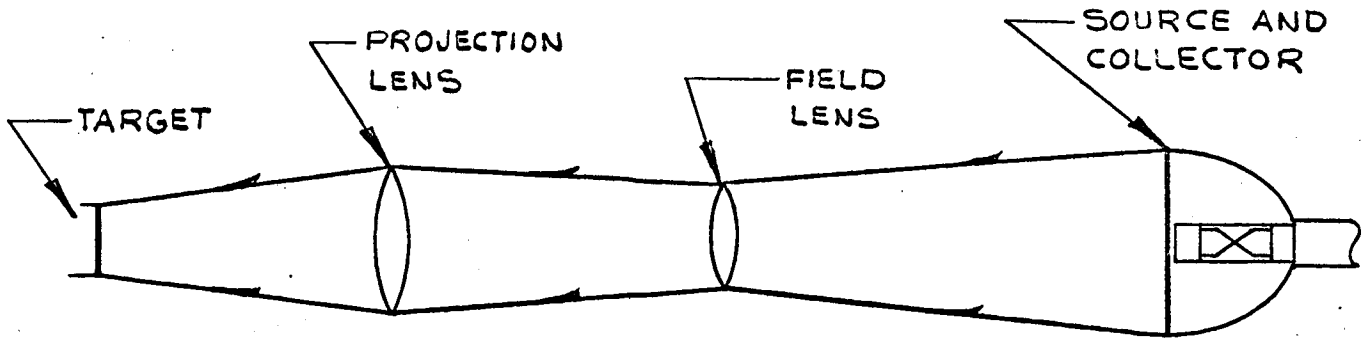
7.4 SYSTEM APPROACH SELECTION

To facilitate evaluation of the Systems Concept Study report, NASA/Ames requested additional detailed information including cost estimates of some optical components in regard to searchlight systems and projection systems. This material was forwarded in a letter to NASA/Ames on 15 October 1963.

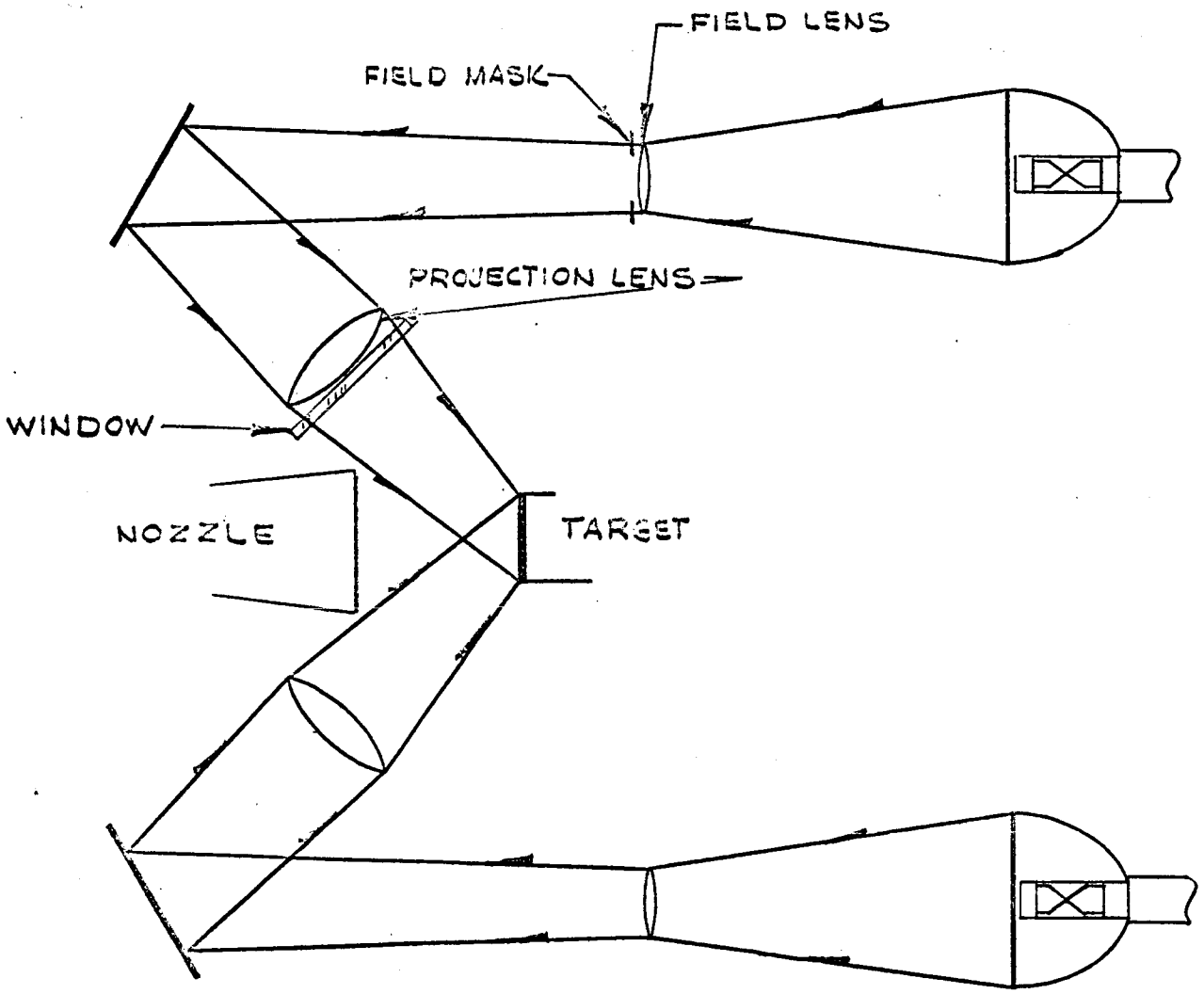
On 18 October 1963, a meeting was held at NASA/Ames to allow Spectrolab personnel to answer questions regarding the technical

material previously transmitted. As a result of NASA/Ames personnel concern regarding the total system cost, rough cost estimates for the radiative heating system were formulated in this meeting. Technical discussions regarding filtering, target size, restraints imposed by the convective heating system and the necessity for chopping were discussed.

In a letter dated 8 November 1963, NASA/Ames informed Spectrolab their choice of projection type system for design study. A field lens diameter of 6" was specified so that the source radiation collector optics might be used in a searchlight system if the projection system approach proved too costly. This letter made many changes to the Statement of Work, including a change of target size from 6" to 4" and elimination of the high intensity mode requirement.



STRAIGHT PROJECTION SYSTEM



FOLDED PROJECTION SYSTEM

FIG. 7.1

PROJECTION (UNCOLLIMATED) SYSTEM

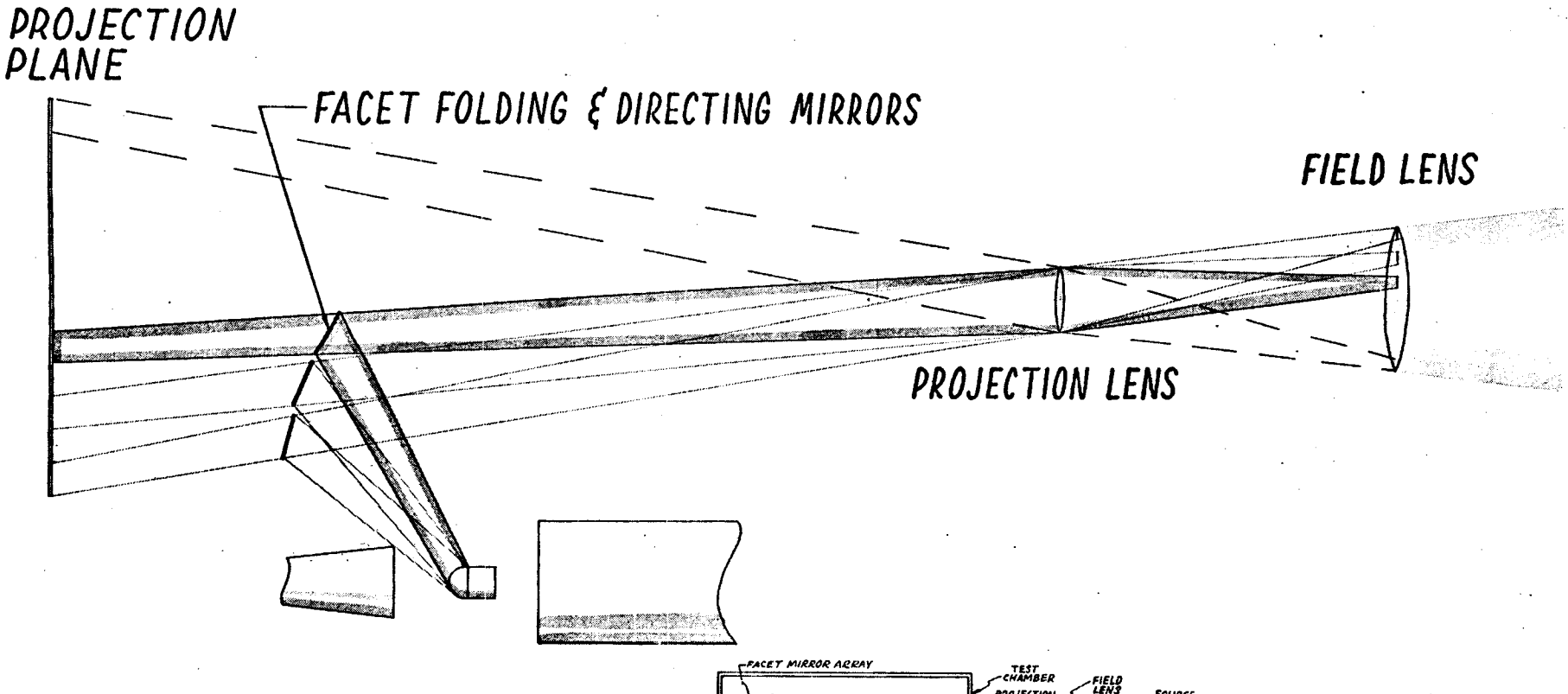
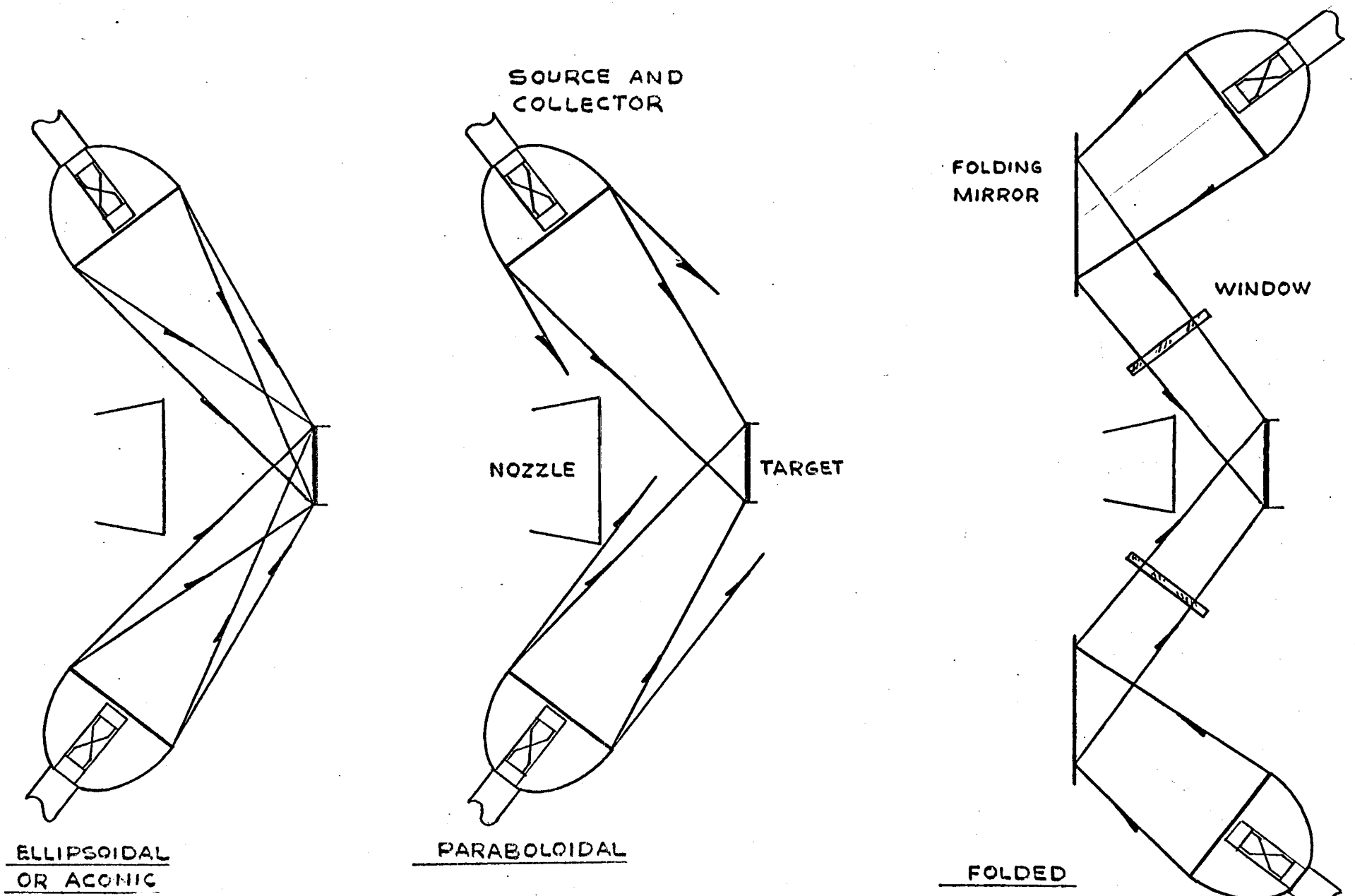


FIG 7.2



SEARCHLIGHT SYSTEMS

FIG 7.3

8. OPTICAL DESIGN DEVELOPMENT

The optical system which was utilized in the final design of the radiative heating system, which is presently being fabricated, evolved from recommendations stemming from the Systems Concept Study. A brief summary of the developments that have transpired regarding the optical system design is presented here.

8.1 OPTICAL DESIGN EVOLUTION

Many system requirement changes and design modifications transpired during the course of the contract. A brief summary of the history of this evolution is presented here including the predicted efficiency and performance data for the various systems as they evolved into the final optical system design.

On 27 September 1963, the study of system concepts for the radiative heating system was completed. As a result of this study, it was recommended that single lamp projection systems utilized in a frontal approach (designated P-series in Systems Concept Report) be selected for detailed study and performance demonstration. At that time, the specifications required two intensity modes, that is, it was required that a 6 inch diameter surface be irradiated at intensities up to 500 BTU/ft^2-sec. and a high intensity mode requiring irradiation up to 3,000 BTU/ft^2-sec. on a 2 inch diameter surface.

The low intensity system was designated P-1 and the high intensity system was designated P-2. The only difference between these two systems was the collector. With a change of collectors, either system could be converted to the other. Systems P-3, P-4 and P-5 were similar to Systems P-1 and P-2, except they consisted of an additional circular row of projection systems. The efficiency factors and performance data of Systems P-1 and P-2 as envisioned in September are tabulated in Tables 8.1 and 8.2 respectively.

The advantages of this system approach were listed as:

a. Control of spillover by masking.

b. Good uniformity obtainable.

c. Mechanical modulation possible.

d. Higher effective solid angle with higher intensity capability.

e. Low susceptibility to degradation.

The disadvantages of Systems P-1 and P-2 were related to their inability to satisfy intensity requirements. Only by adding the second row of projection systems could the low intensity requirement be satisfied and even with the second row of lamps, the high intensity requirement could not be satisfied without sacrificing filtering.

The approximate parameter dimensions which would satisfy the conversion from Systems P-1 and P-2 are listed in Table 8.1.

Upon the request of NASA/Ames, additional information was requested to supplement the Systems Concept Report. This data was transmitted to NASA/Ames on 15 October 1963, and included new efficiency tables, new system comparison chart, and graphs showing anticipated intensity distribution at the focal plane of the aconic collector proposed for System P-2. The new efficiency tables depicted a System P-20 which was identical to the P-2 system, except a lens was substituted for a window.

Several changes in the various efficiency factors were also made. These changes included slight reductions in mirror reflectivities and an increase in the efficiency of performing uniformity filtering; also, a slight increase in energy conversion efficiency was predicted. A major change was associated with the adjustment of the arc utilization efficiency factor to account for the smaller clear aperture of the field lens required to accommodate the smaller 3" diameter target. This adjustment was also applicable to System P-2, but was apparently overlooked. The efficiency factors and system performance data predicted for System P-20 are tabulated in Tables 8.1 and 8.2 respectively.

On 18 October 1963, a meeting was held at NASA/Ames to discuss the results of the Systems Concept Study and to answer questions regarding the technical material that was transmitted on 15 October 1963. At this meeting, the possibility of using a P-series which would utilize more than one row of projection systems was ruled out due to simple economics. The merits of selecting a system to irradiate a 4 inch diameter target as a modification of the P-2 system were discussed. These merits, based upon the assumption that the system does not have to be capable of converting to a different size target, included the following:

a. Higher efficiency than a comparable design for a 2 inch or 3 inch diameter target (due to radiometric limitations, the P-2 system had previously been designed for a 3 inch diameter target).

b. Shorter optical path by approximately 5 feet.

c. The irradiation of a 6 inch diameter target would be possible by removing elliptical mask, if intensity fall-off on target edge would be tolerable.

On 8 November 1963, Spectrolab received a letter relating the decision of NASA/Ames that Spectrolab should perform their detailed study and demonstration on a projection type system which would irradiate a 4 inch diameter model size. Among the many changes of the Statement of Work, enclosed in this letter was the requirement that the field lens diameter not exceed 6 inches. This was based upon the reasoning that the collector design would then be suitable for use in a searchlight type of radiative heating system if the projection type system proved too costly. Thus, the requirements for dual intensity mode were eliminated and the intensity requirement for the 4 inch diameter target was specified as at least 1,088 BTU/ft^2-sec.

The Statement of Work was also changed to provide for complete cutoff of radiation and wavelengths greater than 6,000 Å. This change resulted in a significant decrease in the spectral filter efficiency factor. To accommodate the 4" diameter target and 6" diameter clear aperture field lens, the distances between the optical elements had to be modified. A 24" diameter collector was maintained and a new distance between collector and field lens of 123" was selected. This change resulted in an increased arc utilization efficiency factor of .77. This system, designated P-40, like Systems P-1, P-2 and P-20, consisted of 15 single lamp projection systems whose projection lenses were arranged in a circular row about the center line of the nozzle. System P-40 parameter dimensions and predicted efficiency factors and performance data are tabulated in Tables 8.1, 8.2 and 8.3 respectively.

On 18 March 1964, it was realized that the collector tooling at that time being fabricated, utilized an interfocal distance different from that required to accommodate the optical system being analyzed. Inadvertently the S_3 dimension depicting the distance between the collector and the field lens was utilized as the interfocal distance of the collector.

Consequently, it was necessary to modify certain system parameters in order to utilize the collector tooling which was well downstream in fabrication.

An investigation was performed to determine what minor changes would be required in the system design to accommodate this collector. A list of possible changes of system parameters to satisfy the system restraints and the collector design was prepared and presented to NASA/Ames personnel on March 20th at Spectrolab. A decision was made at that time to proceed with a design based upon use of fourteen projection lenses where the distance from the projection lens to target was 38 inches in lieu of 41 inches previously contemplated.

This change in itself would have resulted in an increased arc utilization factor efficiency. However, at that time it was recognized that the radiation source under development would not meet the design goals associated with arc length and radiance. The original goals set forth for the radiation source development program were to produce a radiation source which would exhibit an average radiance of approximately 7,000 Watts/cm^2-str., with a nominal arc length of approximately 8 mm and with an output power of approximately 50 KW. For purposes of predicting system performance, an average arc radiance of 3,200 Watts/cm^2-str. and an arc length of approximately 14 mm was used. As a result of these estimated source parameters, a new arc utilization efficiency was calculated to be .55. As previously defined, the arc utilization represents the percentage of radiation incident upon the clear aperture of the field lens relative to the total radiation incident at the field lens plane.

As a result of the low spectral filter efficiency factor, which was predicted to satisfy the requirement of reflecting all radiation above 6,000 Å, a decision was made by NASA/Ames to modify the spectral requirements to accept the spectral distribution that would be obtained by the use of a water cell approximately 1 cm thick. This would result in a near complete cutoff of all radiation above 1.1 microns. Preliminary calculations indicated that this would result in an efficiency factor of approximately .78 for spectral filtering.

The parameter dimensions for this system designated P-40A are tabulated in Table 8.1 and the predicted efficiency factors and performance data are tabulated in Tables 8.2 and 8.3 respectively.

	PARAMETERS	SYSTEMS P-1	P-2 & P-20	P-40	P-40A
N	Number of Optical Subsystems	15	15	15	14
D_a	Collector Diameter	16	24	24	24
D_f	Field Lens Diameter	12	12 (6 used)	6	6
D_p	Projection Lens Diameter	12 (8 used)	12	12	12
S_3	Distance between Collector and Field Lens	164	164	123	114.5
S_2	Distance between Field Lens and Projection Lens	82	82	61.5	57.25
S_1	Distance between Projection Lens and Target Plane	41	41	41	38.16
D_T	Target Diameter	6	3	4	4
α	Angle of inclination between Optical System and Target	50°46'	50°46'	50°46'	50°52'
S_t	TOTAL Optical Path	287"	287"	225.5"	209.9"
	$S_1 + S_2 + S_3 = S_t$	23.9'	23.9'	18.8'	17.5'

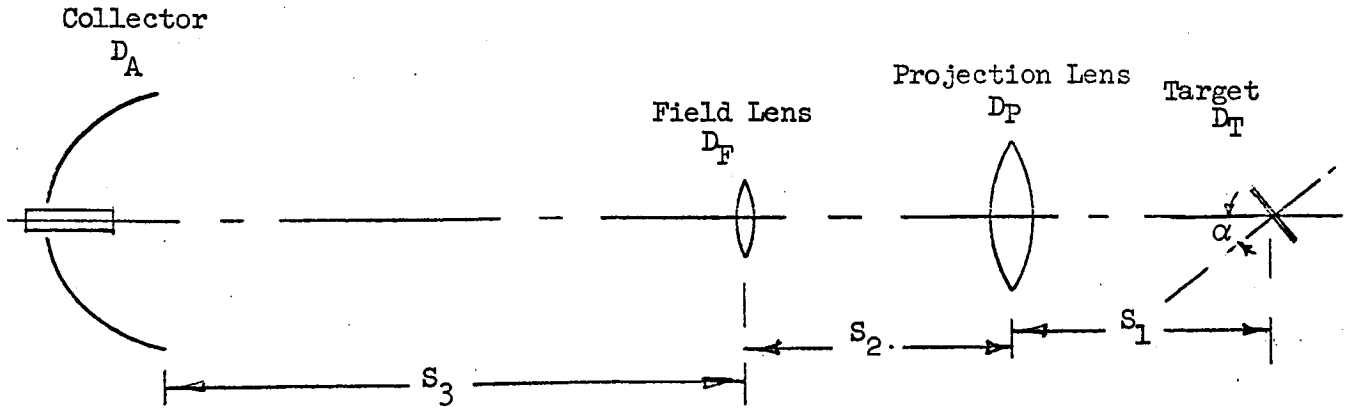


TABLE 8.1 System Dimensions

	SYSTEM				
	P-1	P-2	P-20	P-40	P-40A
OPTICAL EFFICIENCY K_1					
Degradation	.90	.90	.90	.90	.90
Collector Reflectance	.86	.86	.84	.84	.84
Mirror	.88	.88	.87	.87	.87
Facet Mirror with Cover	—	—	—	—	—
Lens	$(.90)^2$	$(.90)^2$	$(.90)^2$	$(.90)^2$	$(.90)^2$
Window	.90	.90	—	—	—
Uniformity Filter	.80	.80	.85	.80	.85
Spectral Filter	.75	.75	.75	.40	.78
Chopping Factor	.90	.90	.90	—	—
COLLECTION EFFICIENCY K_2					
Arc & Image Utilization	.72	.72	.54	.77	.55
Elliptical Mask & Spillover	$\cos\alpha = .637$	$\cos\alpha = .637$	$\cos\alpha = .637$	$\cos\alpha = .637$	.60
Flux Collection	.72	.72	.72	.65	.67
ENERGY CONVERSION K_3	.30	.30	.35	.35	.35
GEOMETRICAL K_4					
Facet Array	—	—	—	—	—
Packing Factor	—	—	—	—	—
Penumbral Loss	—	—	—	—	—
OPTICAL EFFICIENCY K_1	.268	.268	.306	.170	.353
SYSTEM EFFICIENCY K_T	.0268	.0268	.0265	.0190	.0273

The System P-40A represents the present geometrical configuration of the radiative heating system being fabricated. Actual system performance, as compared to the predicted system performance given in Table 8.3, is presented in Section 15.0 titled "System Performance."

8.2 OPTICAL SYSTEM SIZING

As indicated in Section 8.1, the multiple single lamp projection system approach was selected for detailed development work. Selection of the dimensional parameters for this system involved many considerations which are discussed below.

8.2.1 Effective Solid Angle of Irradiation

Since the primary performance goal for the radiative heating system was to obtain the maximum intensity on the specified target size, the total solid angle of irradiation utilized by the optical systems become the primary factor associated with the resulting target intensity. In Section 6, it was shown that the intensity E on the target is equal to the product of the effective source radiance as attenuated by the system optics, total effective solid angle in which the target is irradiated, and the cosine of the inclination angle. Expressed mathematically, the target intensity E is given by the following equation:

Attenuated Source Radiance
Effective Solid Angle of Irradiation
Cosine of Inclination Angle

$$E = (kR)\ (N\pi \sin^2\theta_2)\ (\cos\alpha) \qquad (8.1)$$

where

R = Effective Source Radiance

k = Optical Efficiency

θ_2 = Half Angle of Irradiation

N = Number of Identical Optical Systems Irradiating the Model Face

The qualifications limiting the application of the above equation are satisfied sufficiently to allow its usage in the optimization of the projection optics and positioning relative to the target plane.

TABLE 8.3 EVOLUTION OF SYSTEM PERFORMANCE ESTIMATES

Input power per source = 150,000 watts

System No.	System Description	No. Lamps N	Efficiency		Target				B Source Radiance (w/cm²-Ster)	Eff Total Solid Angle of Irradiation We (N²sin⁴θcosφ)	Limiting Radiometric Intensity EeKiBWe (watts/cm²)
			Total K_T	Optical K_1	Dia (cm)	Area (cm²)	Power (KW)	Intensity (w/cm²)			
P - 1	One row single lamp projection systems-frontal approach (6" Dia target)	15	.0268	.268	15.24 (6 inches)	182.42	67.5	370	7000	.268	503
P - 2	System P-1 modified to accommodate 3 inch target (see Note 1)	15	.0268	.268	7.62 (3 inches)	45.60	60.30	<1201	7000	.64	1201
P - 20	Same as P-2 except efficiencies were revised & window deleted	15	.0265	.306	7.62 (3-inches)	45.60	59.63	1308	7000	.64	1372
P - 40	Similar to P-20 with geometry & efficiencies modified to satisfy spec changes (see Note 2)	15	.0190	.170	10.16 (4 inches)	81.08	42.75	527	7000	.64	762
P - 40A	Similar to P-40 except 14 lamps & efficiency changes (See Note 3)	14	.0273	.353	10.16 (4-inches)	81.08	57.33	707	3200	.678	718

NOTES: (1) System P-2 is accomplished by substituting 24-inch diameter collector for 16-inch diameter collector utilized in System P-1. See System Concept Report for further description.

(2) Specification changes requiring 4-inch diameter target, 6-inch diameter field lens, deletion of chopping, and maximum rejection of energy above .6 microns along with additional radiation source data required system modifications and hence new efficiency estimates.

(3) Efficiency data reflects larger arc size and latest change in filter requirements. 1 cm thickness of water for spectral filtering is included.

Upon examination of the above equation, 8.1, it is seen that maximizing the product of the effective angle and the cosine of the inclination angle will result in the maximum target intensity with given radiation source parameters.

8.2.2 Projection Lens Packing

Upon sizing the projection lenses and their locations relative to the target, in attempting to maximize the product of the effective solid angle and the cosine of the inclination angle, it was necessary to fully evaluate the entire packaging problem. This problem of packaging in projection lenses of diameter D_p, a distance S_1 from the target at a minimum inclination angle α, without vignetting at the nozzle, is discussed in the Systems Concept Report.

Figure 8.1 illustrates the geometrical configuration of the nozzle, target, and projection lenses. It is noted that the effective solid angle term in Equation 8.1 can be presented as a function of the projection lens diameter and the distance from projection lens to target. The angle of inclination α can also be shown to be a function of these same two parameters, as well as the nozzle target geometrical configuration. From Figure 8.1, the following geometrical relationships are noted.

$$\alpha = \gamma + \tan^{-1} \frac{D_p}{2S_1} \tag{8.2}$$

where $$\gamma = 90^\circ - \phi - \tau \tag{8.3}$$

ϕ is a known quantity when the nozzle target configuration is specified. τ is solved by noting the following relationship:

$$\frac{\sin \tau}{D_I/2} = \frac{\sin \phi}{\sqrt{\frac{D_p^2}{4} + S_1^2}} \tag{8.4}$$

$$\tau = \sin^{-1} \frac{D_I \sin \phi}{2\sqrt{\frac{D_p^2}{4} + S_1^2}} \tag{8.5}$$

Thus substituting Equations 8.5 and 8.3 into 8.2, the following expression for α is obtained.

$$\alpha = 90^{\circ} - \phi - \sin^{-1}\left[\frac{D_I \sin\phi}{2\sqrt{D_p^2/4 + S_1^2}}\right] + \tan^{-1}\frac{D_p}{2S_1} \qquad (8.6)$$

The above expression for the inclination angle α is defined as the minimum inclination angle possible without vignetting at the nozzle.

There is another relationship, however, associated with the inclination angle that is of equal importance. This relationship is the one related to packaging N lenses in a single row. The inclination angle must be sufficiently large to allow for the packaging of the lenses allowing for adequate clearance without interference for the lens holders. An approximate relationship was developed for evaluating the functional relationship between the inclination angle and the projection lens diameter and spacing between diameter and target. This relationship is given in Equation 8.7.

$$\tan \pi/N = D_p + E/2\ S_1 \sin\alpha \qquad (8.7)$$

The above equations were utilized in sizing a projection optics and its position relative to the target plane. The original work performed in this optimization, which is included in the Systems Concept Report, was performed for a 6" diameter target. The work was later refined to account for the subsequent change in target size and number of optical systems.

8.2.3 Geometrical Relationships

The basic optical system selected for development consisted of a multiple relay type projection system. An optical schematic of the basic projection system is given in Table 8.1. Such a system must satisfy the following basic geometrical relationships.

$$D_a/D_p = S_3/S_2 \qquad (8.8)$$

$$D_f/D_t = S_2/S_1 \qquad (8.9)$$

where D_a = Collector Diameter

D_p = Projection Lens Diameter

D_f = Field Lens Diameter

D_t = Target Diameter

S_1 = Distance from Projection Lens to Target

S_2 = Distance Between Projection Lens and Field Lens

S_3 = Distance Between Field Lens and Collector

Combining the above equations, we eliminate S_2 and obtain the following equation:

$$\frac{D_f \, D_a \, S_1}{S_3 \, D_t \, D_p} = 1 \qquad (8.10)$$

These equations along with those equations developed for sizing of the projection optics provided the main tools for sizing the complete optical system. Other factors taken into consideration included the recognition of the degradation problems that the projection lens would be subjected to from model ablation products. This consideration was made irrespective of the packaging problem and the inclination angle. Other factors which had to be considered were associated with the size of the optical elements because of economic considerations.

8.2.4 System Parameter Selection

Analysis of the packaging problem associated with the projection lenses resulted in the selection of 12" diameter projection lenses

located at approximately 41" from the target at an inclination angle of approximately 51°. This selection was based upon utilizing 15 optical channels. The subsequent change to 14 channels allowed a reduction in the distance between the projection lenses and target to 38". In the final selection of the optical system, NASA/Ames specified that a 6" diameter field lens be utilized in order to allow for possible utilization of the collectors as a searchlight system for irradiation of a 6" diameter target in the event that the overall costing of the radiative heating system exceeds their funding. Thus, with these parameters established, the ratio of the collector diameter to distances between collector and field lens became fixed. This ratio defines, in essence, the cone angle of irradiation incident upon the field lens. Generally speaking, any selection of collector diameter and distance from collector to field lens which satisfies this cone angle would result in approximately the same system performance. However, in considering the size of the radiation source which must be fitted within the collection optics, a 24" diameter collector was selected in order to maximize the collection of radiation from the radiation source. A distance from 114" between the collector and the field lens was required to satisfy the selection of 24" for the diameter of the collector. To accommodate the above selected parameters, the distance between the projection lens and the field lens of approximately 57" became a requirement.

8.3 OPTICAL LENS ANALYSIS

After the basic geometrical system parameters were established, the detailed optical design was initiated. A first order computation of power and speed was made for both lenses. The results indicated that the field lens would present no difficulties in design due to its low speed. However, the projection lens speed was such that the aberrations produced would have an effect on the final image size, and consequently would affect the system efficiency. It was therefore decided that three design approaches would be investigated and carefully compared both from an analytical and practical standpoint.

8.3.1 Spherical Lenses

Since the same procedure was used for designing both the field lens and the projection lens, it will be sufficient to discuss the techniques generally and then have specific results in tabular form at the end of the section. (See Table 8.4)

The aberration most detrimental to the system is spherical aberration. Using the first order equations 8.11 - 8.14, an approximate shape of the lens for minimum spherical aberration was determined in four steps:

Position Factor $P = (S' - S)/(S' + S)$ (8.11)

Shape Factor $Q = -2(N^2 - 1)P/(N + 2)$ (8.12)

First Radius $R_1 = 2f(N - 1)/(Q + 1)$ (8.13)

Second Radius $R_2 = 2f(N - 1)/(Q - 1)$ (8.14)

where S' = image distance

S = object distance

N = index of refraction

f = focal length

After the above equations were applied, a paraxial ray trace was made to find the focal length. The ratio of the resultant focal length to the desired focal length gave a multiplying factor. Multiplying all the radii by this factor resulted in a lens which had the proper focal length. Using equations 8.15 - 8.19, a check was made of the third order coma, which should be near minimum.

$$\Phi = \bar{y}u - y\bar{u} \quad (8.15)$$

$$\phi = 1/f' \quad (8.16)$$

$$\beta_2 = \frac{\phi\Phi y^2}{N}(N + 1) \quad (8.17)$$

$$\beta_1 = \frac{\phi\Phi y^2}{N}\left[(2N+1)\frac{u}{y} - \left(\frac{\phi N}{N-1}\right)N\right] \quad (8.18)$$

$$F = \beta_1 + \beta_2 C_1 \quad (8.19)$$

where f' = effective focal length

$\bar{y}$ = height of chief ray at entrance pupil

$\bar{u}$ = angle of chief ray at entrance pupil

y = height of axial paraxial ray

u = angle of axial paraxial ray on right side of lens

N = refractive index of lens

F = coma contribution

u_{-1} = angle of axial paraxial ray at left side of lens

C_1 = curvature of first surface = $1/R_1$

After the algebraic approximations were made, the lenses were trigonometrically traced on the LGP-30 digital computer. After a few surface bendings, a lens was selected with minimum spherical aberration. A quick check showed negligible coma present at the usable field angles, thus the lens designs were complete from the geometric standpoint. The projection lens, however, had enough spherical aberration to warrant investigation of aspherizing the last surface.

TABLE 8.4

Lens Aberrations

	SPHERICAL	COMA 3rd ORDER
Field Lens	- .714"	.010"
Projection Lens	- 4.927"	.101"

8.3.2 Aspheric Projection Lens

Using the lens shape for minimum spherical aberration and near minimum coma, the last surface of the lens can be aspherized, resulting in zero spherical aberration.

At this point, it was decided to compare the two designs and their effects at the target plane. This comparison was qualitative and not quantitative.

In Figure 8.2, the projection lens is shown with rays traced to several image planes which lie perpendicular to the optical axis. The lens has spherical surfaces, hence spherical aberration is present. The blur circles at each of the planes are shown.

Figure 8.3 shows the same lens but imaging on an inclined target plane. Blur circle comparisons for three different positions on the target are shown.

Figure 8.4 is the same as Figure 8.2 except this time the lens has been aspherized and thus zero spherical aberration is present.

Figure 8.5 is the same as Figure 8.3 except the lens has been corrected for spherical aberration.

The results of these traces can be explained another way in terms of uniformity. If the lens has no spherical aberration, as in Figure 8.5, the image at X_2 is a point; however, images at X_1 and X_3 are ellipses. Consequently, if we have a uniformity at the field lens like that shown in Figure 8.6, the result at the target would be that shown in Figure 8.7. If we use a projection lens with spherical aberration, the result of imaging the distribution of Figure 8.6 would be that shown in Figure 8.8. The effect of superpositioning this intensity distribution from two diametrically opposing optical channels is shown in Figure 8.9.

One can conclude from the above analysis that correcting for spherical aberration does not help much; in fact, it contributes to a buildup of energy in the center of the target.

8.3.3 Tilted Projection Lens

An approach which is used in photography to compensate for a tilted focal plane was evaluated and is shown in Figure 8.10. The aberration which is of most concern here is astigmatism. If rays are traced through the projection lens at an angle equal to the tilt angle, the astigmatism may be easily determined using the following equations, 8.20 and 8.21.

$$\frac{1}{S'_t} = \frac{1}{\cos\phi}\left(\frac{N\cos\phi'}{\cos\phi} - 1\right)(C_1 - C_2) - \frac{1}{S} \qquad (8.20)$$

$$\frac{1}{S'_s} = \cos\phi\left(\frac{N\cos\phi'}{\cos\phi} - 1\right)(C_1 - C_2) - \frac{1}{S} \qquad (8.21)$$

where

ϕ = angle of chief ray at lens

ϕ' = angle of chief ray within the lens

N = refractive index of lens

C_1 = curvature of surface 1

C_2 = curvature of surface 2

S = object distance

S'_t = tangential image distance

S'_s = sagittal image distance

The values for S'_t, S'_s and the resulting blur circle are given in Table 8.5.

T A B L E 8.5

Blur Circles

ϕ	S'_s	S'_t	Blur Circle At Best Focus
20°	36.261"	29.810"	1.003"

The blur circle given above is about 33" from the lens. At the target, the blur circle would be at least twice as large, and hence further investigation of this technique was not considered justified.

8.3.4 Summary

In the detailed analysis of the optical system, it was found that the only important aberration existing in the system was that of spherical aberration of the projection lens. Correction of this aberration by aspherizing the projection lens was evaluated with results indicating that this approach would adversely affect the intensity uniformity distribution and would not increase the target power after uniformity filtering. Also, correction of the spherical aberration by tilting the projection lens in order to obtain better symmetry was found to be undesirable because the considerable amount of astigmatism introduced would result in a decrease of target power. It was thus concluded that with this optical system which irradiates an inclined target plane, the use of spherical surfaces were warranted since alternate corrective measures did not seem to improve overall performance or had a negative effect.

8.4 MASK ANALYSIS

Minimum irradiation outside of the heating zone was specified as a desired performance characteristic of the radiative heating system. Due to the orientation of the nozzle directly in front of the model, each optical train of the radiative heating system irradiates the model with an inclination angle of approximately 50.4°. The 4" diameter target plane is therefore viewed from the projection lens of each optical channel as an ellipse. The projection lens images the clear aperture of the field lens onto a plane inclined to the target plane with a demagnification factor of .667. Since the projection lens sees an ellipse whose major axis is equal to the diameter of the clear aperture of the field lens imaged at the target, a significant amount of radiation spills over at the target. To minimize this spillover without reducing the target intensity, it was proposed in the Systems Concept Study that a mask be utilized near the field lens location to reject radiation which would normally miss the target. Under ideal circumstances, the mask should be imaged sharply around the target eliminating all spillover of energy. Referring to Figure 8.11, the image positions of points P_1 and P_2 were computed utilizing the following first order equations.

$$f_p = \frac{(OC)(OD)}{OC+OD} \tag{8.22}$$

$$L_1 = \frac{f_p\ OP1}{OP1-f_p} = 60.9 \text{ inches} \tag{8.23}$$

$$L_2 = \frac{f_p\ OP2}{OP2-f_p} = 53.8 \text{ inches} \tag{8.24}$$

where $O = 50.4°$

$OD = 57$ inches

$OC = 38$ inches

$OP1 = 36.46$ inches

$OP2 = 39.54$ inches

Thus, we see that the images of points P_1 and P_2 straddle the field lens plane where L_1 corresponds to the distance from the projection lens to point MP_1 in Figure 8.11 and L_2 corresponds to the distance to MP_2. Although these computations neglect the power of the field lens, they are sufficiently accurate to indicate that in order to have a sharp image of the mask at the target, the mask would lie partly in front and partly in back of the field lens. Since the mask would have to be positioned either in front or behind the field lens, it was recognized that complete elimination of the spill-over would not be possible. Two methods were opened for determining the optimum mask geometry. One method consisted of an analytical study which would trace the perimeter of the target image near the field lens to determine the approximate mask shape. The second method consisted of an experimental design test program utilizing the prototype optical system. The second method was chosen as it appeared to be the most direct method and also more economical.

On May 20, 1965, the mask was empirically designed placing its position directly downstream of the field lens and positioned normal to the optical axis. The final mask design was an ellipse whose equation is $X^2/10.37 + Y^2/7.10 = 1$. This resulted in a mask approximately 6.44" long along the major axis and 5.33" across the minor axis. The image of this mask at the target allows a small amount of spillover to insure no reduction in target intensity. The report of this test program where the mask was empirically recorded is in Development Memorandum No. 272-47 titled "Elliptical Mask for Radiative Heating System Field Lens" and is included in the Appendix.

8.5 COLLECTION OPTICS

The general type of collecting optics selected for use in the development of the radiative heating system was established early in the program and is best described as a surface of revolution about the center line of the optical axis coincident with the center line of the radiation source. This selection was based primarily upon Spectrolab's previous experience in solar simulation where such types of collecting optics were found to be the most efficient means of collecting the radiant flux from radiation sources and directing this flux into the clear aperture of an optical system.

As a result of the Systems Concept Study, Spectrolab recommended use of the Spectrolab Aconic* type collector in the radiative heating system. The principle of design associated with this type of collector had previously been used by Spectrolab in the design of collectors for the NASA/Ames 10 sun solar simulator. The Spectrolab Aconic collector is similar to that of ellipsoidal type collectors except that the basic design principle allows for some control of the intensity distribution at the clear aperture of the optical system. The clear aperture plane coincides with the conjugate focus plane of the equivalent ellipsoid. Utilizing the aconic design principle results in maximum power throughput and a more uniform target intensity distribution.

Many factors influence the design of efficient collecting optics for use with the radiative heating system. The most efficient design, or optimum collecting system is one which maximizes the usable power entering the clear aperture of the optical system at the field lens plane. This requires that the product of the various efficiency factors associated with the collecting optics be a maximum. These efficiency factors discussed in Section 6.2 consist of three basic efficiency factors. They are flux capture, which is defined as the percentage of radiation emitted from the radiation source that is incident upon the collecting optics and arc utilization which is defined as the percentage of the total radiation reflected from the collecting optics that is incident upon the transfer optics. The third efficiency factor is associated with uniformity filtering since the amount of radiation which must be rejected in order to obtain target intensity uniformity is a function of the intensity distribution of the radiation entering the clear aperture of the optical system. This intensity distribution is a direct result of the design and quality of the collecting optics.

*Patent Pending

8.5.1 Compatibility with Radiation Source

To optimize the collecting optics for the radiative heating system, it was necessary to have an intimate knowledge of the radiation source characteristics. The basic source characteristics needed included an accurate polar intensity distribution of the radiation source. Such a distribution defines the directional aspects of the radiation emitted from the radiation source. Also needed were micro-radiance distributions of the arc itself. This type of distribution describes the radiant distribution of the arc as viewed from a given direction and also provides the necessary information regarding overall size and geometry of the arc. The polar intensity distribution is essential data for determining the distribution over the collector and for determining the flux collection efficiency. The physical size of the arc and its micro-radiance distribution is a very important source parameter since this data is necessary to determine the distribution of power at the field lens plane of the optical system. From this power distribution, the arc utilization efficiency is determined as well as the amount of radiation which must be rejected in order to achieve intensity uniformity at the model. The physical size and geometry of the radiation source is also important from a packaging standpoint. The packaging restraints can dictate certain minimum collector dimensions for maximum efficiency design.

8.5.2 Basic Collector Sizing

As indicated in Section 8.1, the specifications for the radiative heating system were modified at the conclusion of the Systems Concept Study. The heating zone was changed to a 4" diameter and the clear aperture of the field lens was limited to 6" or less in diameter. As discussed in Section 8.2 titled "Optical System Sizing," a projection lens diameter of 12" was chosen consistent with the lens packaging problems and the distance between the projection lenses and the model face. From the basic geometrical relationships given in Section 8.2.3, the selection of these parameters established the ratio of the collector diameter to the distance between the collector and the field lens. In essence, this established the cone angle of irradiation for the radiation irradiating the transfer optics from the collection optics. Upon establishing the ratio of collector diameter to distance between collector and field lens plane at approximately .21, the relationship between cost and system performance to collector diameter was evaluated. Results

of this evaluation indicated slightly higher efficiencies and lower fabrication costs with smaller collector diameters and associated shorter optical paths. A detailed graphical study was then performed to determine the minimum collector diameter which would be compatible with the expected size of the radiation source. This evaluation resulted in the selection of a 24" diameter collector since a smaller diameter would have caused problems in the packaging of the relatively large radiation source due to source removal from collecting optics and from potential problems resulting from irradiation of the end of the radiation source which was to be cantilevered through the collector. Selecting a diameter of 24" necessarily fixed the distance between the collector and field lens of the system at approximately 114".

8.5.3 General Method of Evaluation

The basic approach taken to evaluate the performance of the many collectors analyzed required the discretizing of the collector into many circular zonal elements. Each of these zonal elements were in essence analyzed separately to determine its contribution of the intensity distribution at the field lens.

The method utilized in determining the intensity distribution from a particular circular zone was accomplished by examining the intensity distribution from a point on the zonal increment. The reflected radiation from this point would be an image of the electrodes and arc at the field lens position in the same manner as if this point was a small aperture in the collector allowing the arc to be imaged at a screen located at a distance equal to the distance between the point and field lens. The size of this arc image at the field lens plane is a function of the magnification factor associated with that particular zone. The magnification factor is equal to the ratio of the distance between the field lens plane and the position on the collector. Thus, it is seen that the zones nearest the arc are associated with the larger magnification factors and hence larger images at the field lens plane.

Thus, the power distribution at the field lens plane from a point on a zone of the collector can be plotted by utilizing the relative micro-radiance distribution of the arc as viewed from that zone of the collector.

Utilizing the symmetry property of the collector, the total relative distribution from the circular ring could be obtained by the process of revolution of this micro-radiance distribution at the field lens plane.

From the polar intensity distribution data, the total power emitted from the radiation source that strikes each zone can be determined. Correcting for collector reflectivity, the total power irradiating the field lens plane from a given zone is known and is equal to the total volume under the relative intensity distribution obtained on the field lens plane from the zone. This information allows determination of the intensity distribution in units of power.

The superposition of the intensity distribution contribution from each circular zonal element then allows determination of the total intensity distribution at the field lens from which calculations as to the total arc utilization could be made. Because of the type of the optical system approach, the power distribution across the field lens has a direct relationship with the power distribution across the target from each optical channel. Because of this characteristic, it was possible to estimate the amount of power that would have to be rejected by use of a uniformity filter to obtain target intensity uniformity. Since the flux collection is also known by knowledge of the power per zone and the collection angle of the collector selected, the product of the flux collection, arc utilization, and uniformity filtering allowed a measure of the performance of a selected collector analyzed.

Using the combination of the computer and graphical techniques, the collector design providing the best uniformity and maximum power input to the optical system is obtained through iteration on the various collector parameters.

8.5.4 Trade-off Study

Since the fabrication of the collector tooling was the longest lead item on the basic development program other than the radiation source development work, Spectrolab was in the position of designing the collecting optics without benefit of having the actual final radiation source characteristics for design inputs. The development of the radiation source for the radiative heating system as described in Volume II of this final report was only getting started at the time the system approach was selected and collector design work initiated. To overcome this hurdle, new emphasis was placed upon the 60 KW radiation source program. Originally, the 60 KW radiation source was to be an off-the-shelf item similar to an

experimental model demonstrated prior to Spectrolab awarding source development contract to Giannini Scientific.

To aid in the development of the 150 KW radiation source and to provide for more representative source data, the decision was made to develop the 60 KW radiation source as the prototype of the 150 KW source. At that time, it was thought that the final radiation source would be a scaled up version of this prototype and that the relative polar and micro-radiance distributions would not change appreciably and would be representative of the final source design. It was therefore planned to utilize the arc characteristics of the 60 KW radiation source as design inputs for the optimization of the collecting optics.

Upon delivery of the 60 KW radiation source to Spectrolab, a test program was initiated to obtain the required radiation source data. The relative micro-radiance distribution and polar intensity distribution data utilized in the design of the collecting optics is given in Figures 8.12 and 8.13.

As a result of a trade-off study in designing the collecting optics utilizing this radiation source data, the predicted intensity distribution on the plane of the field lens was determined as illustrated in Figure 8.14. This was based upon having an arc of 8 mm in length and 6 mm in diameter which was the anticipated size of the arc for the final radiation source. For comparison purposes, the intensity distribution which would be obtained by utilizing a 24" diameter ellipsoid with the same collection angle and same arc characteristics is superimposed on the same curve. Based upon the above assumptions, the arc utilization for the aconic collector was computed to be 76.2% as compared to 52.3% for the ellipsoid. It is also obvious from the two types of distribution that the radiation from the aconic collector would result in minimum filtering to obtain target intensity uniformity relative to the ellipsoid which exhibits a high peak intensity in the center of the lens and drops to a very low intensity level at the edge of the lens.

To substantiate the validity of the method of analysis and the method of design of the aconic type collector, the intensity distribution from a 10" diameter aconic type collector as used on the NASA/Ames 10 sun solar simulator was compared to the original predicted distribution. The observed and predicted curves for this collector are illustrated in Figure 8.15. The straight ellipsoid equivalent for the 10" diameter collector is compared against the aconic 10" diameter collector in Figure 8.16. At the time of finalizing the collector design, it was anticipated that the source parameters would differ somewhat from those used in the collector study. The three key source parameters were polar

distribution, micro-radiance distribution and arc geometry. The degree of variation of these parameters which would necessitate a design change of the collector contour was examined. Results of this examination indicated that, while variations in the polar intensity distribution could affect the selection of the optimum collection angle, the most significant changes would result from a change in the electrode geometry which could affect the micro-radiance distribution. It was not anticipated, however, that there would be any radical changes in either of these parameters. It was also noted that the function of the aconic collector, as compared to an ellipse, is to build up energy at the edge of the field lens where the larger area associated with the periphery of the lens has great significance in system efficiency.

It was therefore concluded that, while changes in expected arc micro-radiance distribution and arc geometry may improve or decrease system efficiency, such changes would have little effect on collector contour required to maximize the system efficiency as long as the profile of micro-radiance from cathode to anode exhibited a negative slope.

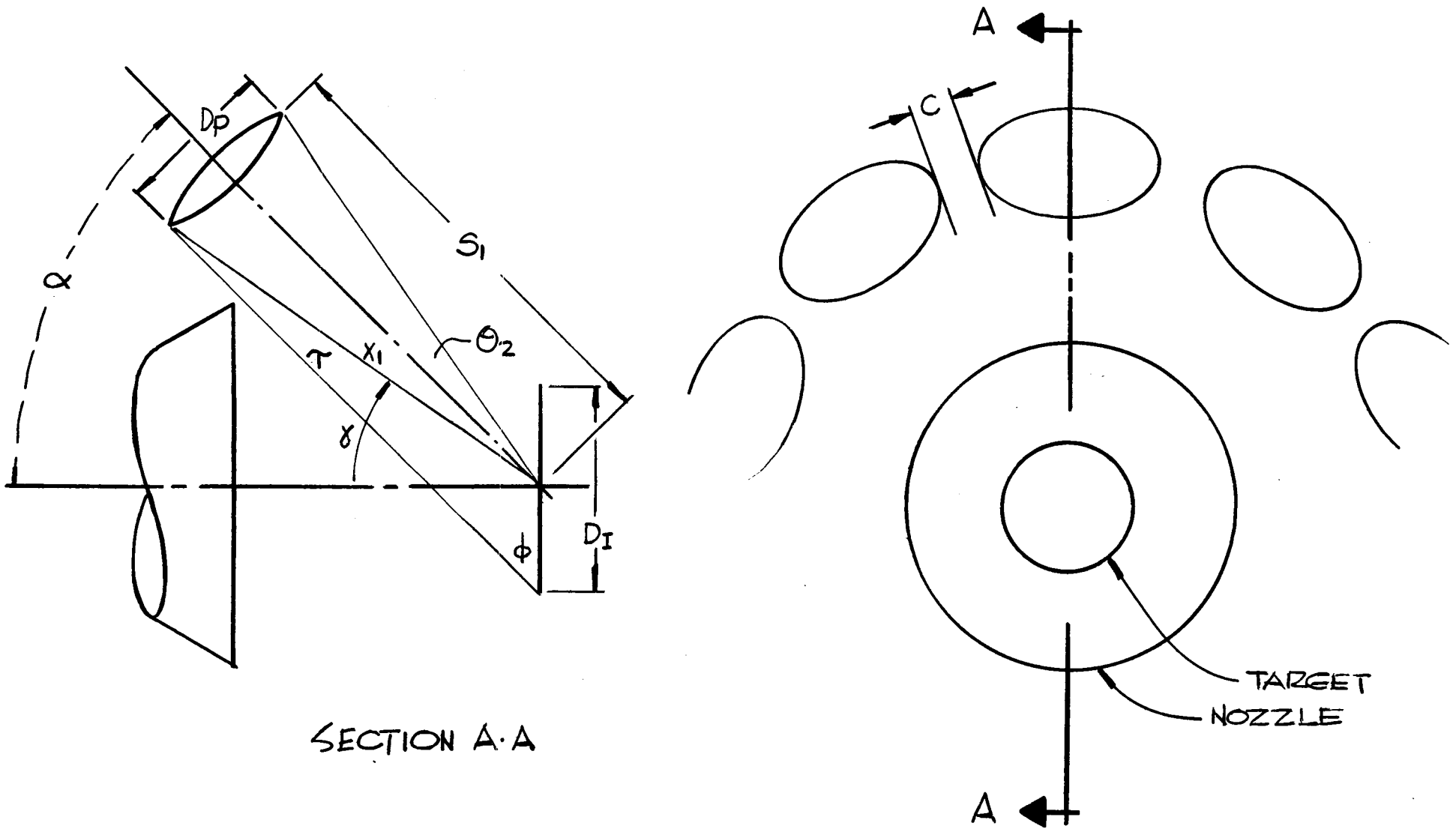


Figure 8.1

Geometrical Configuration of Projection Lens, Target and Nozzle

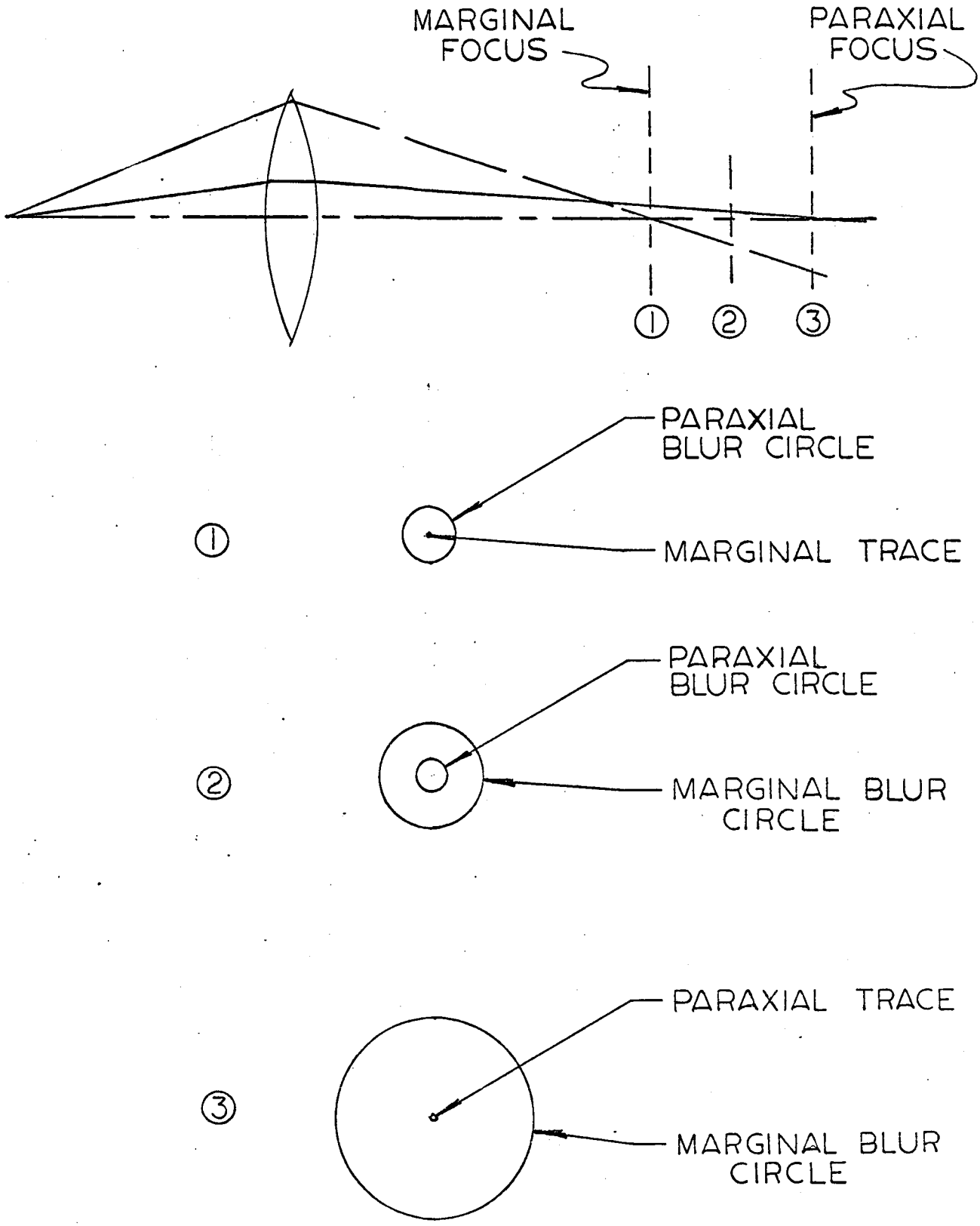


FIGURE 8.2-TARGET NORMAL TO AXIS, LENS WITH SPHERICAL ABERRATION

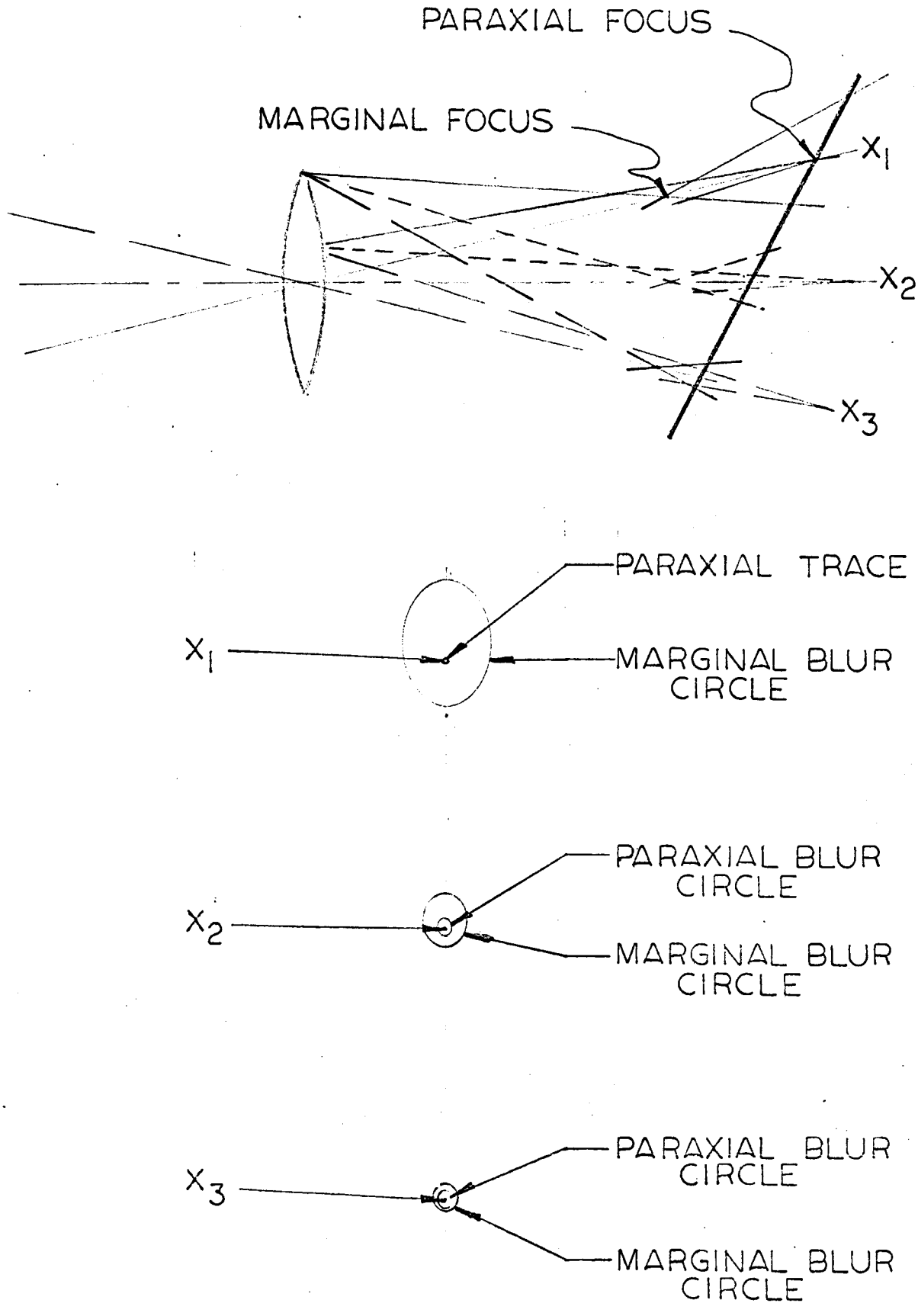
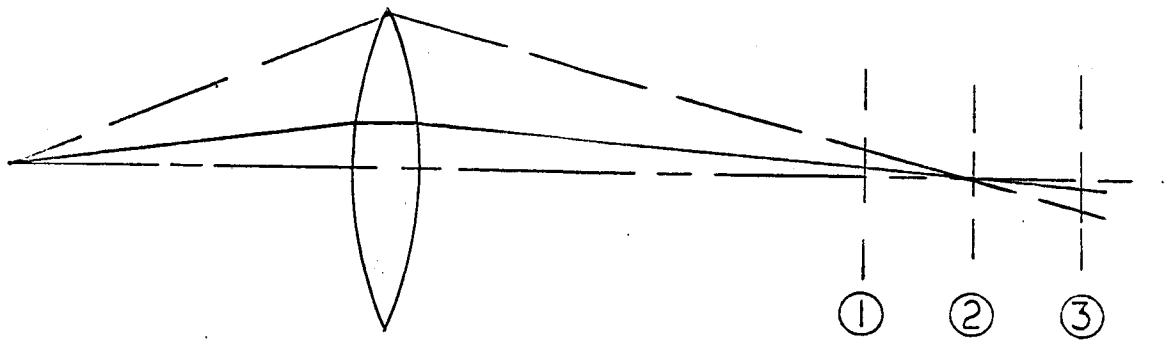
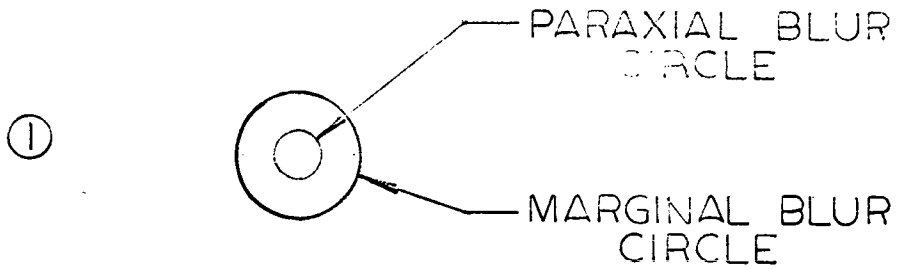


FIGURE 8.3 - INCLINED TARGET, LENS WITH SPHERICAL ABERRATION.





②

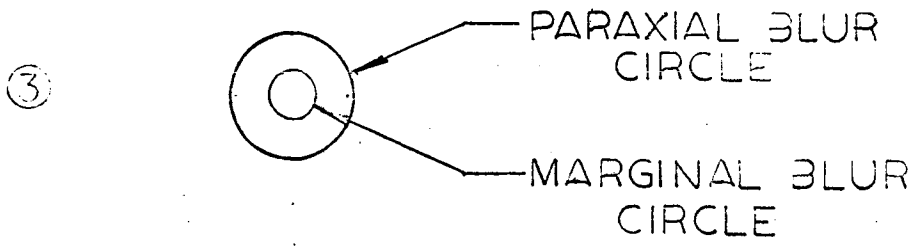
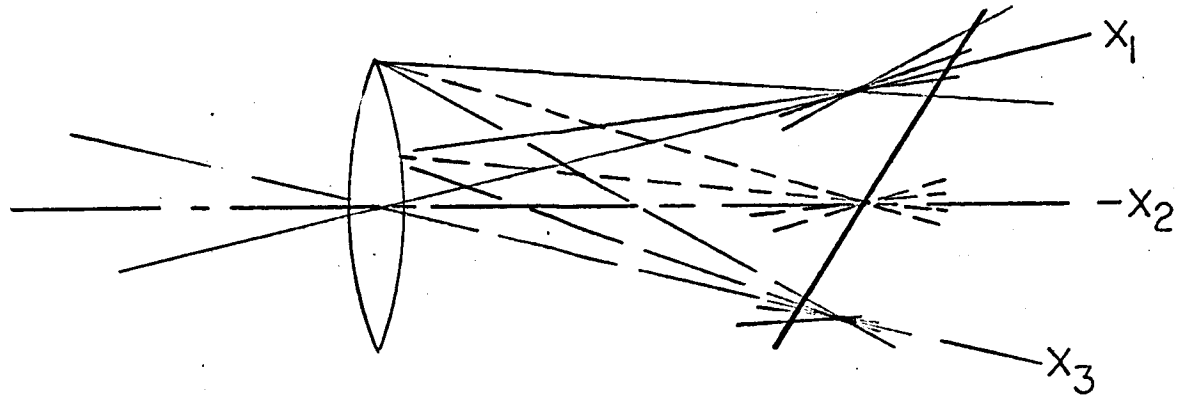
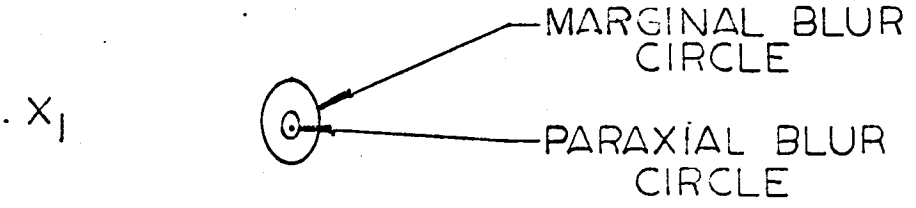


FIGURE 8.4—TARGET NORMAL TO AXIS
NO SPHERICAL ABERRATION





X_2

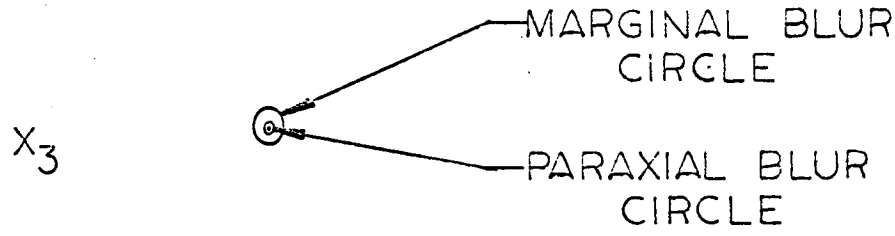


FIGURE 8.5 — INCLINED TARGET, NO SPHERICAL ABERRATION

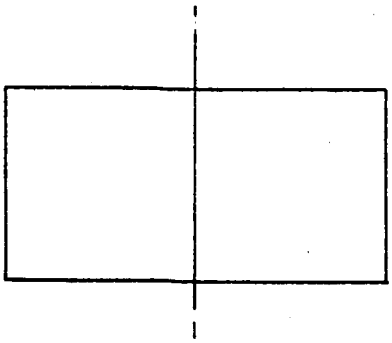


FIG. 8.6 Postulated Intensity Distribution Across Field Lens Clear Aperture

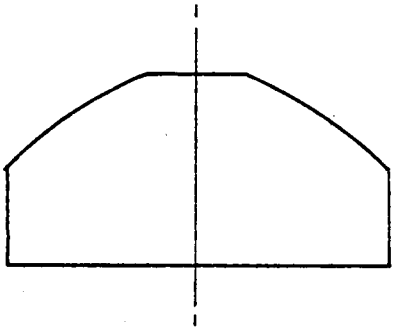


FIG. 8.7 Intensity Distribution Across Inclined Target Using Aspherized Projection Lens

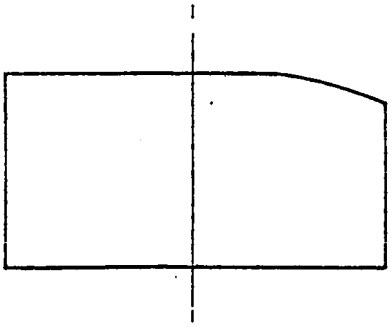


FIG. 8.8 Intensity Distribution Across Inclined Target Using Spherical Projection Lens

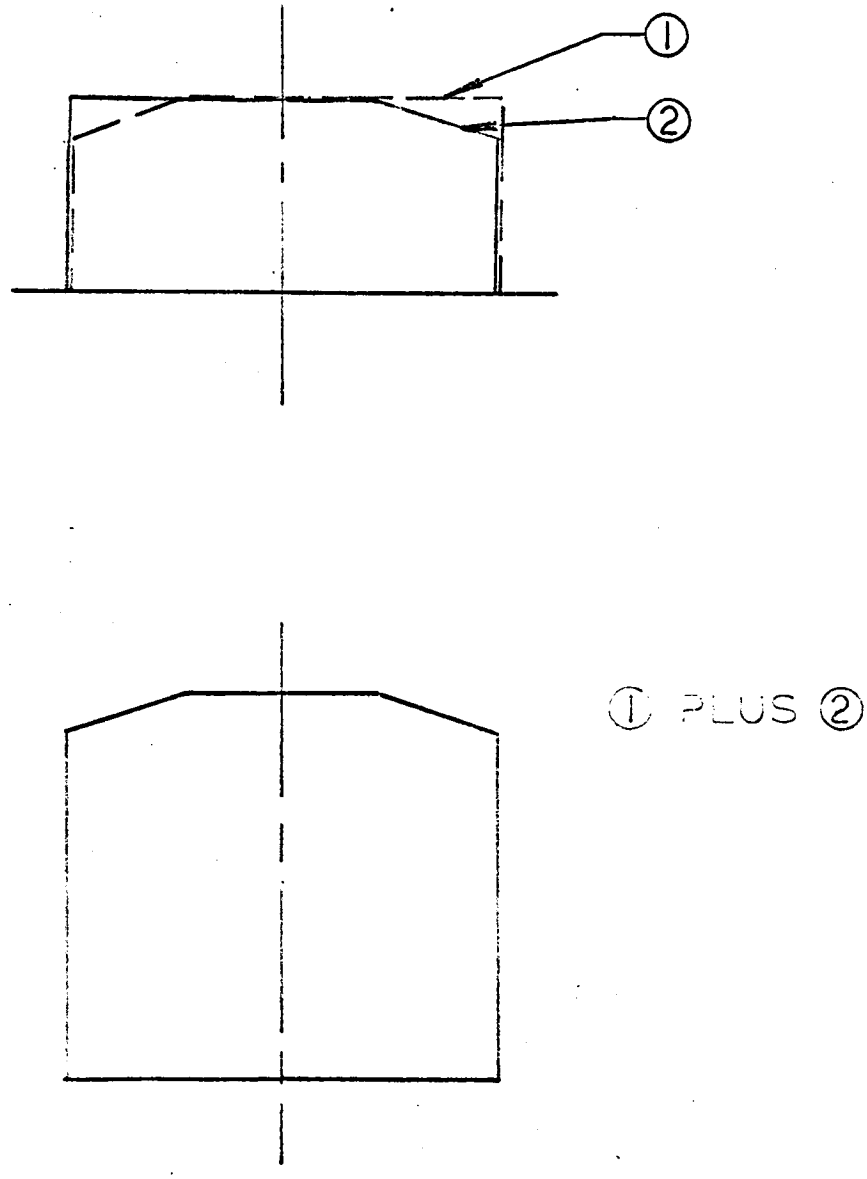


Figure 8.9 Superposition of Intensity Distributions From Diametrically Opposite Optical Channels

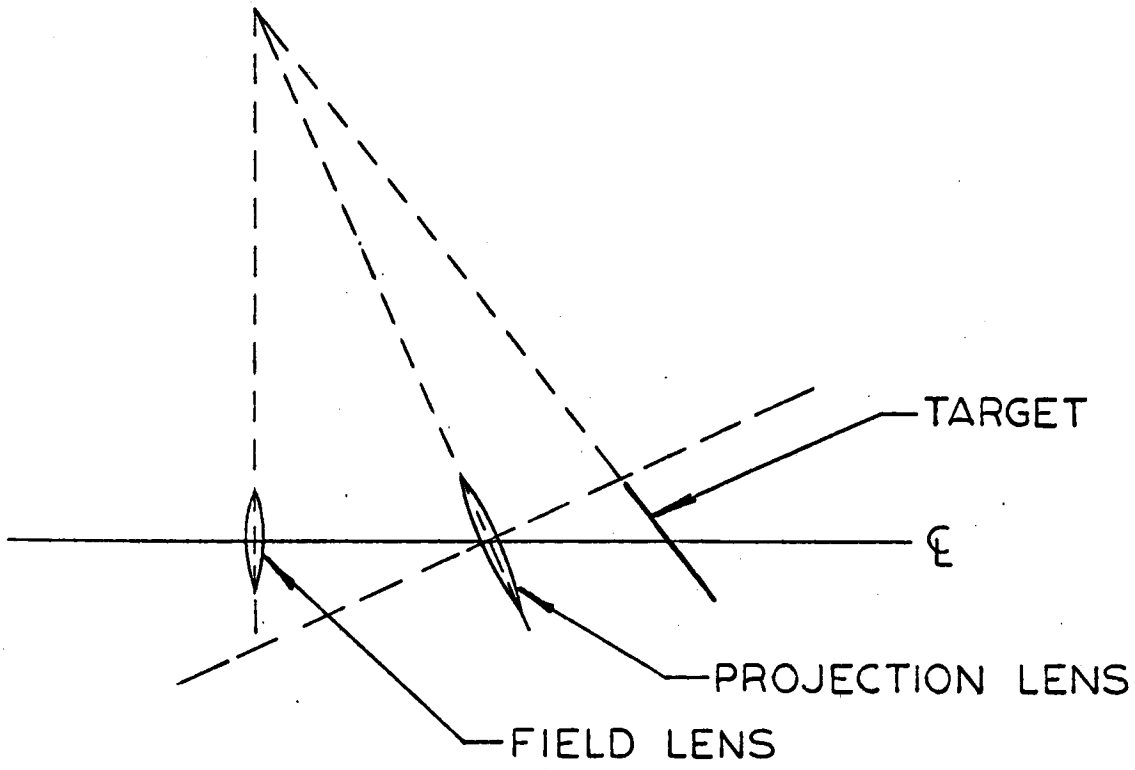


FIGURE 8.10-TILTED PROJECTION LENS

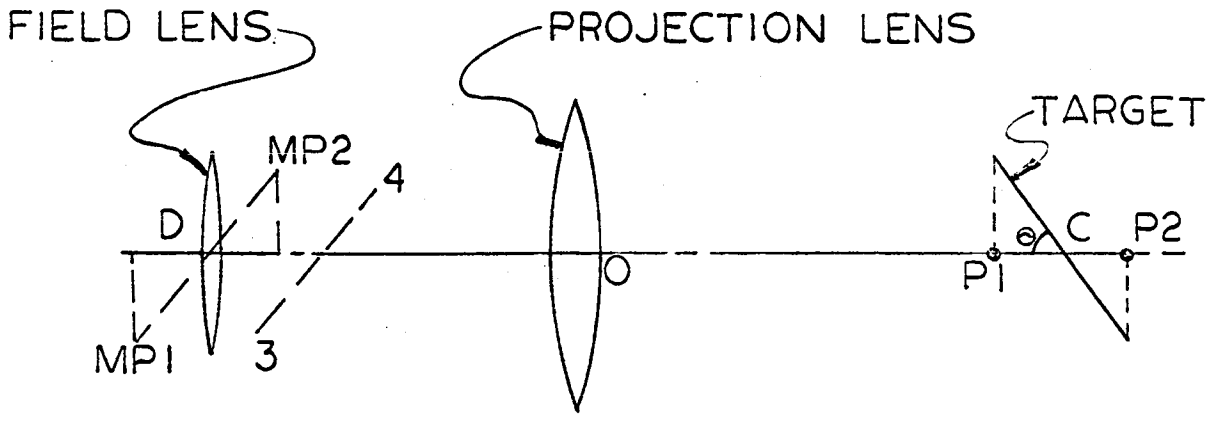
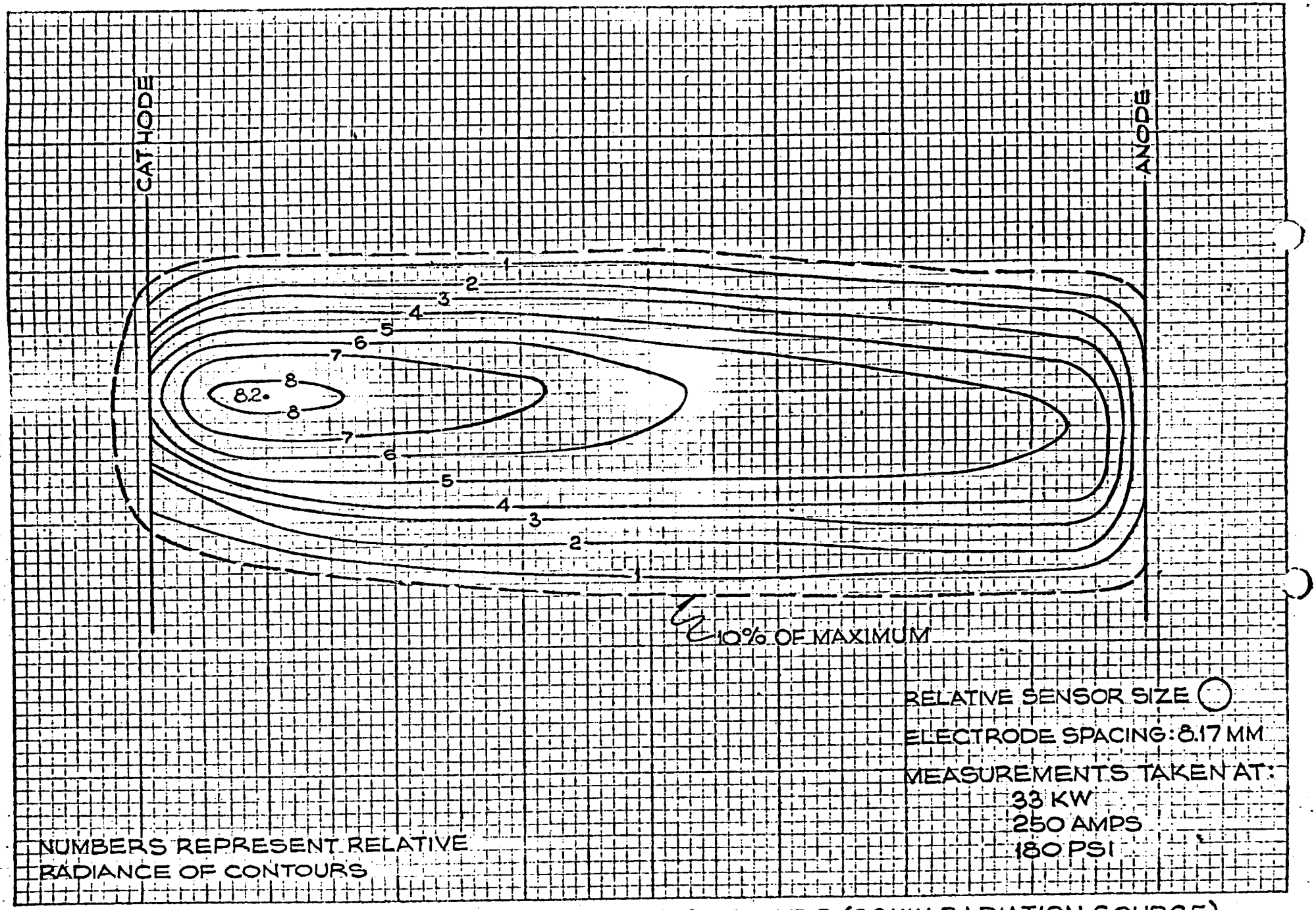


FIGURE 8.11 — MASK ANALYSIS



ARC IMAGE MICRO-RADIANCE CONTOURS (60KW RADIATION SOURCE)

Figure 8.12

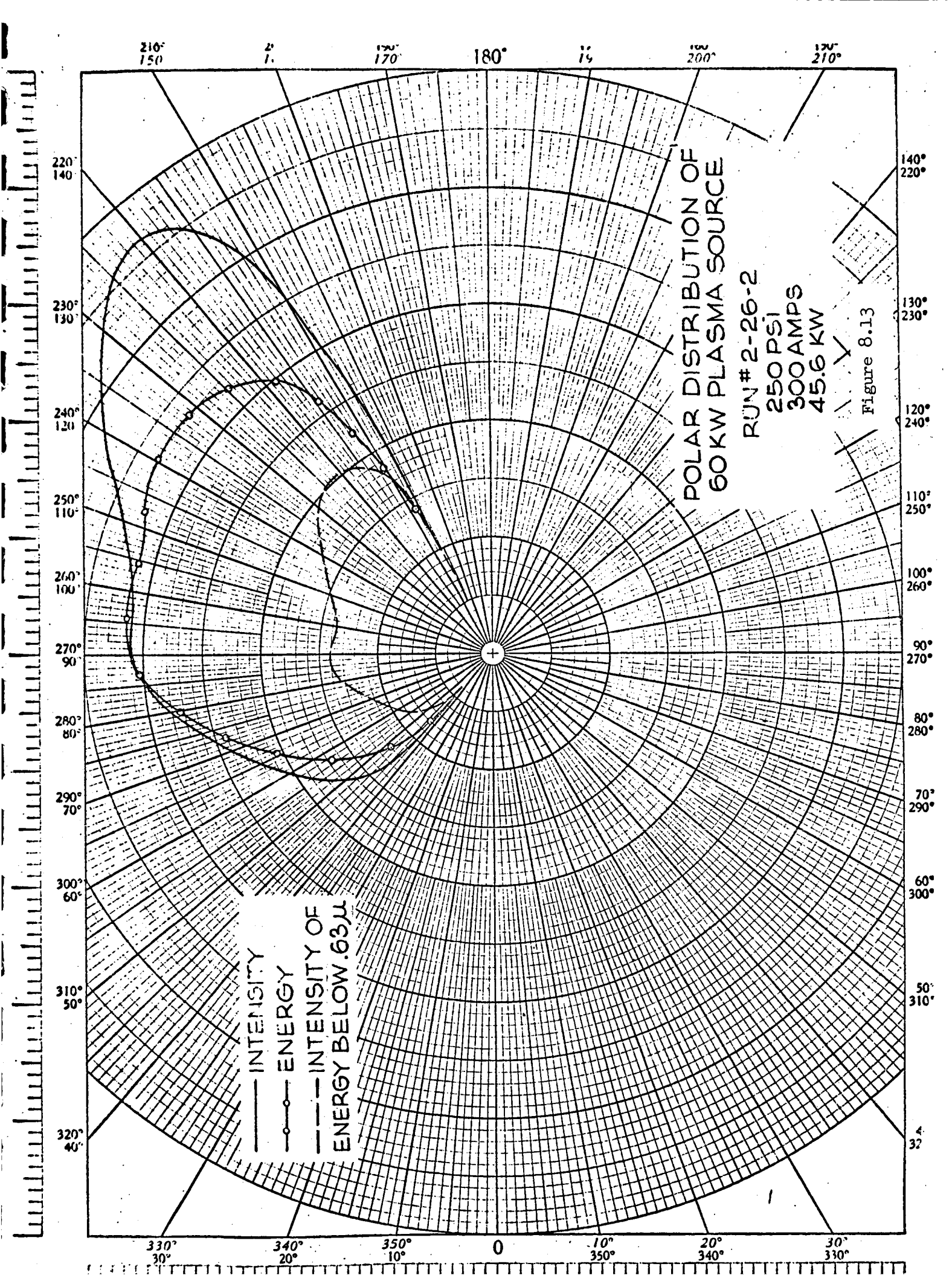

POLAR DISTRIBUTION OF
60 KW PLASMA SOURCE
RUN # 2-26-2
250 PSI
300 AMPS
45.6 KW
INTENSITY
ENERGY
INTENSITY OF
ENERGY BELOW .63μ
180°
0
210°
150°
220°
140°
230°
130°
240°
120°
250°
110°
260°
100°
270°
90°
280°
80°
290°
70°
300°
60°
310°
50°
320°
40°
330°
30°
340°
20°
350°
10°
10°
350°
20°
340°
30°
330°
140°
220°
130°
230°
120°
240°
110°
250°
100°
260°
90°
270°
80°
280°
70°
290°
60°
300°
50°
310°

Figure 8.13

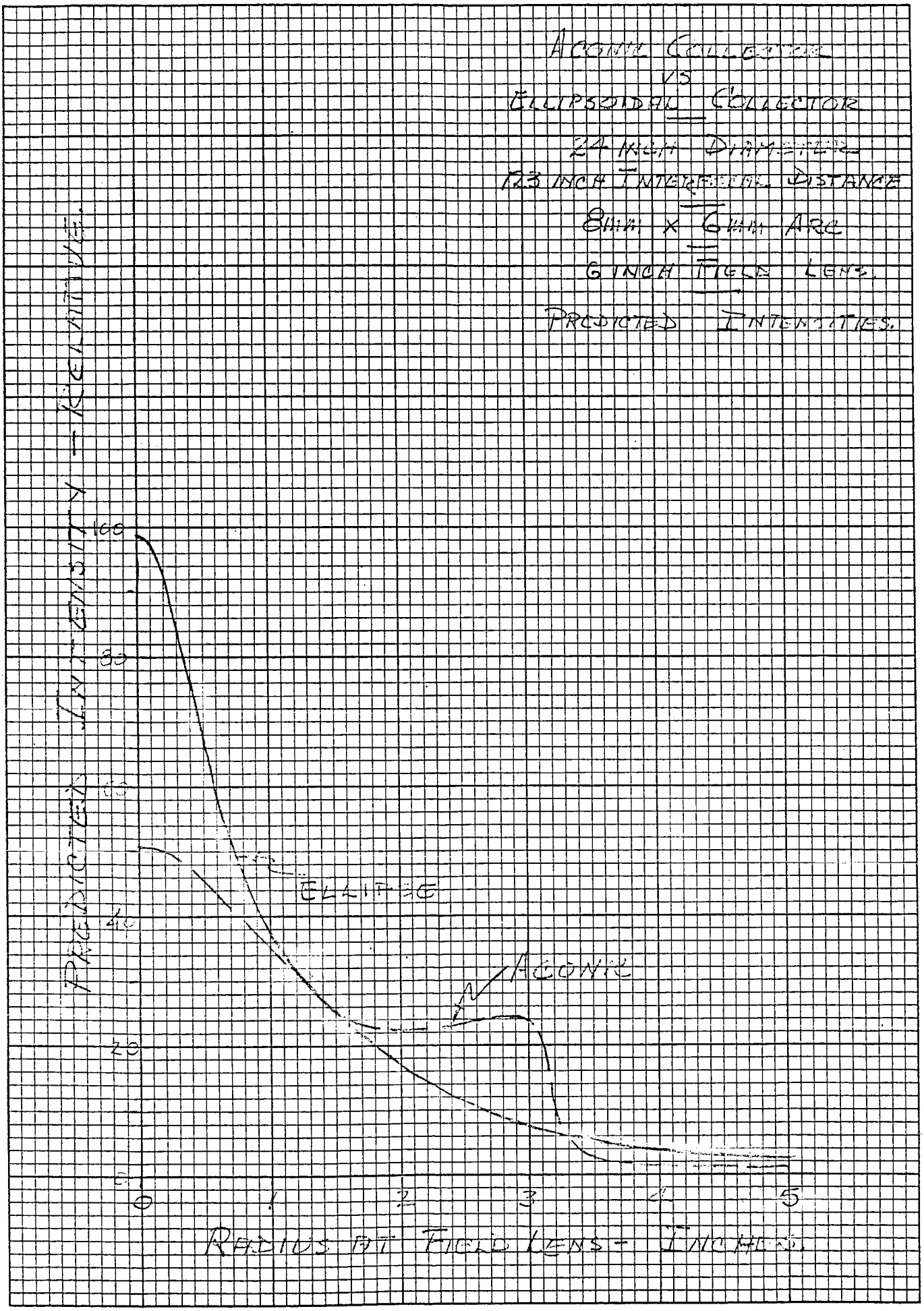

ACONIC COLLECTOR
VS
ELLIPSOIDAL COLLECTOR
24 INCH DIAMETER
23 INCH INTERFOCAL DISTANCE
8mm x 6mm ARC
6 INCH FIELD LENS
PREDICTED INTENSITIES.
PREDICTED INTENSITY - SUNS
100
80
60
40
20
0
ELLIPSE
ACONIC
0
1
2
3
4
5
RADIUS AT FIELD LENS - INCHES

FIGURE 8.14

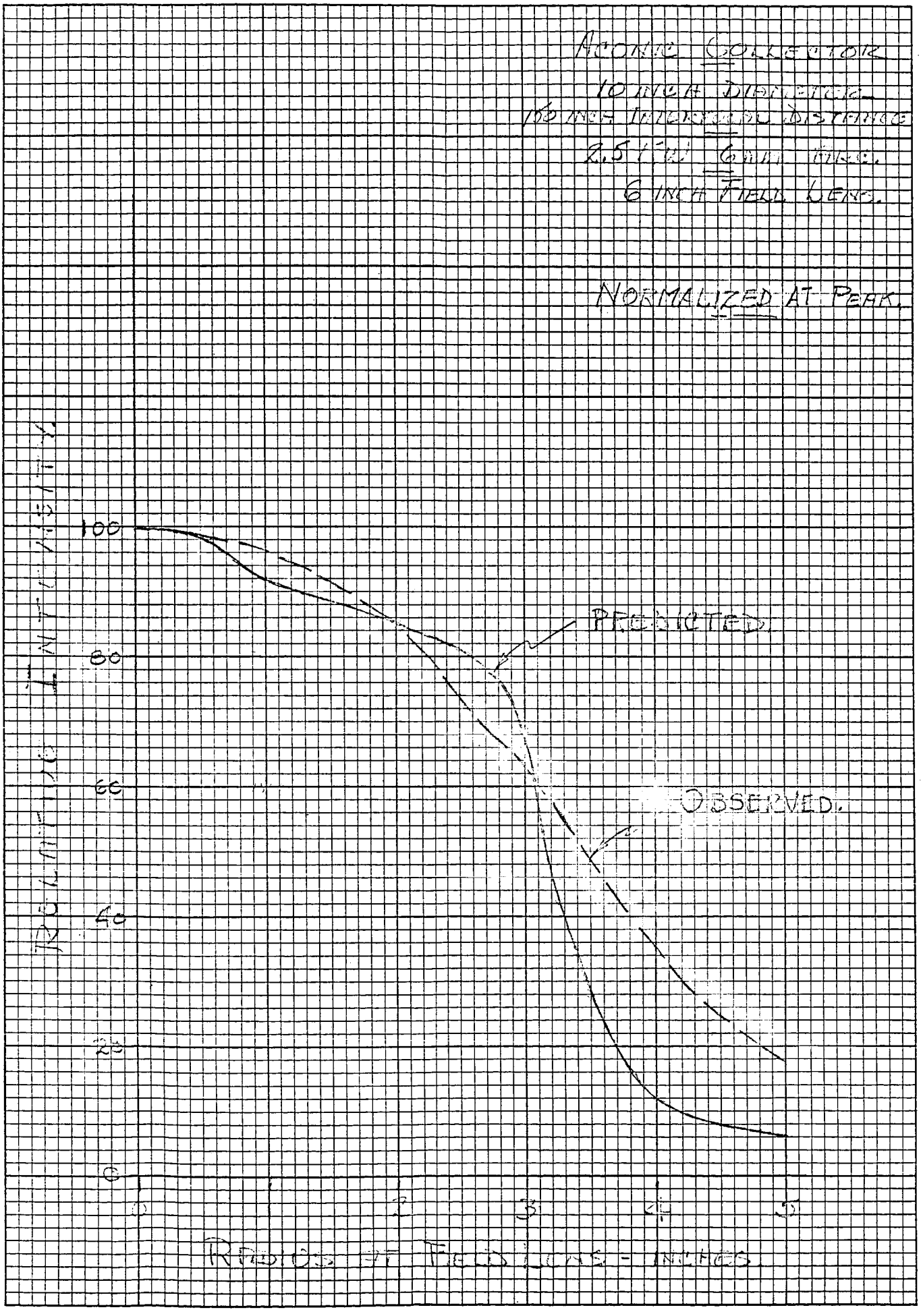

ACOUSTIC COLLECTOR
10 INCH DIAPHRAGM
100 INCH INTERNODAL DISTANCE
2.5 KHz 6 mm TUBE
6 INCH FIELD LENS
NORMALIZED AT PEAK
PREDICTED
OBSERVED
100
80
60
40
20
0
0
1
2
3
4
5
RADIUS OF FIELD LENS - INCHES

FIGURE 8.15

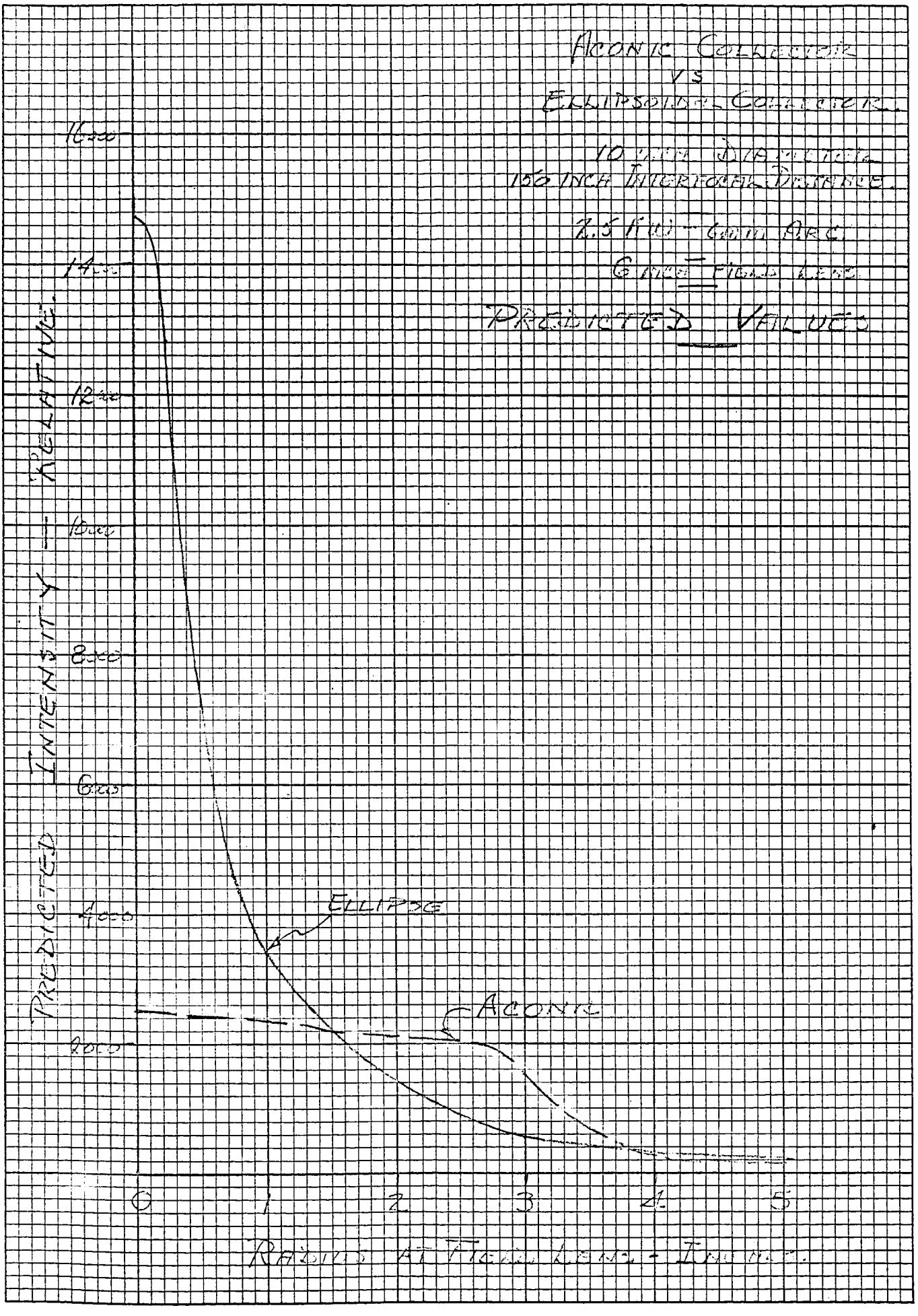

ACONIC COLLECTOR
VS
ELLIPSOIDAL COLLECTOR
10 INCH DIAMETER
150 INCH INTERFOCAL DISTANCE
2.5 KW - 600 AMP ARC
CONCENTRIC FIELD LENS
PREDICTED VALUES
PREDICTED INTENSITY - RELATIVE UNITS
16000
14000
12000
10000
8000
6000
4000
2000
ELLIPSE
ACONIC
0
1
2
3
4
5
RADIUS AT FIELD LENS - INCHES

FIGURE 8.16

9. THERMAL LOADING ANALYSIS

The thermal loading of the various components of the radiative heating system depends upon the efficiencies (N_i) of the individual components. These efficiencies are defined as follows:

N_1 = Source Conversion Efficiency - Percentage of the Input Electrical Power Converted into Radiant Flux Emitted by Arc Source.

N_2 = Flux Collection Efficiency - Fraction of the Emitted Radiation from Radiation Source Which is Incident upon Collector.

N_3 = Collector Efficiency - Total Reflectivity of Collector Mirror Surface.

N_4 = Arc Utilization - Fraction of Power Reflected by Collector Which is Incident upon Clear Aperture of Field Lens.

N_5 = Field Lens Efficiency - Fraction of Incident Radiation Transmitted by Field Lens.

N_6 = Mask Efficiency - Fraction of Radiation Transmitted by Field Lens Which Passes Unobstructed by Mask.

N_7 = Filter Efficiency - Fraction of the Total Incident Power Transmitted by Combination Water Cell - Uniformity Filter.

N_8 = Folding Mirror Efficiency - Total Reflectivity of Folding Mirror.

N_9 = Projection Lens Efficiency - Fraction of the Total Radiation Incident Upon the Projection Lens Which is Transmitted.

9.1 THERMAL LOAD DISTRIBUTION

The approximate thermal load distribution per optical channel is shown in Table 9.1. It is noted that in this table the efficiency factors are listed in a sequence which allows calculating the power throughput as the radiation goes from the radiation source

through the various optical elements to the target. For the most part, the efficiency values utilized were based upon experience and/or analysis of the individual components. To insure a conservative thermal load analysis, an input power of 150,000 watts was utilized. This allows for the anticipated upgrading of the final radiation source to 150,000 watts from the present 130,000 watts. Since many tests will be run on the radiative heating system without utilizing the water cell/uniformity filter, the thermal load distribution chart considers the worst case when this particular component is removed from the system. An arc utilization efficiency of .60 was used which is higher than the value obtained in the prototype demonstration testing. Utilization of this higher efficiency factor allows for eventual use of a radiation source with a shorter electrode spacing and equivalent output power capability.

Of the electrical input power per radiation source system, approximately one-third is converted to radiant power. The remainder is dissipated at the source electrodes and is carried away with the coolant water. That radiation emitted from the radiation source which fails to strike the collector is intercepted by a water-cooled baffle. Over 14,000 watts are dissipated by this baffle. The absorbence of this baffle is on the order of 90% thus approximately 1800 watts is reflected to the surroundings in the enclosure. The collector utilized is water-cooled, thus the power absorbed at the collector is carried off directly with the water. A water-cooled field lens holder and mask intercept the radiation spillover at the field lens clear aperture. The majority of this waste radiation is absorbed by the mask and the remainder is reflected to the surroundings. Of the energy incident upon the field lens, approximately 13% is rejected by reflection and absorption. The reflected component to this radiation is directed back towards the source array structure. Of the radiation absorbed, a portion is conducted to the field lens holder and the remainder is re-radiated to the surroundings. The elliptical mask which rejects approximately 38% of the incident radiation is water-cooled, thus the majority of the absorbed power is conducted to the cooling water. The uniformity filter-water cell, when used, rejects approximately 33% of the usable radiation. Almost all of this rejected radiation with the exception of the reflection component is absorbed in the separate closed loop water system provided for the water cells. The radiation is then folded by a water-cooled aluminum mirror which directs the radiation towards the projection lens. The radiation rejected by the folding mirror is by absorption and is carried directly into the cooling water. Radiation rejected

At the projection lens as at the field lens is by reflection and absorption. The reflection component of this rejected power is redirected to the surroundings. The absorbed component is partially conducted to the water-cooled projection lens holder and partially reradiated by the projection lens. The total power dissipation by the 14-channel system is shown on Table 9.1 and is obtained simply by multiplying the power dissipation from one channel by 14.

9.2 LENS ABSORPTION ANALYSIS

Absorption data were required as basic inputs for an analysis to determine the operating temperature of the lenses, especially the projection lens where a vacuum seal requirement exists. Calculations were performed to determine the total power absorption and transmission for these lenses. It was found that there would be a 6.6% absorption of power by the field lens with a total transmission of approximately 86.9%. The remaining 6.5% of the radiation would be accounted for by reflections. For the projection lens, the absorption was found to be 7.6%, transmission 85.9%, and reflection 6.5%. The detailed analysis giving these results is found in Development Memorandum No. 272-95 and is included in the Appendix. Caution is urged in the use of these absorption numbers inasmuch as they appear to be higher than experience dictates. The accuracy of the calculations is very dependent upon the accuracy of the source spectral distribution. The spectral distribution of the radiation emanating from the radiation source had not as yet been measured at the time of this analysis although the data used does not differ significantly from the actual spectral distribution. Also, as pointed out in the analysis, the accuracy of the results are extremely dependent upon the accuracy of the transmission data utilized.

9.3 LENS TEMPERATURE ANALYSIS

An analysis was made in order to predict the operational temperatures that the field lens and projection lens would obtain under steady-state conditions. This analysis is presented in Development Memorandum No. 272-96 and is included in the Appendix. Results of this analysis indicated that the steady-state temperature of the field lens would be approximately 721°K. In this analysis, it was assumed that the lens was insulated from the holder and thus the only mode of heat transfer considered was that of radiation. In the analysis of the steady-state temperature of the projection lens, an attempt was made to account for the absorption of radiation originating at the target and gas cap and absorption of radiation which is reflected from the target, as well as the absorption of the incident power from the radiation source. Results of this analysis indicate that the steady-state temperature of the projection lens will be approximately 610°K.

APPROXIMATE THERMAL LOAD DISTRIBUTION

Efficiency Factor	Ni	Power Through Put	Power Dissi-pated	Source H. E's	Collector H. E's	Collector Baffle H. E	Field Lens Baffle & Holder H.E's	Mask H. E	Unif. Filter H. E	Folding Mirror H. E	Proj. Lens H. E	Enc.
Input Electrical Power	-	150,000										
Power Conversion	.33	49,500	100,500	100,500								
Flux Collection	.67	33,200	16,300			14,500						1800
Collector Reflect-ance	.84	27,800	5,400		5,400							
Arc Utili-zation	.60	16,700	11,100				9,500					1600
Field Lens Trans.	.87	14,500	2,200		100		400					1700
Mask	.62	9,000	5,500				250	5,150				100
Uniformity Filter (*when not used)	1* (.67) when used	9,000							(1820) when used			
Folding Mirror Reflectance	.84	7,560	1,440							1,440		
Proj.Lens Trans.	.86	6,500	1,060								300	760
1 Channel	Power Dissipation		143,500 watts	100,500	5,500	14,500	10,150	5,150	(1820)	1,440	300	5960

Table 9.1

THERMAL LOAD DISTRIBUTION PER CHANNEL

10. PROJECTION LENS VACUUM SEAL DEVELOPMENT WORK

The projection lens of each optical channel also act as a vacuum interface between the chamber and the radiative heating system. Due to absorption of radiation from the radiation source and from the target, analysis indicated that the lens would operate at a relatively high temperature, in excess of 600°F. Since no standard off-the-shelf type vacuum seals were available for this application, a small development program was initiated in order to develop a vacuum seal for this application. After investigation of available sealing methods, two devices were chosen for test. One was a thin walled, silver plated, stainless steel O-ring. The other was a V-face seal made from Inconel-X plated with soft Watts nickel.

The application of the stainless steel O-ring in the standard recommended approach would result in excessive compressive forces against the quartz lens. Hence, the approach using the O-ring was slightly unorthodox in that the seal was attempted on the periphery of the lens. With this approach, the O-ring is compressed by forces parallel with the optical axis and restrained in such a manner that it would distort against the lens periphery.

The Inconel-X V-face seal approach also was designed for use at the periphery of the lens. The open end of the V pressed against the edge of the lens while the other edge of the V rested against the lens holder. The V is then expanded by applying pressure to a solid copper O-ring placed within the V-seal.

To perform the various vacuum tests, a test fixture was constructed with a lens holder designed to accommodate the V-seal and a pyrex disk shaped to simulate the quartz projection lens. The edge of the disk was coated with a layer of copper approximately .002" thick to allow the seal to seat more readily on the edge of the disk. A vacuum pump capable of attaining a pressure of 0.015 mm or 15 microns of Mercury was connected to the vacuum chamber below the pyrex disk. Several vacuum tests were made using this V-ring seal. The lowest pressure obtained using this seal with the vacuum pump used was 12 mm of Mercury. More important was the leak rate which was calculated to be 1.4×10^{-2} cu ft/min. The results of this test are given in Development Memorandum No. 272-9, which is included in the Appendix.

Upon completion of the vacuum tests of the V-ring seal, the lens holder was modified to accommodate the O-ring seal and vacuum

tests were repeated. For this seal, a pressure of 2.0 mm and a leak rate of 2.73×10^{-3} cu ft/min. was obtained at room temperature. The description of this test and the associated leak rate calculations are given in Development Memorandum No. 272-12, which is included in the Appendix.

Subsequent tests using the O-ring seal at elevated temperatures were undertaken. The pyrex surfaces were vacuum plated with a thin coating of gold in order to increase the absorptivity of the lens to allow heating at elevated temperatures with the use of heat lamps. Three 375 watt industrial heat lamps were used to irradiate the highly absorbing lens. As the steady-state temperature of 60°C was approached, the vacuum chamber pressure dropped from 2.0 to 1.5 mm of Mercury, and the leak rate fell to 2.2×10^{-3} cu ft/min. In order to attain even higher temperatures, a hot plate heating element was placed directly on the pyrex plate surface. The temperature under these conditions rose at a rate of approximately 2° per minute and attained a temperature of approximately 150°C when a crack appeared, starting at the edge of the lens blank, and extending approximately 2" towards the center. There was no indication that the failure was in any way due to the O-ring seal. The test results for these tests are presented in Development Memorandum No. 272-19, which is included in the Appendix. No further vacuum seal development work was attempted after these tests. The pressure and leak rate data obtained using the O-ring vacuum seal was evaluated by NASA/Ames and deemed satisfactory for the radiative heating system application.

11. SPECTRAL FILTER STUDIES

The initial spectral distribution requirement for the radiative heating system required a close spectral match to the desired spectral distribution depicted in Figure 4 of the Statement of Work, which is reproduced here as Figure 11.1. At the initiation of this program, the best estimate of the output spectral distribution from the final radiation source was obtained from Giannini Scientific (formerly Plasmadyne) from a 20 KW vortex stabilized plasma arc using argon gas. Comparison of this lamp's output spectral distribution and the desired spectral distribution indicated a close similarity, although it was clear that some filtering would be required in order to satisfy the required tolerance limits. In Figure 11.2 the superposition of the plasma arc distribution over the desired spectral distribution with tolerance limits is illustrated. The distribution is adjusted so that without filtering the distribution falls below the upper tolerance limit, except in the region beyond .7μ where excess power would be eliminated through filtering. For such a configuration, the energy distribution still falls below the minimum tolerance requirements in the spectral region of .37μ to .41μ, but elsewhere would meet the specifications.

In Figure 11.3 are shown the derived filter transmittances for the case of minimum filtering to meet the specification tolerance limits, the complete filter to meet the desired distribution, and the maximum filtering condition to meet the lower tolerance level. Thus, the primary goal, in order to minimize rejection of power, was to provide a filter design characteristic which would approach as closely as possible the minimum filter characteristic.

On 8 November 1963, NASA/Ames modified the Statement of Work to delete the radiation source chopping requirements because of economic considerations. For instrumentation considerations, the spectral requirements were modified to require rejection of all radiation above .6μ. With this new requirement, various techniques for rejecting radiation above .6μ were studied. Both transmissive type filters and reflecting type filters were considered for satisfying this specification. Of considerable concern was the durability of the filters to the high intensity radiation to which they would be subjected. Transmissive type filters to satisfy this application would have to reject by reflection and/or absorption of the radiation above .6μ where reflective type filters would be required to reflect the wavelength bandwidth of interest from .2μ to .6μ and either absorb or transmit radiation above .6μ.

Initial investigations resulted in rejecting the possibility of using a transmitting type filter due to aspects of obtaining undesirable absorption in the ultraviolet portion of the spectrum. This absorption was undesirable from two standpoints: (1) Excessive rejection of usable radiation in the ultraviolet portion of the spectrum especially since the source was expected to be rich in ultraviolet radiation and (2) in maintaining the performance characteristics of the filter at the relatively high temperatures that would be obtained with the considerable ultraviolet absorption. The rejection of radiation above .6μ would mainly be via reflection thus would not impose a considerable thermal problem. With this decision, the main development work was directed towards the design of a reflecting type filter which would transmit the vast majority of the undesirable radiation. Since the optical system already required the use of a folding mirror, attention was directed toward using this mirror as the spectral filter. The initial design concept called for use of a large quartz plate which would support multiple filter segments covering its front surface.

In this manner with proper filter design, the incident radiation in the bandwidth of .2μ to .6μ would be reflected while the power at longer wavelengths would be transmitted through the mirror with minimum absorption.

Two studies were initiated:

(1) A study to determine the design problems associated with fabrication of a filter to satisfy the performance requirements and

(2) A test program in order to prove out the durability of the reflecting coating under high intensity irradiation.

11.1 COLD MIRROR DEVELOPMENT WORK

The initial approach taken to design a cold mirror filter that would satisfy the required performance characteristics was to take a conventional standard cold mirror filter which had been vacuum deposited on a quartz substrate. The performance of this standard cold mirror filter would nearly satisfy all portions of the specification with the exception of the ultraviolet portion of the spectrum which it transmitted. Work was initiated to use this standard filter as the rear face of the filter plate and to design an ultraviolet reflecting filter which could be deposited on the front face. In a parallel effort, the design of the complete filter to satisfy the specification was initiated. The results of these initial development studies were summarized in Development Memorandum No. 272-97, which is included in the Appendix.

11.2 FILTER THERMAL DEGRADATION TEST

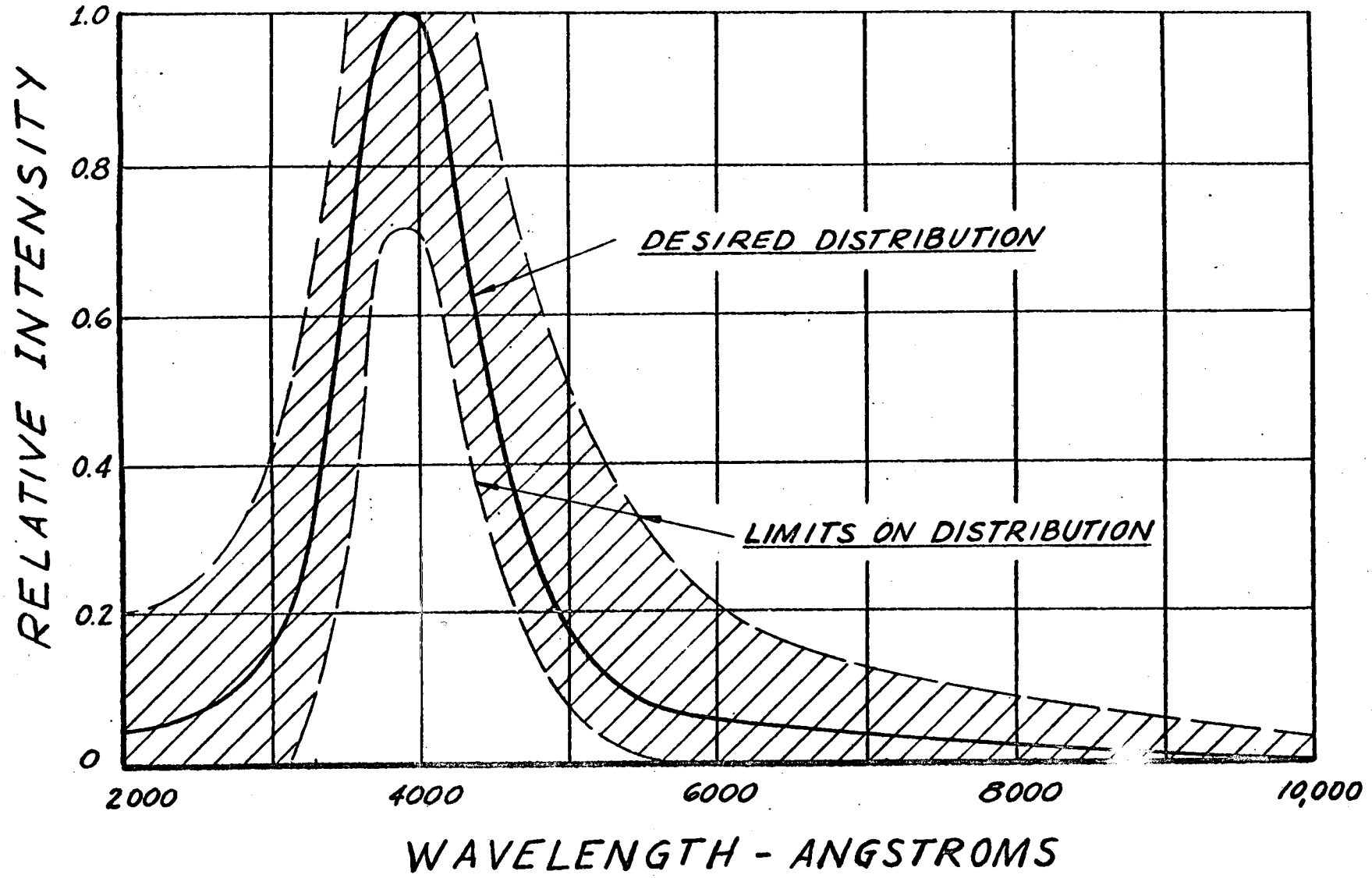
To determine the thermal stability and durability of the spectral filters developed, high intensity irradiation tests were set up. The radiation source used for the thermal tests was the 60 KW radiation source delivered as the prototype of the 150 KW radiation source. A 10" diameter aconic aluminized collector with integrated water-cooling jacket was fabricated and installed about the 60 KW source. The transmission of the filters tested were measured prior and after thermal irradiation tests in order to determine the degree of degradation. The test consisted of 4.5 minutes of irradiation at each of the following intensity levels: 19.2 Watts/cm^2, 28.3 Watts/cm^2, 37.4 Watts/cm^2 and 44.1 Watts/cm^2. Small changes in transmission were noted and determined to be a result of oxidation of some layers of the multi-layer coating. This type of oxidation is normally expected and results in decreased absorption without significantly changing the reflectivity. This oxidation is not continuous with continuous exposure, but reaches a saturation level before any important change in reflectivity takes place. Results of these tests gave an indication that it was feasible to obtain coatings which would withstand the thermal environment.

11.3 WATER CELL FILTER

The possibility of using water in the transmission filter was explored. Small water cells with provisions for one-half and one centimeter of water between two (2) one-eight inch GE 101 quartz plates were constructed. The transmission of these two cells with and without water were measured on the Cary Model 14 spectroradiometer and is presented in Figures 11. 4 and 11. 5.

In addition, the transmission of samples of tap water was measured and compared with the transmission of distilled water. No significant difference in transmission was found. Inspection of the transmission curve of the water cell, with and without water, shows no attenuation at the UV end of the spectrum because of the water. Water begins to absorb radiation at approximately .8μ and at 1μ is absorbing approximately 40% of the incident radiation. At 1.2μ, approximately 70% is absorbed and by 1.4μ, almost all the radiation is absorbed by the water. Although the water filter approach did not satisfy the long wavelength curoff at 6,000Å, as required per specification, it did offer certain attractive features such as simplicity and higher target intensities.

On 24 April 1964, NASA/Ames modified the spectral filtering requirements to allow 40% of the radiation to fall outside of the bandwidth of .2μ to .6μ which allowed the use of the water cell filter. Main factors influencing this decision included higher target intensity and lower system costs. Another advantage obtained by the use of this design approach was that one of the quartz plates of the water cell could be utilized as a water-cooled substrate for the uniformity filter without adding any additional quartz air interface reflection losses.



SPECIFIED SPECTRAL DISTRIBUTION

Figure 11.1

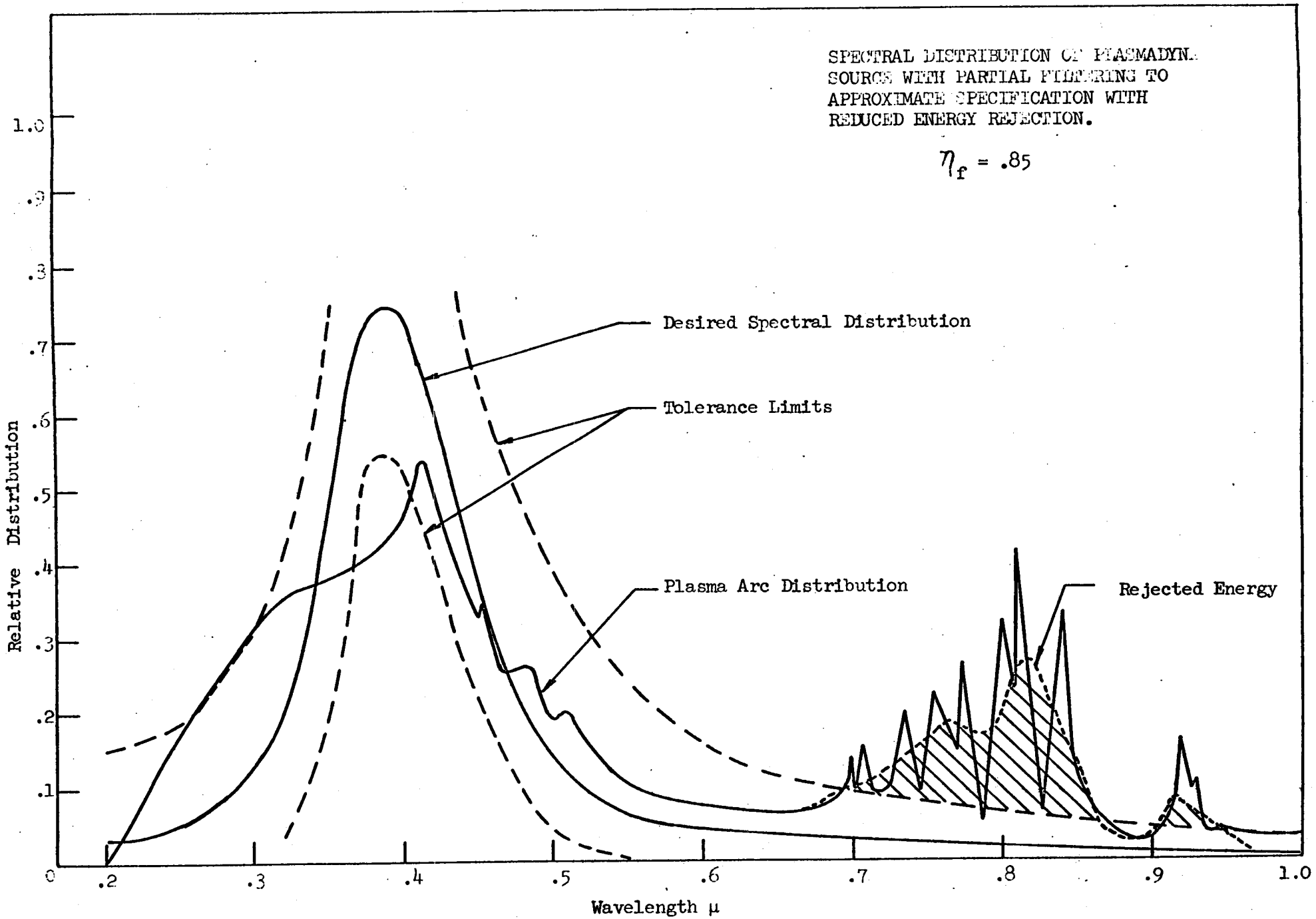

SPECTRAL DISTRIBUTION OF PLASMADYN. SOURCE WITH PARTIAL FILTERING TO APPROXIMATE SPECIFICATION WITH REDUCED ENERGY REJECTION.
η_f = .85
Desired Spectral Distribution
Tolerance Limits
Plasma Arc Distribution
Rejected Energy
Relative Distribution
1.0
.9
.8
.7
.6
.5
.4
.3
.2
.1
0
.2
.3
.4
.5
.6
.7
.8
.9
1.0
Wavelength μ

Figure 11.2

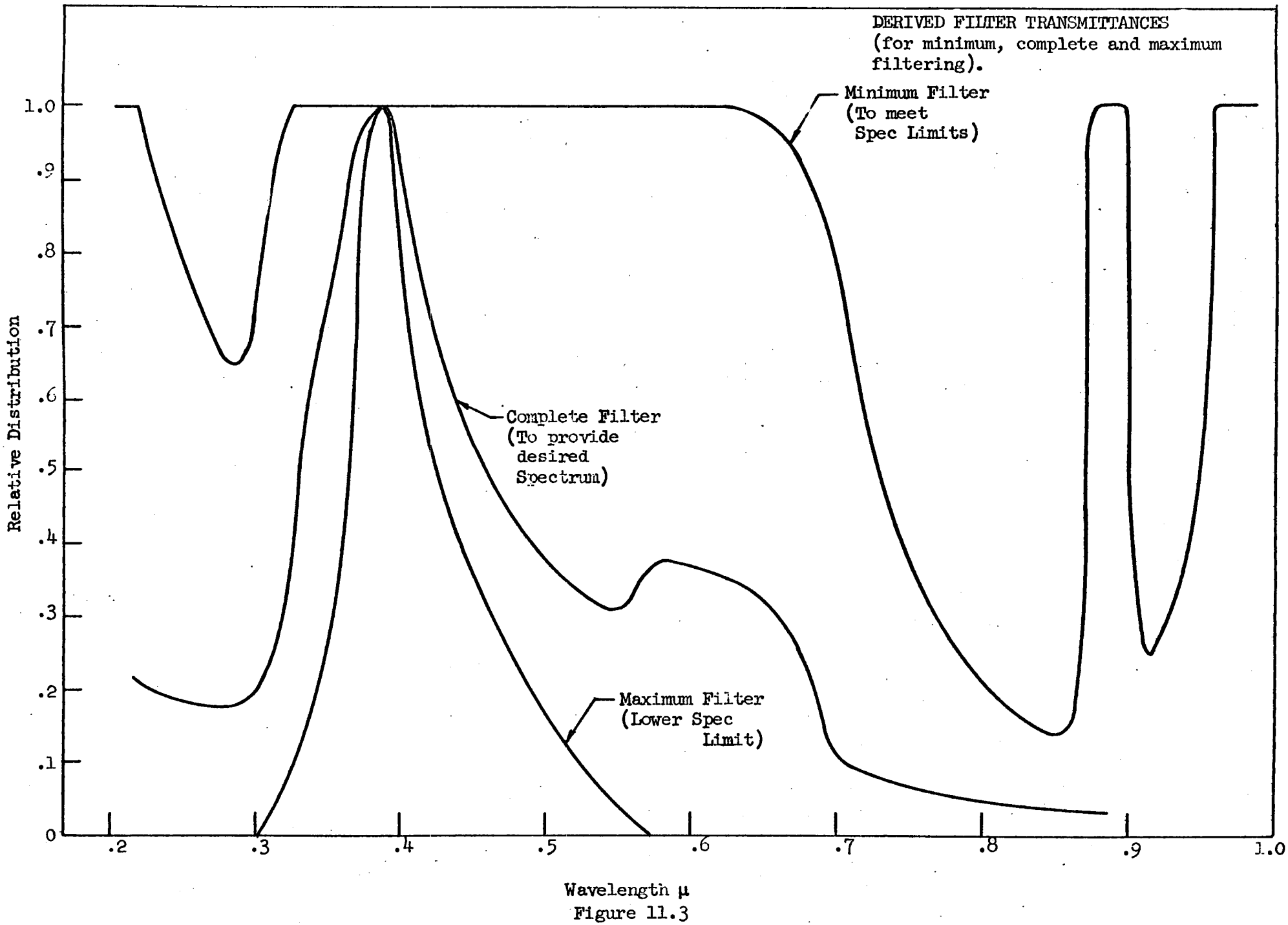

DERIVED FILTER TRANSMITTANCES
(for minimum, complete and maximum filtering).
Minimum Filter
(To meet
Spec Limits)
Complete Filter
(To provide
desired
Spectrum)
Maximum Filter
(Lower Spec
Limit)
Relative Distribution
1.0
.9
.8
.7
.6
.5
.4
.3
.2
.1
0
.2
.3
.4
.5
.6
.7
.8
.9
1.0
Wavelength μ

Figure 11.3

K+E 7 X 10 INCHES MADE IN U.S.A.
KEUFFEL & ESSER CO.

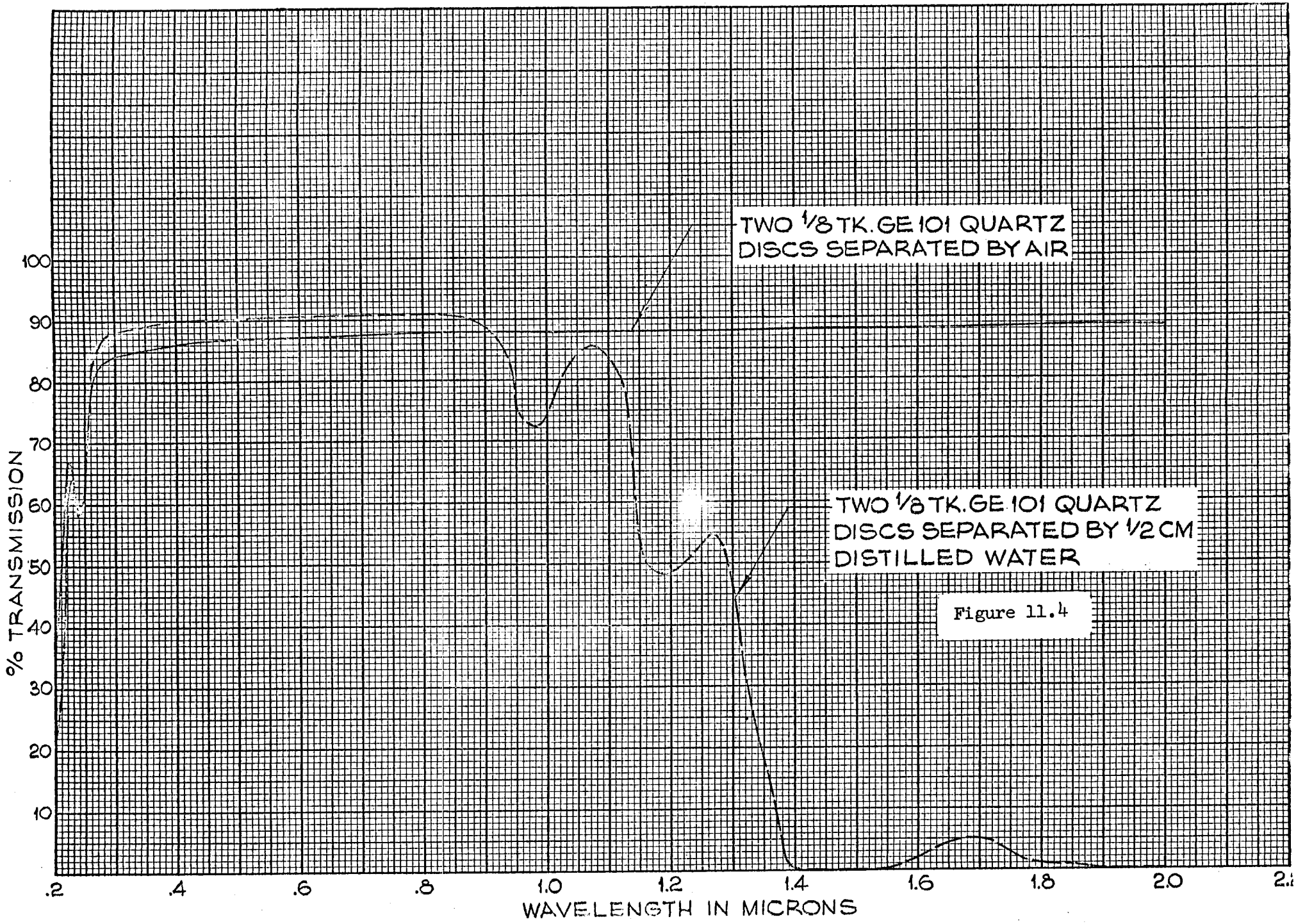


Figure 11.4

KEUFFEL & ESSER CO.

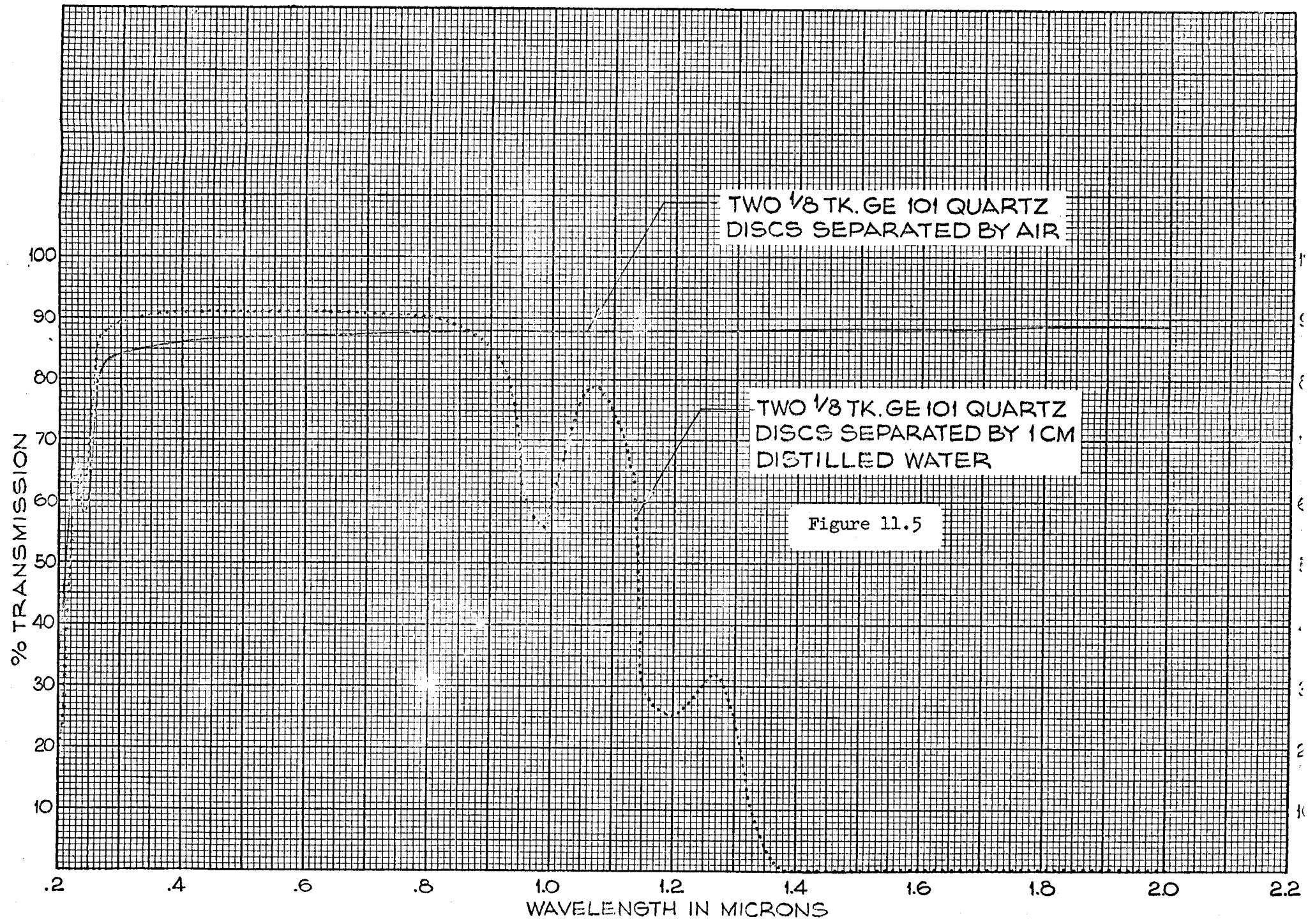


Figure 11.5

12. PROTOTYPE OPTICAL SYSTEM COMPONENTS

From the optical design development work as reported on in Section 8, an optical design for the radiative heating system was formulated. Per the Statement of Work, it was required to fabricate and assemble a prototype system including the final radiation source to allow for performance demonstration tests.

12.1 PROTOTYPE REQUIREMENTS

After selection of the projection type system for design study, it was agreed that the prototype would consist of at least the following elements:

a. Field lens and mount.

b. Projection lens and mount.

c. Collector mirror, cooling provisions, and collector reflector holder with adequate alignment provisions.

d. Folding mirror and mount.

e. Water-cooled mask and aperture plates for field lens assembly.

f. Beam douser and support.

g. Spectral and uniformity filters.

h. High power radiation source system including control console, power supplies, recirculator system and source holder.

i. Suitable system supporting fixtures.

12.2 QUARTZ SELECTION

Corning 7940-Optical Grade fused quartz was selected for the material to fabricate the prototype lenses. This selection was based upon a short trade-off study between performance, quality and cost. This material is a synthetic grade of quartz (fused silica) and exhibits excellent UV transmission characteristics. It does exhibit certain water absorption bands in the infrared portion of the spectrum, but since specifications called for

minimum transmission at those wavelengths, the absorption bands were considered of little importance. Special UV grade quartz was rejected primarily on the basis of cost. Also, experience seems to bear out the suspicion that any gain in UV transmission by using UV grade quartz over an optical grade synthetic quartz is minimum. Other qualities such as striae, bubbles, strain, etc., were identical for the two material grades.

12.3 OPTICAL TOOLING AND FABRICATION

12.3.1 Lenses

The design of the projection and field lens for the prototype system specified spherical surfaces, thereby allowing standard tooling and optical shop methods to be used in the fabrication of these elements.

12.3.2 Collector Mirror

Early in the program, the electroforming technique was established as the method for fabrication of the collector mirror. This method required the fabrication of an electroforming mandrel as the basic tooling for the electrolytic plating. A short program to investigate various mandrel materials was undertaken. Three basic materials investigated included 304 and 316 stainless steel and kanigen plated 2024 aluminum. The samples were first machined and then polished utilizing standard polishing techniques. Several electroformings each were made from the stainless and kanigenized aluminum samples. Results of this investigation indicated that the kanigen plated aluminum surfaces took a much better polish and hence resulted in more specular appearing electroformed parts than the parts electroformed from the stainless steel mandrels. Not all of the attempted electroforming over the kanigenized aluminum sample mandrels were successful. The first two attempts resulted in loss of the sample mandrels. As a result of this investigation, the stainless 304 or 316 was deemed preferable over the kanigenized aluminum for the mandrel material primarily because of minimum risk. The 304 stainless was eventually utilized in lieu of 316 stainless because of delivery considerations in obtaining a forged billet.

A computer program was used to determine the coordinates of the mandrel and of a jig bore cutter for fabrication of a cam for contouring the stainless billet. Because of the accuracy required,

100 coordinates per inch were calculated allowing the cam to be fabricated on a jig bore machine to within ± .0002 inches. The cam was then used in conjunction with a tracer lathe in the machining of the stainless steel forging to the proper contour. Inspection of mandrel indicated a slope error of less than 4 minutes of arc. The machined mandrel was then optically ground and polished in preparation for collector electroforming.

Because of the high heating loads that the collector would be subjected to, a direct water bath cooling technique was selected. The cooling jacket was fabricated by the spinning process and bonded to the collector. The inlets and outlets were designed in such a manner to provide reasonable circulation about the collector with a minimum pressure drop at a flow rate of approximately 2 gpm. Subsequent tests with this collector instrumented with thermocouples resulted in maximum collector surface temperatures on the order of 100°F and a total water temperature rise of approximately 15°.

12.3.3 Folding Mirror

A water-cooled rectangular mirror was fabricated for the prototype system from a flat aluminum plate which was kanigenized, optically polished, and vacuum coated with aluminum. The mirror mounting allowed rotation about two mutually perpendicular axes and translation in two mutually perpendicular directions so that all necessary adjustments anticipated during alignment procedures could be made precisely.

12.4 MECHANICAL COMPONENTS

The following is a brief description of those mechanical components used in the prototype system.

12.4.1 Douser

A water-cooled aluminum douser was placed between the field lens and projection lens so that the radiation could be occluded prior to reaching the target for instrumentation purposes and personnel safety. The douser was approximately 1" thick with a number of internal baffles forming a Labyrinth for the water flow so that all parts of the douser would be cooled. The douser was hinged so that it would swing about a vertical axis like a gate. Mechanical remote control was provided. A picture of the installed douser is shown in Figure 14.9.

12.4.2 Water-cooled Apertures and Mask

Water-cooled stainless steel apertures were fabricated to restrict the clear aperture of the field lens in the prototype system. For initial tests in the prototype, a water-cooled stainless steel mask with a circular opening was used instead of the elliptical mask. This mask was placed close to the field lens on the side facing the projection lens and its image was formed in the projection plane at the target. The empirical elliptical mask studies performed with the prototype as reported in Section 8.4 were attached to this water-cooled mask.

12.4.3 Backstop Calorimeter

A brass double walled conical backstop was constructed for use in the prototype system behind the target area in order to absorb the target radiation. A picture of this conical backstop is shown in Figure 5 of Development Memorandum No. 272-18, which is included in the Appendix.

12.4.4 Collector-Source Mount

The design approach selected for the collector-source mounting system required that the collector holder provide adjustments for aligning the collector relative to a fixed radiation source and also provisions for aligning the fixed source and combined source and collector holder to the optical axis. This approach of aligning the collector relative to the source in lieu of adjusting the source relative to the fixed collector was primarily selected because of the many utility attachments required at both ends of the radiation source, including electrical, water and gas. A side view of the collector mounting system, as fabricated for the prototype optical system, is shown in Figure 12.1. The collector assembly is attached to a vertical L-shaped aluminum weldment by means of three (3) threaded rods, which terminate at ball joints in the three (3) lugs on the mounting ring, which is welded onto the collector cooling jacket. The collector is suspended from the upper rod, and is raised and lowered by turning the knob at the top of the assembly. This knob is not shown in Figure 12.1 because it was temporarily replaced with a pulley and wire arrangement to allow for remote alignment. The two lower threaded rods are also supported by ball joints where they pass through the vertical weldment, and hence cannot support any part of the collector weight. Turning of the three rods separately allows the collector to be tilted in any direction. Turning of the three rods in unison allows the collector to be translated along the optical axis for focusing purposes. Remote controls for these rods are visible in the photograph.

A fifth adjusting screw, not visible in the photograph, moves the bottom of the collector at right angles to the optical axis as it swings about the top support. Thus, every adjustment necessary to place the collector in the correct position relative to the radiation source is provided. Precise adjustment is a necessary requirement since misalignment of the collector would seriously degrade target intensity and uniformity.

The radiation source is supported through the large opening in the vertical plate weldment and does not partake of the motions listed above. The required adjustments for aiming the lamp collector system in the correct direction are provided by the three vertical adjusting screws attached to the horizontal plate through ball joints. The source axis can be tilted and raised or lowered by turning these adjusting screws. The entire assembly can be translated from side to side by simply loosening the lock nuts.

A spring loaded support rod was utilized to support the cathode end of the source and its water-cooled cables in order to minimize external loading on the quartz envelope.

12.4.5 Lens Holders

For thermal control purposes, the lens holders on the prototype optical system were designed with water-cooling provisions. The primary purpose for cooling the lens holders was to keep the holders at a near constant temperature in order to minimize dimensional changes upon heat up or cool down. Although the lenses operate at a relatively high temperature, it was deemed desirable to minimize the conductive thermal path between the lens and lens holder in order to minimize thermal gradients across the lenses. Because of the high intensity levels of lens irradiation, a problem of finding a suitable spacer for the lens-holder interface was experienced. To assist in the selection of a suitable material, a test program was conducted where selected materials were irradiated at a level of 38 Watts/cm^2 with the following results:

Glass Reinforced Epoxy - Epoxy evaporated in 30 seconds.

Micalex - Distorted in 2 minutes.

Porcelain Insulator - Cracked in 3 minutes.

Copper and Beryllium Copper Springs - Softened and burned in 2 minutes.

Unfired Lava - No change in 8.7 minutes.

Fired Lava - No change in 5 minutes.

On the basis of these test results, lava (anhydrous aluminum silicate) was selected for the spacer material for both the field and projection lenses. In the "green" for unfired state, this material can be machined easily. However, after heating to about 2,000°F, it becomes a hard rock-like material with low thermal conductivity. Also, it was noted that upon firing, this material exhibited certain permanent dimensional changes. Although the dimensional changes were small, it was deemed undesirable to utilize this material as spacers in the fired state. Further investigation of this material indicated that up to a temperature of 1200°F, no permanent dimensional changes are experienced. Since this temperature is considerably higher than the maximum anticipated operating temperature of a spacer in the radiative heating system, the decision was made to utilize lava in its unfired state for the separator spacers.

No adjustments were provided for the projection lens holder since none would be available in the radiative heating system. The field lens holder was provided with adjustments to allow for vertical and horizontal translation.

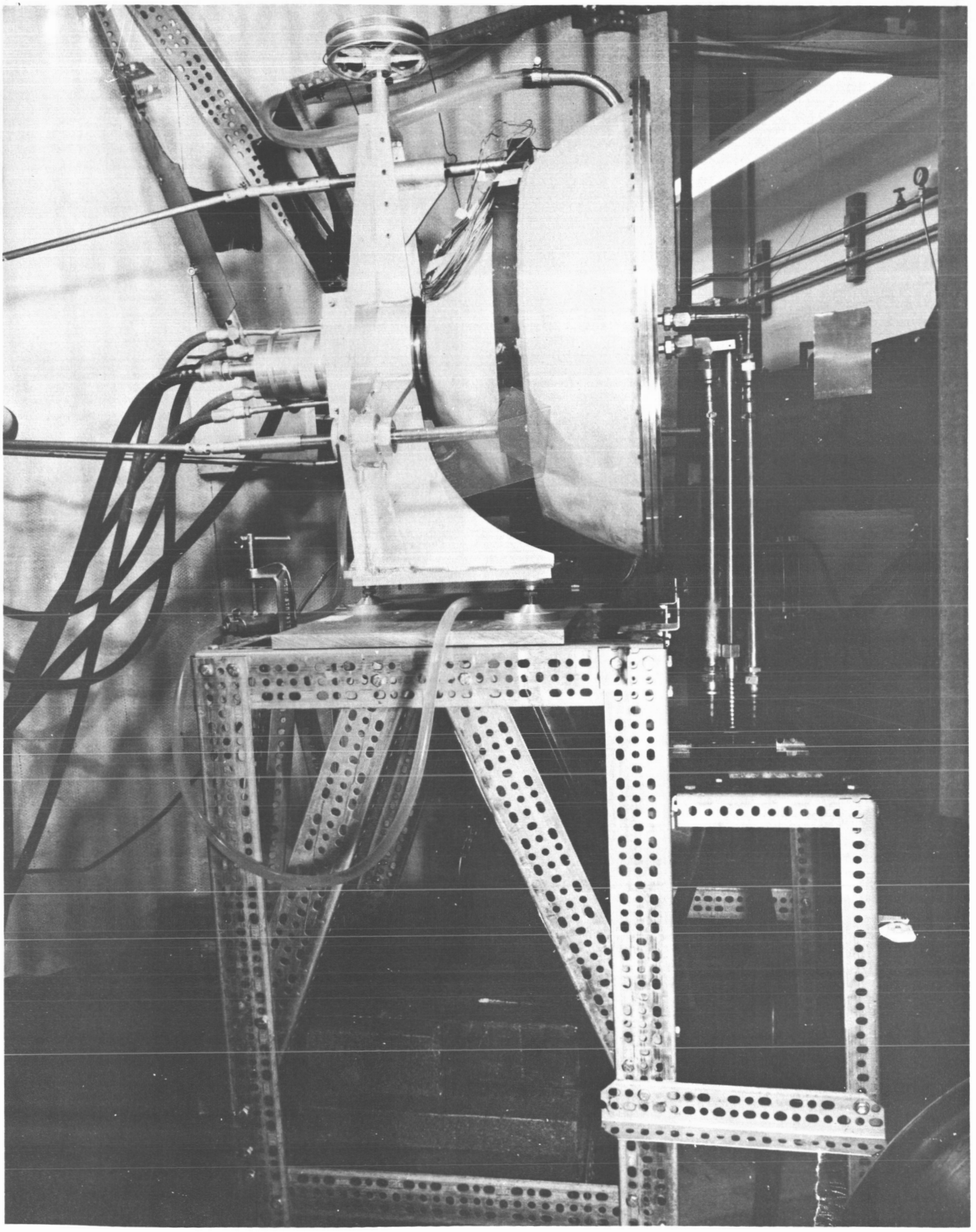


Figure 12.1 - Source-Collector Mounting System

13. INSTRUMENTATION

Instrumentation was required on this program in order to measure and monitor the radiation source characteristics. Instrumentation was also required for measurement of the output intensity distribution of the prototype optical system. Instrumentation for measurement of the spectral distribution of both the radiation source and the target radiation was also required.

13.1 SENSORS

Two Eppley thermopiles, Serial Numbers 6132 and 5013, were utilized during the test program to measure the absolute intensity of the arc radiation. Both of these sensors were of the single-junction constantan-manganin type with water cooling provisions. In continuous operation, these thermopiles are capable of measuring a maximum flux density of approximately 2 Watts/cm^2. Thermopile Number 5013 was calibrated by Spectrolab on September 20, 1963 at Table Mountain using Spectrolab's pyrheliometer as a secondary standard. Thermopile Number 6132 was subsequently calibrated from thermopile 5013, utilizing a Spectrolab Model X-25 solar simulator as a calibrating source. The calibration of these two thermopiles is recorded on Development Memorandum No. 272-13, which is included in the Appendix.

Used in conjunction with the water-cooled thermopile was a remotely operated water-cooled shutter. This permitted observations of short duration so as to avoid temperature changes in the sensitive element of the thermopile. Figure 1 of Development Memorandum No. 272-22, which is included in the Appendix, shows this assembly attached to the scan arm used in obtaining the absolute polar intensity distribution of the radiation source. For making micro-radiance measurements, a 1P28 multiplier phototube with an S-5 response was used. This sensor was utilized inside a shielded metal box with a 1/8 inch diameter aperture. Between the aperture and the photomultiplier were four thin quartz diffusers, each with one fine ground surface.

Solar cell intensity monitors were utilized for monitoring the output intensity of the radiation during tests. The cell output was connected to a strip chart recorder in order to display the solar cell output and obtain an intensity time history.

For the high intensity levels associated with the target irradiation two Hy-Cal "Asymptotic" calorimeters of the circular foil type were used for intensity measuring devices. These calorimeters, Serial Numbers 11146 and 12492, were capable of withstanding intensity levels of 60 and 120 BTU/ft^2-sec. respectively. The sensing area of these Hy-Cal calorimeters were exposed and subject to deterioration. Hence, it was renovated as often as necessary by deposition of camphor soot after careful removal of the used coating. A transient (slug) calorimeter, furnished by NASA/Ames, was also used on one occasion for measuring the target intensity and for purposes of comparison with the response of the Hy-Cal radiometer.

13.2 OPTICAL VIEWING INSTRUMENTATION

Because of the high intensity radiation levels and possibility of experiencing a violent failure of the radiation source envelope, the radiation source was operated within a separate room with a wall separating the radiation source from the test personnel. The general radiation source area was observed by viewing through sheets of welders glass. The arc itself was viewed through a similar filter after the radiation had been reflected from a plain flat quartz plate. In order to see small details of the electrodes and arc during source operation, a 10-power Gaertner telescope was used. The radiation was first reflected from a "cold mirror" to remove the infrared radiation. It was next reflected from the plain glass surface of a Herschel wedge, as used in astronomical telescopes for viewing the sun. The radiation then passed through a dense welders glass and into the telescope. All elements except the cold mirror were shielded from direct radiation.

The measurement of differences in radiance in different parts of the arc required scanning a relatively large projected image of the arc. Ideally, this image should be produced by an aberration free optical system. Such systems, resembling complex camera lenses, would be damaged by the arc radiation if placed near enough to the arc to obtain the required magnification. As a compromise, a single quartz plano-convex lens working at F/16.4 and a magnification factor of approximately 11 was used.

13.3 MECHANICAL INSTRUMENTATION

To measure the polar intensity distribution of the final radiation source, a remotely operated scanning arm was constructed. With

the Eppley attached to this scanning arm, the sensor was rotated along an arc of a circle in a plane containing the arc axis at a radius of 30 inches. The construction of this scanning arm is described and illustrated in Development Memorandum No. 272-22 which is included in the Appendix of Volume II.

To explore the power intensity distribution over a plane such as the target or a lens, a water-cooled scanning device was constructed to move a suitable sensor in two coordinates across the plane to be scanned. This device was also used for making micro-radiance scans with the photomultiplier sensor. This scanner is described and illustrated in Development Memorandum No. 272-18, which is included in the Appendix.

13.4 SPECTRAL DISTRIBUTION MEASUREMENT INSTRUMENTATION

Two spectroradiometers were used at various times during this program to measure the spectral distribution. Earlier in the program, the G-11 spectroradiometer which was designed and built at Spectrolab was used to measure the spectral distribution of several preliminary vortex stabilized radiation sources at Giannini Scientific. This instrument is a single pass grating monochromator working at F/11. It covers the range of 0.3 to 1.0 microns using S-1 and S-5 photomultiplier detectors.

The primary instrument utilized for measurement of the radiation spectral distribution was the Spectrolab P-20 spectroradiometer system. This system utilizes a double-prism modified Perkin-Elmer Model 350 monochromator which exhibits low stray irradiation and narrow bandwidth resolution. It is used with both an RCA 1P28 photomultiplier tube having sufrasil quartz window and two impedance matched Ektron PbS detectors cemented back-to-back. In the wavelength range from 0.45 microns to 2.7 microns, the PbS detector is employed and the 1P28 photomultiplier is used for the wavelength range from 0.2 microns to 0.7 microns, with the two detectors overlapping in the 0.7 to 0.45 micron region. An NBS calibrated 1000 Watt quartz iodine standard lamp is used to calibrate the spectral radiometer system. A rotating magnesium carbonate diffuser reflecting block is used as a part of the fore optics to direct radiation from either the radiation being measured or radiation from the standard lamp towards the entrance slit of the monochromator and an optically identical manner. The radiation is modulated at 160 cycles per second prior to entering the entrance slit of the monochromator. The radiation is then dispersed and

the radiation incident to the detector generates a signal of 160 cps. The signal is demodulated and amplified by a Perkin-Elmer 107 amplifier. These signals are displayed on a Moseley 680 strip chart recorder through an impedance matching Dymec DC amplifier for visual checking of intensity versus wavelength. In addition to the analog display on the strip chart recorder, the output signal is digitized by a nonlinear systems digital data collecting system. The digital data collecting system consists of an analog-digital converter, a digital voltmeter with automatic ranging network from 1 millivolt to 100 volt scale, an automatic wavelength marker, and a 12-channel binary tape punch. The 12-channel tape which contains all the information regarding intensity versus wavelength of the measurement is directly read into a Fortran program compatible with an IBM 7090 computer for data reduction. A block diagram of this measurement setup is given in Figure 13.1. This spectroradiometer system was used for all spectral distribution measurements of the output radiation from the final radiation source and the prototype optical system.

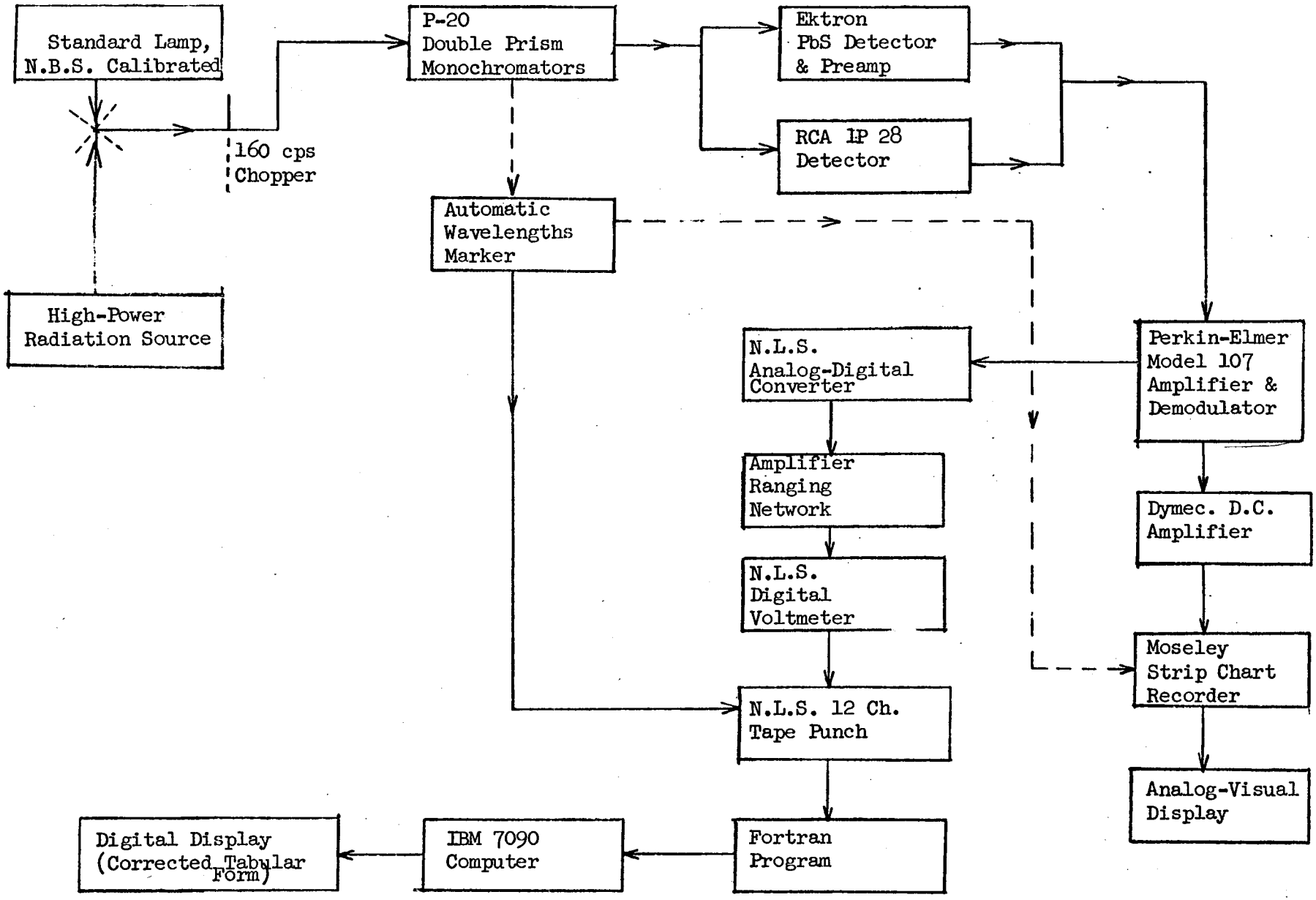


Figure 13.1 Block Diagram of Spectral Measurement and Data Reduction System

14. PROTOTYPE TESTING

The testing of the prototype optical system was accomplished in conjunction with testing of the final radiation source. Those tests associated with the optical system or components are reported on here. Those tests associated only with the final radiation source are presented in Volume II of this final report.

14.1 TEST SITE DESCRIPTION

An enclosure approximately 12 ft. x 17 ft. with a 15-foot high ceiling was utilized for testing of the final radiation source integrated with the prototype optical system. Only the final optical element, which is the projection lens, was positioned outside of the enclosure to allow for access to the target area for instrumentation purposes. Several movable 4 ft. x 8 ft. corrugated transite shields were fabricated and used to protect switch panels and associated instrumentation within the enclosure. Figure 14.1 is a photograph of the control area directly outside of the enclosure showing the control console and the input water distribution system with associated monitoring provisions. Figure 14.2 is another photograph showing the outside of the enclosure at the end of the optical train. The projection lens is visible in this photograph and the target plane is located directly in front of the conical backstop calorimeter. The uniformity scanner is also shown and is oriented in a position for target plane intensity scans. Figure 14.3 is similar to Figure 14.2 with the exception that protective covers are in place to protect personnel from the high intensity radiation. Figure 14.4 is a photograph of the enclosure as seen looking through the enclosure door. The installed folding mirror is seen in the center of this picture. The field lens assembly, obscured in this picture, is located between the folding mirror and the large circular aperture located in the left portion of the picture. The radiation source collection system, not shown in this view is located to the right adjacent to the test enclosure wall. Figures 14.5 and 14.6 show the radiation source-collector assembly installed in the test enclosure. Figure 14.4 also shows the viewing optics for monitoring source operation during prototype testing. In Figure 14.6, the mechanical linkages associated with remote collector alignment utilized in this test program are seen.

Figure 14.7 is a view showing a portion of the optical train consisting of the field lens assembly, douser, projection lens

and target area. A closeup of the field lens assembly is given in Figure 14.8. Another view of the field lens assembly and installed douser is shown in Figure 14.9. Figure 14.10 is a rear view of the installed folding mirror with alignment provisions. A closeup of the water-cooled scanning device is given in Figure 14.11.

To remove ozone generated during radiation source operation, a 7,000 cfm blower was installed to exhaust through the roof of the test site giving approximately two air changes per minute. Fresh air from the laboratory flowed into the test chamber through openings at the floor level. These openings were shielded to prevent radiation being reflected into the laboratory.

14.2 ALIGNMENT

The prototype optical system design requires that the collector produce a purposely distorted image of the plasma arc at the field lens. The field lens images the collector onto the projection lens and the intensity distribution at the field lens is projected into the vicinity of the target by the projection lens. While the system is not required to produce images of high resolution, accurate alignment is required in order to attain maximum target irradiation and proper distribution of the power on the target.

Since the projection lenses in the radiative heating system will be fixed without adjustment capability, the prototype projection lens holder was positioned without adjustments except those necessary to place it normal to the optical bench axis. With the projection lens mounting position fixed, the axis of this lens becomes the optical axis of the entire system, and all other optical elements must be aligned to this lens. The following basic alignment procedures were followed:

14.2.1 Initial Positioning

Adjustment provisions for all components were set near the middle of their range. With a leveling tape measure, the support stands for the folding mirror, source collector holder assembly, and optical bench were positioned in the correct relationship to each other with their optical axes at the same level.

14.2.2 Optical Bench

The projection lens holder was mechanically centered and made square with the bench. The field lens assembly was positioned the proper distance from the projection lens. Utilizing a modified Gaertner telescope, Model M-511, mounted in the projection lens holder and a mirror positioned in the field lens holder, allowed fastening of the field lens holder parallel with the projection lens holder. Substituting the target for the mirror allowed the field lens holder to be centered.

14.2.3 Folding Mirror

With the telescope still positioned in the projection lens holder, a target was centered on the folding mirror. The folding mirror assembly was then moved so that the target was centered on the optical axis. The target was then placed at the source holder and the folding mirror adjusted to position the target on the optical axis.

14.2.4 Source-Collector Axis

The telescope was then removed from the projection lens holder and placed in the lamp holder. A target was placed in the projection lens holder and the source holder was adjusted to site on the target. The system was aligned when the telescope sites on the target without requiring lateral or vertical adjustment of the source holder.

14.2.5 Alignment Check

The alignment of the entire optical system was checked focusing the telescope successfully on the test zone target, projection lens target, and field lens target. All targets should appear centered on the telescope crosswire intersection when they are all correctly centered on the single optical axis. The angular adjustment of the field lens holder can be checked by attaching the field lens target mirror and focusing on the reflected image of the telescope. Figure 14.14 shows the telescope mounted in the projection lens holder.

14.2.6 Field Lens Alignment

To remove the effects of any centering error obtained in the fabrication of the field lens, the telescope was mounted in the aligned source holder. With the field lens installed, the field lens holder was adjusted normal to the source axis until the test zone target was centered on the telescope crosswire intersection.

14.2.7 Projection Lens Centering Error Compensation

Since the projection lens holder is fixed in position, the effects of centering errors in the manufacture of this lens cannot be removed. However, it is possible to compensate for such errors by tilting the folding mirror. With the lenses in place and the telescope mounted in the aligned source holder, the folding mirror was adjusted slightly in order to bring the test zone target center to the intersection of the telescope crosswires.

14.2.8 Collector Alignment

The optical axis of the collector must coincide with the source axis. The initial method utilized for aligning the collector to the source holder consisted of positioning an alignment lamp with a small filament (.120" x .062") in the radiation source holder so that the filament occupied the position of the brightest part of the radiation source arc. An aluminum disk with eight apertures was placed across the large opening end of the collector as shown in Figure 14.12. Each aperture isolates light from a small area of the collector and the curvature of this area forms a filament image on the screen placed at the field lens holder. Figure 14.13 shows the eight resulting images. The small images are formed by light passing through the outer four holes and the larger images are formed from the four inner holes. The collector adjustments were manipulated in the attempt to bring these images to their correct positions. For this method of collector alignment, it is necessary that the aperture plate be correctly centered on the collector axis. No simple way to accomplish this was found.

The use of the aperture plate was eventually abandoned and in its place an aperture cylinder was used. This cylinder, with holes arranged in four groups of three each, was placed around the alignment lamp. The collector alignment lamp assembly was adjusted by moving the lamp so that its filament is centered within the perforated cylinder and at the correct distance from the base of the fixture. By observing the middle hole of any group of three, the lamp filament is silhouetted against the diametrically opposite hole when the fixture is correctly adjusted. During alignment, a light from the filament passes through eight openings in the alignment fixture cylinder and is reflected from eight different portions of the collector reflecting surface, resulting in eight beams of light forming eight filament images on the field lens target as obtained using the aperture plate. Manipulation of the collector focus adjusting knobs allowed moving these images with respect to each other and to the field lens target.

This basic method for collector alignment was adopted for the alignment of the radiative heating system and incorporated in the NASA/Ames Alignment Manual A-11054(RP39) dated 20 January 1966 for the radiative heating system.

14.2.9 Final Alignment with Source Operating

With the radiation source operating, the final focus adjustment of the collector about the radiation source was made utilizing remote control provisions. Utilizing a radiometer at the target plane, the collector was focused about the radiation source to obtain maximum average edge intensity at the target plane.

14.3 COMBINED RADIATION SOURCE - OPTICAL SYSTEM TESTING

The first series of tests to evaluate the prototype system were initiated on 7 October 1964. The primary purpose of this initial test series was to obtain sufficient performance data of the combined prototype radiation source-optical system in order to predict the performance of the radiative heating system utilizing the prototype system design. Those tests performed included the following:

a. Intensity scans for determination of the intensity distribution at the projection plane of the optical system utilizing a 6-inch and a 7-inch clear aperture at the field lens.

b. Intensity scans for determination of the intensity distribution at the target plane utilizing 6-inch and 7-inch clear apertures at the field lens.

c. Intensity scans for determination of the intensity distribution at translated target plane positions utilizing a 7-inch diameter clear aperture at the field lens.

d. Intensity scans across the minor axis of the target plane (as viewed from the projection lens) at various radiation source currents utilizing a 7-inch diameter clear aperture at the field lens.

These tests, which represent Runs 5 through 9, are reported on in Development Memorandum No. 272-18, which is included in the Appendix. The sensor used in these tests was the Hy-Cal No. 1 sensor (Serial Number 11146). The tests were performed without spectral or uniformity filters in the optical train.

The intensity data acquired from the minor axis scans at current levels from 900 to 1550 amps were utilized in conjunction with the overall target intensity distribution data obtained with a radiation source current of 1,000 amps to predict the performance of the 14-lamp radiative heating system without uniformity or spectral filtering.

The edge and peak intensity values obtained from the minor axis scans at the various current levels were utilized to obtain extrapolation factors that could be applied to the overall target intensity distribution data obtained at 1,000 amps. The validity of this method used for extrapolation of target edge intensities as a function of current was subject to the assumption that the relative target intensity distribution does not vary with source current. Based upon the extrapolation factors, an average edge intensity of 7000 BTU/ft^2-sec. for 1550 amps operation was predicted for a 14-lamp radiative heating system. This prediction turned out to be relatively high compared to subsequent edge intensity tests. During these tests, Hy-Cal No. 1 radiometer was subjected to intensity levels grossly exceeding its intensity rating. This factor, plus subsequent degradation of radiation source cathode, were considered attributable factors to the higher intensity value prediction.

In Test Run 10, the Hy-Cal No. 1 sensor was compared with the Eppley thermopile #6132 and a NASA Radlab radiometer. These sources were positioned at varying distances from the final radiation source based upon their relative sensitivities. The results of this test indicated that, based upon factory calibration factors, the Hy-Cal No. 1 sensor reads approximately 16.5% higher than the Eppley thermopile for the same flux intensity. Data obtained from the Radlab radiometer indicated that either the radiometer had malfunctioned or the instrumentation associated with the radiometer was faulty. This sensor comparison test is reported on in Development Memorandum No. 272-15, which is included in the Appendix.

Subsequent to Test Run No. 10, Hy-Cal No. 2 (Serial Number 12492) was procured. This sensor has a lower sensitivity than the Hy-Cal No. 1 sensor and therefore more suitable for the prototype target scan tests.

Prior to utilizing this new sensor in prototype tests, it was decided to perform another sensor comparison test. For this test, the Eppley thermopile, Serial Number 6132, and both Hy-Cal Numbers 1 and 2 were utilized in a similar test setup. The results

of this test, which are included in Development Memorandum No. 272-21, indicated large discrepancies between the three sensors. In this test, the Hy-Cal No.2 sensor was located approximately 10.17" from the radiation source. The mounting of this sensor at this close proximity to the radiation source was required because of its low sensitivity. To make the sensor comparison, it was assumed that each receiver received a flux density which is inversely proportional to the square of its distance from the arc.

Trips were made by Spectrolab personnel to Hy-Cal to evaluate their calibration procedures and techniques. No criticisms could be found in regard to the calibration techniques used at Hy-Cal.

In order to compare the two Hy-Cal sensors, a sensor comparison test at the projection plane of the optical system was conducted. Readings from both sensors were obtained at the center of the projection plane and at a radius of 2 inches. Fairly close agreement was obtained from the two sensors although difficulty was experienced in maintaining system operating parameters during the acquisition of the data. The results of this sensor comparison test are given in Development Memorandum No. 272-31, which is included in the Appendix.

A run was made on 28 January 1965 in order to compare the Spectrolab No. 2 radiometer with a slug calorimeter obtained from NASA/Ames. Results of this test are given in Development Memorandum No. 272-33, which is included in the Appendix. In this comparison test, the Hy-Cal radiometer indicated an intensity level approximately 10% higher than the slug calorimeter.

On 19 and 22 February 1965, combined target edge intensity and sensor comparison tests were performed. Edge intensity at 12 equally spaced discrete points along the periphery of the 4" diameter circle representing the edge of the target in the target plane were measured utilizing the Hy-Cal No. 2 radiometer and the NASA slug calorimeter. These tests were all made with the radiation source current at 1550 amps. The results of these tests are presented in Development Memorandum No. 272-39, which is included in the Appendix. In Figure 1 of this development memorandum, the intensity values from both radiometers are plotted as a function of position around the periphery of the target area. Again, as experienced in the sensor comparison tests reported in Development Memorandum No. 272-33, the Hy-Cal No. 2 sensor indicated 10% to 15% higher intensities than the slug calorimeter.

On 25 and 28 May 1965, the last attempt was made to obtain a correlation between the Hy-Cal radiometers and the Eppley thermopile No. 6132. Every attempt was made to reduce the errors inherent in such a calibration type test. The sensors were mounted at what was thought to be accurately determined dimensions from the radiation source. The water-cooled shield, utilized on previous sensor tests, was removed from the Eppley thermopile so that its normal 45° field of view was not obstructed. Several modifications in the instrumentation were made in order to minimize sensor loading problems. Both the water-cooled Hy-Cal sensors were freshly coated with camphor soot to provide an absorptivity of approximately .95 to .96. The results of this sensor comparison test is given in Development Memorandum No. 272-46, and is included in the Appendix. Again, as in previous sensor comparison tests where the sensors are positioned at varying distances from the plasma arc depending upon their relative sensitivity factors, large discrepancies were experienced after correcting for the factory calibration factor, distance factor, and instrumentation loading.

14.3.1 Water Cell Transmission Test

Test Runs 22.1, 22.2 and 22.3 were made to determine the transmission of the water cell. One double scan was made without the water cell, two with the water cell installed, and two more runs without the water cell. Hy-Cal sensor No. 2 was utilized and positioned on-axis and at a radius of 1 inch and 2 inches at the projection plane. The results of these tests are given in Development Memorandum No. 272-26, which is included in the Appendix. The transmission of the water cell was found to be approximately 0.68 for on-axis rays and approximately 0.66 at a 1" radius and 0.65 at the 2-inch radius.

14.3.2 Field Lens Intensity Distribution

Field lens intensity distribution data were obtained during Runs 24 and 25. A total of 25 intensity scans, each of vertical separation of 1/2", were made on the field lens plane using the Hy-Cal No. 2 radiometer. From this data, a plot of iso-intensity lines was constructed and calculations were performed to determine the total power incident upon the field lens plane and that passing through 6 and 7-inch diameter apertures. The calculated power passing a 6-inch diameter clear aperture baffle was determined to be approximately 7.8 KW. The power passing a 7-inch diameter clear aperture baffle was 9.4 KW. The calculations resulting in these numbers are presented in Development Memorandum No. 272-32, which is included in the Appendix.

14.3.3 Target Intensity as a Function of Gas Flow

On 4 March 1965, a test was made in order to determine possible increases of target intensity due to reductions of gas flow. The results of this test are given in Development Memorandum No. 272-40, which is included in the Appendix. The results of this test indicated that, by reducing the indicated gas flow from 22 cfm to 16 cfm, an increase of target edge intensity of 9.5% was obtained. Associated with this increase in edge intensity was almost a similar increase in arc voltage.

14.3.4 Target Edge Intensities at Reduced Diameters

Tests were performed to determine the relative intensities at the edge of targets at slightly reduced diameters. The results of these tests are given in Development Memorandum No. 272-41, which is included in the Appendix. An average edge intensity increase of 8.6% was obtained for a 3.75" diameter target relative to the average edge intensity for a 4" diameter target. For a 3.5" diameter target, the average edge intensity increased by 14.8%.

14.3.5 Collector Focus Sensitivity

On 3 March 1965, tests were performed to determine the sensitivity of the collector focus on target intensity. At discrete focus settings, intensity readings at the target were made at points 2" above and below target center and at 2" to the left and right of center. The focus adjustment screws which have 16 threads per inch were set at 1/2 turn increments. The results of this test are included in Development Memorandum No. 272-42, which is included in the Appendix.

14.3.6 Uniformity Filter Tests

An aluminum dot pattern uniformity filter was deposited to the outer quartz surface nearest the target on the water filter. Based upon evaluation of the unfiltered intensity distribution of a 14-lamp radiative heating system and based upon a 1-lamp intensity distribution as obtained in Run 8.1 reported on in Development Memorandum No. 272-18, the filter exhibited 100% transmission at a 5.5" diameter and 50% transmission at the center. The transmission varied from 100% to 50% in a spherical manner from the center to the 5.5" diameter. Seven continuous horizontal scans were made across the target plane with the uniformity filter in place. The scan locations were chosen to give 12 equally spaced points around the edge of the target in order to obtain a good average value of edge intensity. Extrapolation of the resulting

target intensity distribution to the intensity distribution that would result in the use of 14 such optical systems indicated a uniformity of ± 8.8% using the initial filter design. It was also obvious from the resulting intensity distribution that, simply by removing the center dots, it would allow an increase of the center transmission slightly which would result in a ± 5.9% system uniformity. The results of this test are given in Development Memorandum No. 272-49, which is included in the Appendix.

14.3.7 Collector Damage Due to Envelope Failure

On 8 February 1965, the outer envelope of the final radiation source failed during a static pressure test at 250 psi. The collector damage was of three types: abrasion, deformation and surface deteoriation. A more detailed description of the collector after this envelope failure can be found in Development Memorandum No. 272-35, which is included in the Appendix. Upon evaluation of the collector, it was estimated that its loss in total reflectivity amounted to approximately 4%. The collector was subsequently realuminized and utilized throughout the remaining portion of the test program.

14.4 TARGET EDGE INTENSITY - 14-LAMP SYSTEM

The following table is a review of the estimated projected 14-lamp system target edge intensity, without water cell losses, that was reported during the period of the test program based upon a radiation source current of 1550 amps.

If we reject the reported intensity values in Item a of Table 14.1, and also assume that a data interpretation error was made in Item b and that the 540 BTU/ft^2-sec. is applicable, then an average of the remaining intensity values obtained using the Hy-Cal #2 radiometer and the slug calorimeter would be approximately 546 BTU/ft^2-sec. This value is considered to be a representative estimate of the average predicted target edge intensity value.

TABLE 14.1

		Target Edge Intensity BTU/ft^2-sec.	Sensor Used
a.	Calculations based upon Run 8.1 target scan data at 1000 amps and Run 9.9 diameter scan data at 1550 amps (D.M. 272-18)	700	Hy-Cal #1
b.	Calculations based upon Run 23.5 target scan data. (Note: Investigation indicated that data interpretation error may have been made. If so, intensity of approximately 540 BTU/ft^2-sec. would result)	435 (See note)	Hy-Cal #2
c.	Calculations based upon intensity readings for one position located 2" above and which is normally point of near minimum intensity (Run 39, D.M. 272-33)	568	Slug Calorimeter
d.	Calculations based upon intensity readings at 4 positions; top, bottom and both sides. (Average of readings at these positions approximate average edge intensity) (Runs 40 and 41)	547	Hy-Cal #2
e.	Calculations based upon intensity readings at 12 equally spaced edge locations. (Test Runs 44.3 and 45.2, D.M. 272-39)	565 496	Hy-Cal #2 Slug Calorimeter

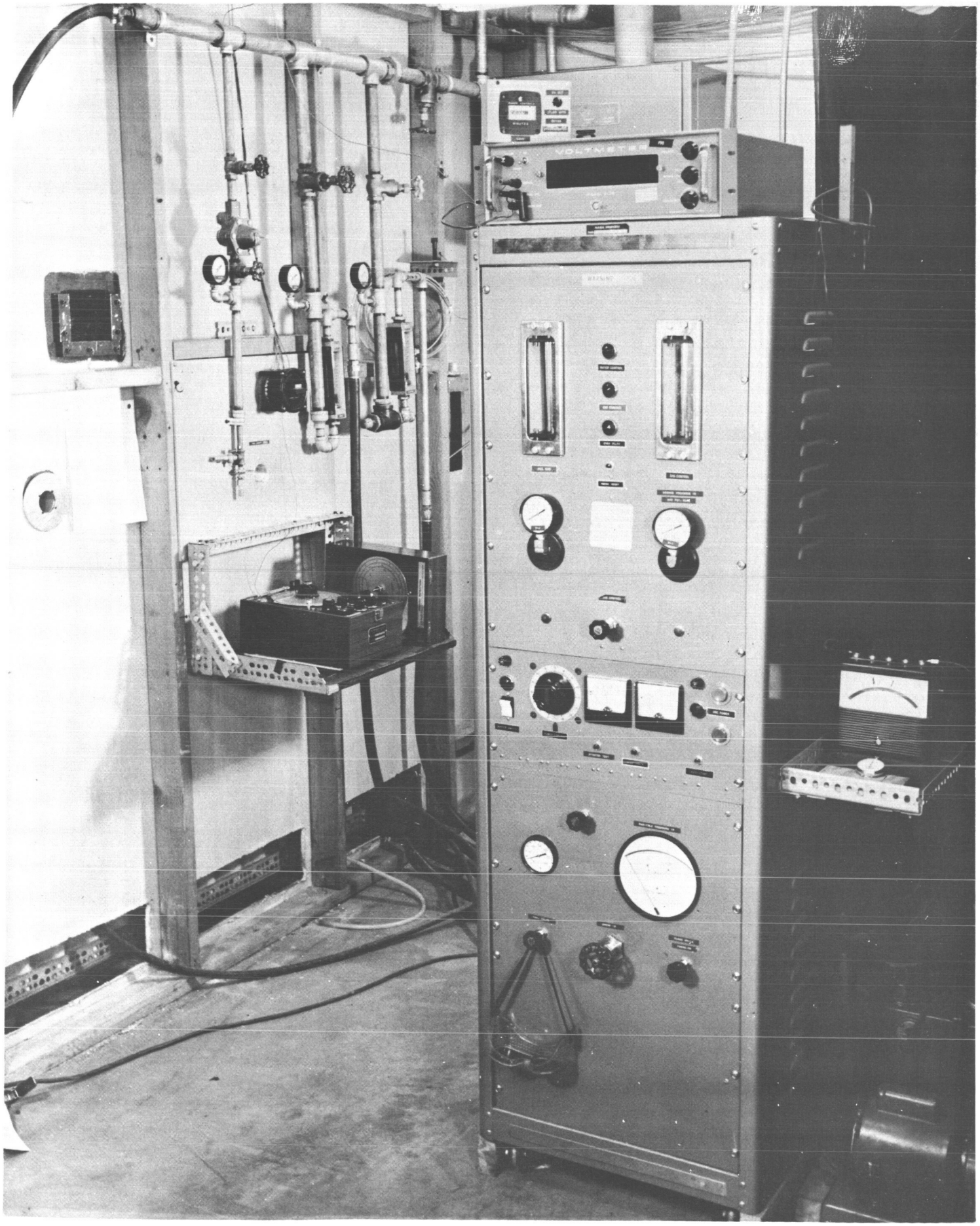


Figure 14.1 - Photograph Viewing Control Console and Input Water Distribution System Outside Test Enclosure

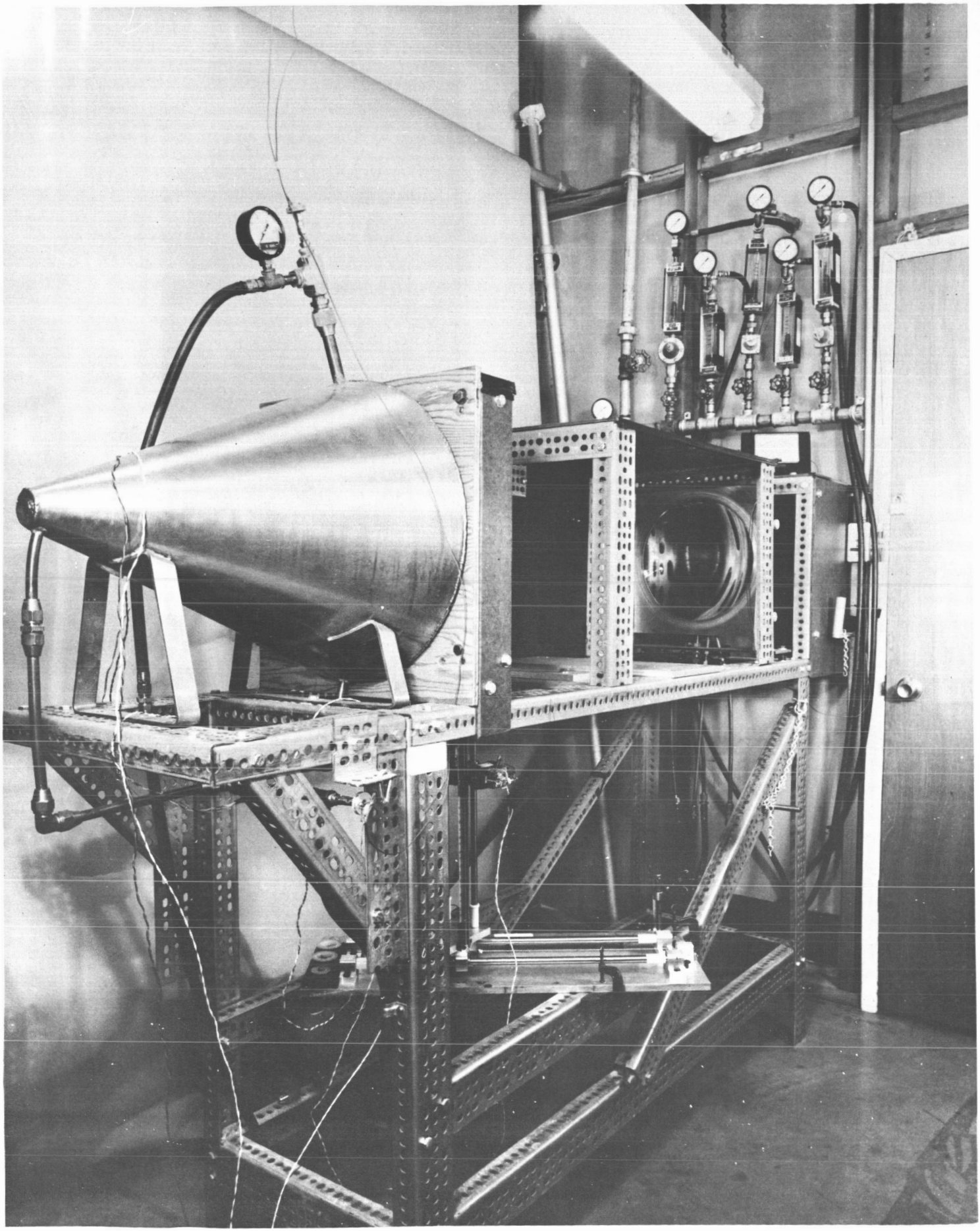


Figure 14.2 - Photograph Viewing Installed Projection Lens, Target Area and Conical Backstop Calorimeter Outside Test Enclosure

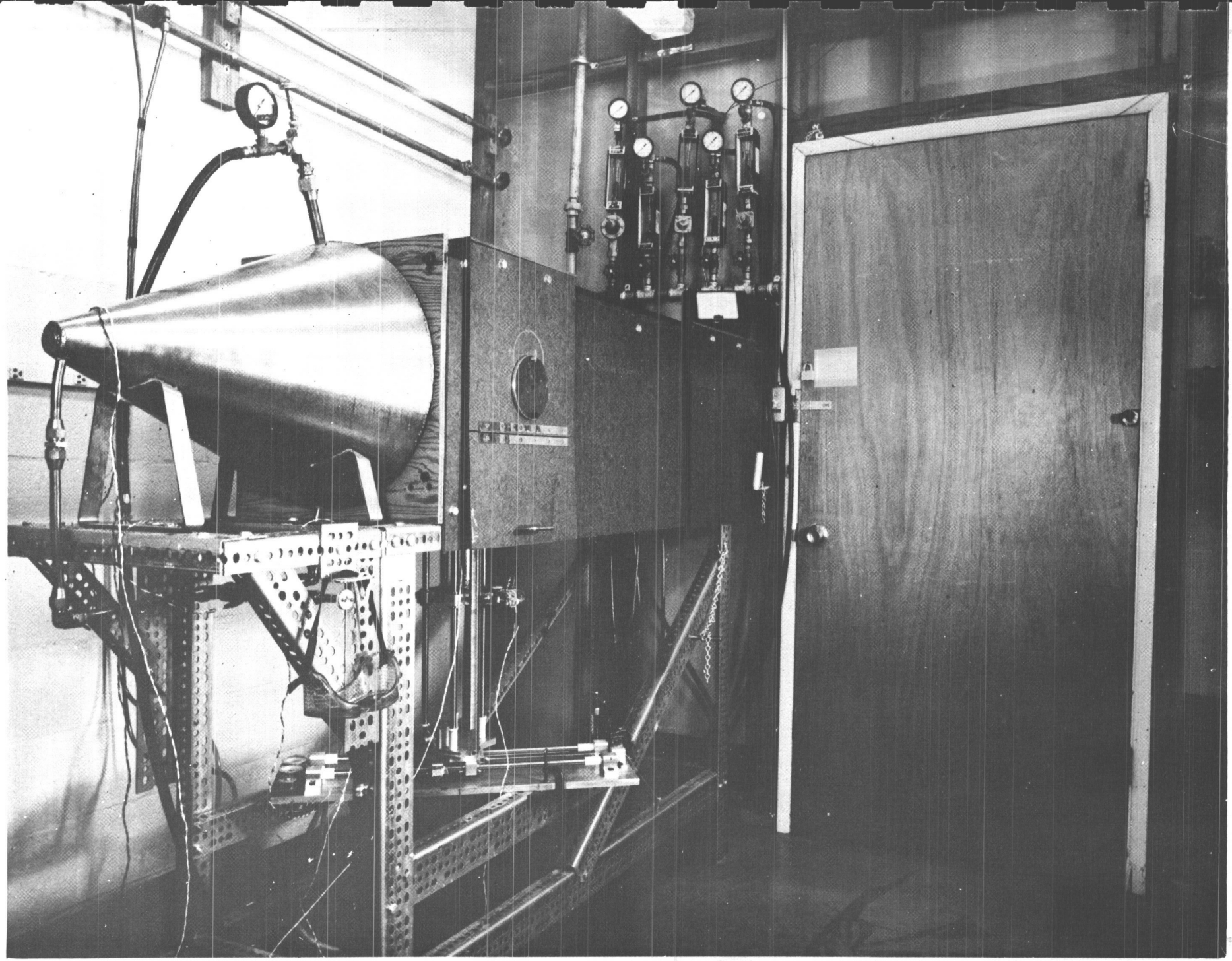


Figure 14.3-View of Target Area with Protective Covers in Place for Target Intensity Scans

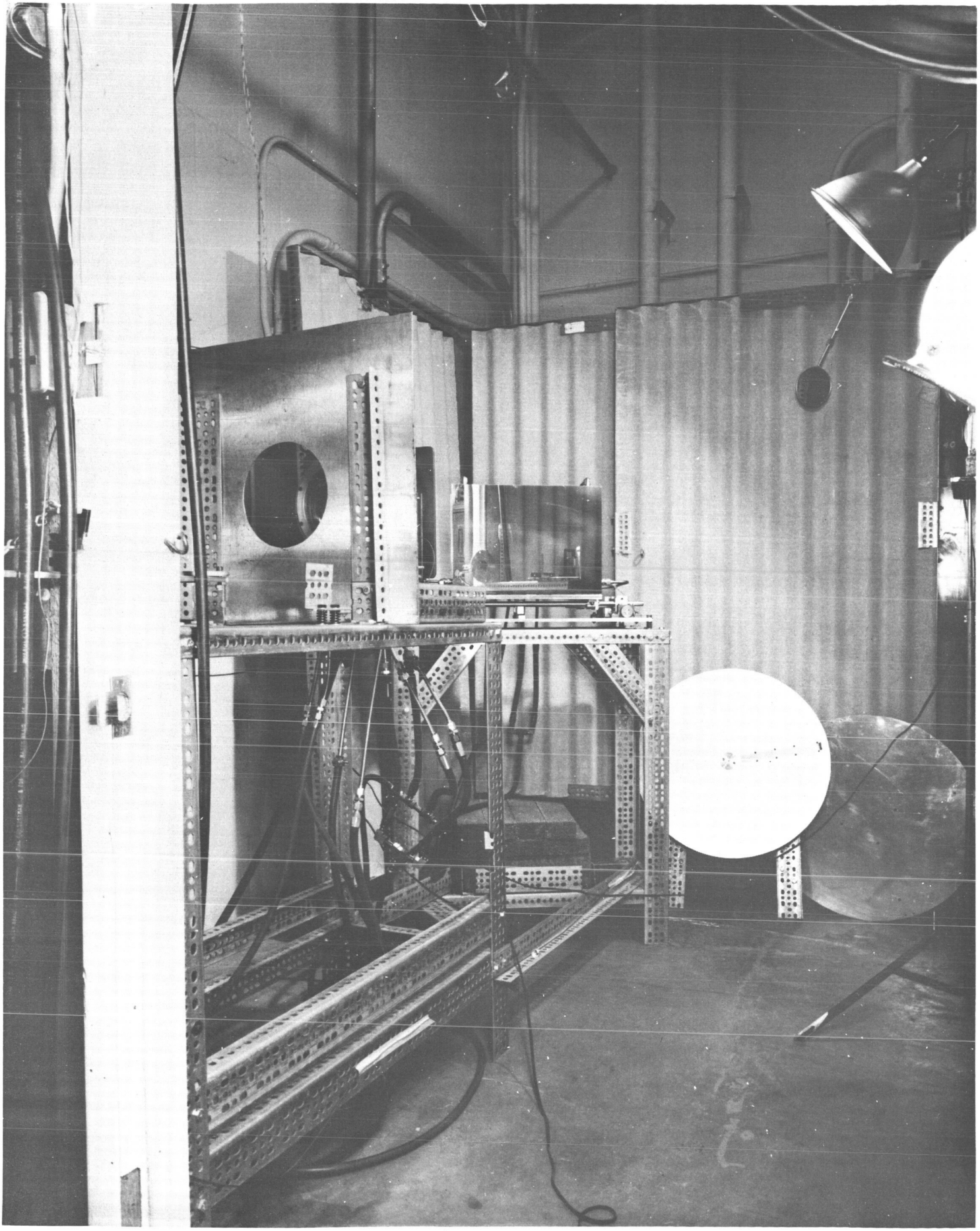


Figure 14.4 - View of Installed Folding Mirror Inside Test Enclosure

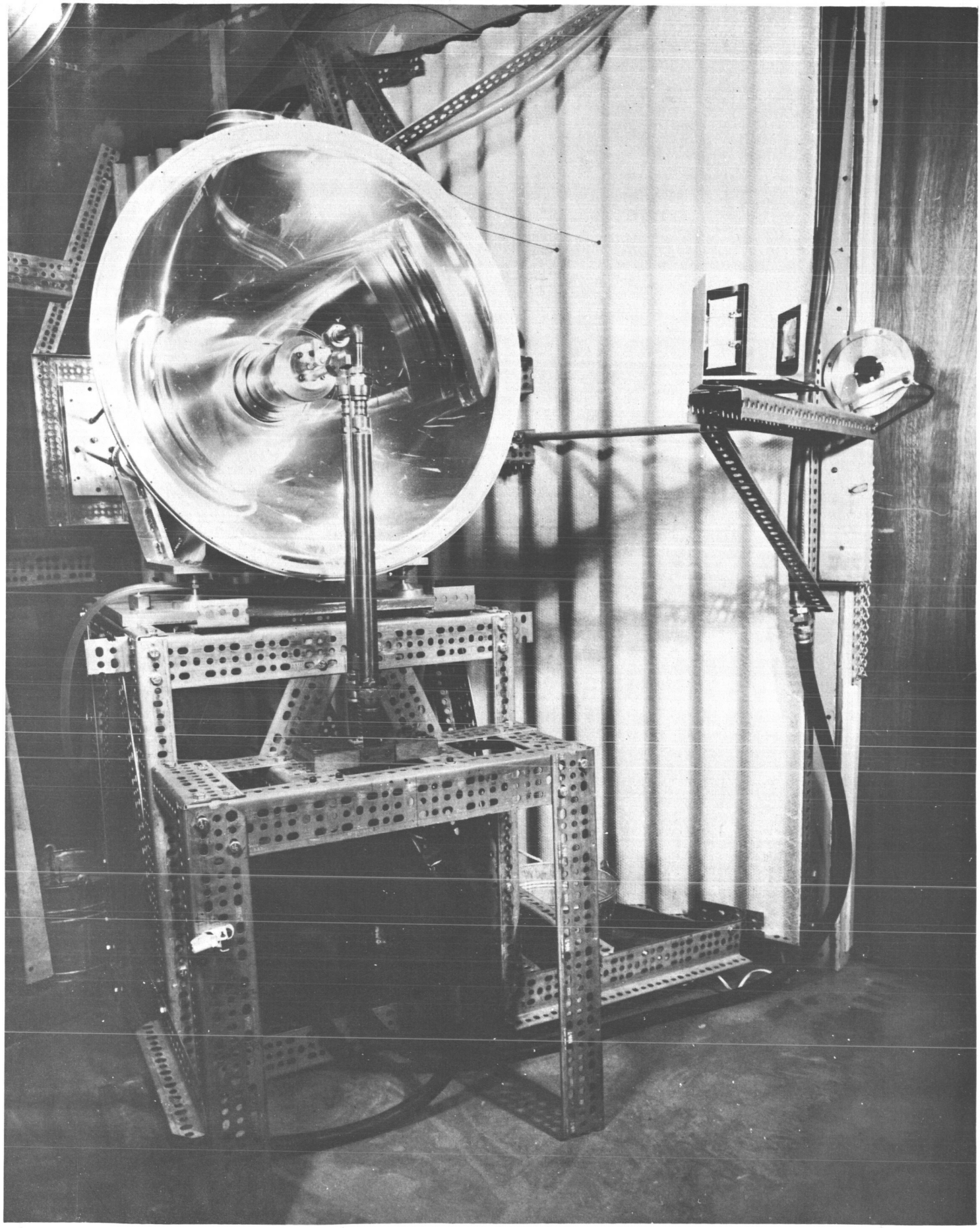


Figure 14.5 - Installed Collector in Test Enclosure Showing Monitoring Optics

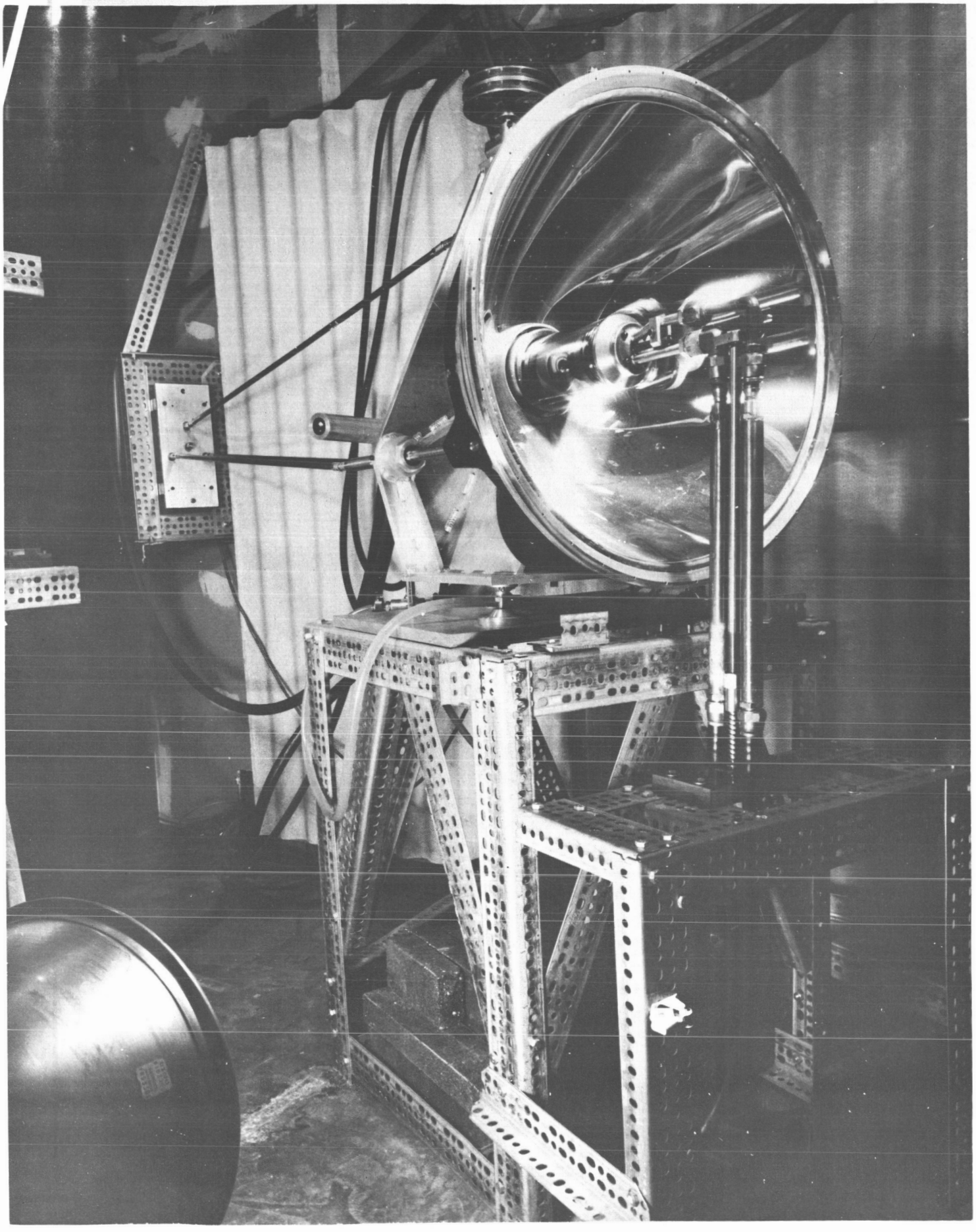


Figure 14.6 - Installed Radiation Source-Collector Assembly in Enclosure Showing Remote Alignment Provisions

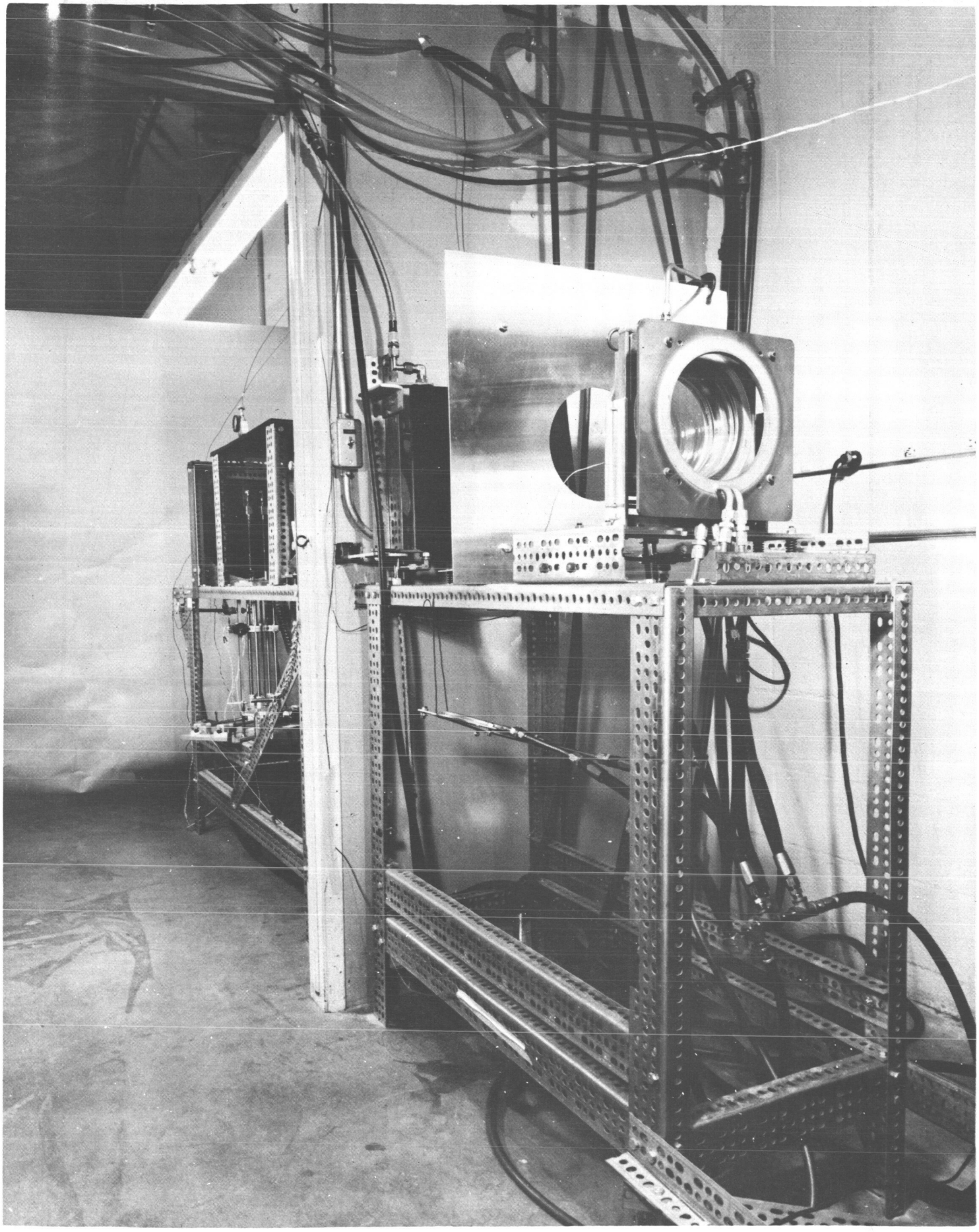


Figure 14.7 - View of Portion of Prototype Optical System from Within Test Enclosure

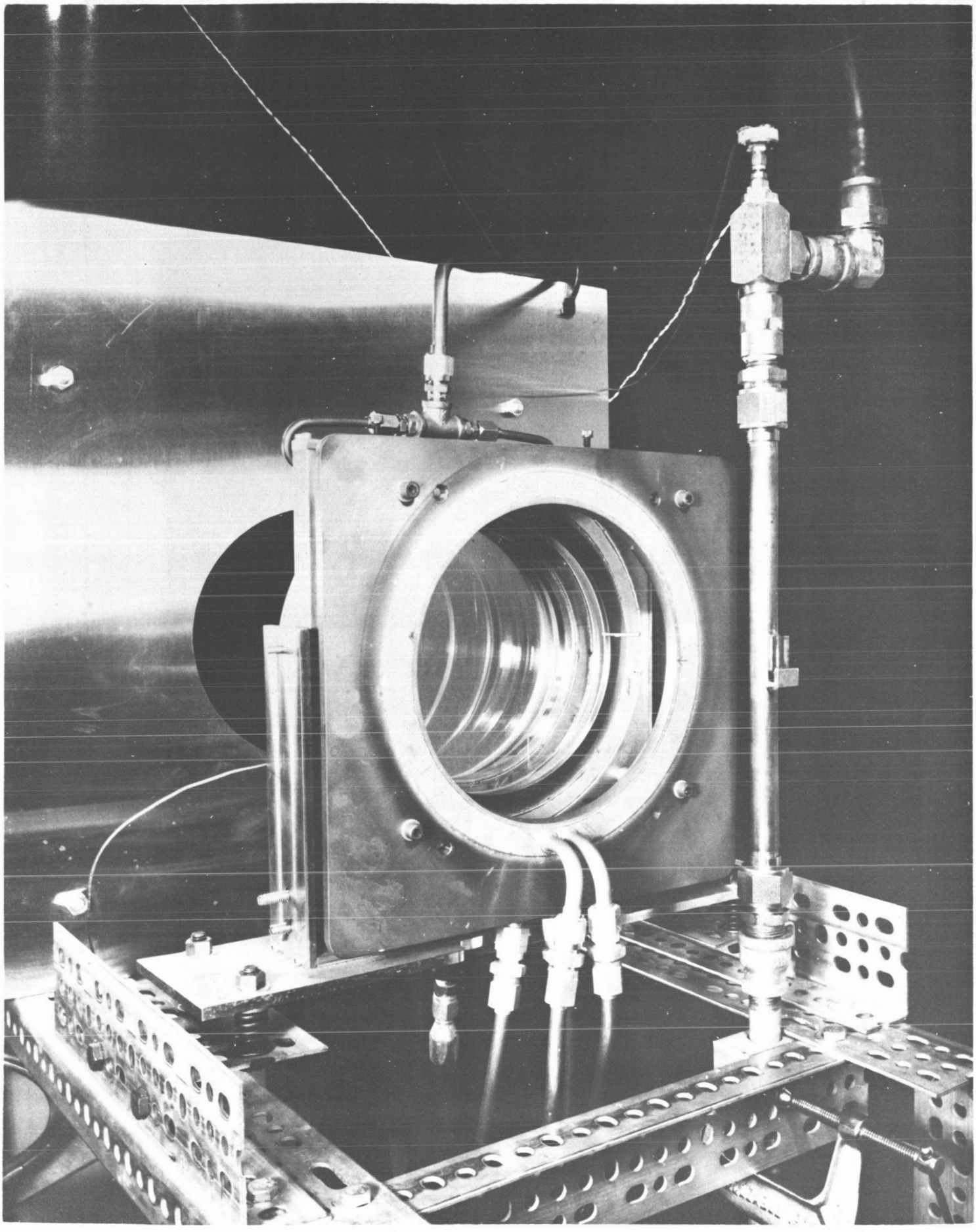


Figure 14.8 - Closeup of Installed Field Lens Assembly

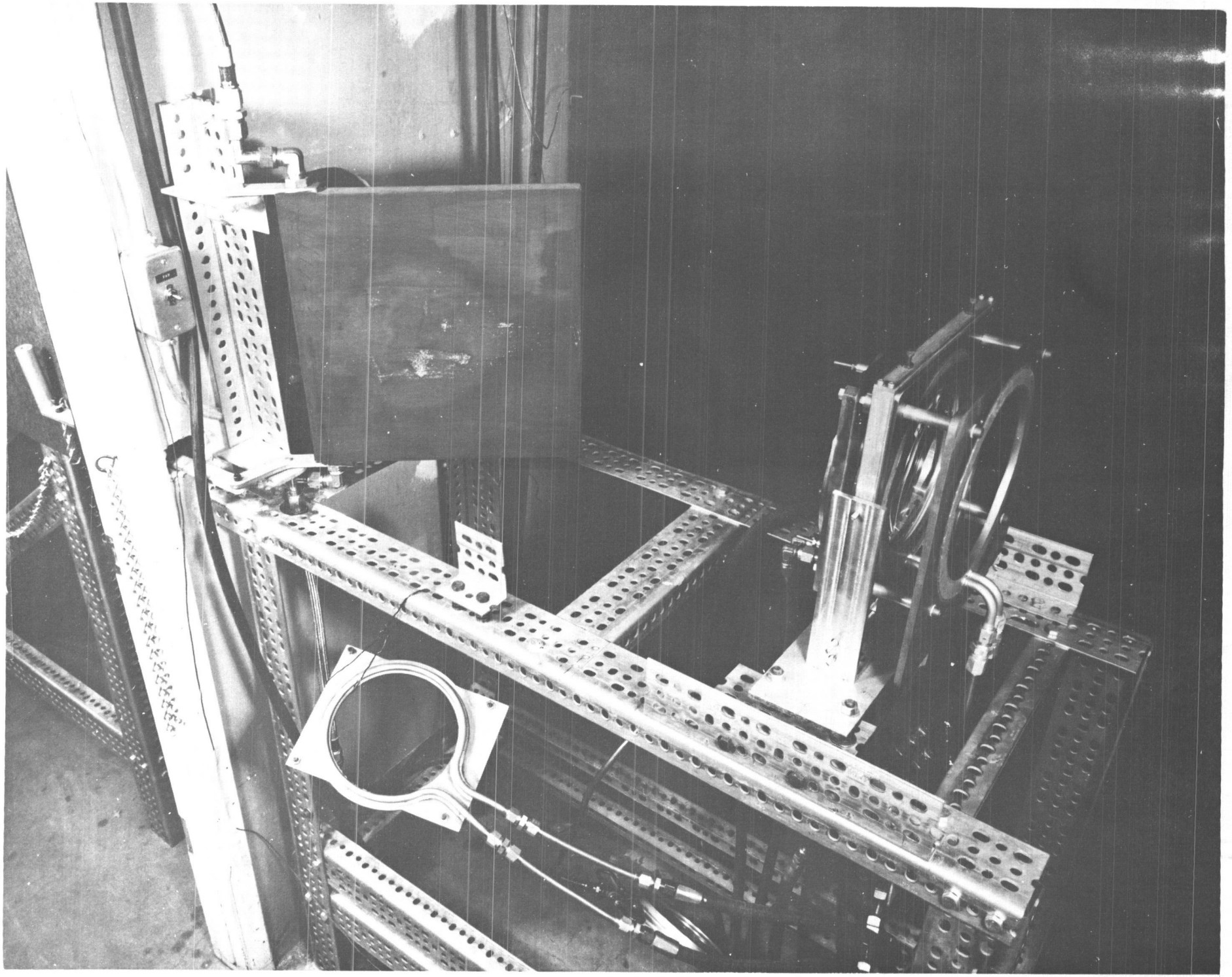


Figure 14.9 - View of Installed Field Lens-Water Cell Assembly and Douser

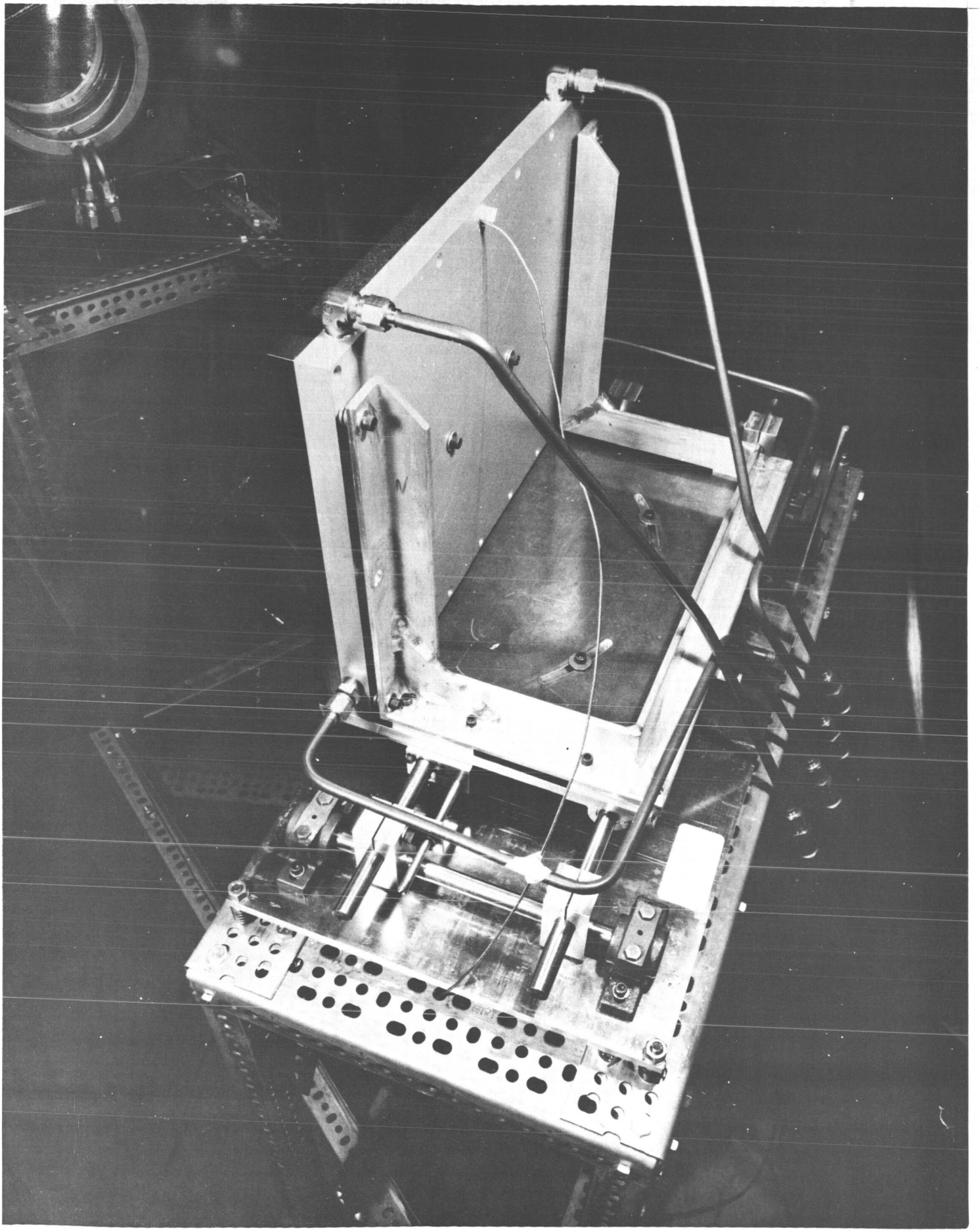


Figure 14.10 - Rear View of Installed Folding Mirror Showing Alignment Provisions

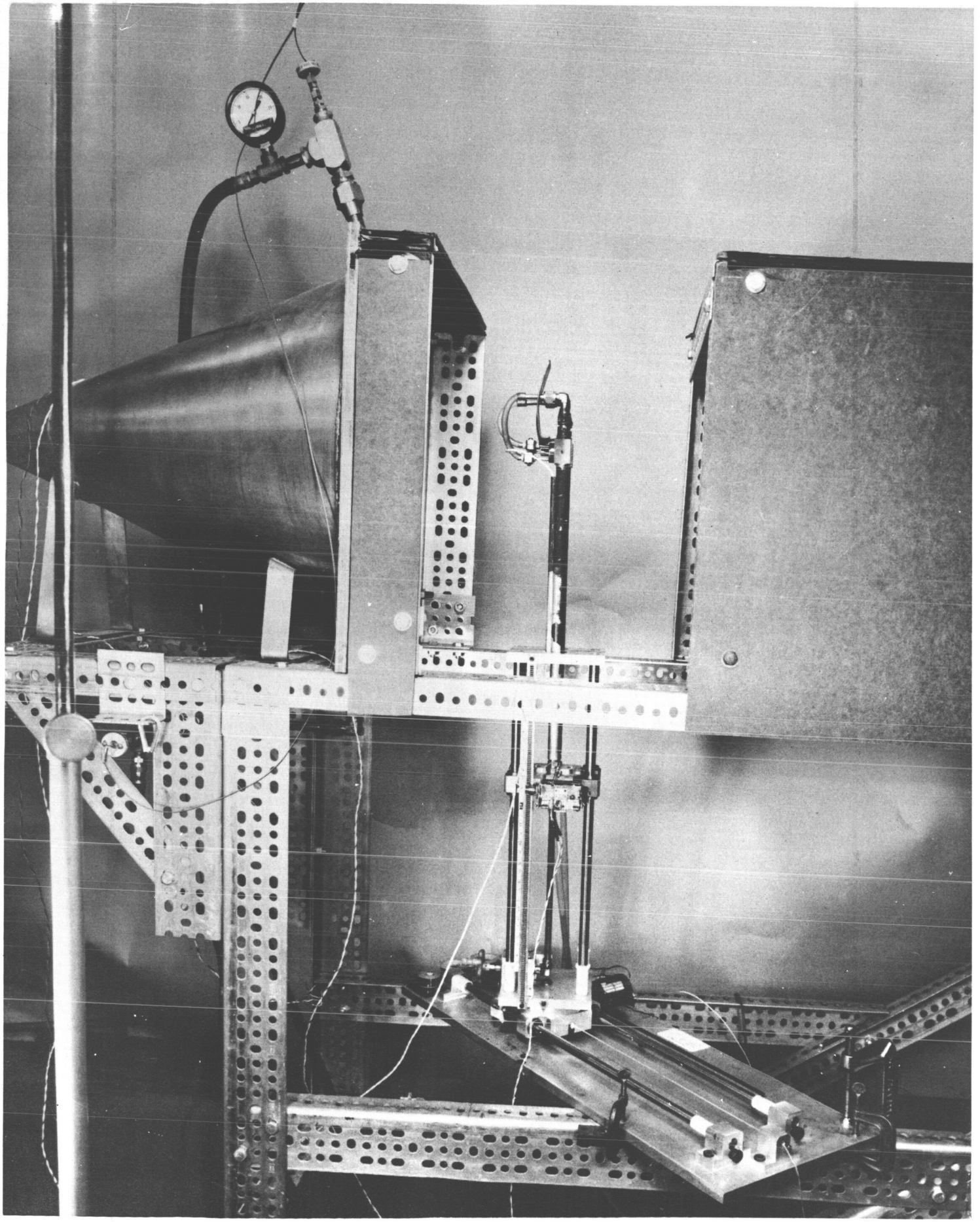


Figure 14.11 - Intensity Scanner Positioned for Target Intensity Scans

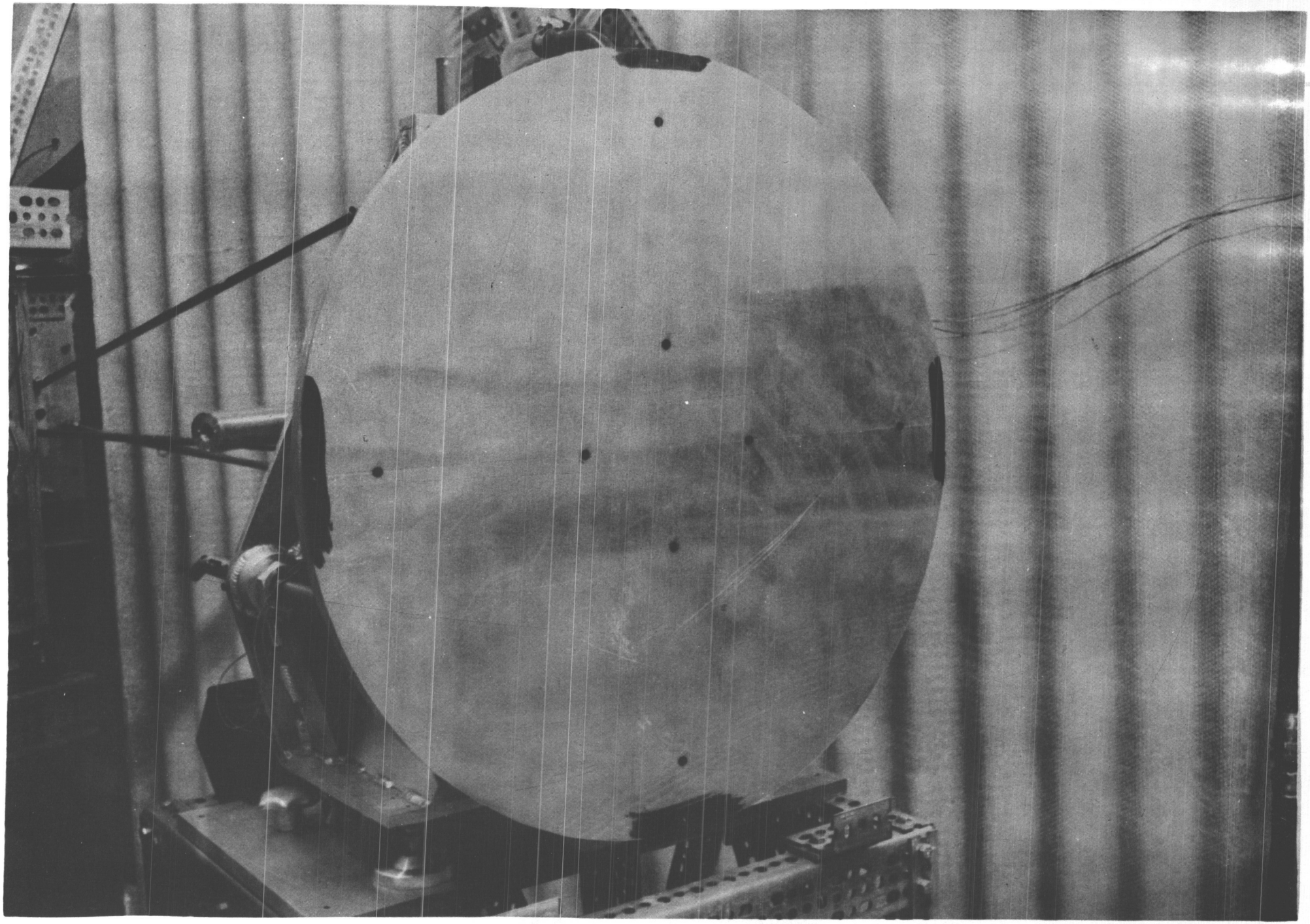


Figure 14.12 Collector alignment disk attached to collector.

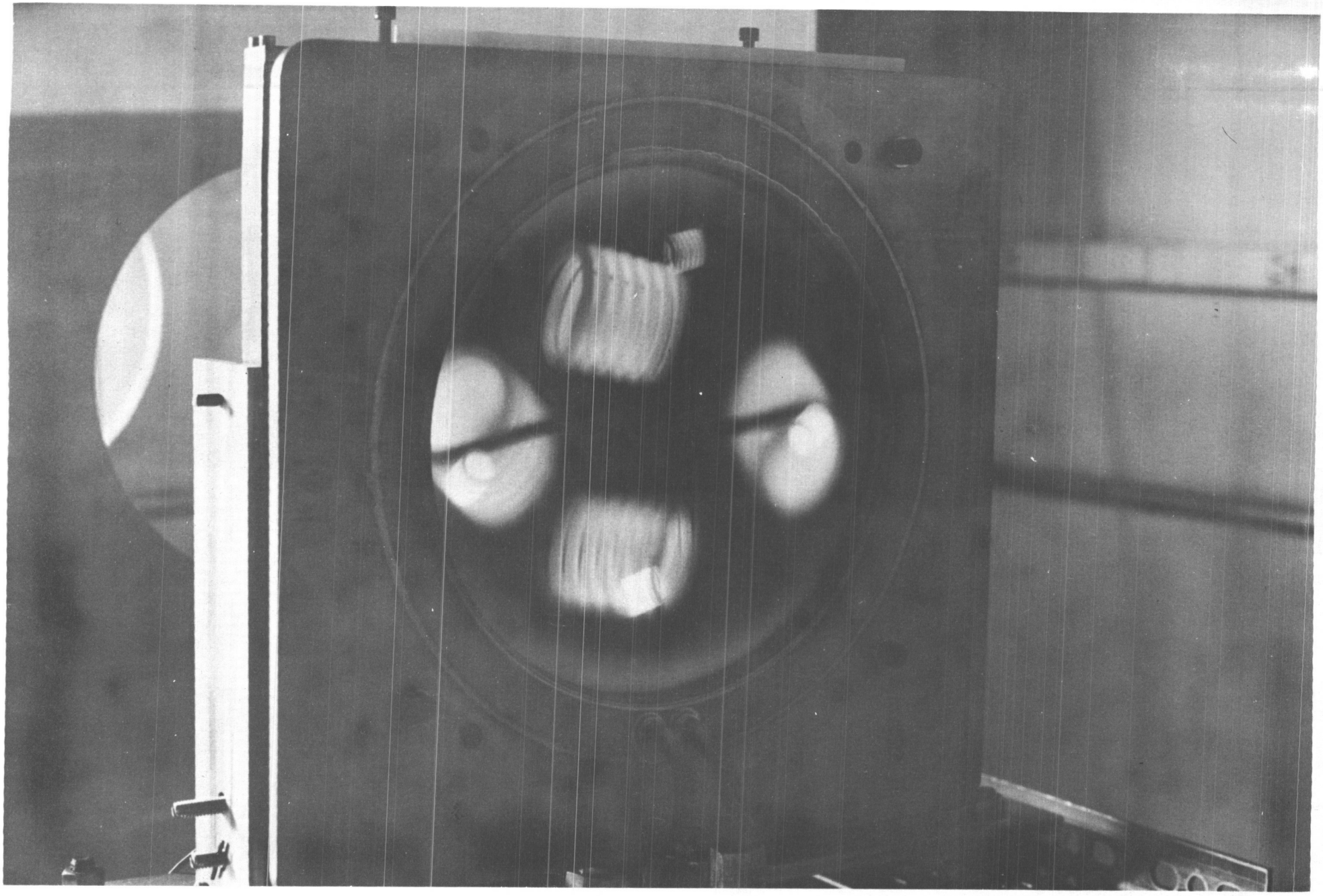


Figure 14.13 Filiment images obtained at field lens using alignment lamp in collector.

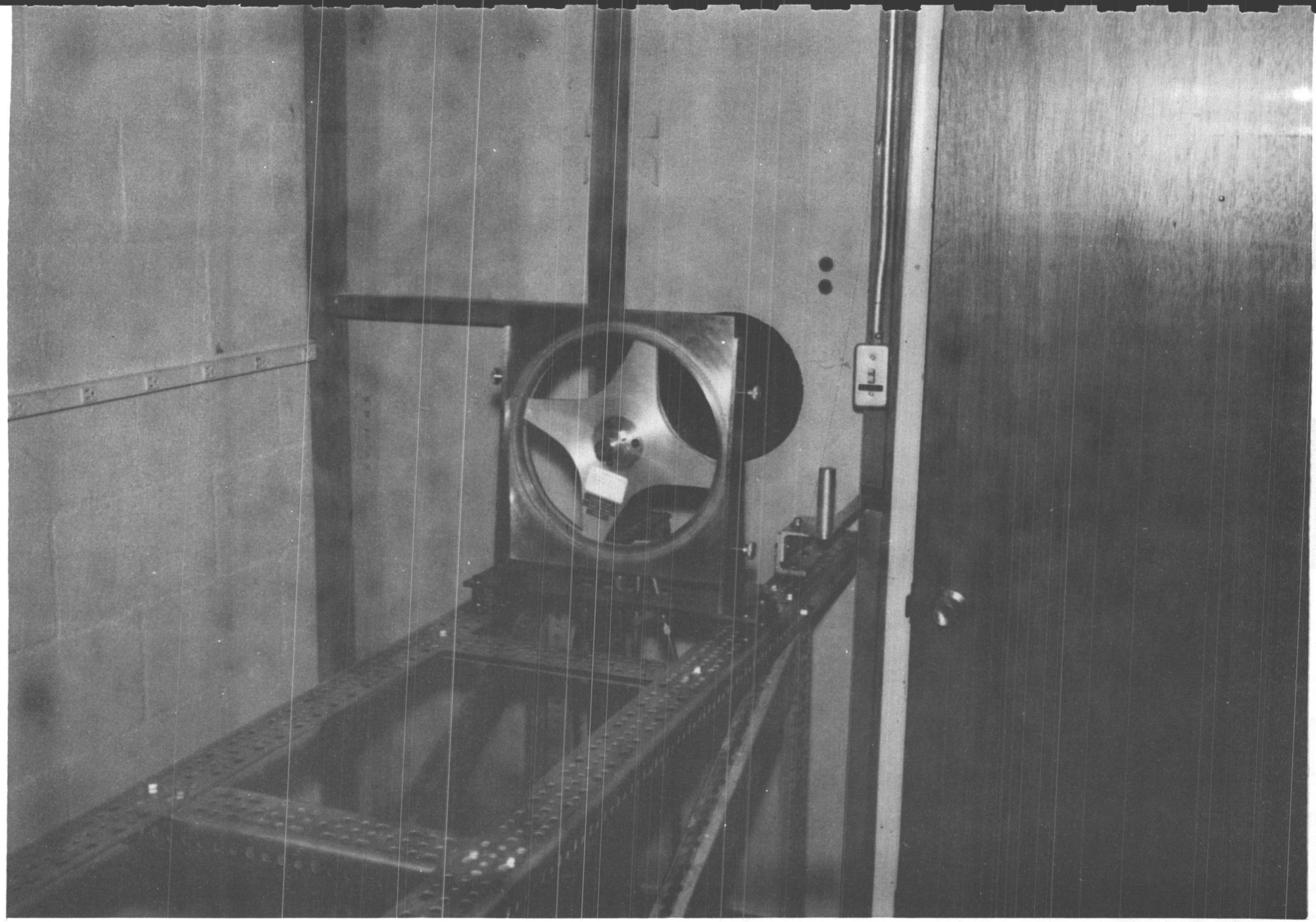


Figure 14.14 Telescope mounted in projection lens holder.

APPENDICES

SPECTROLAB

DEVELOPMENT MEMORANDUM NO. 272- 9

SUBJECT: Vacuum Seal Development Work

WRITTEN BY: John Nagle
DATE: September 29, 1964
JOB NUMBER: 6002-14

The O-ring was returned to Spectrolab by Tetraflour and on the 8th of September, testing was resumed. On the first attempt, a partial vacuum was produced in the test chamber but it was apparent that the leak rate was appreciable.

Following this test, the V-ring seal and the O-ring were removed from the test chamber and inspected. There was no apparent deformation in either the V-ring or the O-ring noted. Since the edge of the lens blank did show a degree of roughness, it was decided to deposit a .002" thickness of copper on this edge, so that the V-ring might grip the edge more securely. In the next test a vacuum of 12 mm of Mercury was obtained and a leak rate determination was made.

LEAK RATE MEASUREMENTS

The leak rate for the vacuum test lens mount was determined by means of the following method:

It was assumed that the leakage would be an isothermal process since the rate of change of pressure within the system was not excessive.

If we consider the ideal gas law,

$$P = \frac{RT}{V} \cdot n \qquad \text{where}$$

P is the pressure in mm of Mercury, T is the absolute room temperature.
V is the volume of the vacuum test mount, V = .243 liter.
n the number of gr-molecular weights of air, within the vacuum test mount and R is the universal gas constant

$$R = 62.4 \quad \frac{\text{mm of Hg - liter}}{\text{Mole-K}^\circ}$$

If there is a leak, the amount of air in moles leaking into the system will be proportioned to the time rate of change of pressure, $\frac{dn}{dt} = \left(\frac{V}{RT}\right) \frac{dp}{dt}$.

Now, the number of moles of air within the vacuum test lens mount at any time will be equal to the ratio of the total mass, m, of air to the molecular weight of air, $M_o = 29.7$ gr/mole.

$$n = \frac{m}{M_o}$$

So that $\frac{dm}{dt} = M_o \frac{dn}{dt}$.

Noting that the density of air is given by the expression

$$\rho_o = \frac{dm}{dv} = 1.29 \text{ gr./liter}$$

it follows that the leak rate in liters per second is

$$\frac{dv}{dt} = \frac{1}{\rho_o} \frac{dm}{dt}$$

Relating this leak rate back to the time rate of change of pressure, we have

$$\frac{dv}{dt} = \left(\frac{M_o}{R \rho_o}\right) \left(\frac{V}{T}\right) \frac{dp}{dt}$$

The factor $\frac{M_o}{R \rho_o}$ is evaluated as

$$\frac{M_o}{R \rho_o} = \frac{29.7}{62.4 \times 1.29} = .369$$

Since the volume of the system is V = .243 liter, the final expression for the leak rate in liter/sec is

$$\frac{dv}{dt} = .0897 \frac{1}{T} \frac{dp}{dt}$$

where dp/dt is as before, the time rate of change of pressures measured in mm of Hg per second, and T is the absolute temperature.

TABLE 1 - LEAK RATE DATA

Trial	Original Manometer Height h_o	Final Manometer Height h_o	P	Average Time t	$\frac{dp}{dt}$
1	12 mm	48 mm	36	2.50	14 mm/sec
2	28 mm	68 mm	40	1.85	22 mm/sec
3	28 mm	108 mm	80	3.55	23 mm/sec
	Temperature 24°C = 301°K				

Since the valve used to isolate the test chamber from the vacuum pump could not be closed instantaneously, the data in Trial One is not valid. Too low a rate of change of pressure is observed since the chamber was being evacuated while the valve was being closed. Trial Two and Three were made with the valve completely closed and, therefore, are significant.

MEASUREMENTS

Using the maximum value of leak rate, as measured in Trial Three, the leak rate was found to be

$$\frac{dv}{dt} = 6.9 \times 10^{-3} \text{ liter/sec.}$$

Using the conversion 1 liter/sec = 2.12 cu ft/min, the leak rate in cu. ft. per minute is

$$\frac{dv}{dt} = 1.4 \times 10^{-2} \text{ cu ft/min.}$$

Upon completion of the test, the O-ring and V-ring were removed from the test chamber and visually inspected, there was again no evidence of deformation for either ring.

PLANNED ACTIVITIES

During the next month, the test chamber will be modified to hold the single O-ring seal. Test will then be performed to determine the feasibility of the use of this seal.

SPECTROLAB

DEVELOPMENT MEMORANDUM NO. 272- 12

SUBJECT: Projection Lens Vacuum Seal Development Work

WRITTEN BY: John W. Nagle
DATE: October 27, 1964
JOB NUMBER: 6002-14

INTRODUCTION

Subsequent to the fabrication of a rigid stainless steel retaining ring, testing was resumed on the single O-ring vacuum seal.

FIRST TEST

For the first test, the 10 x 32 machine screws which hold the retaining ring in place were torqued to a value of 65 lb-in. Upon evacuation of the test chamber, a pressure of 2.5 ± .02 of Mercury was attained. Leak rate data is as follows:

$$\frac{dp}{dt} = 5.0 \text{ mm/sec} \qquad T = 297°K \qquad V = 334 \text{ cc}$$

The volume has been increased from the previously reported value as a result of a change in the manometer connection. The leak rate is calculated using the expression derived in the Development Memorandum No. 272-9, i.e.

$$\frac{dv}{dt} = .369 \left(\frac{V}{T}\right) \frac{dp}{dt}$$

The leak rate was calculated to be

$$\frac{dv}{dt} = 2.07 \times 10^{-3} \text{ liter/sec}$$

Using the conversion: 1 liter/sec = 2.12 ft^3/min, the leak rate in ft^3/min is

$$\frac{dv}{dt} = 4.39 \times 10^{-3} \text{ } ft^3/\text{min}$$

Following this test, the retaining ring was removed and inspected. It was noted that there was the anticipated flattening of the top surface of the O-ring.

SECOND TEST

For the second test, the seal was reassembled with the 10 x 32 machine screws torqued uniformly to 50 lb-in. Upon evaluation, a pressure of 2.0 $\pm$ .02 mm of Mercury was attained. Leak rate data is as follows:

$$\frac{dp}{dt} = 3.1 \text{ mm/sec} \qquad T = 297°K \qquad V = 334 \text{ cc}$$

Using the previous expression, the leak rate was calculated to be

$$\frac{dv}{dt} = 1.29 \times 10^{-3} \text{ liter/sec} = 2.73 \times 10^{-3} \text{ ft}^3/\text{min}$$

A possible explanation for the improvement noted between the first and second tests would be that in the process of removal and subsequent reassembly of the retaining ring, a more uniform distribution of the load upon the O-ring surface resulted.

PLANNED ACTIVITIES

Although further compression of the O-ring may result in improved values of the pressure and leak rate, there is also the possibility that a mutilation of the O-ring might result. Therefore, the thermal vacuum testing of the seal will be started, upon the completion of which, further tests will be performed to determine the minimum possible pressure and leak rate which may be attained at room temperature.

SPECTROLAB

DEVELOPMENT MEMORANDUM NO. 272- 13

SUBJECT: Thermopile Calibration

WRITTEN BY: Henry Lee
DATE: October 27, 1964
JOB NUMBER: 6002-60

INTRODUCTION

Two Eppley thermopiles, #6132 and #5013, were irradiated by the same light source to establish the calibration ratio between the two thermopiles.

METHODS OF CALIBRATION

Each thermopile was, in turn, mounted on an optical bench and orientated in the same manner for the calibration measurement. Spectrolab Model X-25 solar simulator was used as the calibration source. The solar simulator output beam is collimated, uniform, and closely filtered.

The half collimation angle of the beam is within $1\frac{1}{2}$ degrees and the intensity uniformity of the beam in any 1" x 1" area on the test plane is within ± 5%. The spectral distribution of the beam is within ± 10% of the N.R.L. Johnson curve in any 1000°A wavelength intervals in the range of 0.25μ to 2.7μ.

The output signal from each thermopile was amplified by a Dymec D.C. amplifier and recorded on a Moseley X-Y recorder. (See Figures 13.1 & 13.2)

Three scans were made for each thermopile with and without the beam falling on the thermopile. During the measurement, the beam intensity was monitored with a 1" x 1" solar cell module and the effect due to beam intensity fluctuation was compensated.

RESULTS

Calibration ratio of thermopile #6132 and #5013 is given in the following table.

	Eppley Thermopile #6132	Eppley Thermopile #5013
Calibration Reading (in Millivolts)	1.225 ± 0.006	1.250 ± 0.006
	1.237 ± 0.006	1.258 ± 0.006
	1.219 ± 0.006	1.268 ± 0.006
Average Reading (in Millivolts)	1.227 ± 0.006	1.259 ± 0.006
Ratio	1.000	1.026

Thermopile #5013, borrowed from NASA/Ames, is the thermopile shipped to NASA on the 10 sun simulator contract. This instrument was calibrated by Tom Bulpitt on September 20, 1963 at Table Mountain using Spectrolab's Pyrheliometer as a secondary standard. Spectrolab's Pyrheliometer had been checked against Heliotek's Pyrheliometer several days earlier and agreed within 1%. The calibration factor adopted by Tom Bulpitt for Thermopile #5013 was 4.80 $mv/w\text{-}cm^{-2}$.

Thermopile #5593, originally procured on contract NAS2-1620 was damaged and returned to Eppley for calibration. To avoid the long delivery quoted for the return of this thermopile, Spectrolab accepted delivery of Thermopile #6132 in place of the damaged instrument.

A summary of the calibration factors for these sensors are given in the table below.

Eppley Thermopile	Eppley Calibration $mv/w\text{-}cm^{-2}$	Spectrolab Calibration $mv/w\text{-}cm^{2}$
5013*	5.60	4.80*
5593	5.47	
6132**	5.24	4.68**

* This sensor with the Spectrolab calibration factor was utilized in Test Runs 1, 2, 3, and 4.

** The Spectrolab calibration factor for Sensor #6132 was obtained by utilizing the calibration ratio determined above as follows:
C.F. = 4.80/1.026 = 4.68 $mv/w\text{-}cm^{-2}$

K+E 10 X 10 TO THE INCH 358-5D
KEUFFEL & ESSER CO. MADE IN U.S.A.

5013

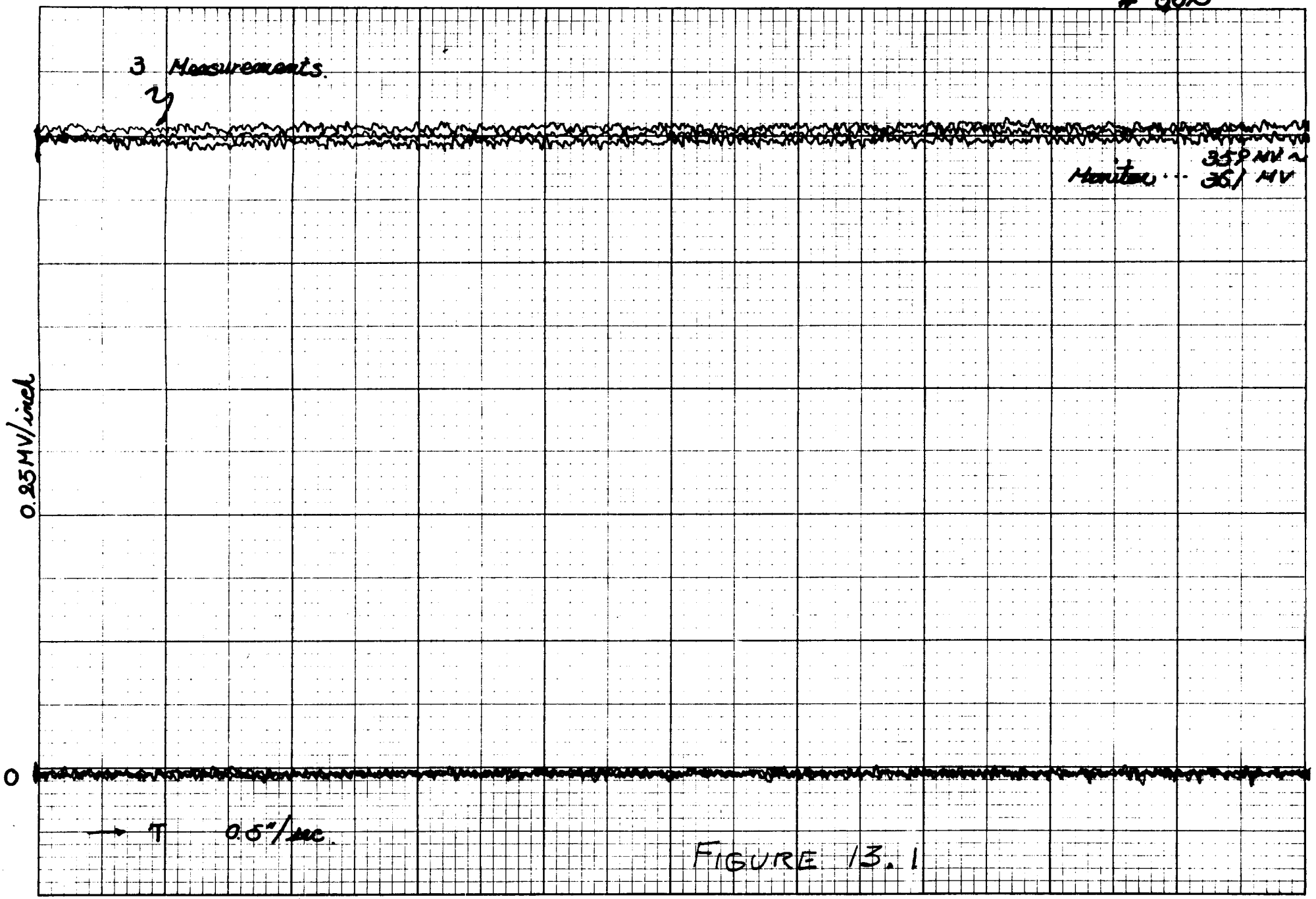


FIGURE 13.1

K+E 10 X 10 TO THE INCH 358-5D
KEUFFEL & ESSER CO. MADE IN U.S.A.

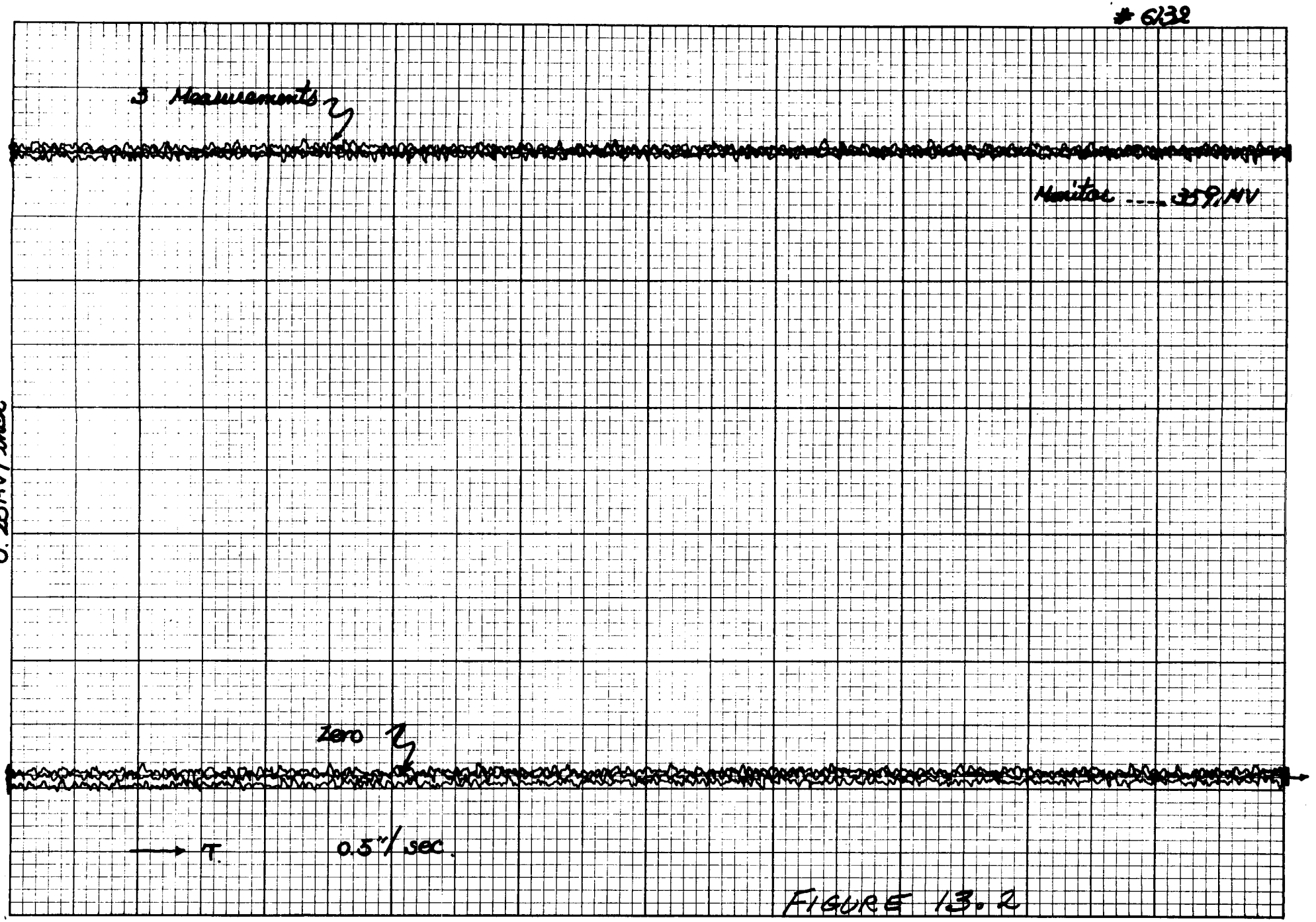


FIGURE 13.2

SPECTROLAB

DEVELOPMENT MEMORANDUM NO. 272- 15

SUBJECT: Comparison of Sensors (Test Run No. 10)

WRITTEN BY: Phil Larraburu and Wagner Schlesinger
DATE: October 29, 1964
JOB NUMBER: 6002-18

The following sensors were compared:

a. Eppley Thermopile #6132.

b. Hy-Cal Asymptotic Radiometer Model C-1300 #11146.
(The black coating of this sensor surface had been damaged by a heavy overload prior to this comparison.)

c. NASA Radlab Radiometer.

Figure 10.1 shows the test setup. The sensors were located at the following distances from the plasma arc.

Eppley - 30.08 inches
Hy-Cal - 19.77 inches
Radlab - 18.25 inches

Since the Eppley is temperature sensitive, it was water-cooled and was placed behind a water-cooled shield with a shutter which was opened momentarily in order to obtain readings. The Hy-Cal and Radlab were exposed continuously to radiation but were water-cooled.

The outputs of the Eppley and Hy-Cal were directly connected to an X-Y recorder (Moseley Model 6S). The sensors were connected alternately to the Y axis. The X axis was manually operated.

The output of the Radlab was connected to the input of a Dymec amplifier and the amplifier output was connected alternately to the X-Y recorder. Two ranges of amplification were used - X1 and X10.

The lamp was run at different power levels. Table 1 summarizes all test results, and graphs illustrating these results are attached to this report (Figures 10-2 and 10-3).

The calibration factors of the sensors are

Eppley 4.68 mv/ per w/cm^2
Hy-Cal 0.149 mv/ per w/cm^2
Radlab 0.0833 mv/ per w/cm^2 (12 $watts/cm^2$ $volt^{-1}$)

The axes of all three sensors were in the same plane normal to the axis of the arc, and were directed through the center of the arc. In this case, we can assume that the flux density per unit area will follow the "inverse square law" and the flux falling on the three instruments would vary in the following ratios:

Eppley $(30.08)^2/(30.08)^2 = 1.00$
Hy-Cal $(30.08)^2/(19.77)^2 = 2.32$
Radlab $(30.08)^2/(18.25)^2 = 2.72$

In order to compare the three sensors, an adjustment must be made for the different distances from sensor to arc. The conversion factors corrected for the distance factors above are:

Eppley $4.68 \times 1 = 4.68$ mv/w cm^{-2}
Hy-Cal $0.149 \times 2.32 = 0.345$ mv/w cm^{-2}
Radlab $0.0833 \times 2.72 = 0.226$ mv/w cm^{-2}

We can now compare the records made by the three sensors. Assume the Eppley thermopile as the reference on the point 10.2, 1000 ampere run.

The Eppley indicated a flux of $\frac{2.1}{4.68} = .449$ $watts/cm^2$

The Hy-cal indicated a flux of $\frac{.180}{.345} = .523$ watts/cm^2

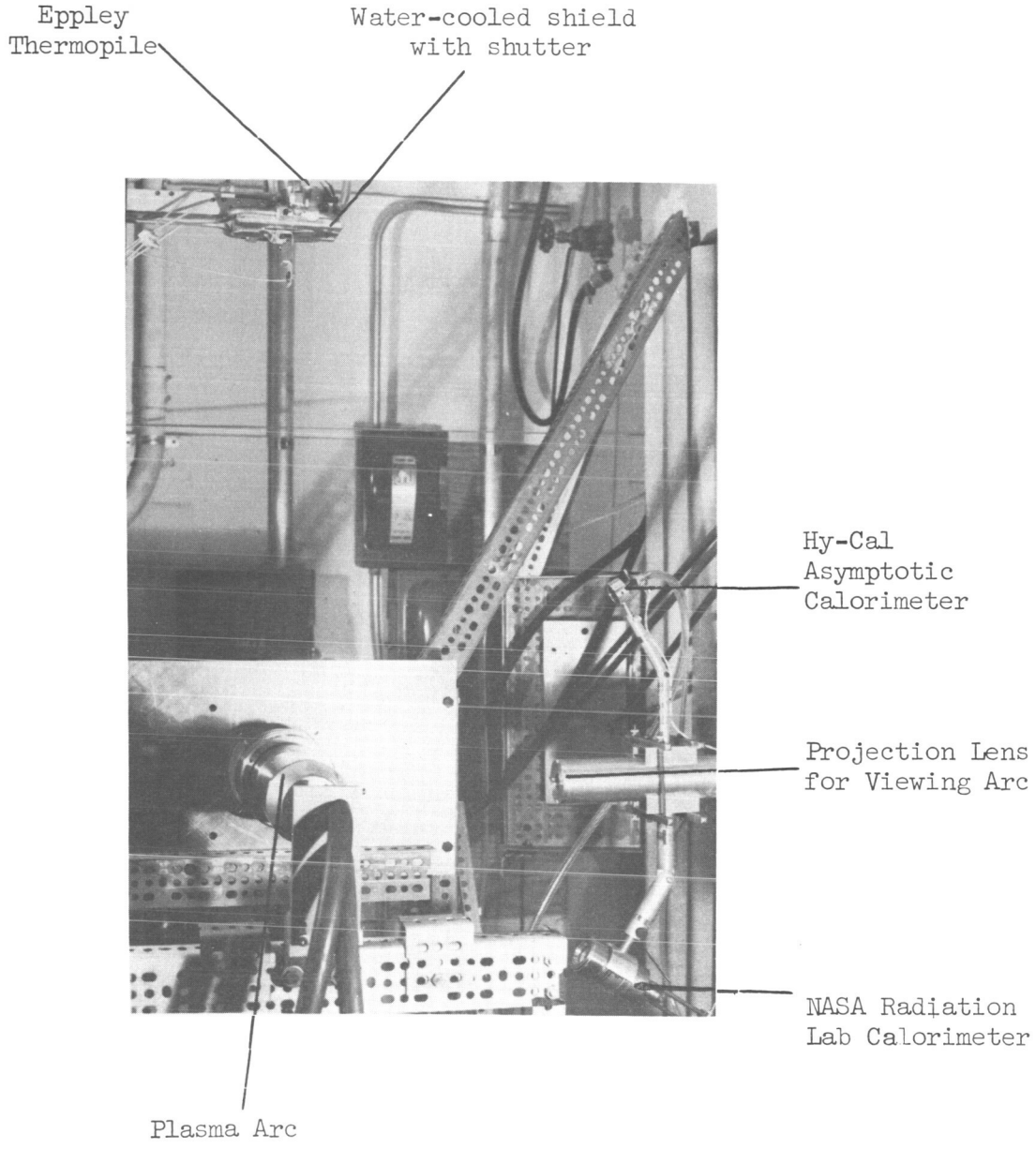
The Radlab indicated a flux of $\frac{.300}{.220} = 1.33$ watts/cm^2

Based upon these results, the Hy-cal reads 16.5% higher than the Eppley for the same flux density.

The Radlab indicated approximately twice the intensity as the Eppley although there is strong reason to suspect the readings recorded for the Radlab radiometer. The voltage signal from this radiometer failed to drop, as expected, after the radiation source was extinguished. The only additional instrumentation utilized with this sensor was the Dymec amplifier and its performance was checked the following work day and was found to be operating satisfactorily. Malfunction of the instrumentation or sensor seems to be indicated.

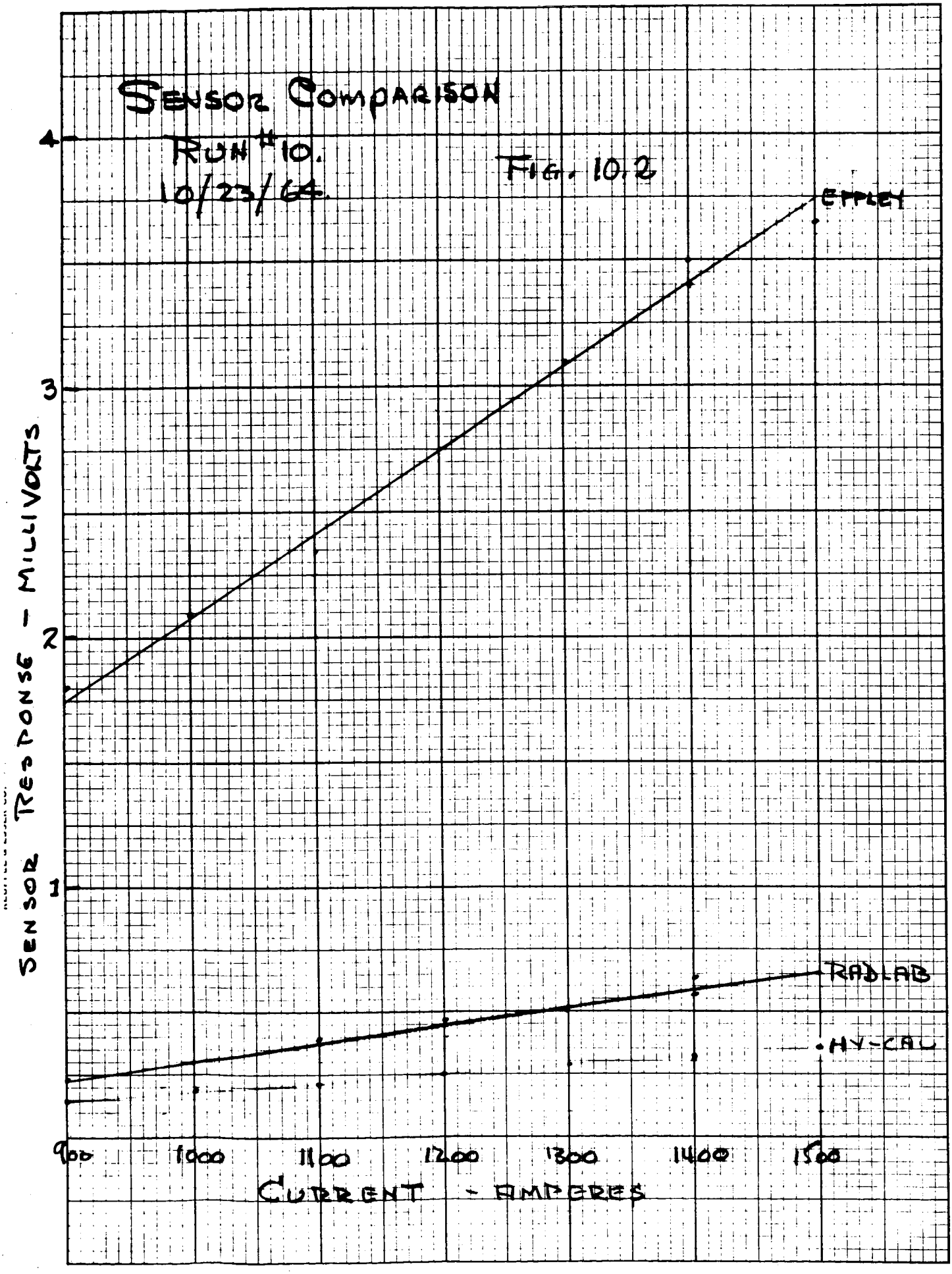
Lamp Current (Amp)	Output - Actual MV			Computed Watts/cm^2 at 30.08 Inches		
	Eppley	Hy-Cal	Radlab	Eppley	Hy-Cal	Radlab
900	1.80	.150	.230	.384	.435	1.05
1000	2.10	.180	.300	.448	.523	1.33
1100	2.35	.210	.390	.502	.608	1.73
1200	2.75	.250	.465	.481	.725	2.07
1300	3.10	.280	.510	.663	.81	2.27
1400	3.50	.320	.630	.746	.926	2.79
1400	3.40	.310	.560	.725	.900	2.48
1500	3.65	.350	.660	.778	1.02	2.93

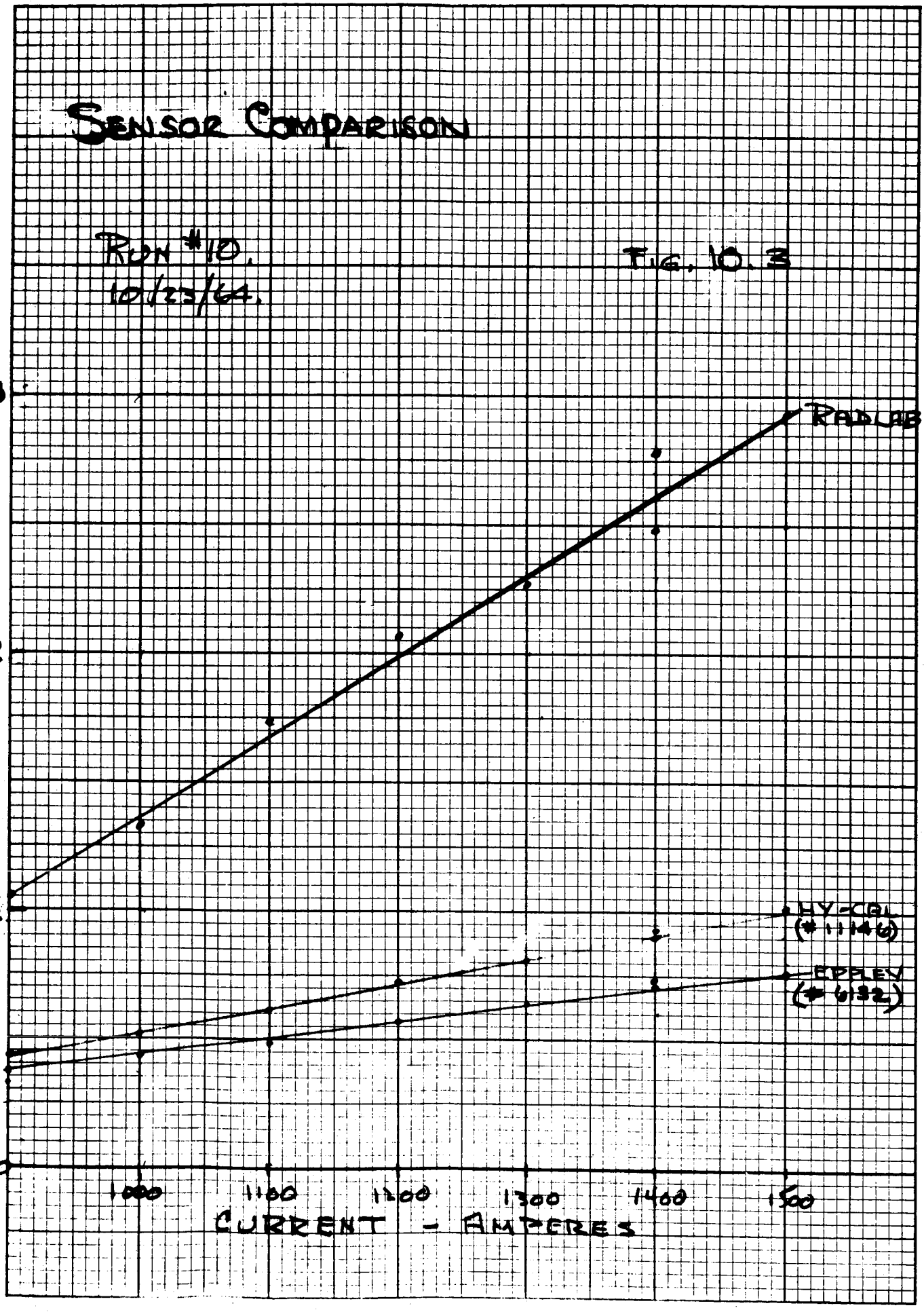
TABLE 1



SENSOR COMPARISON
TEST SET-UP

Figure 10.1


SENSOR COMPARISON
RUN # 10.
10/23/64.
FIG. 10.2
EPPLEY
RADLAB
HY-CAL
SENSOR RESPONSE - MILLIVOLTS
4
3
2
1
900
1000
1100
1200
1300
1400
1500
CURRENT - AMPERES


SENSOR COMPARISON
RUN #10.
10/23/64.
FIG. 10.3
FLUX DENSITY — WATTS/CM² AT 30.00 INCHES
3
2
1
0
RADLAB
HY-CAL (#1146)
EPPLEY (#6132)
1000
1100
1200
1300
1400
1500
CURRENT - AMPERES

SPECTROLAB

DEVELOPMENT MEMORANDUM NO. 272-18

SUBJECT : Prototype Evaluation Testing, Runs 5 through 9

WRITTEN BY: Phil Larraburu and Wagner Schlesinger
DATE : November 2, 1964
JOB NUMBER: 6002-45

INTRODUCTION

The primary purpose of these tests was to obtain sufficient performance data of the combined prototype radiation source-optical system in order to predict the performance of the radiative heating system utilizing the present system design. Source performance data accumulated during these tests are presented in Development Memorandum No. 272-16.

SUMMARY OF TESTS PERFORMED

The tests performed in this prototype evaluation test program included the following:

a. Determination of intensity distribution at the projection plane of the optical system utilizing a 6" and a 7" clear aperture at the field lens.

b. Determination of the intensity distribution at the target plane utilizing 6" and 7" clear apertures at the field lens.

c. Determination of intensity distribution at translated target plane positions utilizing a 7" clear aperture at the field lens.

d. Determination of the intensity distribution across the minor axis of the target plane (as viewed from the projection lens) as a function of source current utilizing a 7" clear aperture at the field lens.

Table 1 provides the correlation between test run number and the test performed. Figures 1 and 2 define the projection plane and target plane.

DESCRIPTION OF EQUIPMENT

Figure 3 shows a picture of the field lens assembly, projection lens assembly, douser, and a portion of the radiation source collector assembly. A picture of the radiation source and the collector assembly is presented in Figure 4. The remote control rods for aligning the collector to the radiation source are also seen in this picture. Figure 5 shows the picture of the uniformity scanner positioned for a target intensity distribution test. Also shown in this picture is the water cooled back stop which can be used as a black body calorimeter when properly monitored. A separate picture of the uniformity scanner is given in Figure 6. The sensor mounted on the water cooled extension arms of the uniformity scanner is the Hy-Cal circular foil radiometer Number 11146 which was utilized for these test runs. (The theory of operation for sensors of this type is described in JOSA, May 1953, page 366 - "An Instrument for the Direct Measurement of Intense Thermal Radiation" by Robert Gardon.) In this memorandum, the longitudinal axis and the vertical axis are referred to as the X and Y axes respectively. During all scans, the voltage of the battery biased potentiometer utilized for a position indicator on the X axis was connected to the X input of an X-Y recorder and the output of the Hy-Cal radiometer was connected directly to the Y input of the recorder.

PRELIMINARY ALIGNMENT

With the uniformity scanner positioned for a projection plane scan, the alignment telescope was placed in the lamp holder and used to locate the optical axis in the target zone and, hence, the center of the projection plane and target plane. The optical axis was then utilized as the origin of the sensor coordinates. Previous to locating the optical axis in the target zone, the collector had been aligned utilizing a dummy lamp in an attempt to position the collector so that its axis would be collinear with the radiation source.

FINAL COLLECTOR ALIGNMENT

The final alignment procedure is based on the following concept: If the collector axis is collinear with the arc, it should then produce at the projection plane an intensity pattern which is symmetrical with respect to the center of

the projection plane and should give circular iso-flux density lines. In Figure 7, the scanning technique utilized for scanning the projection or target plane is illustrated. If the collector is aligned with respect to the Y axis, a scan along the X axis will produce a symmetrical scan with the peak centered at X = 0. On the other hand, scans along $X_2(Y=2)$ and $X_{-2}(Y=-2)$ should result in intensity profiles which are superimposable if we have symmetry about the X axis.

TEST RESULTS

In Test Run 5.1 and a portion of Run 5.2, projection plane scans were made in conjunction with collector alignment adjustments. When the alignment was deemed satisfactory, the collector was focused. This was achieved by moving the collector back and forth along the optical axis until the intensity readings along the edge of the 4 inch diameter projection plane were maximum. The test was conducted with a 6" clear aperture mask at the field lens. The reduced data from this scan is presented in Figure 8. It shows that the highest iso-intensity lines are not perfectly centered with respect to the X axis. This indicates either slight mis-alignment of collector or collector distortion. It is believed that the method utilized to attach the cooling jacket to the collector resulted in a small amount of distortion to collector.

In Test Run 5.3, a target plane intensity distribution scan was made. For this test, the uniformity scanner is rotated 51° about the Y axis. The sensor is rotated so that it remains parallel to the optical axis. This is accomplished in order to avoid the problem of accurately determining the angular absorptivity of the sensor surface. Intensities obtained in this manner were reduced by the area factor which equals the cosine of 51°. The data taken in Run 5.3 are presented in Figure 9.

No data were obtained in Test Run 6 due to system problems. (See DM 272-16) In Run 7.1, an effort to improve the collector alignment was made. With a 7" clear aperture at the field lens, a projection plane scan was accomplished. The data from this scan are presented in Figure 10.

In Run 8.1, a target scan was completed with the 7" clear aperture at the field lens. The reduced data for this scan are given in Figure 11. In Runs 8.2 and

8.4, target intensity scans were obtained after translating the uniformity scanner from d = 38.16 to d = 40.22 and 42.28 respectively. These two tests were performed in order to obtain information regarding the optical system design and may aid in the eventual selection of projection plane location relative to target plane.

Target intensity distribution data as a function of source currents were obtained in Test Run 9. A diameter scan on the X axis was obtained for current levels of 900 amps through 1550 amps. A plot of these intensity scans is presented in Figure 12.

TARGET INTENSITY DISTRIBUTION FOR 14 LAMPS

It is assumed that the target intensity distribution from each optical system in the radiative heating system is characterized by the distribution presented in Figure 11 obtained from Run 8.1 test data. To obtain the intensity distribution that would result from a 14 lamp system, it is necessary to superimpose the intensity distribution 14 times with the proper angular displacements. The following method was used.

The Y axis of the target plane for each optical system makes an angle of 360/14 degrees or nearly 26° with the Y axis of the adjacent optical system. The 14 Y axes separated by this angle are shown in Figure 13. Point 1, radius 1, can be considered to be on the Y axis of lamp 1 which is 26° from the Y axis of lamp 2, and 2 x 26° from the Y axis of lamp 3, etc. Hence, the total intensity at point 1, radius 1 will be the sum of the intensities at point 1 radius 1, point 1 radius 2, point 1 radius 3 and so on for all fourteen radii. In other words, by making a summation for a point, we obtain the flux density for 14 points which fall on the same diameter. A similar procedure will give the total intensity for 14 lamps at any specified point on all 14 radii.

Figure 14 shows the computed iso-flux density lines representing the summation, by the above method, of a 14 lamp system utilizing the intensity distribution presented in Figure 11. The intensity profile of this distribution is given in Figure 15.

PREDICTED PERFORMANCE OF RADIATIVE HEATING SYSTEM

To predict the performance of the radiative heating system based upon 14 lamps and operation at higher current levels, the relationship between the average edge intensity as a function of current is required. The target diameter intensity distribution data obtained in Run 9 as presented in Figure 12 are utilized in obtaining extrapolation factors which, in turn, can be applied to the performance data resulting from Run 8.1. From Figure 12, the average target edge intensities were tabulated and then normalized about the edge intensity obtained in the 1,000 amp run, resulting in the extrapolation factors. The validity of such a method is based upon the assumption that the relative target intensity distribution does not vary with source current. A rough check of this assumption was made taking the ratio of the peak and average edge intensity from Figure 12. These ratios varied between 1.532 and 1.618 in a random manner. It was thus concluded that the relative intensity distribution does not change significantly with source current and that the method used to obtain the extrapolation factors is valid. Table 2 shows the tabulation of the extrapolation factors obtained from Test Run 9. Utilizing these extrapolation factors and the current and source voltage data obtained in Run 9 with the average edge and peak intensities obtained in Run 8.1 at 1,000 amps, the edge and peak intensities associated with the other current levels were calculated and tabulated in Table 2. Figure 16 shows the edge and peak intensities plotted as a function of current. It must be recognized, however, that these runs were not made with the uniformity water cell in place. This water cell will reduce the target intensity by approximately 22%. Also, in subsequent tests to compare the Eppley thermopile with the Hy-Cal sensor, it was found that the Hy-Cal radiometer indicated significantly higher intensities than the Eppley on the order of approximately 13% to 30%. If further investigations indicate that the Eppley represents the more accurate indication of intensity, then the results that have been presented in this Development Memorandum will have to be reduced.

TABLE 1 - PARAMETERS FOR TEST RUNS 5 - 9

Point No.	Current Amp	Total Voltage	Gas Pressure	Distance d(inches)	Angle α	Clear Aperture Baffle	Test Performed
5.2	1000	82.1	250	38.16	0°	6"	Projection Plane
5.3	1000	82.1	250	38.16	51°	6"	Target Plane Scan
7.2	1000	80.9	250	38.16	0°	7"	Projection Plane
8.1	1000	81.2	250	38.16	51°	7"	Target Plane Scan
8.2	1000	81.2	250	40.22	51°	7"	Target Plane Scan
8.4	1000	83.7	252	42.28	51°	7"	Target Plane Scan
9.1	900	81.4	250	38.16	51°	7"	Diameter Scan
9.2	1000	83.3	252	38.16	51°	7"	Diameter Scan
9.3	1100	87.2	248	38.16	51°	7"	Diameter Scan
9.4	1200	89.7	247	38.16	51°	7"	Diameter Scan
9.5	1300	94.1	250	38.16	51°	7"	Diameter Scan
9.6	1400	97.6	250	38.16	51°	7"	Diameter Scan
9.7	1450	100.3	252	38.16	51°	7"	Diameter Scan
9.8	1500	101.6	252	38.16	51°	7"	Diameter Scan
9.9	1550	103.6	254	38.16	51°	7"	Diameter Scan

From Run 8.1 at 1000 amps at 250 psi, the average
Peak Intensity = 5.77 inches (recorder deflection)
Edge Intensity = 3.167 inches (recorder deflection)
Scale Factor = 2 mv/inch
Calibration Factor = .19 mv/Btu-ft^{-2}-sec^{-1} (Absorbed)
Absorptivity Factor = .89
Area Correction Factor = Cos 51° = .63

Average Edge Intensity = 23.59 Btu/ft^2-sec (one lamp) = 330 Btu/ft^2-sec (14 lamps)

Average Peak Intensity = 42.98 Btu/ft^2-sec (one lamp) = 601.72 Btu/ft^2-sec (14 lamps)

	(1)	(2)	(3)	(4)	(5)	(6)	(7)	(8)	(9)
Test Point	Current	Total Voltage	Source Voltage	Relative Edge Intensity Run 9	Relative Peak Intensity Run 9	Ratio (5)/(4)	Extrapolation Factor (4) Normalized	Ave. Edge Intensity (7) Times 330.26 (Btu/ft^2-sec)	Ave. Peak Intensity (7) Times 601.72 (Btu/ft^2-sec)
9.1	900	81.4	69.1	32.1	49.2	1.532	.838	276.8	504.2
9.2	1000	83.3	69.5	38.3	59.3	1.540	1	330.26	601.72
9.3	1100	87.2	71.8	45.0	72.8	1.618	1.175	388.1	707.0
9.4	1200	89.7	72.7	51.5	81.5	1.582	1.345	444.3	809.3
9.5	1300	94.1	75.6	60.6	96.1	1.585	1.582	522.5	951.9
9.6	1400	97.6	77.5	68.6	108.0	1.574	1.791	591.6	1077.7
9.7	1450	100.3	79.4	76.3	118.5	1.553	1.992	658.0	1198.6
9.8	1500	101.6	80.0	78.3	122.3	1.561	2.044	675.1	1230
9.9	1550	103.6	81.2	81.3	129.2	1.589	2.122	700.9	1277

Table 2
Extrapolated Performance Tabulation
14 Lamp System

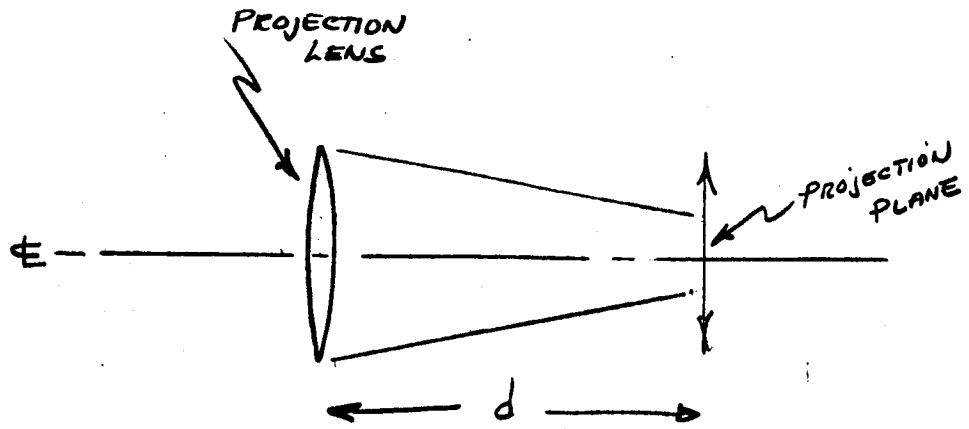


FIGURE 1

PROJECTION PLANE SCAN CONFIGURATION

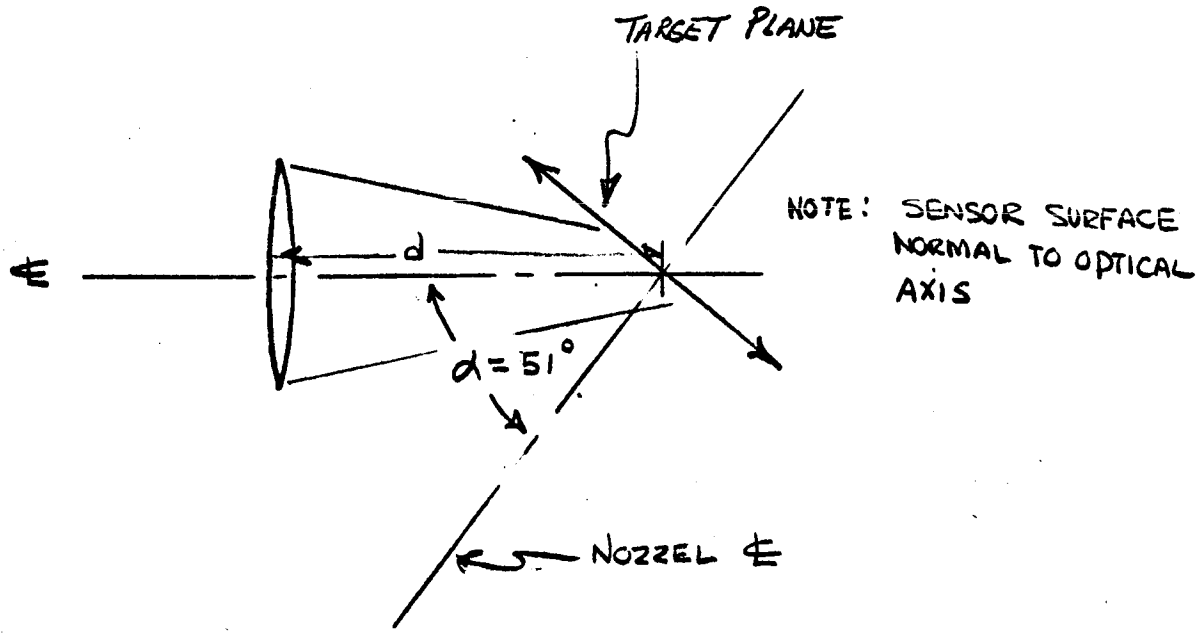


FIGURE 2

TARGET PLANE SCAN CONFIGURATION

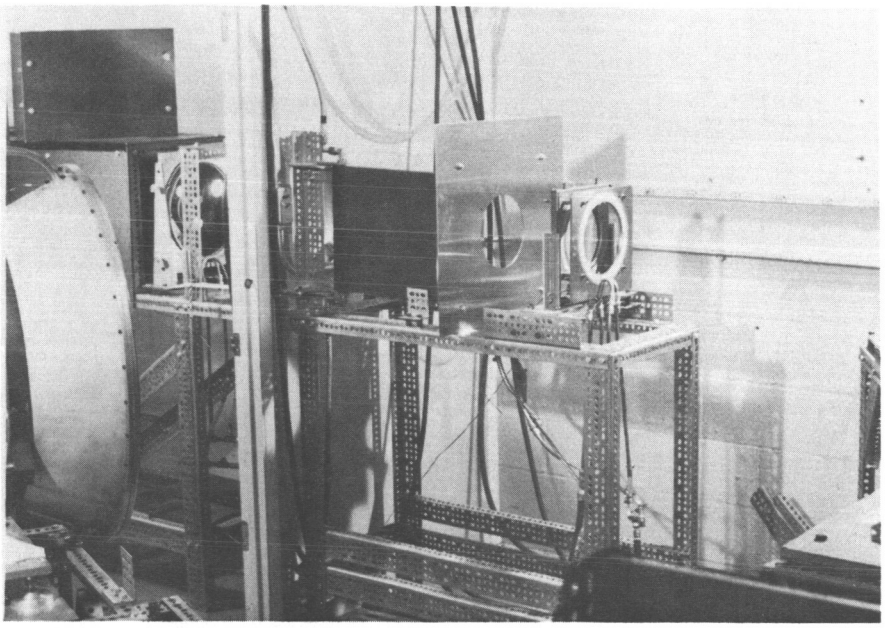


Figure 3 - Prototype System Components

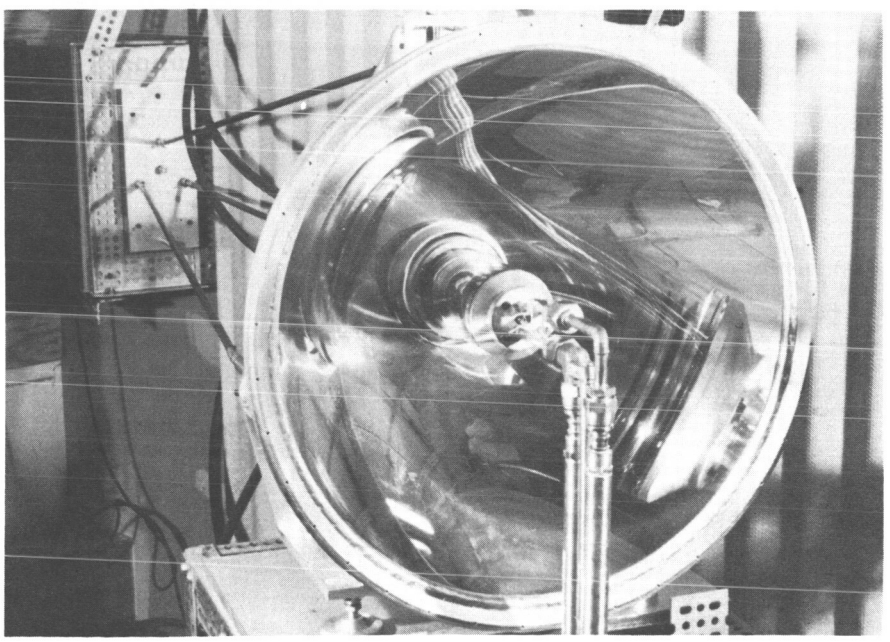


Figure 4 - Radiation Source - Collector Assembly

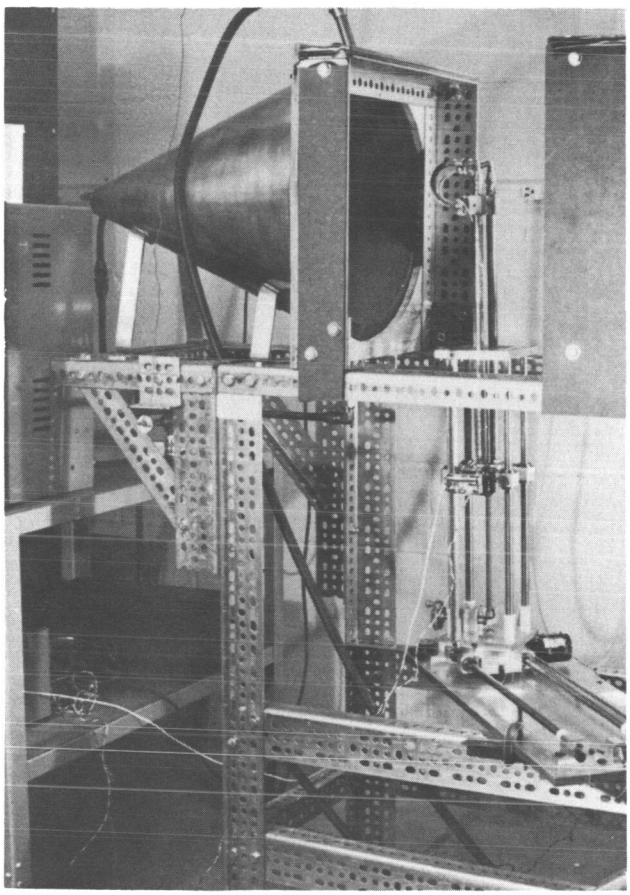


Figure 5 - Uniformity Scanner and Watercooled Back Stop

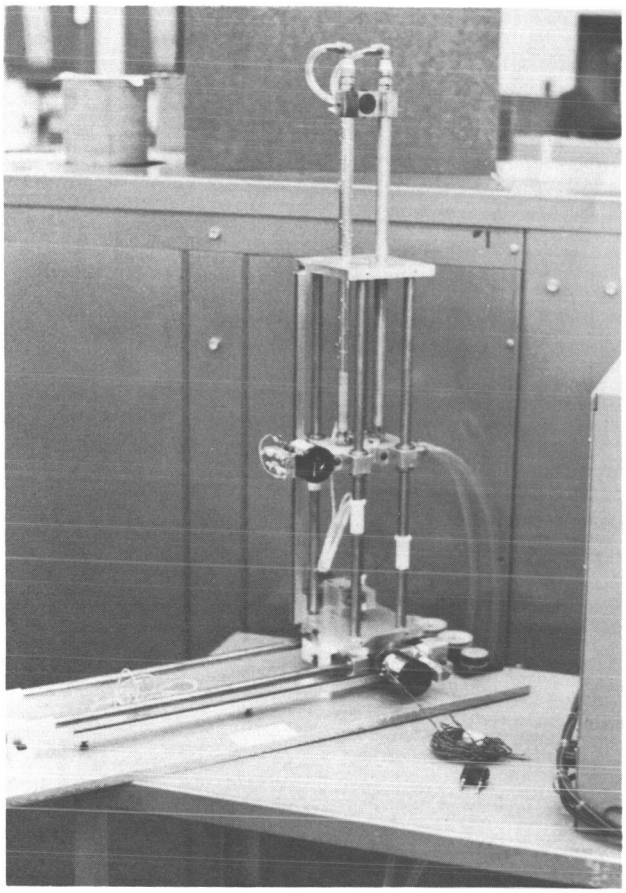
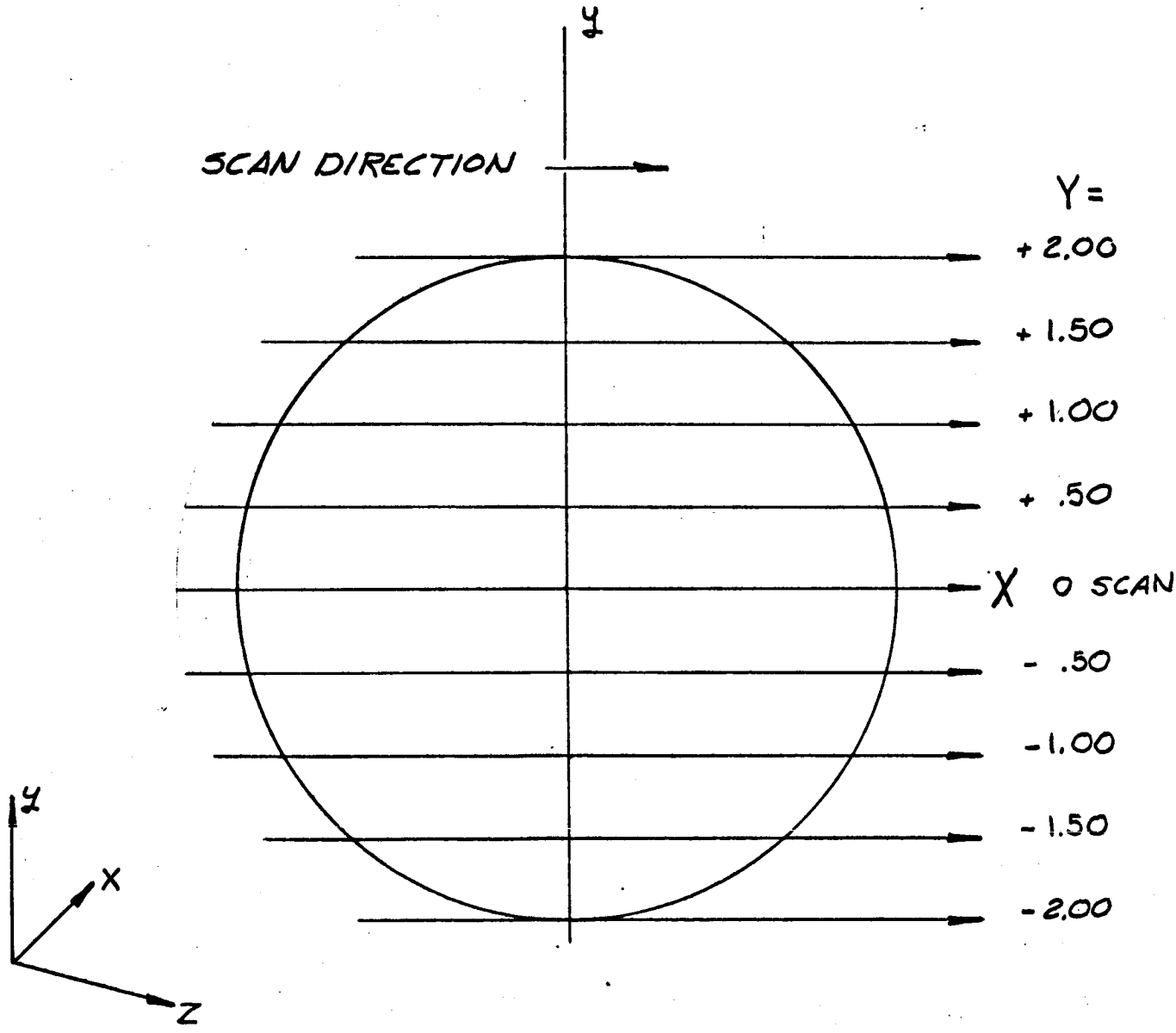
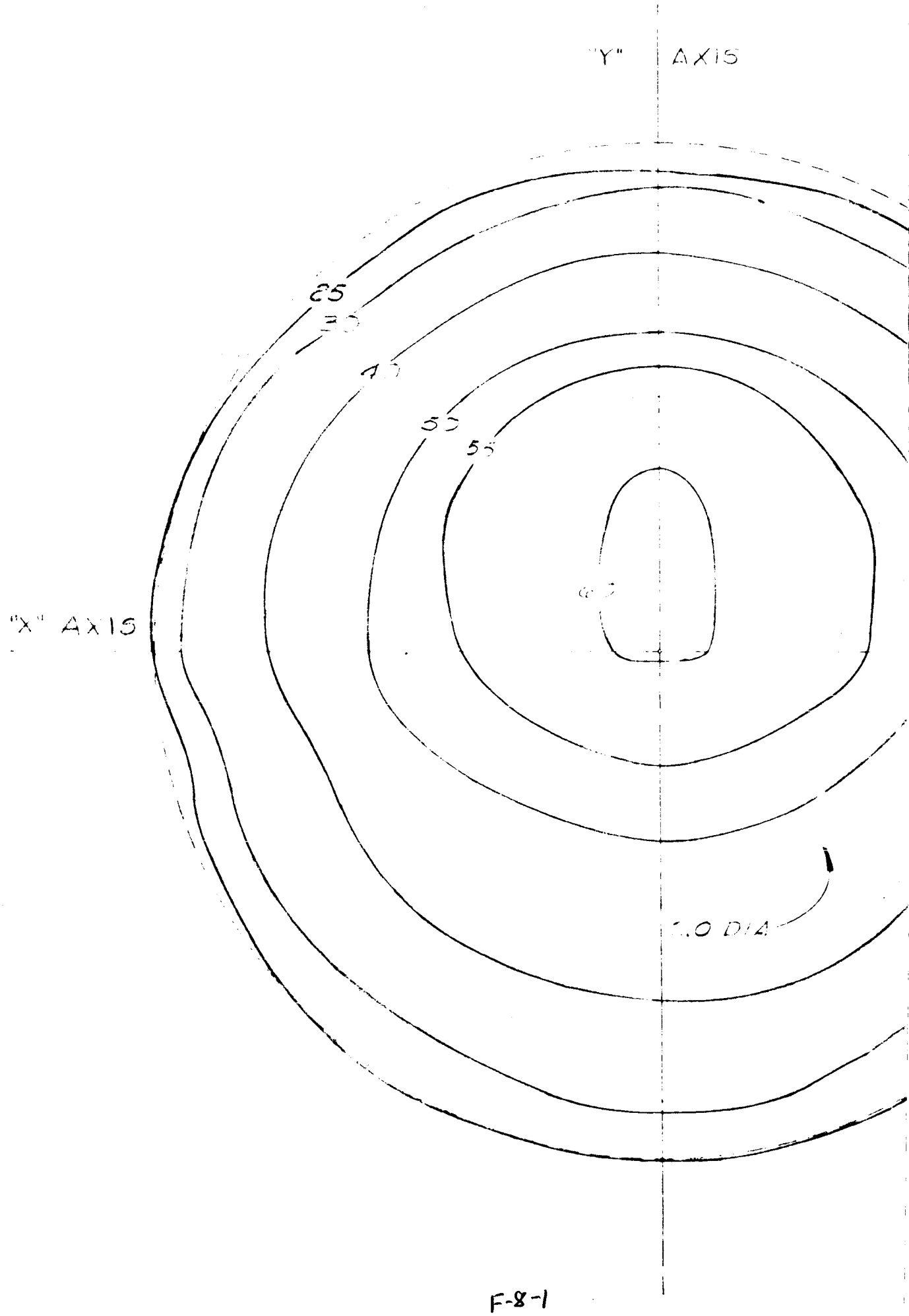


Figure 6 - Uniformity Scanner with Sensor Mounted



SCANNING TECHNIQUE

FIGURE: No. 7



F-8-1

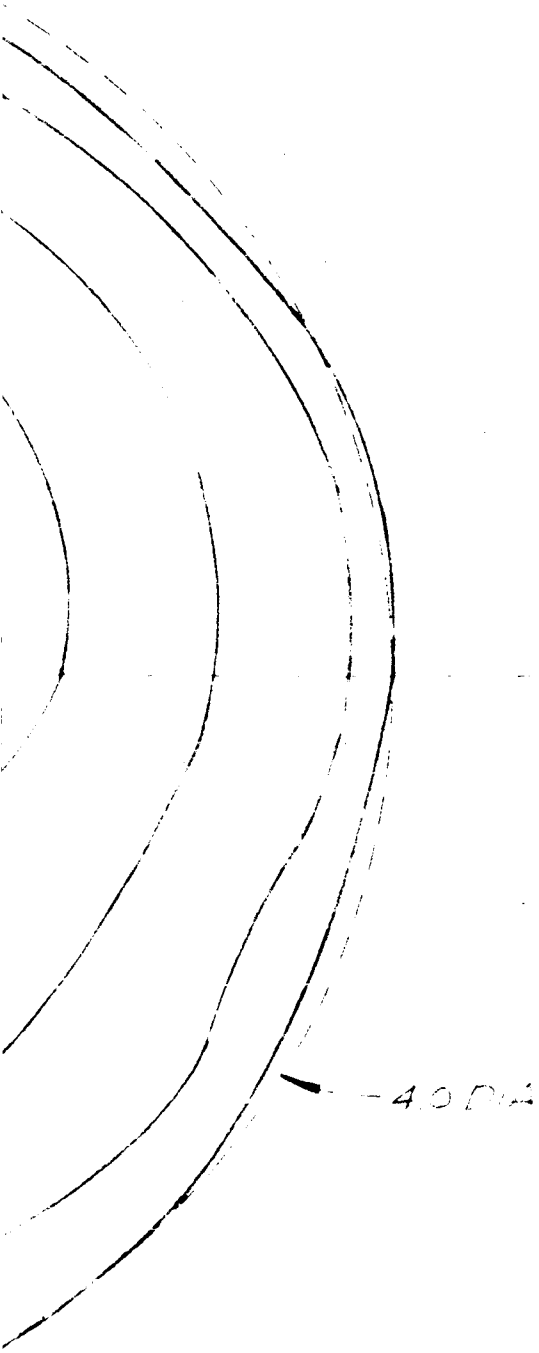


FIGURE [illegible]

PROJECTION BEAM INTENSITY DISTRIBUTION

RUN No. 5-C

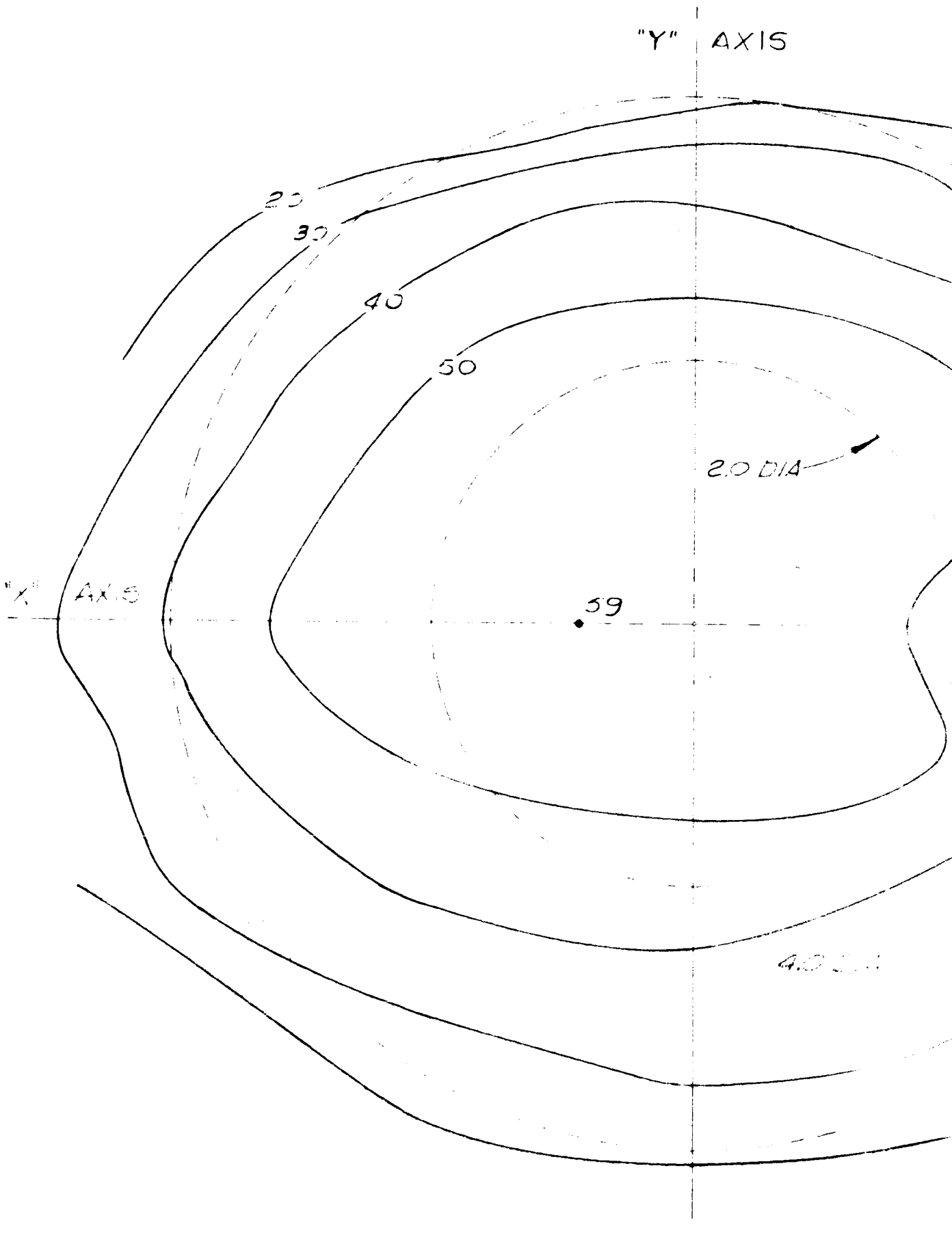
[illegible] DIAMETER

[illegible]

INTENSITY: MULTIPLY NUMBERS

BY 1.15 TO OBTAIN

UNITS IN BTU/FT.² SEC.



F-9-1

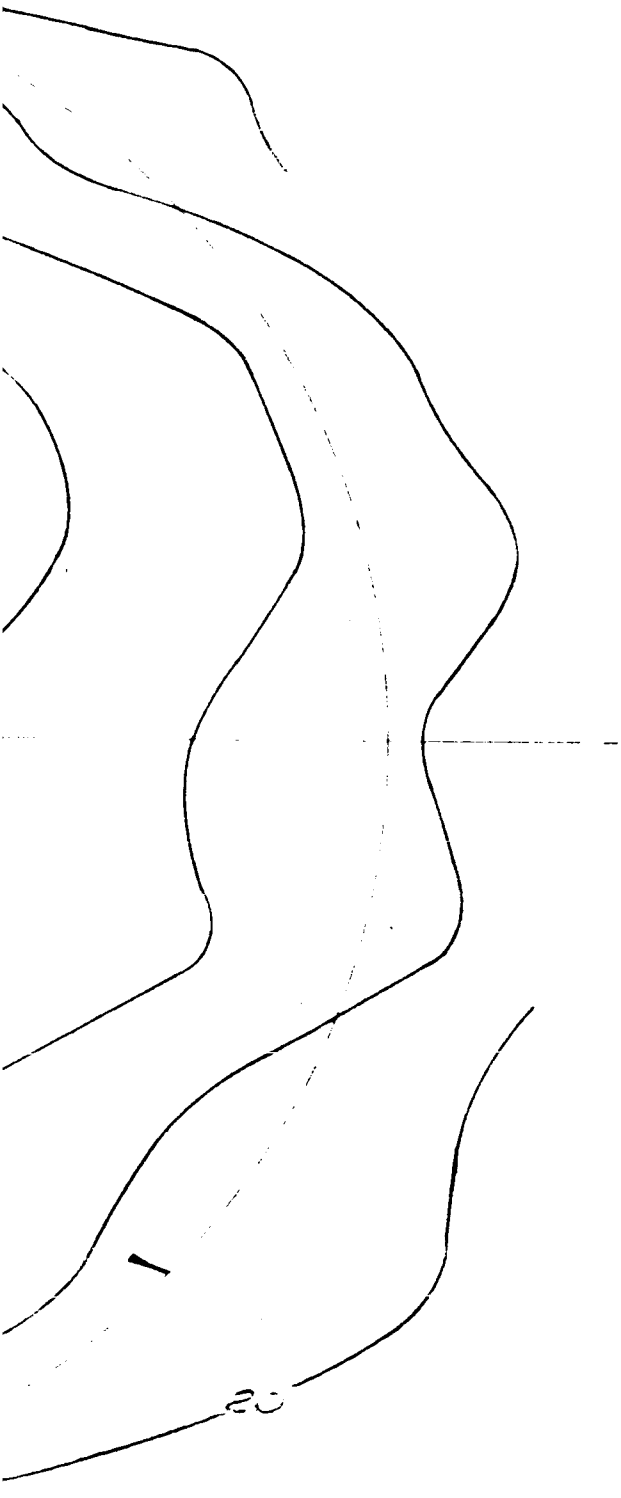


FIGURE No. 9

TARGET PLANE INTENSITY DISTRIBUTION

RUN No. 5-3

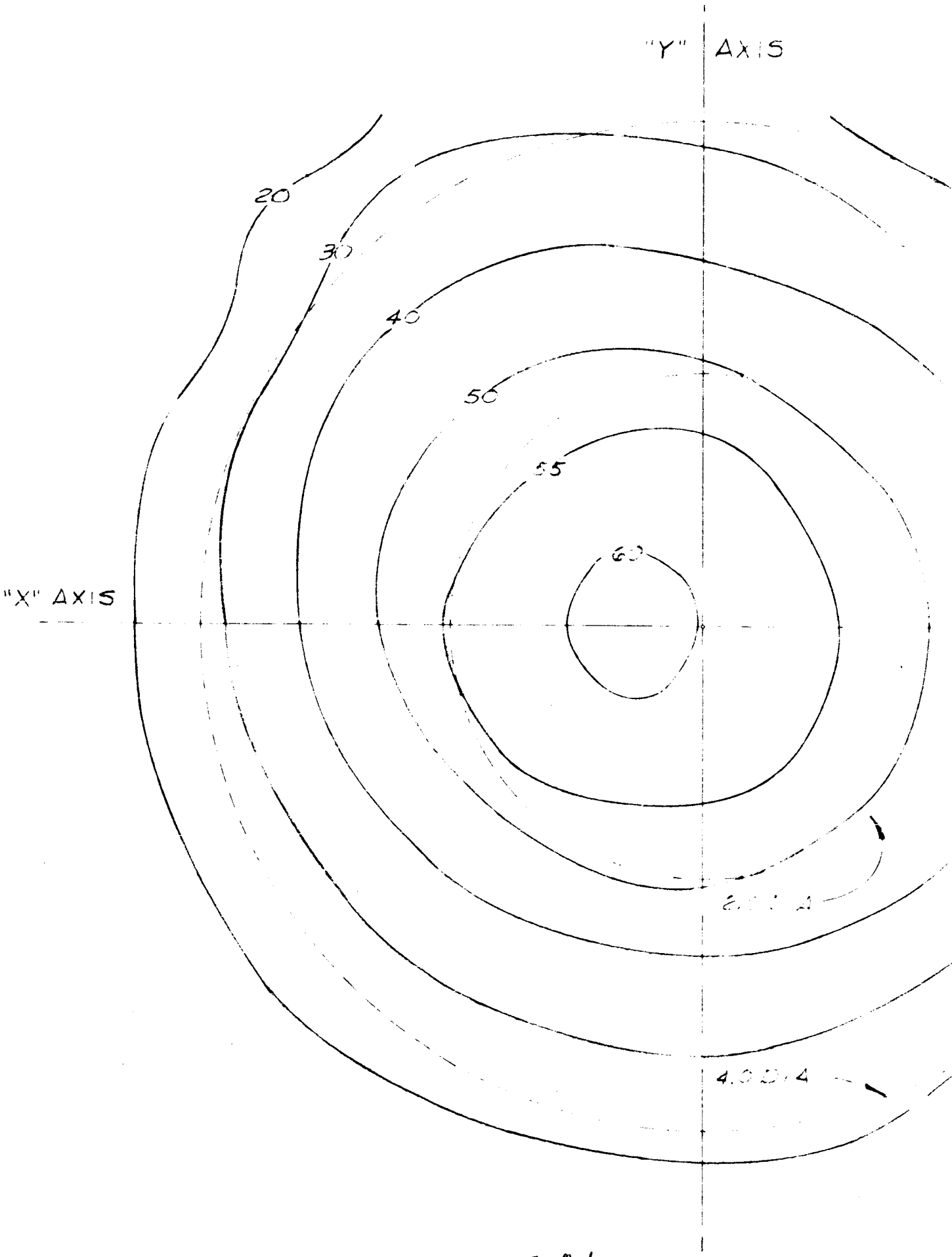
BAFFEL 6.0 INCH DIAMETER

DISTANCE 38.16 INCHES

INTENSITY: MULTIPLY NUMBERS

BY .745 TO OBTAIN

UNITS IN FT-LB/FT^2-SEC.



F-10-1

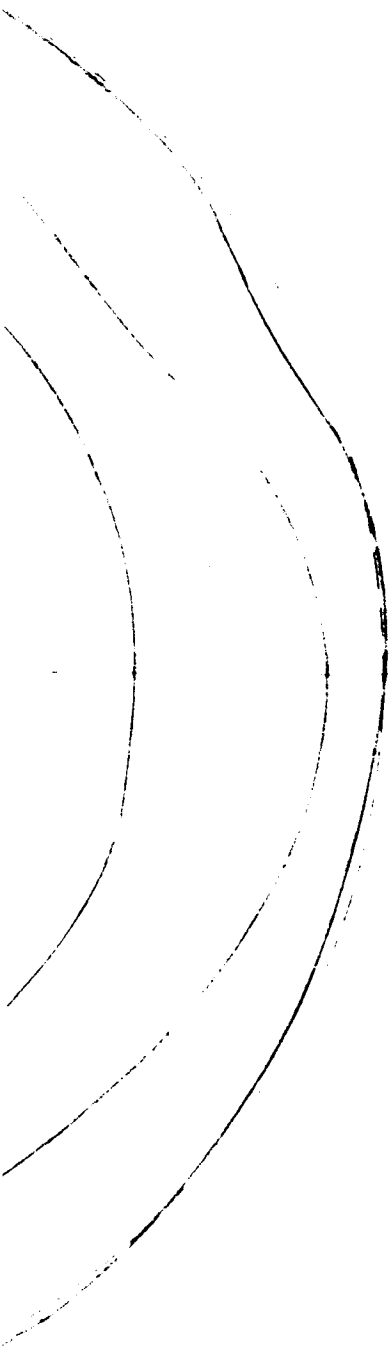
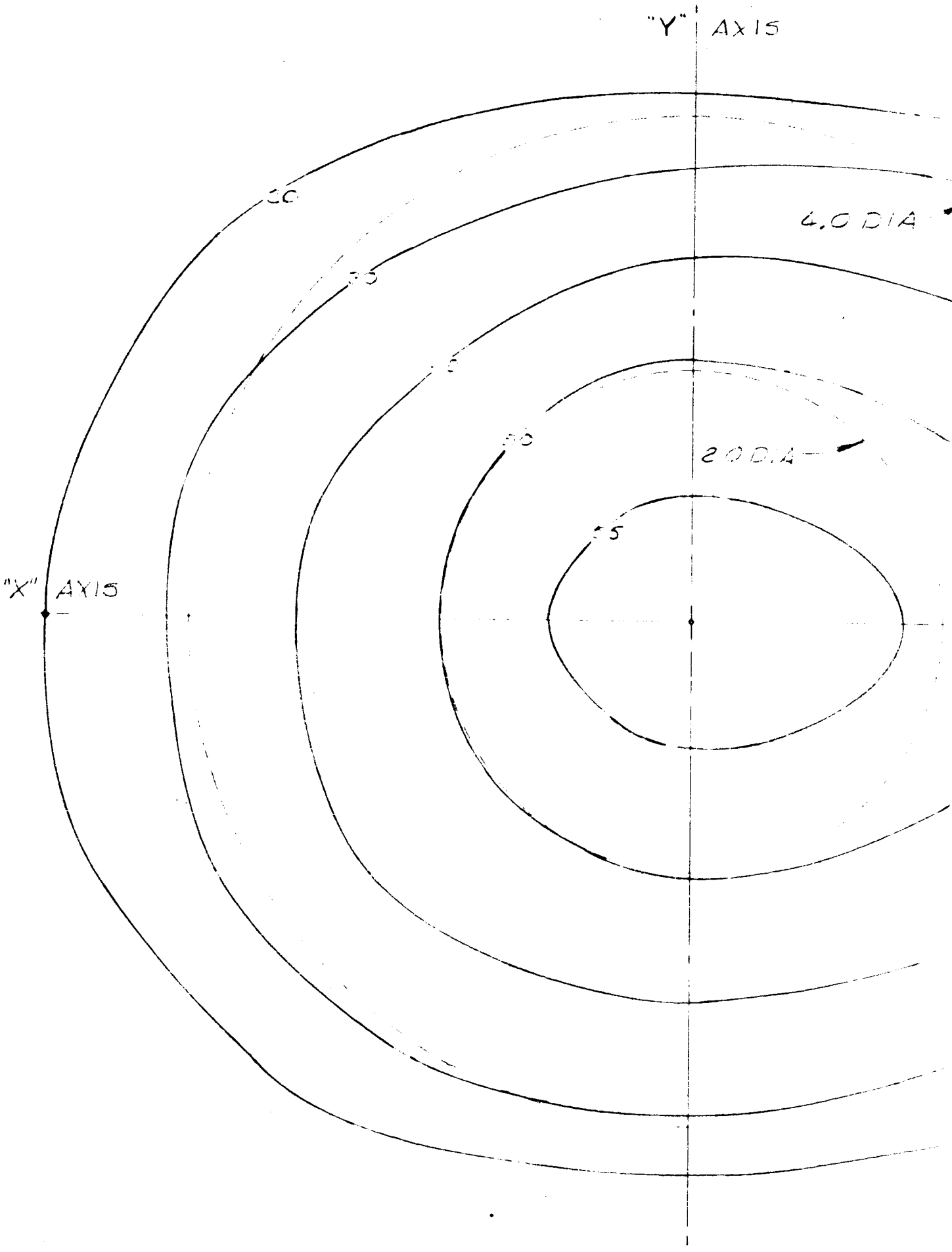


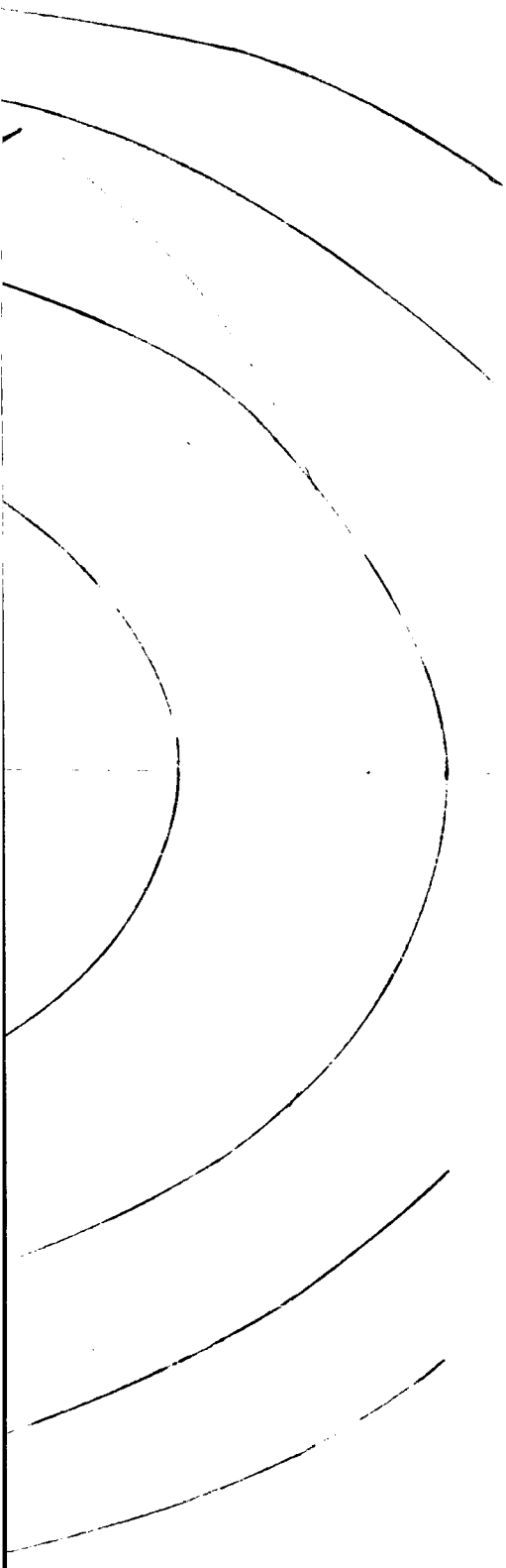
FIGURE No. 10

RUN No.

F-10-2



F-11-1



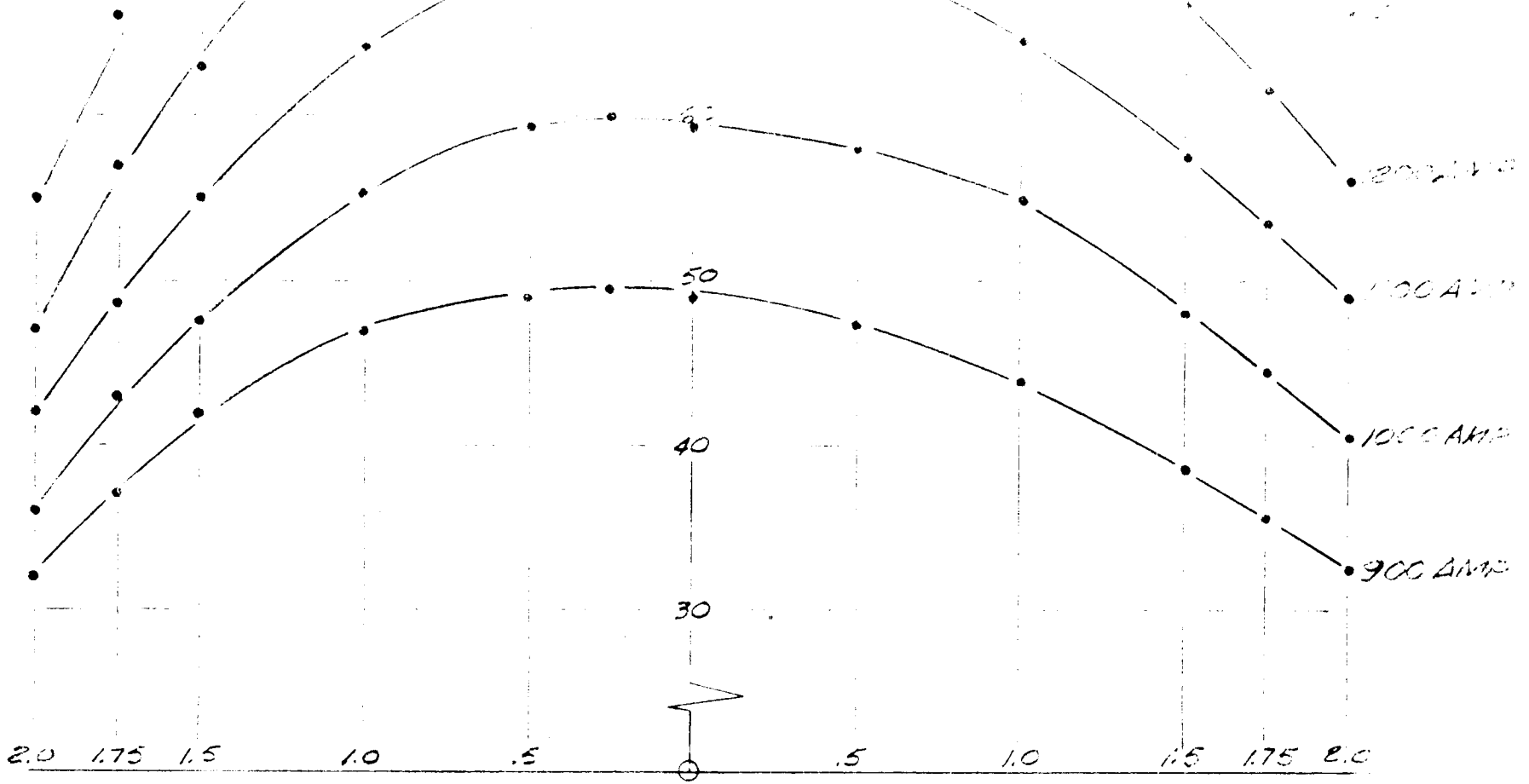
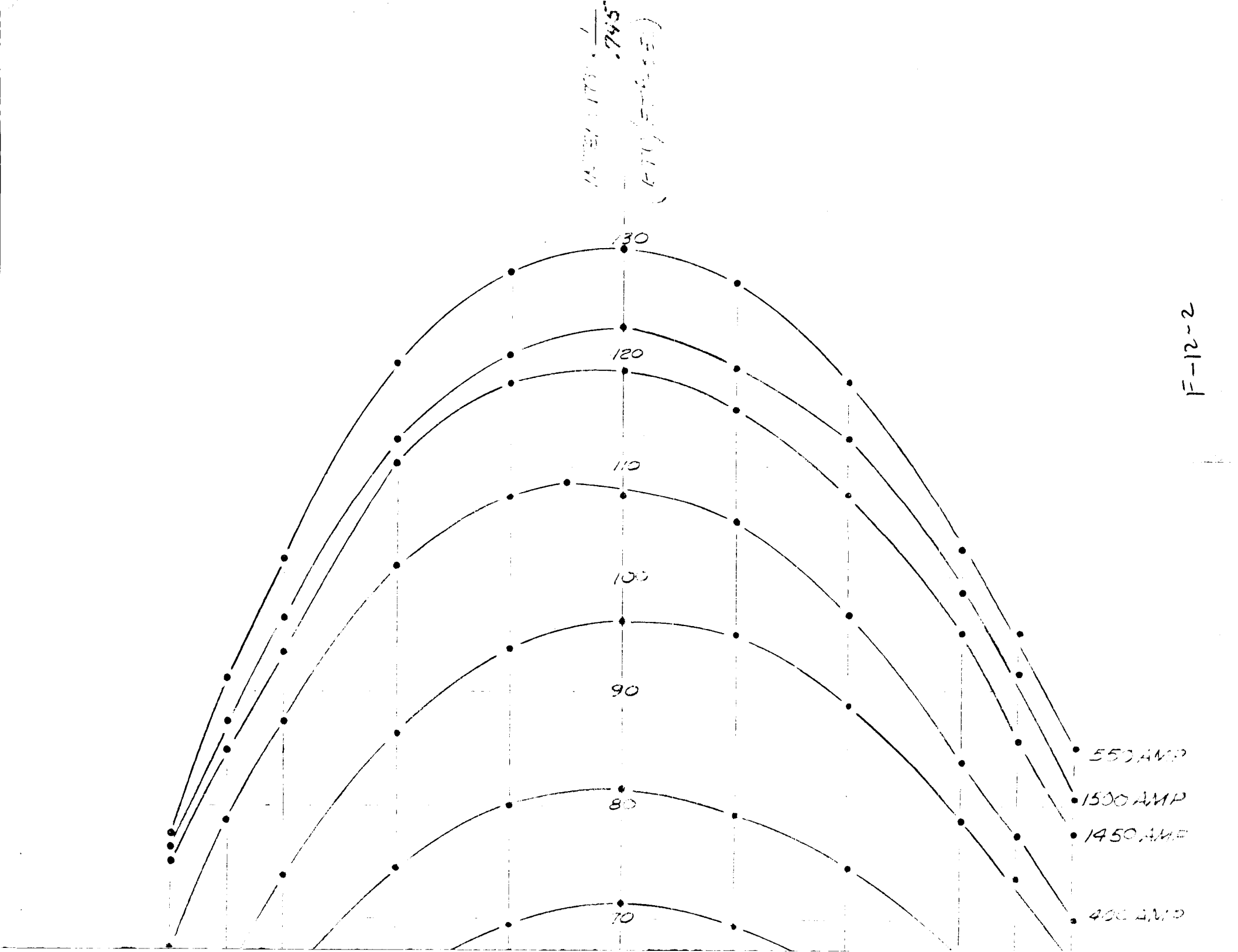
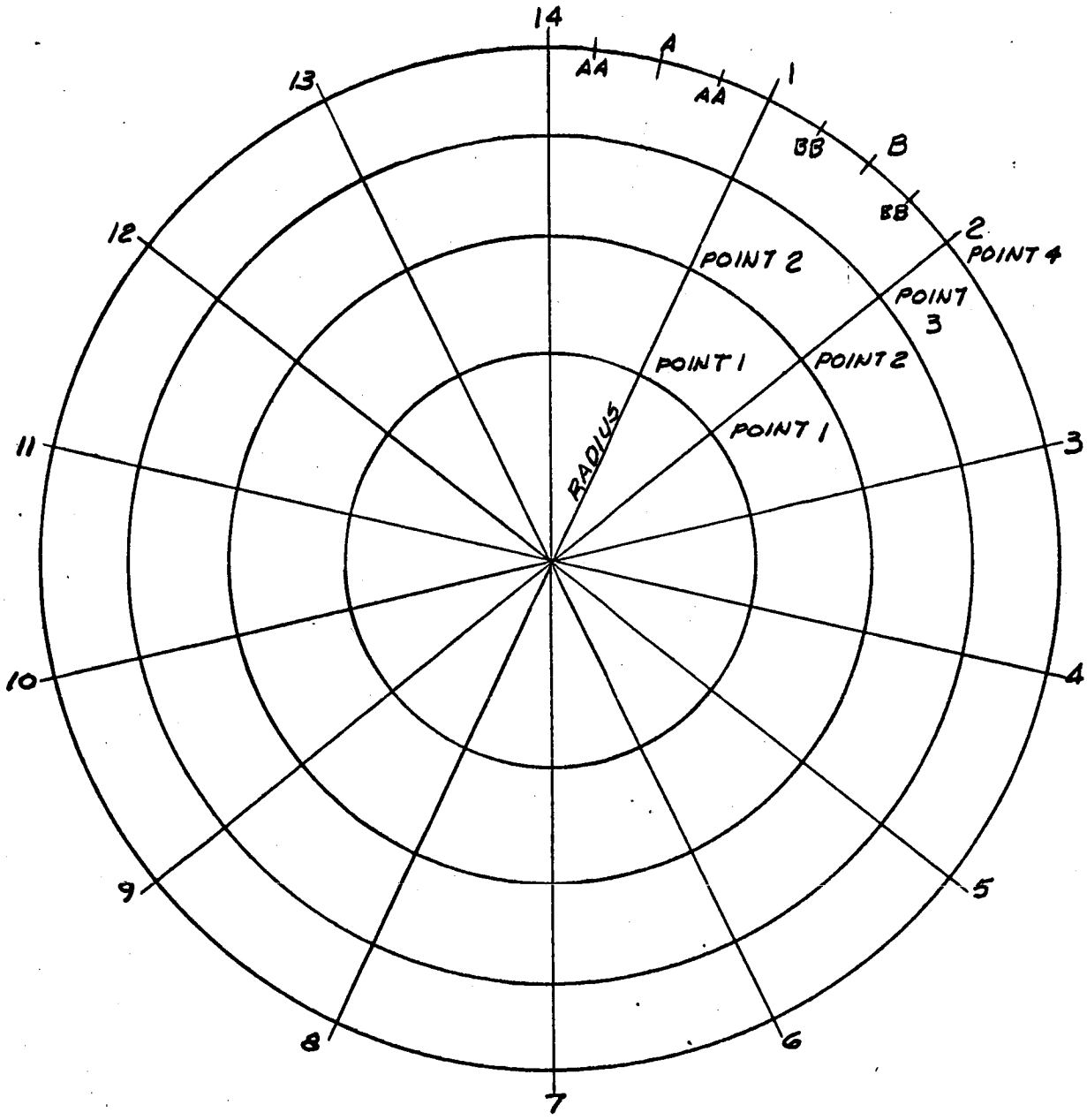


FIGURE 12

TARGET
DIAMETER (1.0) INTENSITY DISTRIBUTION
VS.
CURRENT

RUN NO. 9
BAFFEL 7.0 INCH DIAMETER
DISTANCE 38.0 INCHES


130
120
110
90
80
70
550 AMP
1500 AMP
1450 AMP



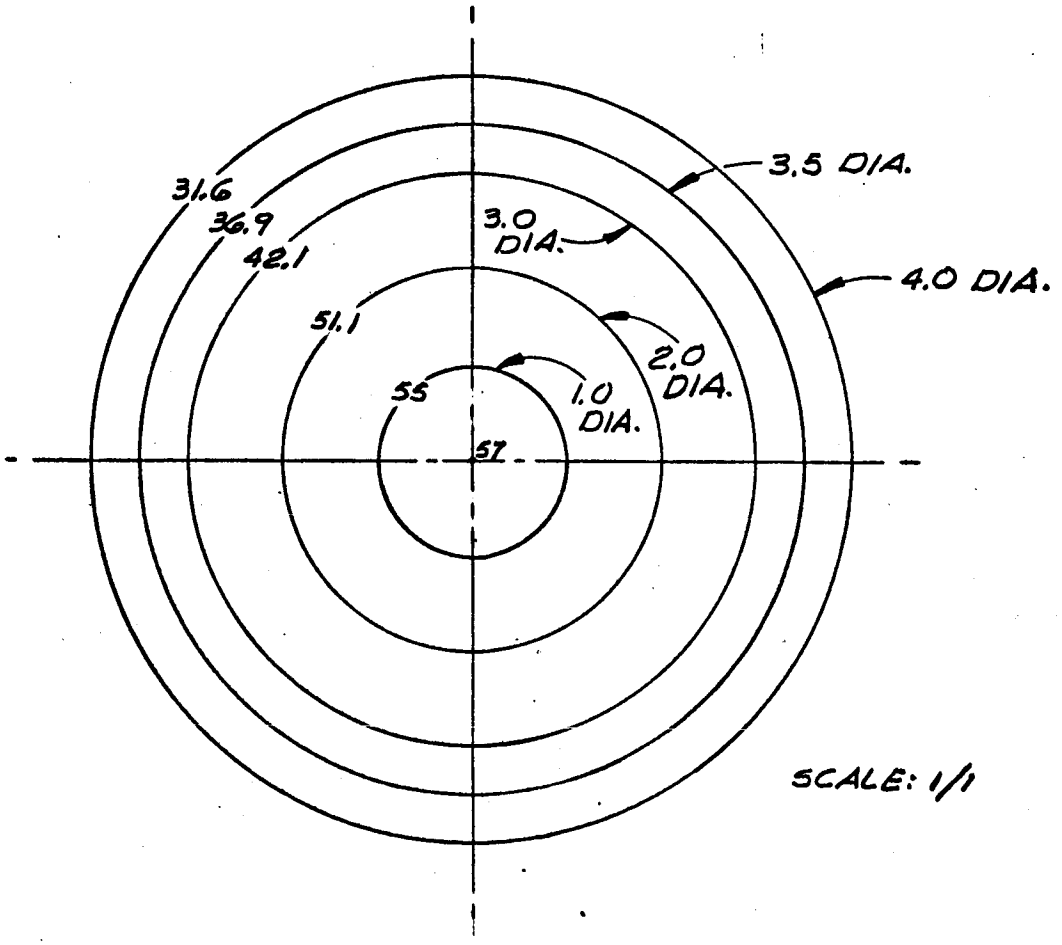
TARGET PLANE COORDINATE SUPERPOSITION (14 SOURCES)

FIGURE: 13

TARGET INTENSITY DISTRIBUTION
14 LAMPS

SIMILAR TO RUN 8.1

INTENSITY: Multiply Numbers by 14 x .470 To obtain units in Btu/ft²-sec



SCALE: 1/1

FIGURE: 14

FIGURE 15

TARGET DIAMETER
INTENSITY PROFILE
14 LAMP SYSTEM

INTENSITY: Multiply NUMBERS by 14 x .470 to obtain units in Btu/ft²-sec

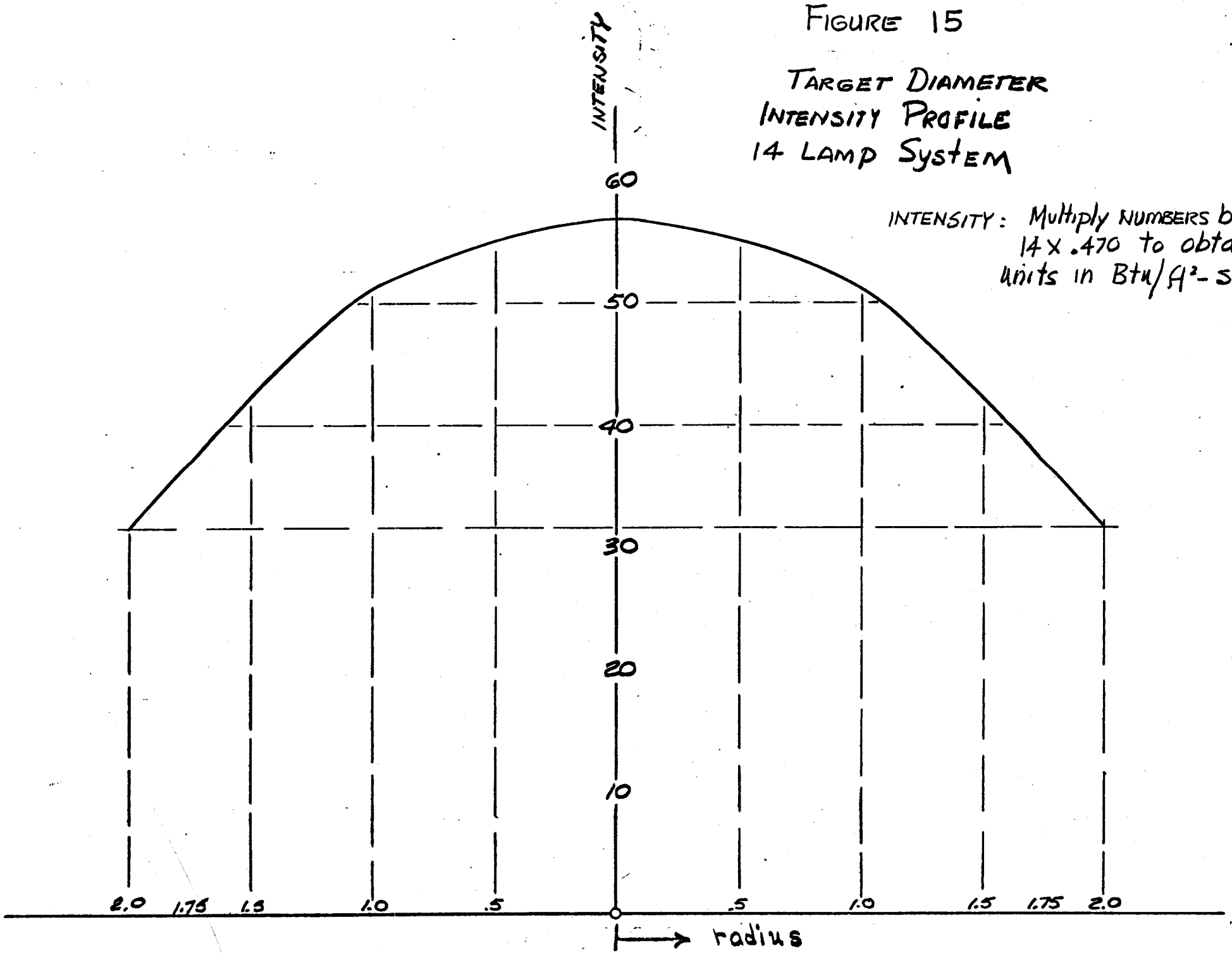
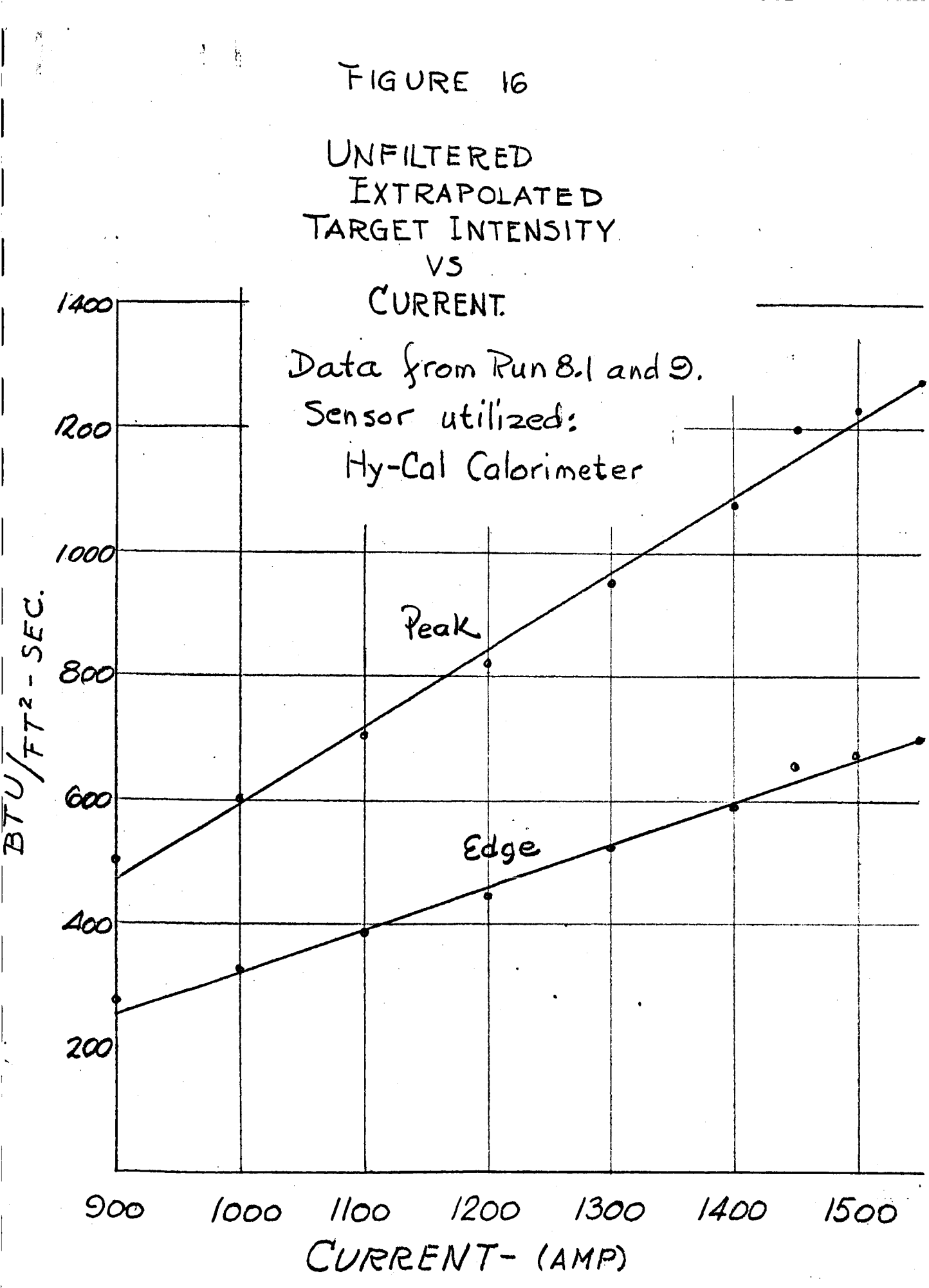


FIGURE 16


UNFILTERED
EXTRAPOLATED
TARGET INTENSITY
VS
CURRENT.
Data from Run 8.1 and 9.
Sensor utilized:
Hy-Cal Calorimeter
Peak
Edge
1400
1200
1000
800
600
400
200
BTU/FT² - SEC.
900
1000
1100
1200
1300
1400
1500
CURRENT - (AMP)

SPECTROLAB

DEVELOPMENT MEMORANDUM NO. 272-19

SUBJECT: Vacuum Seal Development Work

WRITTEN BY: John Nagle
DATE: November 5, 1964
JOB NUMBER: 6002-14

The O-ring vacuum seal was tested at elevated temperatures in order to evaluate its ability to maintain a seal.

FIRST TRIAL

Using radiant energy from three 375 watt General Electric industrial heat lamps, the temperature of the lens blank was elevated to a steady state temperature of only 60°C, an increase of only 36°C over room temperature. The pressure within the chamber was observed to drop slightly from 2.0 ± .02 mm of Mercury to 1.9 ± .02 mm of Mercury. Leak rate data is as follows:

$$T = 297°K \qquad V = 334 \text{ cc} \qquad \frac{dp}{dt} = 2.5 \text{ mm/sec}$$

Using the expression derived in Development Memorandum No. 272-9, i.e.,

$$\frac{dv}{dt} = .369 \left(\frac{V}{T}\right) \frac{dp}{dt}$$ the leak rate was found to be

$$\frac{dv}{dt} = 1.04 \times 10^{-3} \text{ liter/sec} = 2.20 \times 10^{-3} \text{ ft}^3\text{/min}$$

SECOND TRIAL

In order to obtain a higher temperature, heat was applied directly to the surface of the lens blank by a heating element. The temperature was increased from room temperature of 24°C to 150° centigrade at a rate of approximately 2 degrees per minute. At this temperature, a crack appeared, starting at the edge of the lens blank, extending two inches towards the center. As a result of this failure, the test was concluded. Just prior to the failure, a measurement of pressure had been made which indicated a pressure of 1.5 ± .02 mm of Mercury. No leak rate data were obtained.

CONCLUSIONS

Although a failure of the lens blank resulted, there is no indication that this failure was associated with malfunction of the O-ring seal. Indications are that it was caused by a defect of the lens blank at its edge, and as a result of thermal stresses, the fracture occurred.

Further, there is positive indication that the anticipated improvement in pressure and leak rate values were realized. It was also noted that, since a great deal of difficulty was encountered in heating the lens blank, there must be appreciable heat conduction through the O-ring vacuum seal. This had not been previously anticipated. As a result of this heat conduction, previously reported evaluations of maximum equilibrium temperature for the projection lens would appear to suggest values of temperature which are too high.

SPECTROLAB

DEVELOPMENT MEMORANDUM NO. 272- 21

SUBJECT: Comparison of Sensors

WRITTEN BY: Wagner Schlesinger WS
DATE: November 25, 1964
JOB NUMBER: 6002-18

The following sensors were compared during Runs 13.4 to 13.10:

Eppley Thermopile (#6132)
#1 Hy-Cal Calorimeter (#11146)
#2 Hy-Cal Calorimeter (#12492)

The test setup was similar to that described in Development Memorandum No. 272-15, in all details except the distances between the sensors and the plasma arc. These distances were:

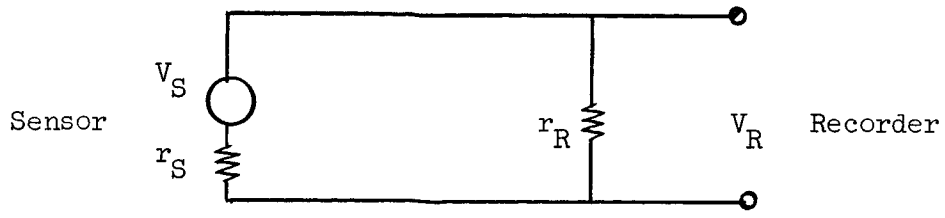
Eppley - 30.08 inches
Hy-Cal #1 - 13.82 inches
Hy-Cal #2 - 10.17 inches

It is assumed that the flux density on each receiver is inversely proportional to the square of its distance from the arc, then the ratios of the flux densities received are as follows:

$$\text{Hy-Cal \#1 to Eppley} = \frac{(30.08)^2}{(13.83)^2} = 4.737$$

$$\text{Hy-Cal \#2 to Eppley} = \frac{(30.08)^2}{(10.17)^2} = 8.748$$

A correction is necessary for the effects of loading of the recorder produced by the sensor circuit resistance. The circuit employed can be represented thus:



where V_S = voltage generated by the sensor

V_R = voltage recorded by the recorder

r_S = resistance of sensor and lead wires

r_R = resistance of the recorder

i = current flowing in the circuit

$$i = \frac{V_S}{r_S + r_R} = \frac{V_R}{r_R}$$

hence $$\frac{V_S}{V_R} = \frac{r_S + r_R}{r_R} = 1 + \frac{r_S}{r_R}$$

The measured values of the resistances are:

Eppley	-	12.0 ohms
Hy-Cal #1	-	1.6 ohms
Hy-Cal #2	-	1.3 ohms

The resistance of the Mosley 6S recorder on the 0.5 mv/inch setting is 1000 ohms.

Substituting these values in the equation above.

Eppley $\frac{V_S}{V_R} = 1.012$

Hy-Cal #1 $\frac{V_S}{V_R} = 1.0016$

Hy-Cal #2 $\frac{V_S}{V_R} = 1.0013$

The calibration factors of the three sensors are:

Eppley	=	4.68 mv/watt cm^{-2}
Hy-Cal #1	=	0.149 mv/watt cm^{-2}
Hy-Cal #2	=	0.0678 mv/watt cm^{-2}

Calibration factor, distance correction factor and loading factor can be combined to give a single conversion factor to obtain flux densities from recorder indication:

Eppley 4.68 x 1.00/1.012 = 4.62 mv/watts cm^{-2} = 0.216 watts cm^{-2}/mv

Hy-Cal #1 0.149 x 4.737/1.0016 = 0.705 mv/watts cm^{-2} = 1.418 watts cm^{-2}/mv

Hy-Cal #2 0.0678 x 8.748/1.0013 = 0.592 mv/watts cm^{-2} = 1.689 watts cm^{-2}/mv

Table 21.1 shows the recorded results, the derived flux densities, and the ratios of the indications of the sensors. The ratios are plotted in Figure 21.1.

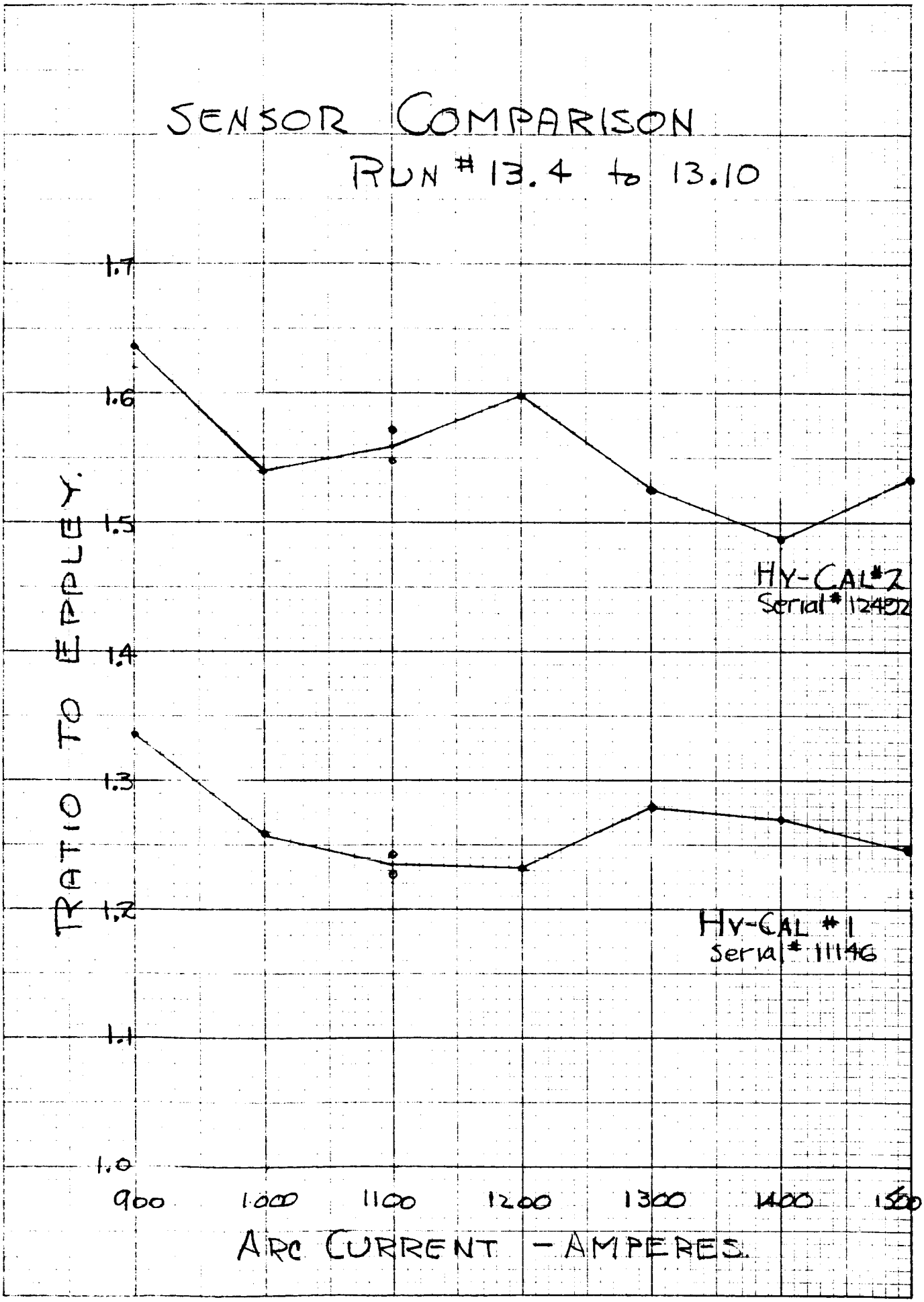

SENSOR COMPARISON
RUN # 13.4 to 13.10
RATIO TO EPPLEY
1.7
1.6
1.5
1.4
1.3
1.2
1.1
1.0
HY-CAL #2
Serial # 12402
HY-CAL #1
Serial # 11146
900
1000
1100
1200
1300
1400
1500
ARC CURRENT - AMPERES

FIGURE 21.1

		EPPLEY		HY-CAL #1 (OLD)			HY-CAL #2 (NEW)		
Point	Amperes	MV Indicated	Watts/cm^2	MV Indicated	Watts/cm^2	Ratio To Eppley	MV Indicated	Watts/cm^2	Ratio To Eppley
13.4	900	1.67	0.361	0.34	0.482	1.335	0.35	0.591	1.637
13.5	1000	1.98	0.428	0.38	0.539	1.259	0.39	0.659	1.540
13.6	1100	2.14	0.462	0.40	0.567	1.227	0.43	0.726	1.571
13.6	1100	2.22	0.480	0.42	0.596	1.242	0.44	0.743	1.548
13.7	1200	2.40	0.518	0.45	0.638	1.232	0.49	0.828	1.598
13.8	1300	2.82	0.609	0.55	0.780	1.280	0.55	0.929	1.525
13.9	1400	3.05	0.659	0.59	0.837	1.270	0.58	0.980	1.487
13.10	1500	3.47	0.750	0.66	0.936	1.248	0.68	1.149	1.532

TABLE 21.1

SPECTROLAB

DEVELOPMENT MEMORANDUM NO. 272-26

SUBJECT: Water Cell Absorption Test

WRITTEN BY: Wagner Schlesinger WS.
DATE: December 18, 1964
JOB NUMBER:

Runs #22-1, 22-2, 22-3

All runs were made at 1540 amps, 250 psi. With collector very close to exact alignment (slight improvement was obtained later), scans were made along one radius from center out to 2". Each scan was recorded as the sensor moved outward and inward, thus with decreasing and increasing flux to eliminate possible time response effects.

One double scan was made without the water cell, two with the cell, then two more without the cell. Solid stops made sure that all scans started and ended at the same positions.

The sensor used was the Hy-Cal #2. The sensitive surface had been cleaned with an alcohol swab and a thin fresh layer of carbon black had been deposited from burning Shell Tellus oil as recommended by Hy-Cal Engineering. This gives a surface with emissivity of 0.96.

The results follow:

Without Cell			With Cell		
On Axis mv	1" Radius mv	2" Radius mv	On Axis mv	1" Radius mv	2" Radius mv
9.00	7.84	4.17	6.07	5.32	2.72
9.20	8.18	4.23	6.13	5.24	2.76
8.80	7.99	4.32	6.12	5.46	
8.90	7.87		6.12	5.20	
9.05	8.24				
9.06	7.98				
9.00	8.02	4.24 Average	6.11	5.31	2.74

Measured at the projection plane, the water cell transmission is:

On Axis	$\frac{6.11}{9.00} = 0.68$
At 1" Radius	$\frac{5.31}{8.02} = 0.66$
At 2" Radius	$\frac{2.74}{4.24} = 0.65$

During the run with the water cell, the water temperature rose from 65°F to a stable value of 78°F. The flow rate was approximately 1 g.p.m.

SPECTROLAB

DEVELOPMENT MEMORANDUM NO. 272-31

SUBJECT: Sensor Comparison in Projection Plane

WRITTEN BY: Wagner Schlesinger WS
DATE: 27 January 1965
JOB NUMBER: 6002-40

In order to compare the Hy-Cal calorimeters #11146 (Spectrolab #1) and #12492 (Spectrolab #2), three runs were made under the following conditions:

			VOLTS		SOURCE POWER	GAS	
DATE	RUN #	AMPERES	SYSTEM	SOURCE	KW	PSI	CFM
1-21-65	34	1550	93.1	70.9	109.6	250	21.5
1-22-65	35	1550	94.3	71.9	111.4	250	23.0
1-25-65	36-1	1550	100.9	78.5	121.7	250	16.0
1-25-65	36-2	1550	98.9	76.5	118.6	250	16.0

It was necessary to replace the source anode between Runs 35 and 36. The collector alignment was carefully adjusted before Run 35 and again after anode replacement before Run 36.

The surface of Hy-Cal #1 calorimeter apparently had been degraded by a 150% overload on an earlier run and it was tested with this surface and with a freshly deposited coating of lamp black from burning Tellus oil.

Hy-Cal #2 was tested with both an old and a fresh layer of the same lamp black.

The calorimeters were mounted in the X-Y scanner and scans were made across the horizontal diameter of the beam at the projection plane. Calorimeter outputs were recorded on the Moseley 6-S X-Y recorder, and were tabulated for the peak value near the axis of the beam, and for points 2 inches to the right and left of the optical axis.

The results are summarized in Table 1, and since all records were not made at exactly the same power level, a detailed tabulation is given in Table 2.

SENSOR COMPARISON IN PROJECTION PLANE

1550 Amps - 250 PSI

Horizontal Diameter Scans

RUN NO.	SENSOR NO.	SURFACE CONDITION	AVERAGE BTU/ft^2-sec AT 2" RADIUS	AT PEAK
35	1	Degraded	52.75	105.3
35	1	Fresh	51.35	105.25
34 & 36-1	2	Old	49.75	109.4
36-2	2	Fresh	49.75	104.7

TABLE 1

SENSOR COMPARISON IN PROJECTION PLANE
1550 Amps - 250 PSI
Horizontal Diameter Scans

Run #34 - 1/21/65. Run #35 - 1/22/65. Run #36 - 1/25/65.
NOTE: Anode replaced between Runs #35 and #36.

RUN NO.	HY-CAL SENSOR NO.	SURFACE	RECORDER MV/INCH	MV RECORDED			ABSORBED BTU/ft^2-sec			EMIS-SIVITY USED	INCIDENT BTU/ft^2-sec			VOLTS		SOURCE POWER KW	GAS FLOW CFM
				LEFT	PEAK	RIGHT	LEFT	PEAK	RIGHT		LEFT	PEAK	RIGHT	SYSTEM	SOURCE		
34	2	Old Soot	2	3.89	9.1	4.03	44.5	105.0	45.5	.96	46.4	109.4	47.4	93.1	70.7	109.6	21.5
35	1	Degraded	2	8.50	17.9	9.05	44.5	93.6	47.5	.89	50.0	104.5	53.4	94.3	71.9	111.4	23.0
35	1	Degraded	5	9.00	18.0	9.00	47.3	94.4	47.2	.89	53.1	106.1	53.0	94.3	71.9	111.4	23.0
35	1	Fresh Soot	2	8.90	18.9	9.75	46.70	99.0	51.0	.96	48.6	103.1	54.2	94.3	71.9	111.4	23.0
35	1	Fresh Soot	5	9.30	19.0*	9.50	48.7	99.6	49.8	.96	50.7	107.4	51.9	94.3	71.9	111.4	23.0
36-1	2	Old Soot	2	5.10	10.5	5.00	58.5	116.5	57.1	.96	53.1	109.4	52.1	100.9	78.5	121.7	16.0
36-2	2	Fresh Soot	2	4.80	10.05	4.75	55.0	115.3	54.3	.96	50.0	104.7	49.5	98.9	76.5	118.6	16.0

* 90% Overload

TABLE 2

SPECTROLAB

DEVELOPMENT MEMORANDUM NO. 272- 32

SUBJECT: Field Lens Scan - Runs 24 and 25

WRITTEN BY: John Nagle
DATE: 2 February 1965
JOB NUMBER: 6002-11

INTRODUCTION

A total of 25 intensity scans, each of vertical separation of 1/2 inch, were made on the field lens plane using the Hy-Cal #2 radiometer. From this data, a plot of iso-intensity lines was constructed and calculations were performed to determine total power incident upon the field lens plane, and that passing through six and seven inch apertures.

INTENSITY MEASUREMENTS

Using the procedure previously described in Development Memorandum No. 272-18, 25 intensity scans were made at 1/2 inch vertical separations across the field lens plane. The Hy-Cal #2 radiometer was used as a detector for these measurements. The data from these scans were reduced and are presented in the iso-intensity plot shown in Figure 1. For these measurements, the folding mirror was rotated approximately 20° so that the field lens plane was translated to a convenient position for operation of the X-Y scanner, which was placed at the appropriate field lens plane distance. The operating conditions for these two runs are summarized in Table 1.

TABLE 1 - Run 24, 25 - Operating Conditions

RUN NO.	DATE	SOURCE VOLTAGE	SOURCE CURRENT	GAS PRESSURE	GAS FLOW RATE	SCAN NO.
24	12/23/64	71.8 V	1560 A	250 psi	20.5 CFM	1 - 12
25	12/28/64	72.2 V	1560 A	250 psi	21.5 CFM	11 - 25

Calibration data for the Hy-Cal #2 radiometer is as follows: One inch vertical displacement on the X-Y recorder corresponds to a 1 mv signal level from the radiometer. Using a radiometer surface absorptivity of .89, 1 mv is equivalent to an intensity level of 94.6 watt/in^2.

RADIAL INTENSITY DISTRIBUTION

In order to evaluate the total power irradiating the field lens plane, a radial intensity distribution was determined. This was accomplished by finding the average intensity for corresponding points, along the coordinate axes. These average values are tabulated in Table II and represented graphically in Figure II.

TABLE II - Average Intensity as Related to Radial Distance from Center of Field Lens Plane

(INCH) DISTANCE	0	.5	1.0	1.5	2.0	2.5	3.0	3.5	4.0	4.5	5.0	5.5
Avg. Intensity (kw/in^2)	.415	.412	.390	.343	.288	.217	.166	.129	.099	.078	.059	.040

POWER TRANSMISSION

Using the radial intensity distribution described in the preceding section, the total power incident upon the field lens may be evaluated by the expression

$$P = 2\pi \int_0^\infty I(r) \cdot r \, dr$$

where I(r) is the radial intensity distribution, and r is the distance from the axis. That power which passes through a baffle of radius R immediately in front of the field lens plane is given by the expression

$$P(R) = 2\pi \int_0^R I(r) \cdot r \, dr$$

The total power reflected by the folding mirror and incident upon the field lens plane was determined to be in excess of 14.8 KW (probably on the order of 17 KW). The total power to pass a 6" baffle was determined to be 7.8 KW while that passing a 7" baffle was 9.4 KW.

It should be noted that values for the 6" and 7" baffles are more reliable than that for total field lens plane power, since total power determinations depend upon a knowledge of intensity at larger radii.

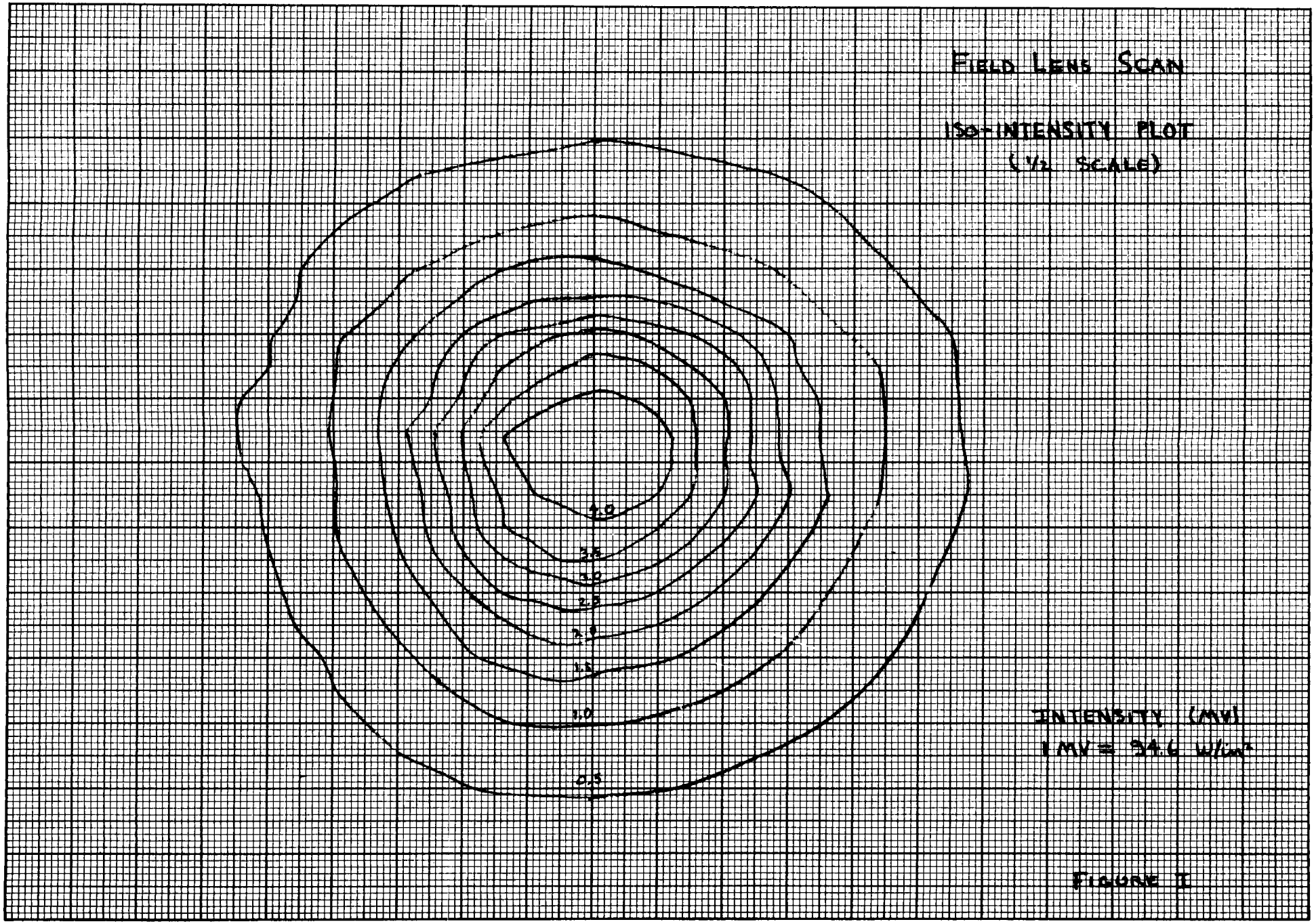

FIELD LENS SCAN
ISO-INTENSITY PLOT
(½ SCALE)
4.0
3.5
3.0
2.5
2.0
1.5
1.0
0.5
INTENSITY (MV)
1 MV = 34.6 w/in²

FIGURE II

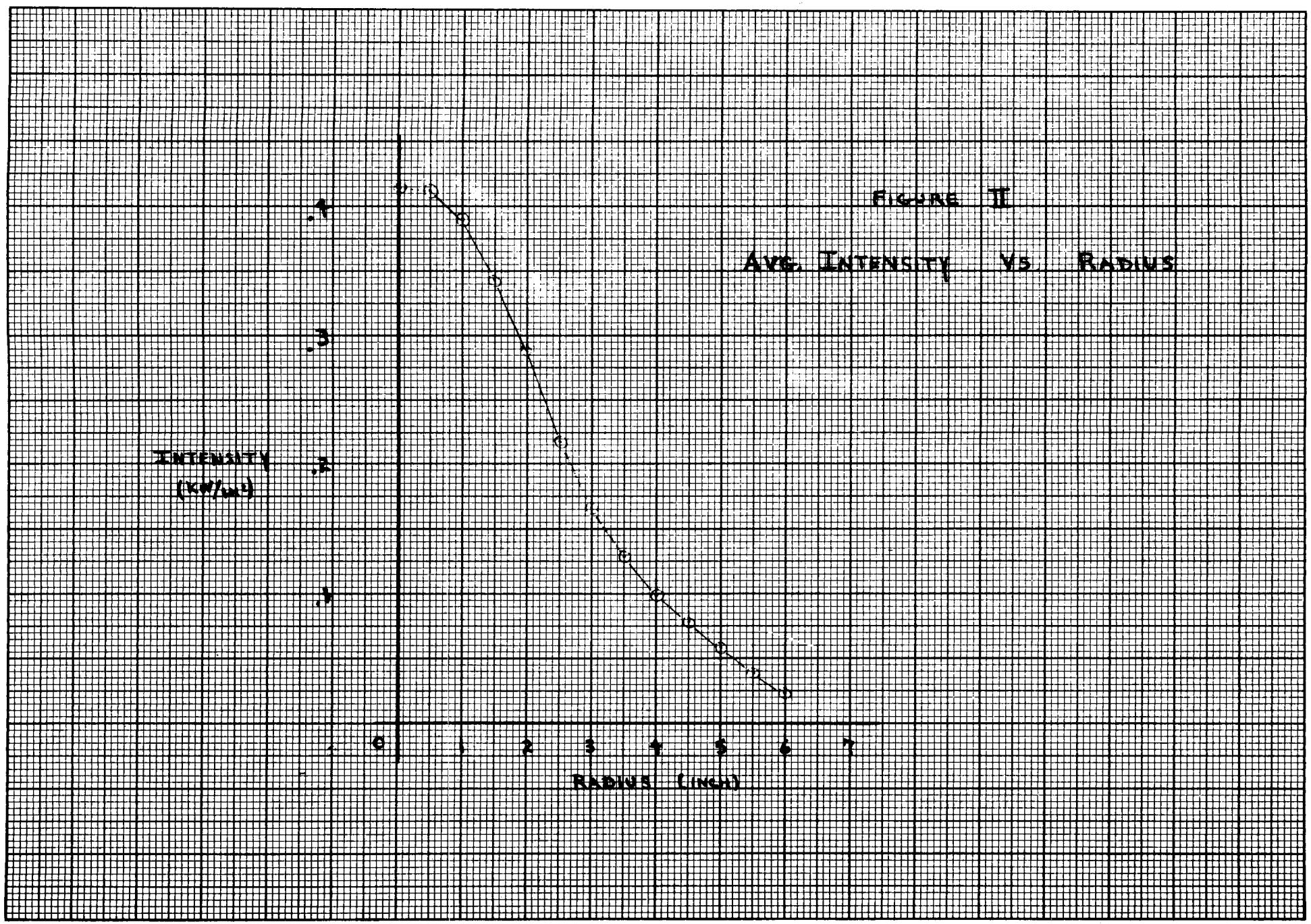


FIGURE II

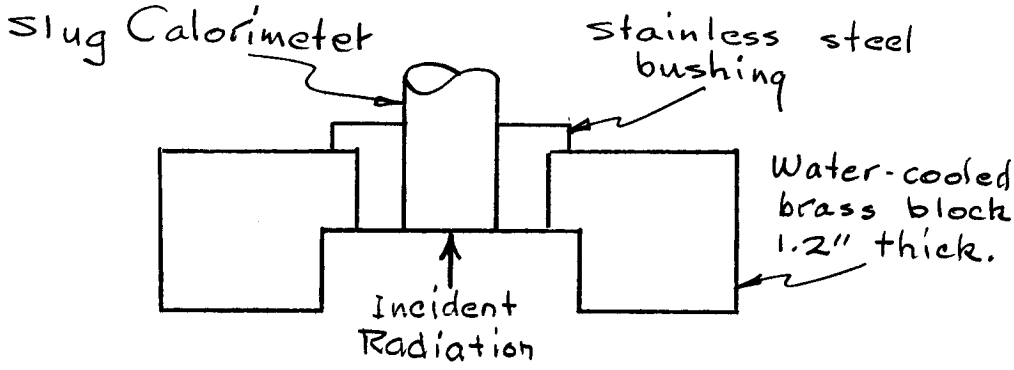
AVG. INTENSITY VS RADIUS

SPECTROLAB

DEVELOPMENT MEMORANDUM NO. 272-33

SUBJECT: Comparison of NASA-Ames Slug Calorimeter with Spectrolab Hy-Cal #2
WRITTEN BY: Wagner Schlesinger WS
DATE: 5 February 1965
JOB NUMBER: 6002-40

A run was made on January 28, 1965 to compare Spectrolab Hy-Cal #2 calorimeter with a slug calorimeter lent by NASA-Ames, and called by them a "transient calorimeter". The sensor in the calorimeter is a copper cylinder 5/16" in diameter and 3/8" long with a chromel-alumel thermocouple embedded in the rear of the cylinder. The calorimeter was placed in the X-Y scanner (as shown in Figure 1) in the position ordinarily occupied by the Hy-Cal calorimeter. Both calorimeters were freshly coated with camphor soot.



(approximately to scale.)

Figure 1

Output of both calorimeters was recorded on a Moseley 6S X-Y recorder. The time scan rates used were checked with a stop watch to ensure accuracy. Exposure times ranged from 3.5 to 5.5 seconds, with maximum outputs up to 9.3 mv. The run was made under the following conditions:

Run	Amps	System Volts	Gas Pressure	Gas Flow
#39	1550	99.2	250 psi	16.0 cfm

Table 1 gives data obtained on the peak intensity on the optical axis made with the Hy-Cal #2. The X-Y scanner was locked in position and the slug calorimeter was substituted for the Hy-Cal. Four readings were made at two different recorder time scan rates. The results tabulated in Table 2 were reduced from the raw data in accordance with the directions furnished by NASA-Ames in "Transient Calorimeter Instructions" furnished with the slug calorimeter.

The calorimeter was then raised to a point two inches above the optical axis and four more readings were made. The results are tabulated in Table 2.

TABLE 1

	PEAK mv	ABSORBED BTU/ft^2-sec	EMISSIVITY CAMPHOR BLACK	INCIDENT BTU/ft^2-sec
Hy-Cal #2	8.77	101.2	0.96	105.5

TABLE 2

PEAK READINGS ON AXIS

Scan No.	Recorder Scan Rate Sec/Inch	Slug Heating Rate * mv/sec	Btu/ft^2-sec	Watts/cm^2
1	1.0	1.55	85.1	96.7
2	1.0	1.58	86.7	98.5
3	0.5	1.69	92.4	105.0
4	0.5	1.67	91.6	104.0
		READINGS TWO INCHES ABOVE AXIS		
1	1.0	1.14	62.6	71.2
2	1.0	1.13	62.1	70.5
3	0.5	1.24	68.0	77.2
4	0.5	1.19	65.2	74.1

* Calibration Factor on Slug Calorimeter, as furnished by NASA-Ames, is 54.8 BTU/ft^2-sec/mv/sec.

SPECTROLAB

DEVELOPMENT MEMORANDUM NO. 272-35

SUBJECT: Damage to 24 Inch Collector Due to Mechanical Failure of Source Outer Envelope
WRITTEN BY: Wagner Schlesinger WS
DATE: 18 February 1965
JOB NUMBER: 6002-54

INTRODUCTION

The outer envelope of the final radiation source failed on February 8 during a static pressure test at 250 psi. Envelope fragments 5/16 inch thick and of various sizes up to about 2 square inches were propelled against the inner surface of the collector. The space between the collector and its surrounding cooling jacket was completely filled with water. The inertia of this water probably considerably reduced the damage.

Collector damage was of three types: abrasion, deformation and surface deterioration. An example of abrasion is shown in Figure 1. This appears to have been caused by a quartz fragment striking broadside on the surface and rebounding without sliding or denting the surface. The frosty or gramular area in this photograph is part of the small region deteriorated apparently by escaping gas. Figures 2 and 3 show deep scratches formed when fragments of quartz struck edge on. Usually some deformation or denting of the collector accompanied these scratches. Figure 4 is an image of the collector formed on a screen at the projection lens by the field lens. A very small light source was positioned near the collector focal point in such a way as to emphasize every defect of the collector (and every irregularity of the light source).

The dents mentioned above appear as dark marks with bright inner borders like those marked "3" on Figure 4, while the scratches in Figure 3 are just above the numeral 4, and those in Figure 2 are just above the numeral 2. The defects in Figure 1 are just above the numeral 1. The dark shadow to the right of the numeral 4 and a similar one 180° away from it are produced by the light source. The faint radial shadows nearly at right angles to the line joining these two dark shadow spots are also produced by the light source. Inspection of Figure 4 and its negative indicate a loss of collector efficiency of about 4%.

Tests with the alignment lamp and aperture plate gave a filament image pattern duplicating that previously recorded. Hence, no general deformation of the collector took place.

The shock of the blow delivered by the cathode end of the lamp when it struck the slotted angle base supporting the source and collector moved the base enough to deflect the optical axis about 1/4 inch at the source.

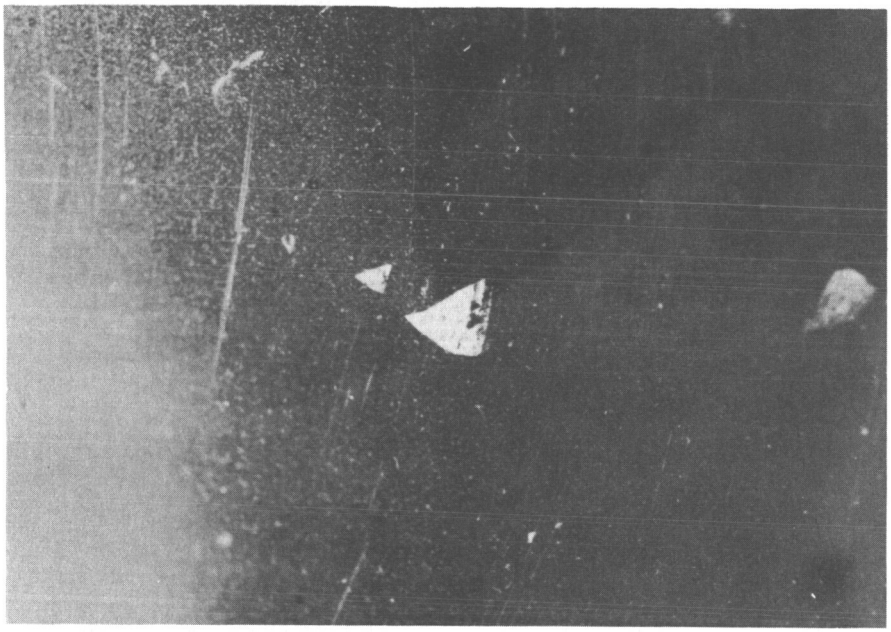


Figure 1

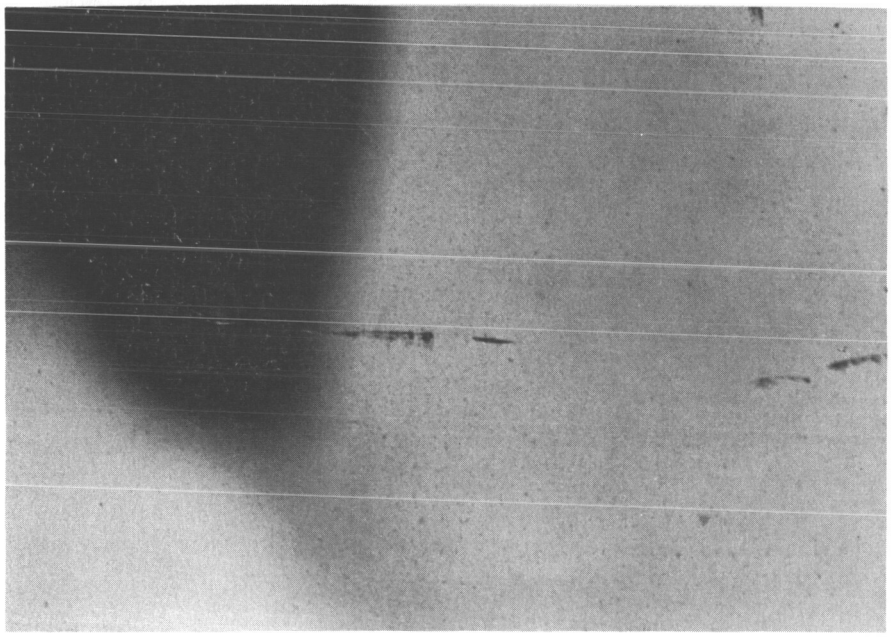


Figure 2

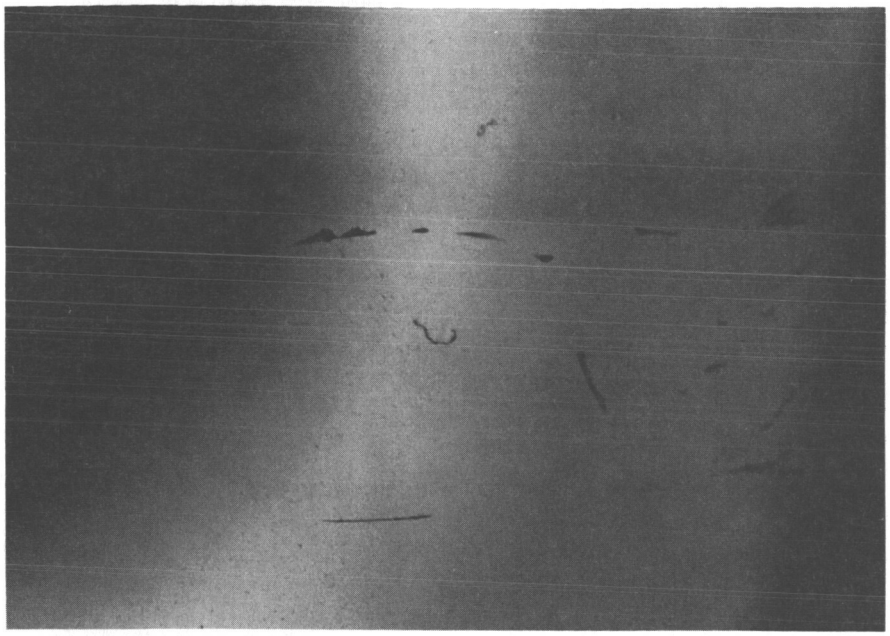


Figure 3

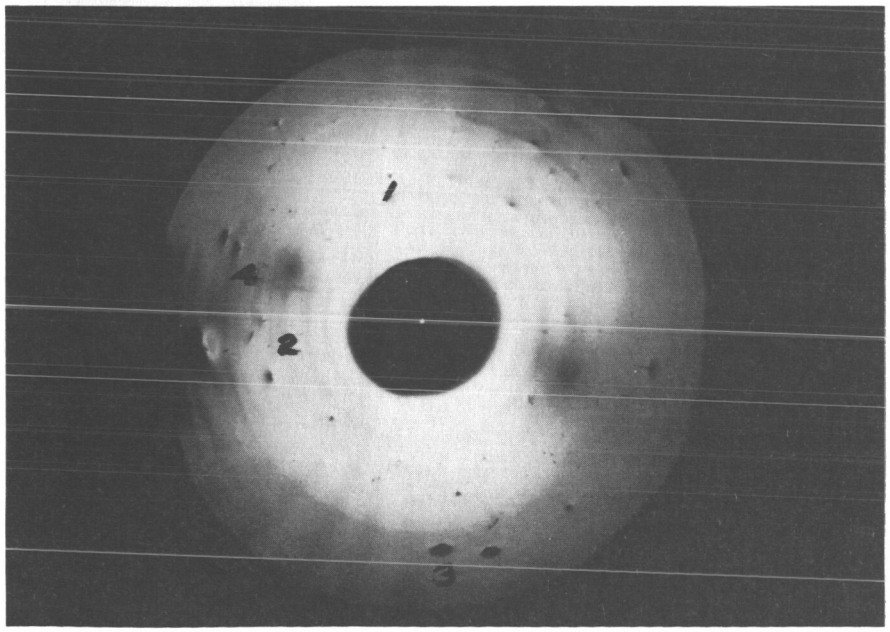


Figure 4

SPECTROLAB

DEVELOPMENT MEMORANDUM NO. 272-39

SUBJECT: Target Edge Intensity and Sensor Comparison

WRITTEN BY: Wagner Schlesinger WS
DATE: 24 February 1965
JOB NUMBER: 6002-11

Runs 44-3 and 45-2 were made under the following conditions:

RUN NO.	DATE	AMPERES	SYSTEM VOLTS	GAS PSI	GAS CFM	SENSOR
44-3	2-19-65	1550	101.2	250	22.0	Hy-Cal #2
45-2	2-22-65	1550	100.2	250	22.0	NASA Slug Calorimeter

Before the first run, both sensors were freshly coated with camphor soot.

The alignment of the optical system was checked with the alignment telescope and the collector was aligned with the aperture plate and alignment lamp. Runs 44-1 and 44-2 were made to adjust the collector using the target plane scanner in order to attain maximum energy along the four inch diameter circle representing the edge of the target in the target plane. All collector adjustments were manipulated for this purpose. After the completion of Run 45, the alignment lamp and aperture plate were used to check the collector alignment. It was found that the final collector position was 0.017" from the initial position obtained before Run 45. The aperture plate alignment method therefore appears to be very accurate, and will be further improved in the future.

The slug calorimeter was mounted as described in Development Memorandum No. 272-33. It was used and the data were reduced in accordance with NASA instructions. Observations were made at twelve equally spaced points around the four inch diameter circle with both sensors. Results are shown in Table 1, and are plotted in Figure 1.

If the previously measured transmission of 0.67 for the water cell filter is applied to the cosine corrected averages in Table I, they become 378 BTU/ft^2-sec for the Hy-Cal #2 and 333 BTU/ft^2-sec for the slug calorimeter.

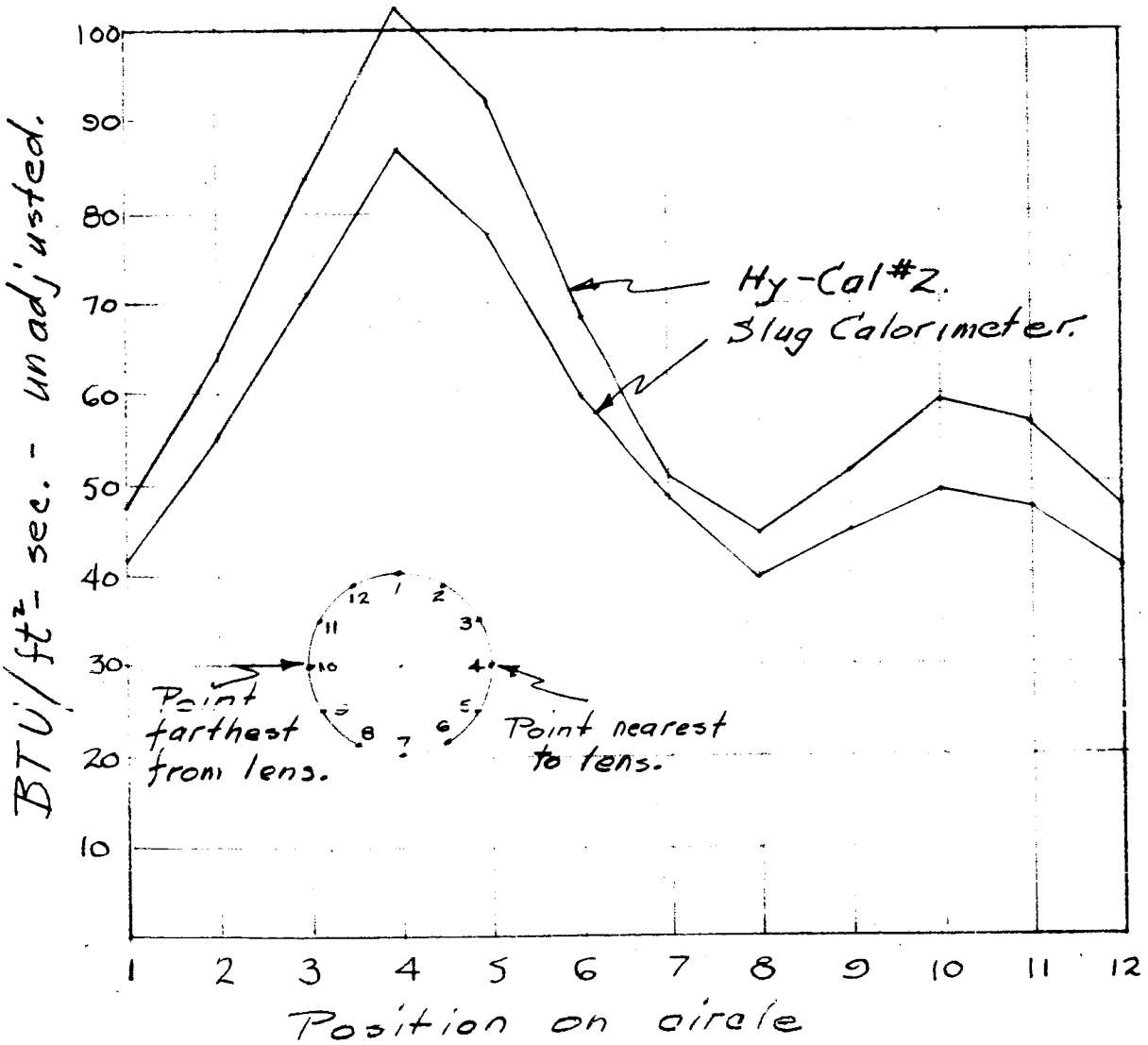

BTU/ft²- sec. - unadjusted.
100
90
80
70
60
50
40
30
20
10
Hy-Cal #2.
Slug Calorimeter.
Point farthest from lens.
Point nearest to lens.
1 2 3 4 5 6 7 8 9 10 11 12
Position on circle

FIGURE 1.

In Development Memorandum No. 272-26, it was estimated that collector efficienty had been degraded by 4% due to the recent outer envelope failure. Hence, all of the above data could legitimately be increased by 4% for this reason.

The NASA instructions for the slug calorimeter do not explicitly state whether the calibration factor of 54.8 (BTU/ft^2-sec)/(mv/sec) is for absorbed or incident energy. It was assumed that the factor is for incident energy, but if this is not the case, all the slug calorimeter data should be increased by 4 to 5%.

Data obtained from Run 39, reported in Development Memorandum No. 272-33, show an average reading at Point 1 of 64.5 BTU/ft^2-sec compared to 41.9 in Table I. This run was made primarily for sensor comparison. The collector adjustment was not carefully checked and may not have produced a symmetrical beam at the projection plane.

TABLE I

Point No.	Hy-Cal #2		NASA Slug Calorimeter		
	mv	BTU/ft^2-sec	Slope	mv/sec	BTU/ft^2-sec
1	3.96	47.6	37.4°	0.765	41.9
2	5.30	63.7	45.3°	1.011	55.4
3	6.96	83.7	52.3°	1.294	70.9
4	8.52	102.4	57.7°	1.582	86.7
5	7.66	92.1	54.8°	1.418	77.7
6	5.70	68.5	47.5°	1.091	59.8
7	4.22	50.7	41.5°	0.885	48.5
8	3.72	44.7	36.0°	0.727	39.8
9	4.28	51.4	39.3°	0.819	44.9
10	4.90	58.9	42.0°	0.900	49.3
11	4.72	56.7	40.8°	0.863	47.3
12	3.94	47.4	37.1°	0.756	41.4
Average Edge Intensity		64.0			56.3
For 14 Sources		896.0			788.2
14 Sources with Cosine Correction (0.63)		564.7			495.8

SPECTROLAB

DEVELOPMENT MEMORANDUM NO. 272- 40

SUBJECT: Effect of Gas Flow Rate Variation on Target Intensity

WRITTEN BY: Wagner Schlesinger WS
DATE: 8 March 1965
JOB NUMBER: 6002-11

On March 4, 1965, Run No. 49 was made in order to determine possible increases in target intensity due to reductions of the gas flow rate and the resulting increases in system voltage. Table 1 summarizes the results.

TABLE 1

Run No.	Gas		System Volts	Source Volts	Amperes	Sensor mv
	psi	cfm				
49 A	250	22	98.7	76.6	1550	5.49
49 B	250	19	101.4	79.3	1550	5.86
49 C	250	16	104.4	82.3	1550	6.04
49 D	250	22	98.7	76.6	1550	5.54

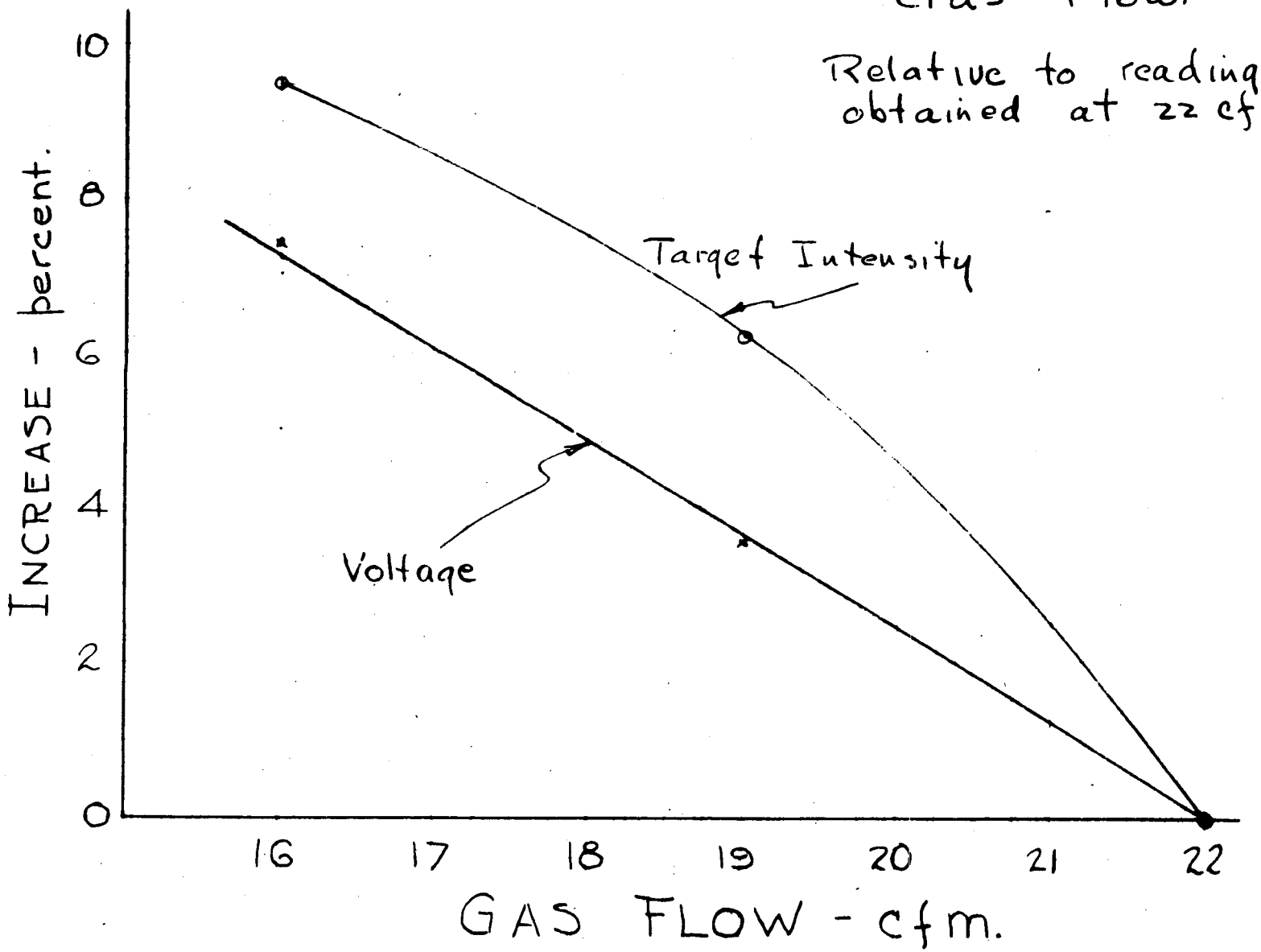
The Hy-Cal #2 sensor was used at a position 1.750" below the center of the target area.

The intensity of 5.86 at 16 cfm is 6.25% greater than 5.515, the average of the two readings at 22 cfm, while the intensity of 6.04 is 9.5% greater than this average. The percentage changes in target intensity and system voltage are plotted in Figure 1.

Target Intensity and Voltage Increase vs Gas Flow.

Relative to readings obtained at 22 cfm.

DM 272-40



SPECTROLAB

DEVELOPMENT MEMORANDUM NO. 272-41

SUBJECT: Target Edge Intensities at Reduced Diameters

WRITTEN BY: Wagner Schlesinger WS
DATE: 8 March 1965
JOB NUMBER: 6002-11

Run No. 48 was made under the following conditions:

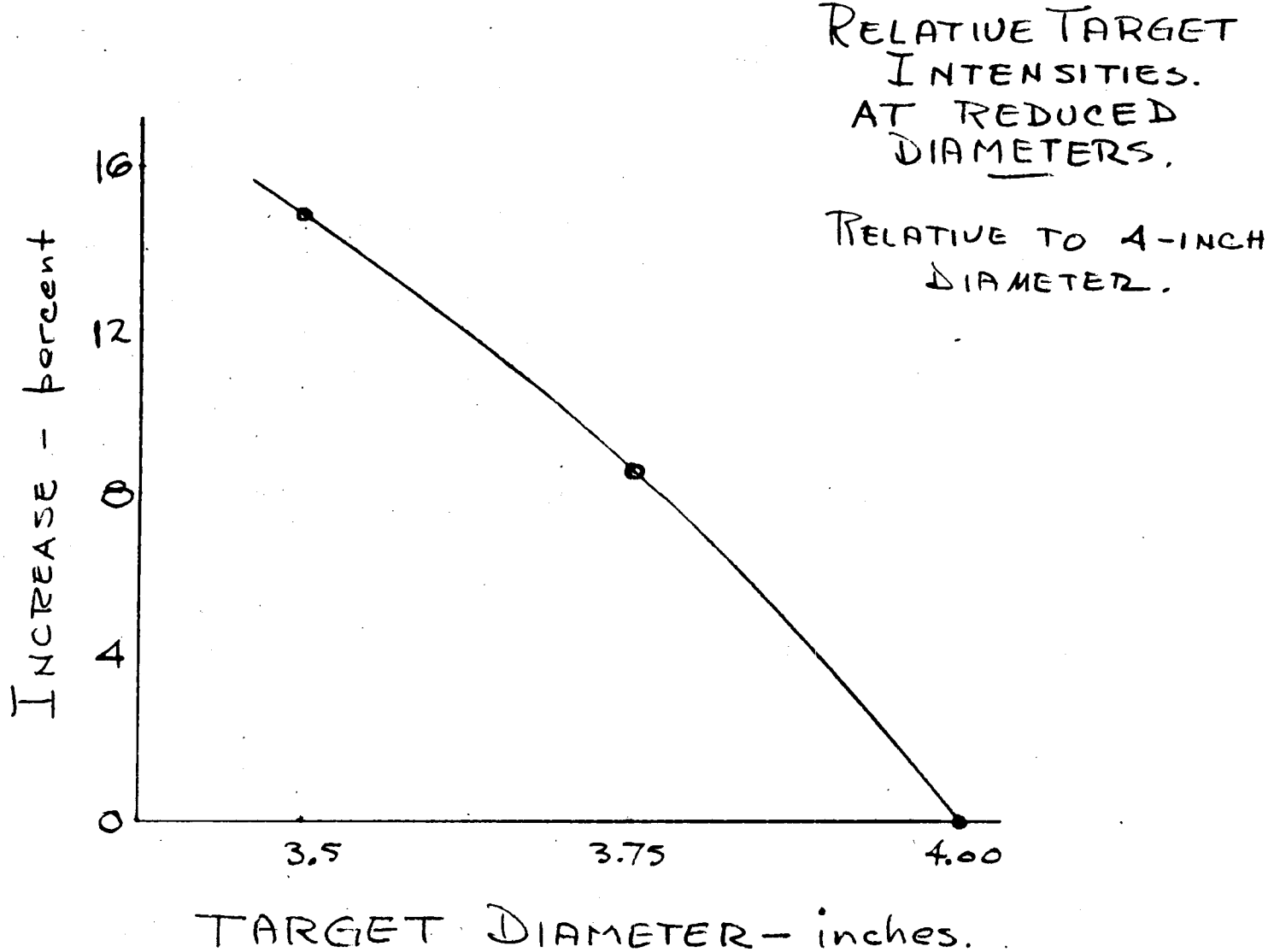
Amperes	1550
System Volts	99.3
Gas Flow	22 cfm
Gas Pressure	250 psi

This run was made in order to determine the relative intensities at the edge of targets of slightly reduced diameters. Intensities were recorded with the Hy-Cal #2 sensor at points 2", 1.875" and 1.750" above and below center. A horizontal diameter scan was also made. The results are given in Table 1 and plotted on Figure 1.

TABLE 1

Run No. 48

Target Diameter	Sensor Response - mv					% Increase over 4"
	Up	Down	Left	Right	Average	
4.00	4.00	4.38	7.55	5.34	5.32	-
3.75	4.62	4.91	8.00	5.60	5.78	8.6%
3.50	5.07	5.42	8.32	5.85	6.11	14.8%



DM 272-41

FIGURE 41.1

SPECTROLAB

DEVELOPMENT MEMORANDUM NO. 272-42

SUBJECT: Target Edge Intensities

WRITTEN BY: Wagner Schlesinger WS
DATE: 8 March 1965
JOB NUMBER: 6002-11

Run No. 46 was made on March 3, 1965 in order to check collector focus after installation of the source which had been reassembled following inspection of the quartz envelopes. At each focus setting, readings were made at points 2" above and below target center and a horizontal target plane diameter scan was made to obtain readings 2" to the left and right of center. The Hy-Cal #2 sensor with fresh camphor soot was used.

The run started with the collector in the position obtained in the last focus adjustment during Run No. 44. The adjustment screws, which have 16 threads per inch, were set at 1/2-turn increments.

The edge intensities are given in Table 1, together with results from Run No. 48-1 reported in Development Memorandum No. 272-41. All runs were made at 1550 amps, 250 psi and 22 cfm gas flow.

The average of the readings at the four listed positions is a good representative of the average edge intensity for the entire target circumference. This is shown by the results tabulated in Development Memorandum No. 272-39. With the Hy-Cal #2, the average for 12 points on the target edge is 1.4% lower than the four-point average; while with the NASA/Ames slug calorimeter, the 12 point average is 1.4% higher than the four-point average.

TABLE 1

Sensor Response - mv

Run No.	System Volts	Target Edge Position 2" Left	2" Right	2" Up	2" Down	Average	Collector Position
46-1	101.3	7.8 mv	4.9 mv	4.0 mv	4.3 mv	5.25 mv	Start
		7.7 mv	5.4 mv	3.8 mv	4.4 mv	5.33 mv	.031" Forward
		7.8 mv	5.4 mv	3.6 mv	4.3 mv	5.27 mv	.063" Forward
46-2	100.5	8.2 mv	5.1 mv	3.9 mv	4.6 mv	5.45 mv	Return to Start
		7.9 mv	5.2 mv	4.1 mv	4.6 mv	5.45 mv	.031" to Rear
		8.0 mv	5.1 mv	4.1 mv	4.6 mv	5.45 mv	.063" to Rear
		8.5 mv	5.3 mv	4.0 mv	4.7 mv	5.63 mv	Return to Start
48-1	99.3	7.55 mv	5.34 mv	4.00 mv	4.38 mv	5.32 mv	-

SPECTROLAB

DEVELOPMENT MEMORANDUM NO. 272-46

SUBJECT : Comparison of Sensors

WRITTEN BY: Wagner Schlesinger WS
DATE : 21 June 1965
JOB NUMBER: 6002-18

Run No. 68 on May 25, 1965 and Run No. 73 on May 28, 1965 were made to compare the following sensors:

Eppley Thermopile (#6132)
Hy-Cal Calorimeter #1 (#11146)
Hy-Cal Calorimeter #2 (#12492)

The test setup was similar to that described in Development Memorandum No. 272-15 and 272-21 except for the following:

(1) The water-cooled shield was removed from in front of the Eppley thermopile so that its normal 45° field of view was not obstructed. The shutter in front of the thermopile was retained and the thermopile was water-cooled.

(2) In Run No. 68 no amplifier was used, while in Run No. 73 a Beckman "Fitgo" amplifier was connected between the sensors and the Moseley 6S X-Y Recorder.

(3) Both water-cooled Hy-Cal sensors were freshly coated with camphor soot. No soot was used on the previous runs.

(4) Lower resistance solid leads were substituted for the coaxial cables previously used with the Eppley Thermopile.

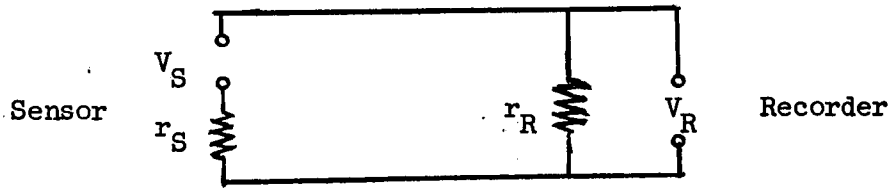
(5) The distances from the sensors to the plasma arc were:

	Run No. 68	Run No. 73
Eppley	29.30 in.	29.30 in.
Hy-Cal #1	9.55 in.	9.67 in.
Hy-Cal #2	9.55 in.	9.42 in.

The flux density falling on each sensor is inversely proportional to the square of its distance from the arc. Hence, the following ratios of flux densities are used.

	Run No. 68	Run No. 73
Hy-Cal #1 to Eppley	$(29.30/9.55)^2 = 9.413$	$(29.30/9.67)^2 = 9.181$
Hy-Cal #2 to Eppley	$(29.30/9.55)^2 = 9.413$	$(29.30/9.42)^2 = 9.675$

A correction is necessary for the effects of loading of the recorder produced by the sensor circuit resistance. The circuit employed can be represented thus:



where V_S = voltage generated by the sensor

V_R = voltage recorded by the recorder

r_S = resistance of sensor and lead wires

r_R = resistance of the recorder

i = current flowing in the circuit

$$i = \frac{V_S}{r_S + r_R} = \frac{V_R}{r_R}$$

hence $\frac{V_S}{V_R} = \frac{r_S + r_R}{r_R} = 1 + \frac{r_S}{r_R}$

The measured values of the resistances were:

Eppley	-	2.20 ohms
Hy-Cal #1	-	1.10 ohms
Hy-Cal #2	-	0.09 ohms

The resistance of the Moseley 6S recorder on the 0.5 mv/inch setting is 1000 ohms.

Substituting these values in the equation above.

Eppley $\frac{V_S}{V_R} = 1.0022$

Hy-Cal #1 $\frac{V_S}{V_R} = 1.0011$

Hy-Cal #2 $\frac{V_S}{V_R} = 1.0009$

This correction is not necessary for Run No. 73 since an amplifier was used.

The calibration factors of the three sensors are:

Eppley	=	4.68 mv/watt cm^{-2}
Hy-Cal #1	=	0.1614 mv/watt cm^{-2} (with camphor black)
Hy-Cal #2	=	0.07330 mv/watt cm^{-2} (with camphor black)

Calibration factor, distance correction factor and loading factor can be combined to give a single conversion factor to obtain flux densities from recorder indications. These flux densities are those which would be measured if all sensors were at the same distance from the source as the Eppley Thermopile.

Run No. 68

Eppley 4.68 x 1.000/1.0022 = 4.670 mv/w-cm^{-2} = 0.2141 w-cm^{-2}/mv

Hy-Cal #1 0.1614 x 9.413/1.0011 = 1.518 mv/w-cm^{-2} = 0.6589 w-cm^{-2}/mv

Hy-Cal #2 0.0733 x 9.413/1.0009 = 0.6893 mv/w-cm^{-2} = 1.4507 w-cm^{-2}/mv

Run No. 73

Eppley 4.68 x 1.000 = 4.68 mv/w-cm^{-2} = 0.2142w-cm^{-2}/mv

Hy-Cal #1 0.1614 x 9.181 = 1.482 mv/w-cm^{-2} = 0.6746

Hy-Cal #2 0.07330 x 9.675 = 0.709 mv/w-cm^{-2} = 1.411

Table 1 shows the recorded results, the derived flux densities and the ratios of the sensor responses. Corresponding data obtained during Run No. 13 adjusted for the same standard sensor distance of 29.30 inches are included for comparison. This run was made with the original Hy-Cal black coating, and the original Hy-Cal calibration was used. The ratios of the sensors to each other are plotted in Figure 1 in groups according to run, while in Figure 2, the same plots are grouped according to sensor. Figure 3 shows the reduced flux densities.

Run No.	Amperes	Eppley		Hy-Cal No. 1			Hy-Cal No. 2			
		MV Indicated	watts/cm^2	MV Indicated	watts/cm^2	Ratio to Eppley	MV Indicated	watts/cm^2	Ratio to Eppley	Ratio to H-C #1
68	1000	1.66	0.355	0.55	0.362	1.021	0.29	0.421	1.186	1.163
68	1300	2.31	0.495	0.78	0.514	1.038	0.41	0.595	1.202	1.158
68	1550	3.12	0.668	1.00	0.659	0.987	0.54	0.783	1.174	1.188
73	1000	2.05	0.439	0.78	.526	1.198	0.40	0.564	1.285	1.072
73	1300	2.54	0.544	1.08	.729	1.340	0.57	0.804	1.478	1.103
73	1550	3.53	0.756	1.48	.998	1.320	0.76	1.072	1.418	1.074
13	1000	1.98	0.451	0.38	0.568	1.259	0.39	0.695	1.540	1.223
13	1300	2.82	0.642	0.55	0.822	1.280	0.55	0.979	1.525	1.191
13	1500	3.47	0.791	0.66	0.987	1.248	0.68	1.211	1.532	1.228

Table 1

SENSOR COMPARISON.

RUNS 13, 68 & 73.

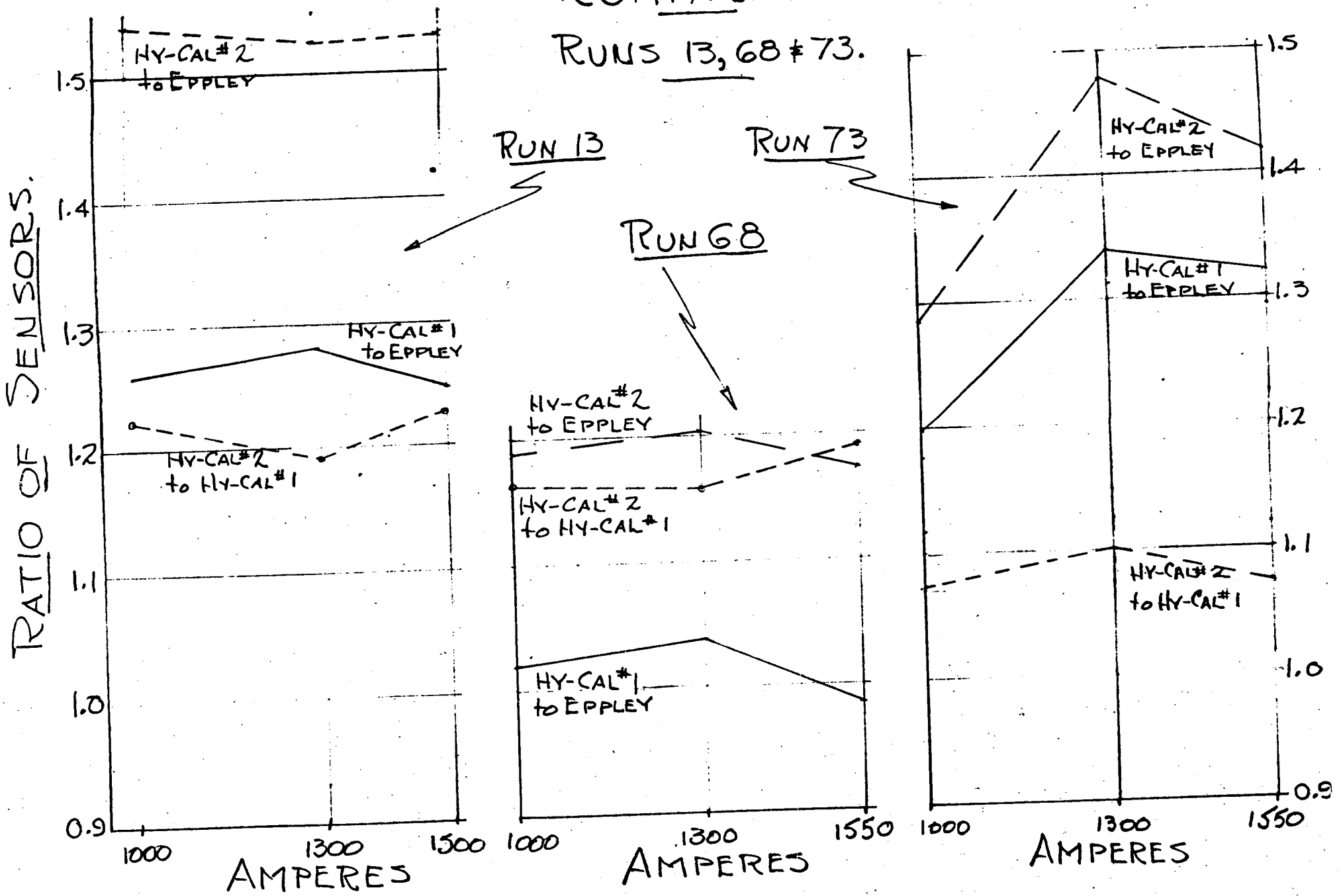


FIGURE 1

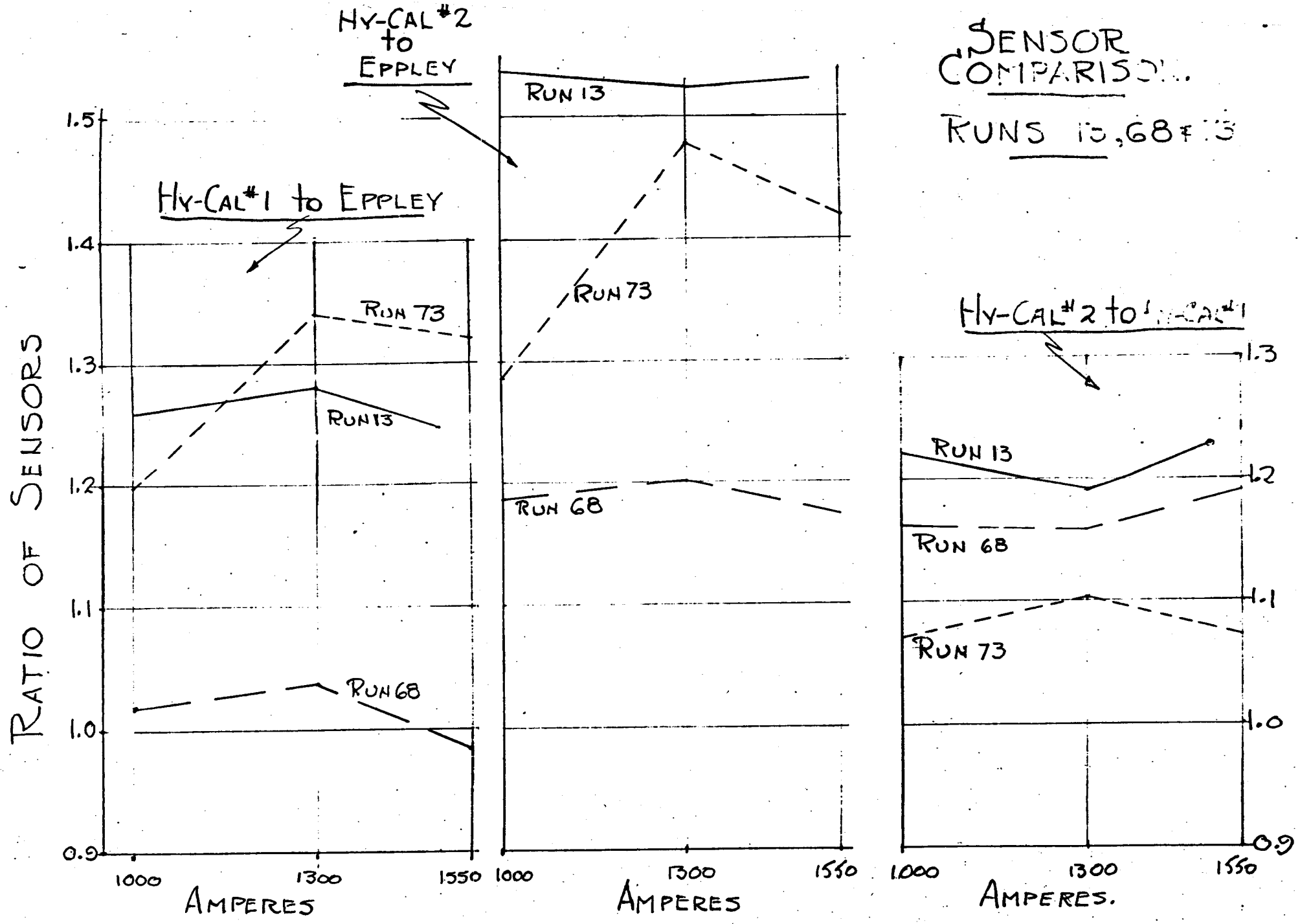
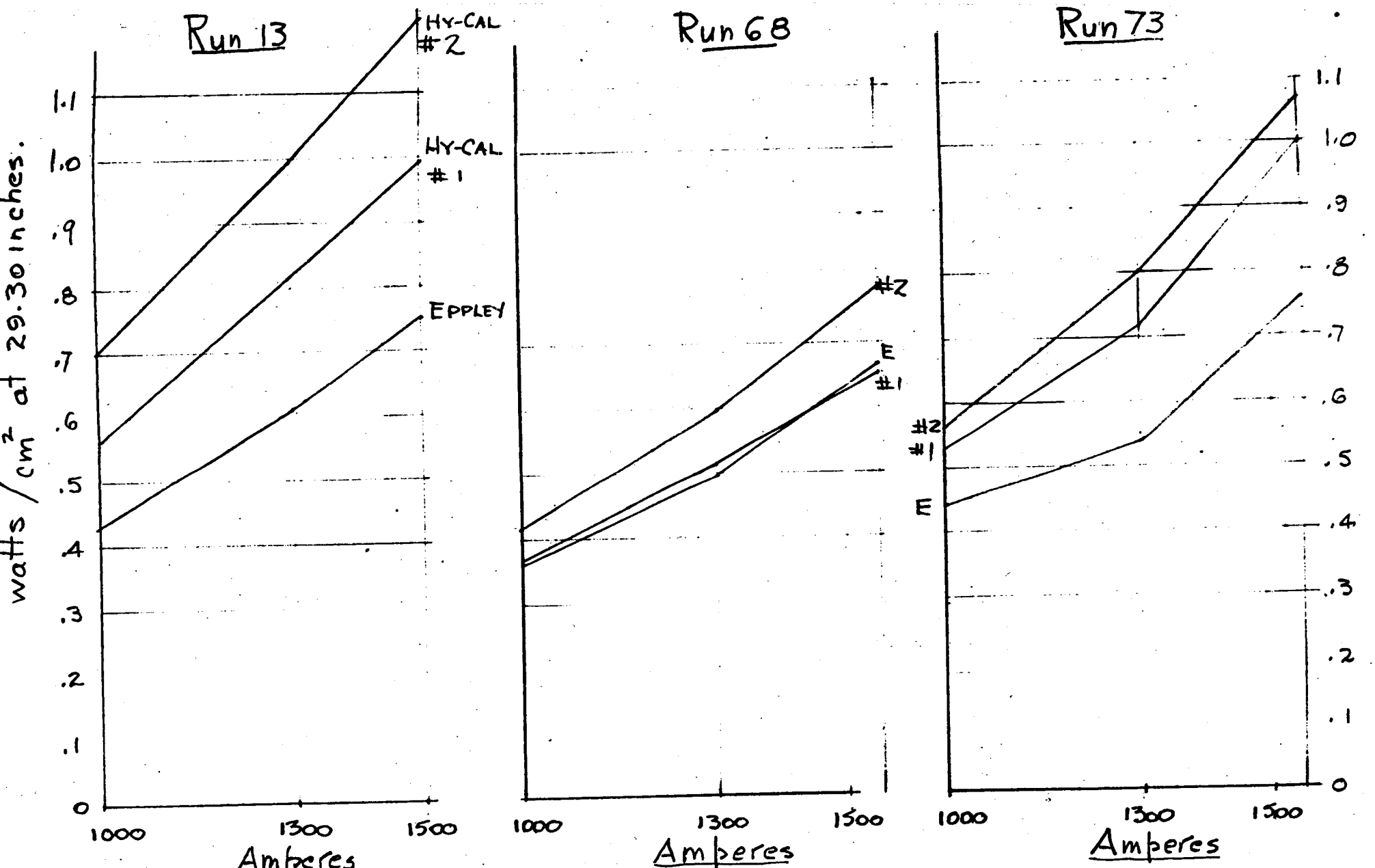

HY-CAL #2 to EPPLEY
HY-CAL #1 to EPPLEY
SENSOR COMPARISON
RUNS 13, 68 & 73
HY-CAL #2 to HY-CAL #1
RATIO OF SENSORS
1.5
1.4
1.3
1.2
1.1
1.0
0.9
RUN 13
RUN 73
RUN 68
1000
1300
1550
AMPERES
AMPERES
AMPERES.

FIGURE 2.



EPPLEY SHIELDED. NO SOOT ON HY-CALS.

EPPLEY NOT SHIELDED. SOOT ON HY-CALS

EPPLEY NOT SHIELDED. SOOT ON HY-CALS. AMPLIFIER USED.

FIGURE 3.

SPECTROLAB

DEVELOPMENT MEMORANDUM NO. 272-47

SUBJECT : Elliptical Mask for Radiative Heating System Field Lens

WRITTEN BY: Wagner Schlesinger WS
DATE : 29 June 1965
JOB NUMBER: 6002-35

On May 20, 1965, the procedure described below was used to design empirically the elliptical mask which is placed between the field lens and the water cell. The purpose of the mask is to reduce to a minimum the spillover of radiation on the sides of the target model. The projection lens forms an image of the mask in the vicinity of the target, and if this image could be made to fit the edges of the target exactly, the spillover would be reduced to zero.

Such a fit is impossible for several reasons. In order to obtain maximum energy, it is necessary to image the field lens, not the mask, on the target. For this reason, the mask image must be slightly behind (downstream from) the target. In addition, the target is not normal to the optical axis but is tilted so that one edge is in front of the mask image and the other edge is behind it, as shown in Figure 1.

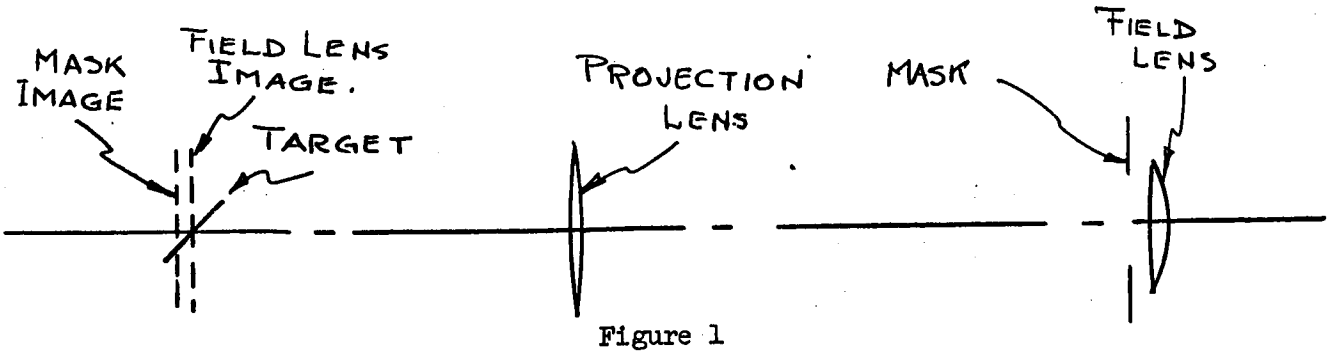


Figure 1

For these reasons, the mask image is out of focus over most of the target. The mask image is further blurred by the sizeable aberrations of the projection lens.

The projection lens also forms an image of the target near the field lens and the mask position, and this image can be used to determine the shape and size of the required mask opening. A thin sheet of metal with a 4-inch diameter opening was set up so that the opening occupied the exact target position. A light source and diffusing screen were placed behind the opening as shown in Figure 2.

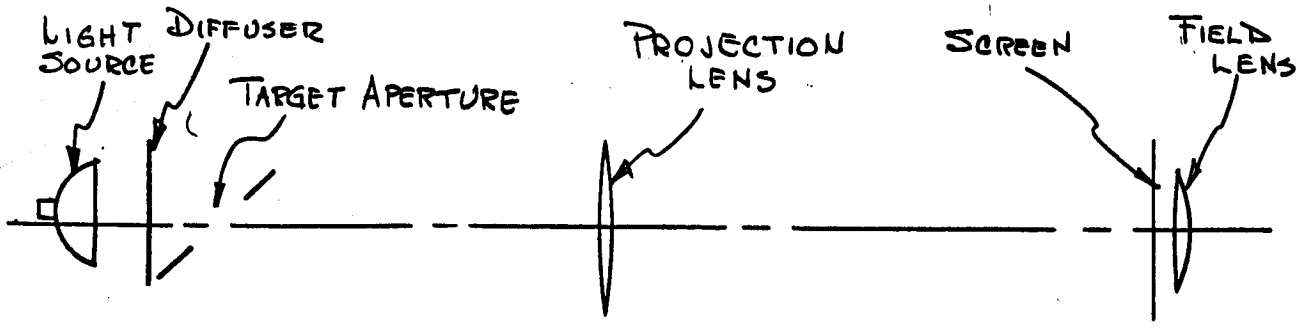


Figure 2

A screen was placed in front of the field lens in the exact position of the mask. An out of focus image of the target aperture appeared on this screen and a tracing was made of the outline of the faintest part of this image. The irregularities of this tracing were smoothed and an opening corresponding to the resulting outline was cut in a temporary mask placed as shown in Figure 3.

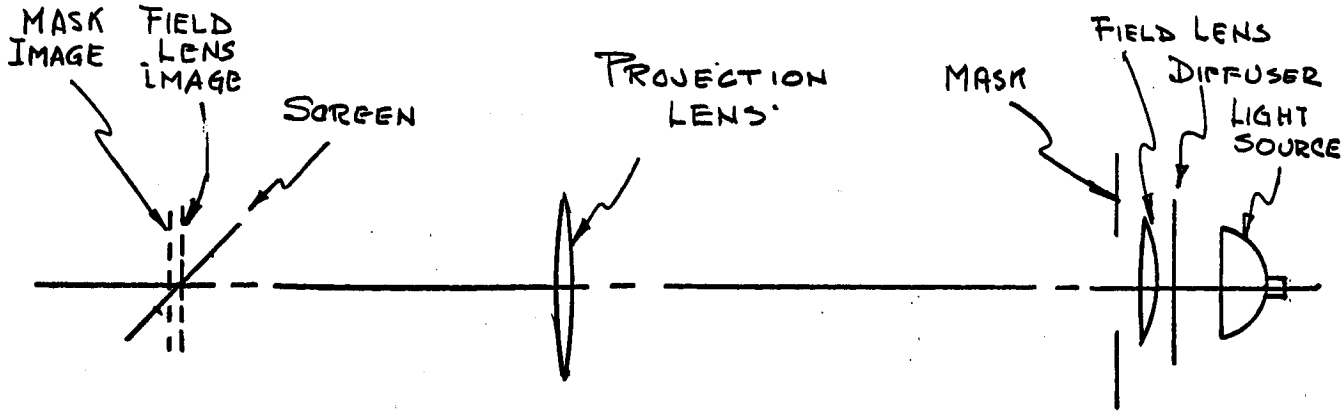


Figure 3

A 4-inch diameter circle was drawn on a white screen which was placed so that the circle coincided with the target position.

A slightly blurred image of the temporary mask was seen on the target screen when the light source illuminated the mask. This image was a little undersized and a new mask was cut with a larger opening. The image of this second mask was slightly oversized. This is desirable in order to avoid any possibility of reducing the intensity of radiation at the edge of the target.

The opening in the mask was 6.44 inches long and 5.33 inches wide. An ellipse was drawn using these figures for the major and minor axes respectively and the mask opening fitted this ellipse almost exactly. Hence, the mask opening is a true ellipse whose equation is

$$x^2/10.37 + y^2/7.10 = 1$$

SPECTROLAB

DEVELOPMENT MEMORANDUM NO. 272-49

SUBJECT : Uniformity Filter Test
WRITTEN BY: Wagner Schlesinger WS
DATE : 23 July 1965
JOB NUMBER: 6002-27

The filter tested consisted of two quartz plates, each 0.312 inch thick, separated by 0.313 inch of flowing tap water. A dot pattern uniformity filter was applied to the outer quartz surface nearest to the target. The filter specification called for 100% transmission at 5.50" diameter and 50% transmission at the center, the transmission to vary from 100% to 50% in a spherical manner. The 5.50" diameter is imaged by the projection lens as a circle slightly smaller than 4.00" in diameter at the projection plane, and hence there is no reduction of intensity at the target edge. The filter was placed in its normal position just downstream from the field lens.

Two runs were made under the following conditions:

Run No.	Amperes	System Volts	Gas cfm	Gas psi	Filter
56	1550	94.5	44	250	in.
57	1550	94.2	44	250	out.

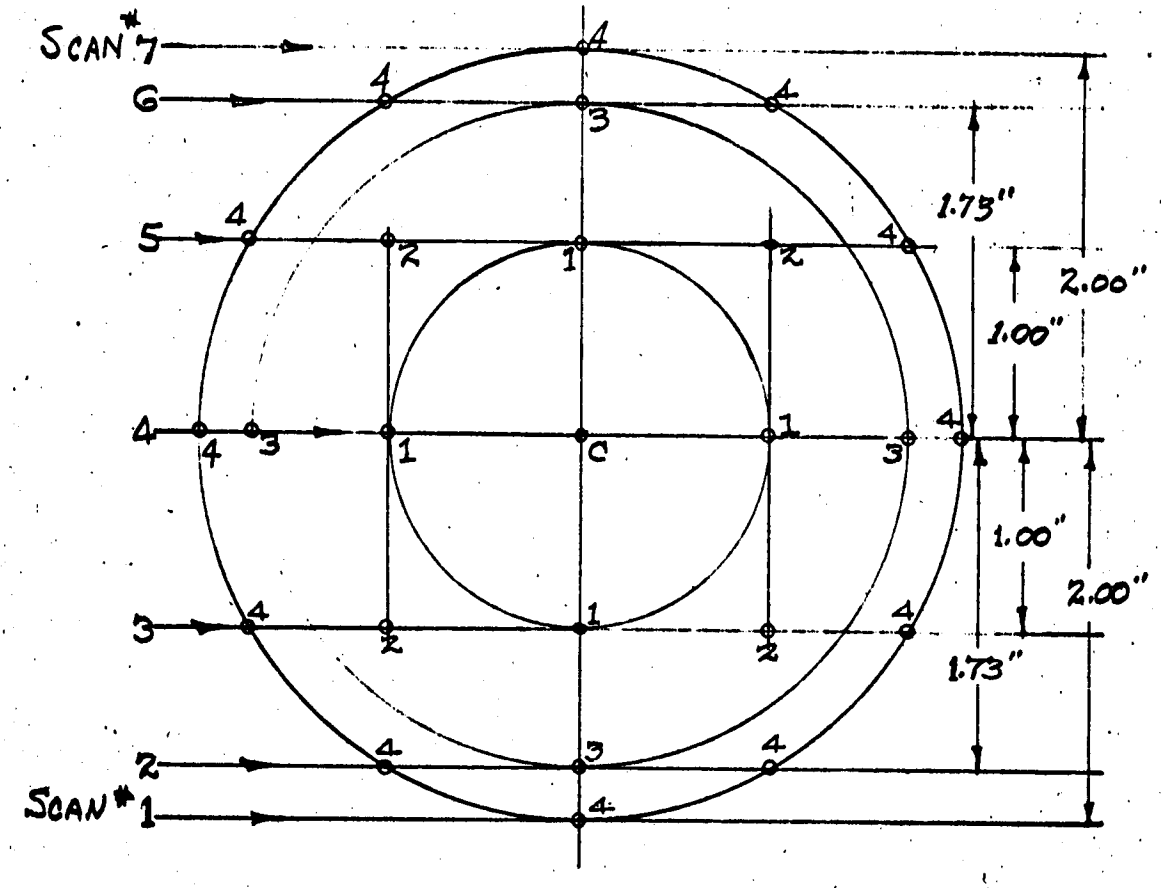
Seven continuous horizontal scans were made across the target plane, as shown in Figure 1, for each run, with the Hy-Cal #2 radiometer. The output of the radiometer was recorded on the Y-axis of a Moseley 6S X-Y recorder. The output of a precision potentiometer geared to the scan carriage horizontal motion was connected to the X-axis of the recorder in order to record the carriage position automatically.

The scan locations were chosen to give 12 equally spaced points around the edge of the target in order to obtain a good average value of edge intensity. However, it is also possible to find symmetrically arranged groups of data points at three other radii as shown by the numbered positions on Figure 1. The raw data from the scan curves are tabulated in Table I, together with reduced averages for the various radii. These averages are plotted on Figure 2. With the filter in place, the edge intensity is reduced to 68% of its value without the filter. Since none of this particular reduction is due to the uniformity dot pattern, it must represent the losses due to the water and the quartz plates. Applying this factor to the unfiltered curve gives points for the dotted curve showing predicted intensity distribution with the quartz-water filter without the uniformity dot pattern.

Maximum and minimum values on the filtered curve represent a uniformity of $\pm$ 8.8%. The existing filter could be improved by increasing the center transmission slightly. The resulting uniformity would become $\pm$ 5.9%.

	RUN NO. 56, WITH FILTER					RUN NO. 57, WITHOUT FILTER				
RADIUS, IN.	0.00	1.00	1.41	1.73	2.00	0.00	1.00	1.41	1.73	2.00
RECORDED MV	2.79	3.40 3.47 3.38 3.08	3.47 3.38 3.17 3.15	3.36 3.02 3.13 3.33	2.53 2.67 3.28 3.53 3.32 2.99 2.58 2.66 2.73 3.05 3.07 2.90	7.82	7.58 7.10 7.05 6.83	6.43 6.27 6.49 5.94	5.07 6.43 4.48 5.85	3.39 2.30 5.05 5.28 4.50 3.53 3.72 4.04 5.33 5.70 5.08 3.80
TOTAL	2.79	13.33	13.17	12.84	35.31	7.82	28.56	25.13	21.83	51.72
AVERAGE MV	2.79	3.33	3.29	3.21	2.94	7.82	7.08	6.19	5.46	4.31
AVE. BTU/FT^{2}SEC	33.54	40.03	39.55	38.58	35.34	94.00	85.10	74.40	65.63	51.81
DITTO, 14 CHANNELS	469.6	560.4	553.7	540.1	494.8	1316.0	1191.4	1041.6	918.8	725.3
14 CHANNELS COSINE CORRECTED	295.4	352.5	348.3	339.7	311.2	827.8	749.4	655.2	577.9	456.2

TABLE I



POINT No.'s	RADIUS
1	1.00"
2	1.41"
3	1.73"
4	2.00"

FIGURE 1.

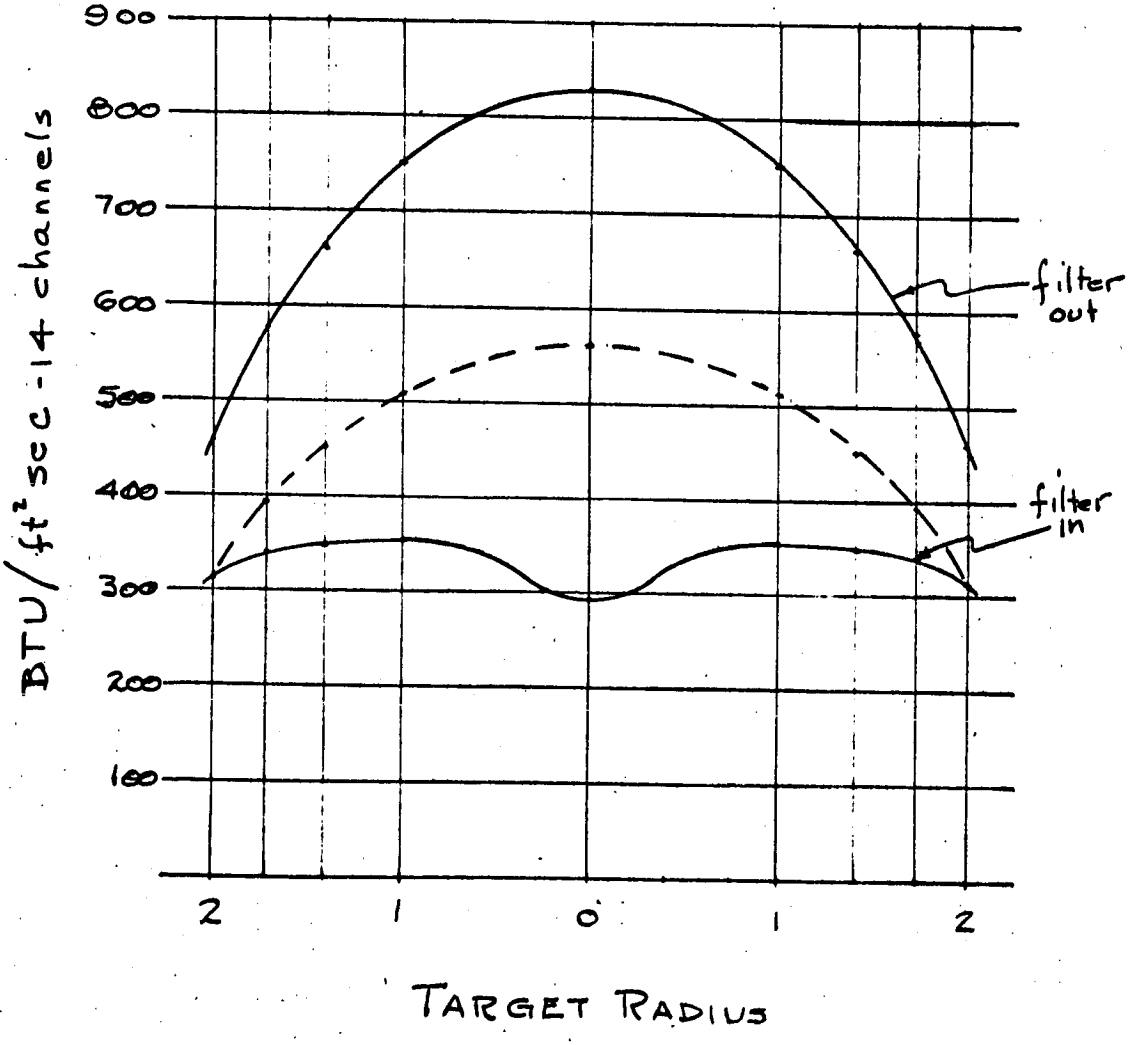

900
800
700
600
500
400
300
200
100
BTU/ft² sec - 14 channels
filter out
filter in
2
1
0
1
2
TARGET RADIUS

FIGURE 2

SPECTROLAB

DEVELOPMENT MEMORANDUM NO. 272-95

SUBJECT : Lens Absorption Analysis for the Radiative Heating System

WRITTEN BY: John Nagle
DATE : 27 July 1964
JOB NUMBER: 6002-15

LENS ABSORPTION ANALYSIS FOR THE RADIATIVE HEATING SYSTEM

The following analysis determines the field lens and projection lens absorbtance and transmittance. The absorption data was required as basic inputs for analysis determining the operating temperature of the lenses, especially the projection lens where a vacuum seal requirement exists. The lens transmission data is needed as an input for efficiency analyses. It must be emphasized that the accuracy of the lens absorption and transmission is dependent upon the accuracy of the source spectral distribution. Since the spectral distribution of the radiation eminating from the final radiation source has not as yet been measured, some caution should be exercised in the use of the values obtained.

SUMMARY: Calculations were performed to determine the total power absorption and transmission for the projection and the field lenses. It was found that there would be a 6.6% absorption of power by the field lens with a total transmission of 86.9%. The remaining 6.5% of the radiation would be accounted for by reflections. For the projection lens, the absorption is 7.6%, transmission 85.9% and reflection 6.5%. Figure I represents the spectral energy distribution incident upon the field lens. Figure II represents the spectral energy distribution transmitted by the field lens and incident upon the projection lens. Figure III represents the spectral energy distribution transmitted by the projection lens and incident upon the target.

I. Absorption of radiation within a lens

The values of absorption for a one centimeter slab of fused silica were computed for each of twenty (20) spectral bands for a range of wavelengths between .25 micron and 3.0 microns.

It is the purpose of this analysis to show how this data may be used to determine values of absorption for slabs which are of a different thickness. In doing so, the following assumption is made: the total effective reflection from both faces will not vary appreciably with thickness of the slab for "thin" slabs.

let

t_{1i} be the transmission for the ith band for a 1 cm slab, taken from Figure IV, "Transmission of a 1 cm Quartz Sample"

R_{1i} be the reflection for the ith band for a 1 cm slab.

A_{1i} be the absorption for the ith band for a 1 cm slab

so that for a 1 cm slab, for the ith band,

$$t_{1i} + A_{1i} + R_{1i} = 1$$

For a slab, which in the limit goes to zero thickness, the absorption will approach zero so that the transmission will be

$$t_{oi} = 1 - R_{oi} \approx 1 - R_{1i}$$

and the transmission through a slab of thickness x will then be given by the expression

$$t_{xi} = t_{oi}\, e^{-\alpha_i x}$$

where α_i, the absorption coefficient, is a constant which must be determined for each band.

The absorption in this distance will be $A_{xi} = 1 - R_{xi} - t_{xi}$

but $1 - R_{xi} \cong 1 - R_{1i} \cong t_{oi}$,

so that

$$A_{xi} = t_{oi}\left[1 - e^{-d_i x}\right].$$

For the 1 cm slab previously considered,

for which x = 1,

$$A_{ii} = t_{oi}\left[1 - e^{-\alpha_i}\right]$$

so that

$$\alpha_i = \ln\left[\frac{t_{oi}}{t_{oi} - A_{ii}}\right]$$

which may be evaluated directly.

Expanding for $\infty > \frac{t_{oi}}{t_{oi} - A_{ii}} > 1$

$$\alpha = \left[\frac{t_{oi}}{t_{oi} - A_{ii}} - 1\right] - \frac{1}{2}\left[\frac{t_{oi}}{t_{oi} - A_{ii}} - 1\right]^2 + \text{higher order terms}$$

Noting that $\left[\frac{t_{oi}}{t_{oi} - A_{ii}} - 1\right] = \frac{A_{ii}}{t_{ii}}$

so that $\alpha_i = \frac{A_{ii}}{t_{ii}} - \frac{1}{2}\left[\frac{A_{ii}}{t_{ii}}\right] + \text{higher order terms}$

It should be noted that since

$$e^{-\alpha_i x} \approx 1 - \alpha_i x + \frac{\alpha_i^2 x^2}{2}$$

the absorption becomes

$$A_{xi} \approx t_{oi}\left(\alpha_i x - \frac{\alpha_i^2 x^2}{2}\right) + \text{higher order terms)}$$

The method for determination of x, the path length will be considered in a later section of this report.

The values of total reflectance were calculated for each of the 20 bands, by means of the method suggested in Appendix F, Technical Report, "Systems Concept Study - Radiative Heating System".

Using the spectral distribution presented in Figure IV, the percentage of total energy was computed for each band. This value was used to "weight" the absorption and transmission value for the respective bands, such that if $\frac{E_i}{\Sigma E_i}$ is the fraction of total energy associated with the i th band,

where $\Sigma E_i = 1$ and A_i and t_i are the absorption and transmission for that band, then the total absorption is $A = \Sigma A_i E_i$ and the transmission is $t = \Sigma t_i E_i$

A resume of these results for the field lens is given in Table I while those for the projection lens are found in Table II.

II. Determination of average path length for the field and projection lens.

The average path length for each lens was determined using the assumption that $\bar{x} = \frac{2\pi \int_0^R x r\, dr}{2\pi \int_0^R r\, dr}$

Where x is the thickness at a distance r from the center of the lens.

Note that the integral $2\pi \int_0^R x r\, dr$ is the volume of the lens, while the integral $2\pi \int_0^R r\, dr$

is the projected area of the lens, so that

$$\bar{x} = \frac{\text{Volume of the lens}}{\text{Area of lens}}$$

Both of these factors may readily be determined from geometric considerations. The results of the calculations are as follows:

For the field lens, $\bar{x}$ = 1.93 cm

and for the projection lens, $\bar{x}$ = 2.94 cm.

III. Spectral energy distribution for the field and projection lenses.

Using the value of transmission for each lens, for the 20 bands selected the percentage of the total energy transmitted for each band was computed using the expression $E_{iT} = \frac{t_i E_i}{\sum_{i=1}^{20} t_i E_i}$

where E_{it} is the fraction of the total energy transmitted associated with the ith band. These values are given in Table I for the field lens, and Table II for the projection lens.

A graphical representation of these distributions are shown in Figures IIand III, for the field and projection lenses respectively.

IV. CONCLUSION

It should be noted that the values of transmission for the 1 cm slab of fused silica have an uncertainty of at least .01 and therefore there will be an uncertainty in the calculated values of the absorption coefficient which is of the same order.

Since the total absorption for a sample of thickness x is given by

$$A_i \approx t_{oi} \alpha_i x$$

the error in the absorption will be

$$dA_i \approx t_{oi} x \, d\alpha$$

that is, proportional to the average lens thickness. For the field lens, $\bar{x} \simeq 2$ cm, so that the possible error in the absorption is of the order of .02 or about 30%. For the projection lens with average path length of approximately 3 cm, the error would be of the order of 50%.

Based on Spectrolab's previous experience with fused silica, it would appear that the evaluation of transmissions indicated are on the low side of normal expectation. If this is the case, the absorption for the field and projection lenses would be lower or of the order of 4 percent total absorption.

In order that these values be predicted with a higher degree of certainty, it is necessary to make more accurate determinations of the absorption coefficients for the twenty spectral bands. This can be done if a thicker sample is used in making the transmission measurements, since the error in the determinations of the absorption coefficient is inversely proportional to the length of the determination sample.

Absorption, Transmission and Energy Distribution Transmitted by Field Lens

Band	t_{1i}	t_{oi}	A_{1i}	A_{1i}/t_{1i}	α_i	A_i	E_i	$A_i \cdot E_i$
1	.813	.932	.119	.146	.136	.215	.0073	.00156
2	.901	.930	.029	.032	.032	.056	.1099	.00615
3	.922	.933	.011	.012	.012	.021	.1383	.00290
4	.921	.933	.012	.013	.013	.023	.0998	.00229
5	.921	.934	.013	.014	.014	.025	.0800	.00200
6	.921	.935	.014	.015	.015	.027	.1104	.00298
7	.920	.934	.014	.015	.015	.027	.1078	.00291
8	.921	.935	.014	.015	.015	.027	.0493	.00133
9	.922	.936	.014	.015	.015	.027	.0367	.00099
10	.921	.936	.015	.016	.016	.029	.0332	.00096
11	.870	.939	.069	.079	.076	.130	.0358	.00465
12	.841	.942	.101	.120	.113	.184	.0437	.00804
13	.860	.940	.080	.093	.089	.146	.0320	.00467
14	.901	.938	.037	.041	.040	.069	.0203	.00140
15	.921	.938	.016	.017	.017	.031	.0165	.00051
16	.921	.939	.017	.018	.018	.032	.0112	.00036
17	.921	.939	.017	.018	.018	.032	.0097	.00031
18	.921	.939	.017	.018	.018	.032	.0073	.00023
19	.820	.945	.125	.152	.141	.225	.0303	.00681
20	.440	.961	.521		.7793	.747	.0197	.01472

$A = .06577$

TABLE I

Absorption, Transmission and Energy Distribution Transmitted by Field Lens

Band				Incident Distribution		Transmitted Distribution
	A_i	R_{ie}	$t_i = 1 - R_{ie} - A_i$	E_i	$t_i E_i$	$E_{it} = t_i E_i / \sum t_i E_i$
1	.215	.068	.717	.0073	.0052	.0060
2	.056	.070	.874	.1099	.0961	.1106
3	.021	.069	.910	.1383	.1259	.1449
4	.023	.067	.910	.0998	.0908	.1045
5	.025	.066	.909	.0800	.0727	.0837
6	.027	.065	.908	.1104	.1002	.1153
7	.027	.066	.907	.1078	.0978	.1126
8	.027	.065	.908	.0493	.0448	.0516
9	.027	.064	.909	.0367	.0337	.0388
10	.029	.064	.906	.0332	.0301	.0346
11	.130	.060	.810	.0358	.0290	.0334
12	.184	.058	.758	.0437	.0331	.0380
13	.146	.060	.794	.0320	.0254	.0292
14	.069	.062	.869	.0203	.0176	.0203
15	.031	.063	.906	.0165	.0149	.0172
16	.032	.062	.906	.0112	.0101	.0116
17	.032	.062	.906	.0097	.0088	.0101
18	.032	.062	.906	.0073	.0066	.0076
19	.225	.055	.720	.0303	.0218	.0251
20	.747	.039	.214	.0197	.0042	.0048

TABLE I

(continued)

$\bar{t} = .869$

$\bar{A} = .066$

$\bar{R} = .065$

Absorption, Transmission and Energy Distribution Transmitted by Projection Lens

Band	t_{oi}	α_i	A_i	E_i	$A_i \cdot E_i$	R_i	$R \cdot E_i$
1	.932	.136	.307	.0060	.00184	.0680	.00040
2	.930	.032	.084	.1106	.00929	.0699	.00773
3	.933	.012	.032	.1449	.00463	.0686	.00940
4	.933	.013	.035	.1045	.00368	.0668	.00698
5	.934	.014	.037	.0837	.00309	.0659	.00552
6	.935	.015	.040	.1153	.00461	.0653	.00753
7	.934	.015	.040	.1126	.00450	.0656	.00741
8	.935	.015	.040	.0516	.00206	.0646	.00333
9	.936	.015	.040	.0388	.00155	.0644	.00250
10	.936	.016	.043	.0346	.00149	.0640	.00221
11	.939	.076	.187	.0334	.00625	.0606	.00202
12	.942	.113	.267	.0380	.01014	.0583	.00222
13	.940	.089	.216	.0292	.00630	.0595	.00174
14	.938	.040	.104	.0203	.00211	.0616	.00125
15	.938	.017	.045	.0172	.00077	.0626	.00108
16	.939	.018	.049	.0116	.00057	.0624	.00072
17	.939	.018	.049	.0101	.00049	.0619	.00062
18	.939	.018	.049	.0076	.00037	.0617	.00047
19	.945	.141	.322	.0251	.00808	.0546	.00137
20	.961	.7793	.864	.0048	.00415	.0386	.00019

TABLE II

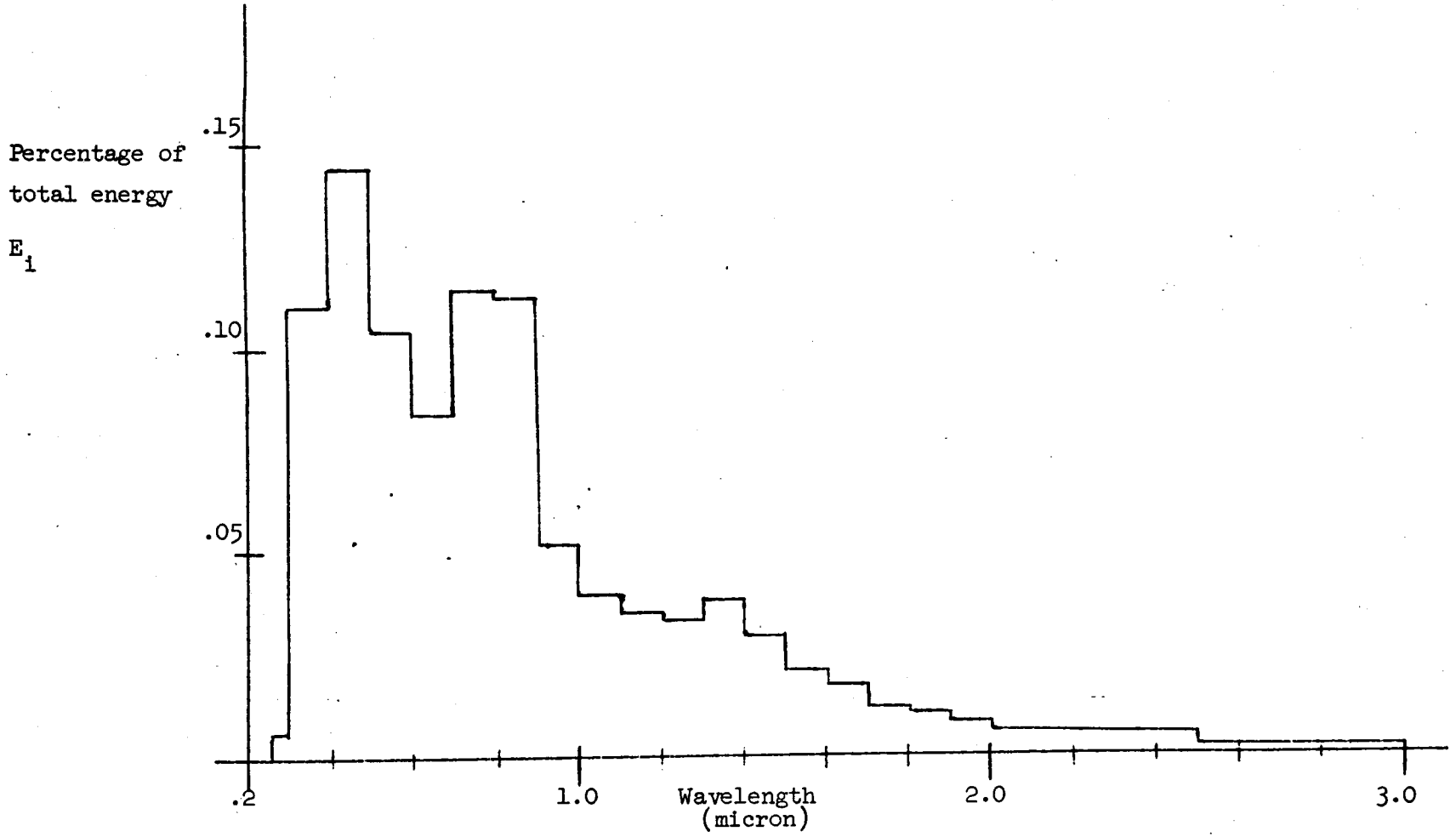
Absorption, Transmission and Energy Distribution Transmitted by Projection Lens

Band	A_i	R_{ie}	$t_i = 1 - A_i - R_{ie}$	Incident Distribution E_i	$t_i \cdot E_i$	Transmitted Distribution $E_{it} = t_i \cdot E_i / \Sigma_i E_i$
1	.307	.0680	.625	.0060	.0038	.0044
2	.084	.0699	.846	.1106	.0936	.1091
3	.032	.0686	.899	.1449	.1303	.1519
4	.035	.0668	.898	.1045	.0938	.1094
5	.037	.0659	.897	.0837	.0751	.0876
6	.040	.0653	.895	.1153	.1032	.1203
7	.040	.0656	.894	.1126	.1006	.1173
8	.040	.0646	.895	.0516	.0462	.0539
9	.040	.0644	.895	.0388	.0347	.0405
10	.043	.0640	.893	.0346	.0301	.0351
11	.187	.0606	.752	.0334	.0251	.0293
12	.267	.0583	.675	.0380	.0257	.0299
13	.216	.0595	.724	.0292	.0211	.0246
14	.104	.0616	.834	.0203	.0169	.0197
15	.045	.0626	.892	.0172	.0153	.0178
16	.049	.0624	.889	.0116	.0103	.0120
17	.049	.0619	.889	.0101	.0090	.0105
18	.049	.0617	.889	.0076	.0066	.0077
19	.322	.0546	.623	.0251	.0156	.0182
20	.864	.0386	.097	.0048	.0005	.0058

TABLE II

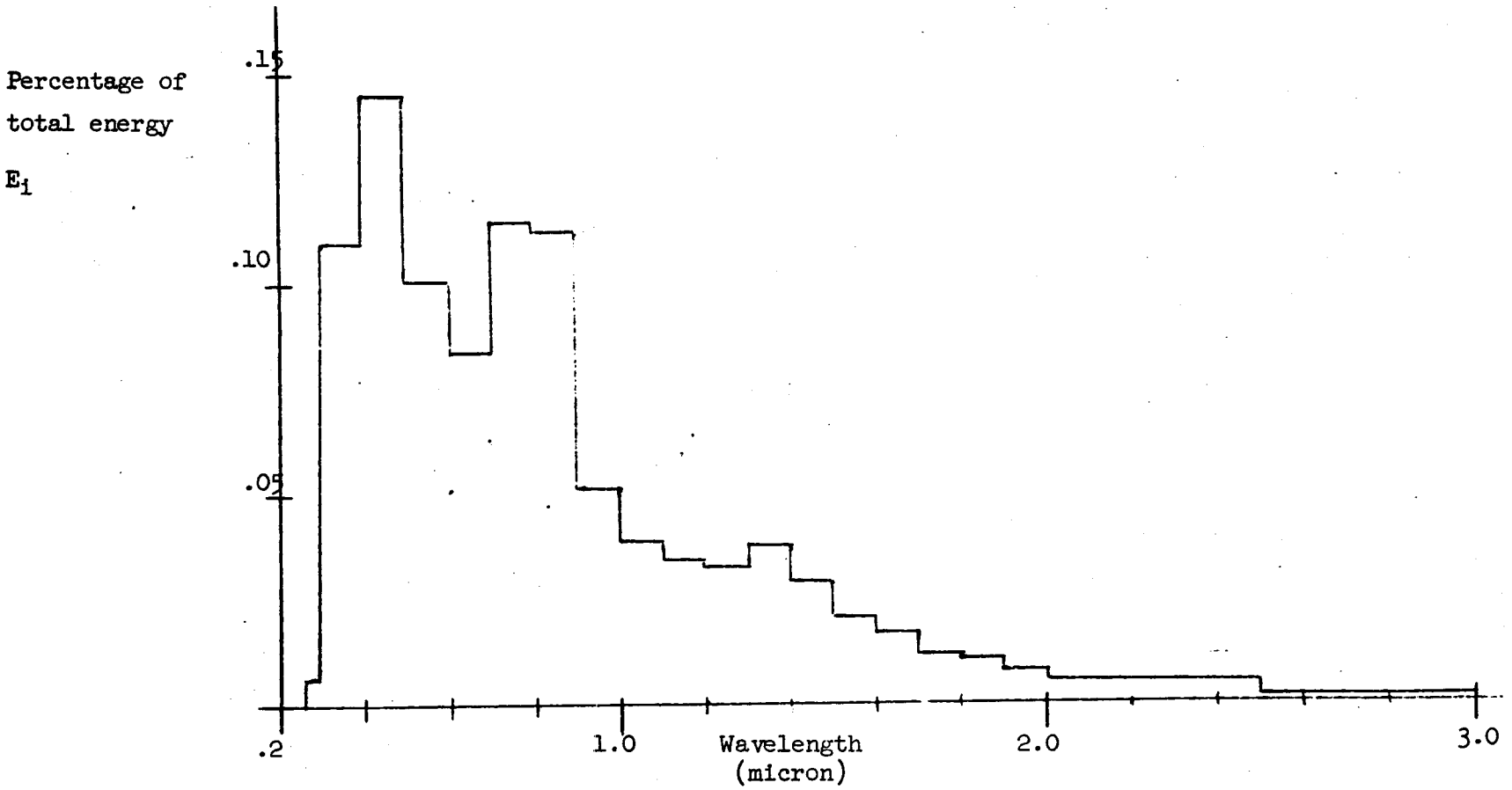
(continued)

$t = .859$
$A = .076$
$R = .065$



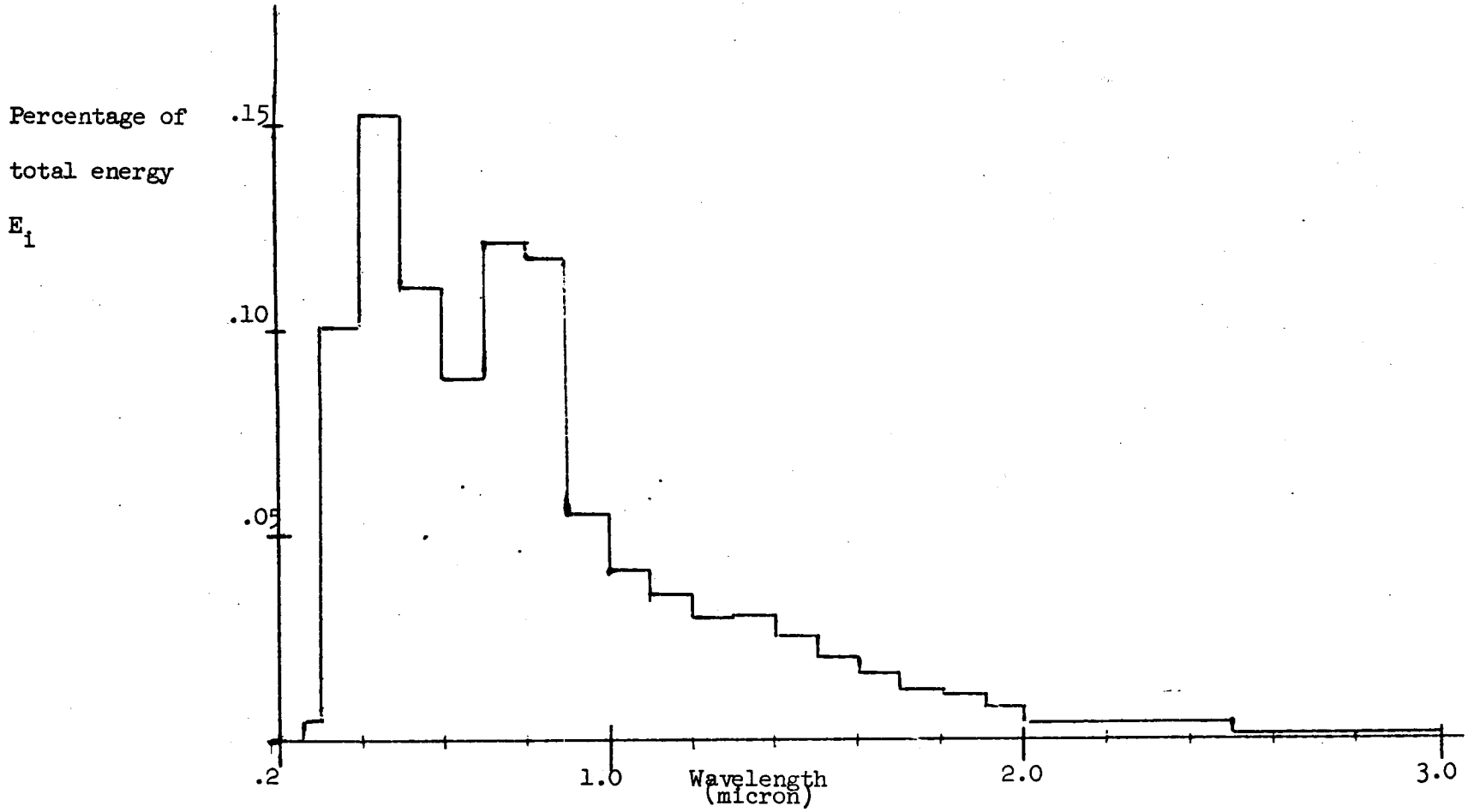
SPECTRAL ENERGY DISTRIBUTION INCIDENT UPON FIELD LENS

Fig. 1



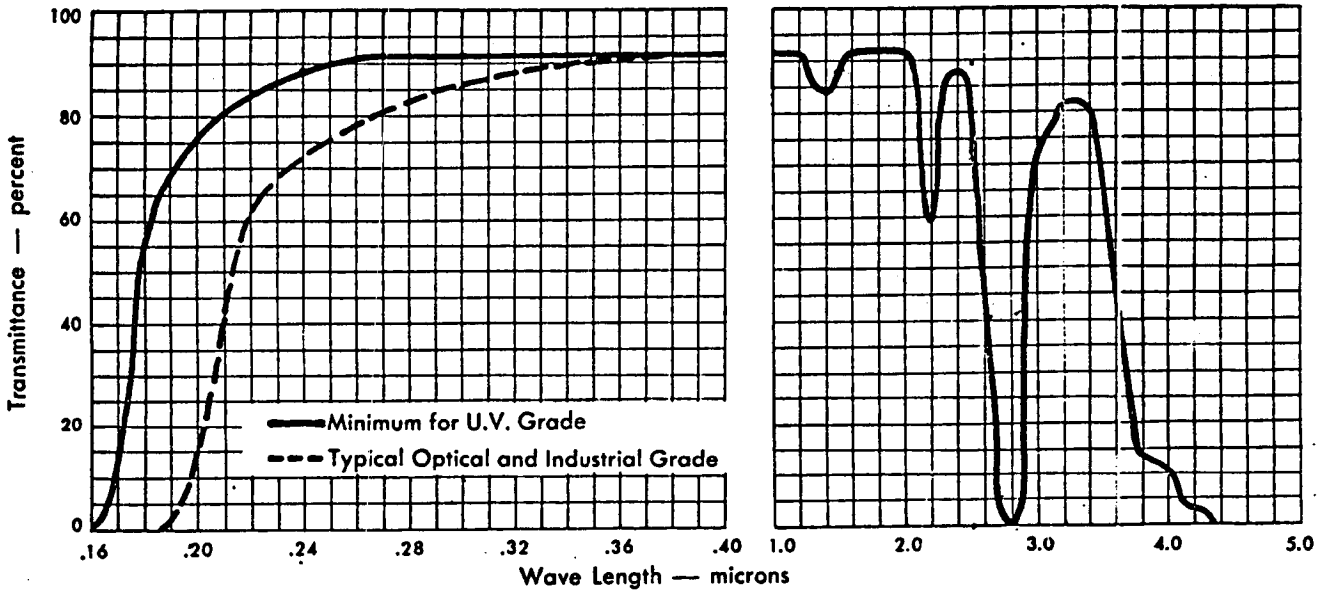
SPECTRAL ENERGY DISTRIBUTION TRANSMITTED BY FIELD LENS

Fig. 2



SPECTRAL ENERGY DISTRIBUTION TRANSMITTED BY PROJECTION LENS

Fig. 3



TRANSMISSION OF A 1 cm QUARTZ SAMPLE

Fig. 4

SPECTROLAB

DEVELOPMENT MEMORANDUM NO. 272-96

SUBJECT : Thermal Analysis for the Field and Projection Lens

WRITTEN BY: John Nagle
DATE : 27 July 1964
JOB NUMBER: 6002-15

Thermal Analysis for the Field and Projection Lens.

As a result of the absorption of energy from the radiation passing through the lenses of the Radiative Heating System, the temperature of these lenses will be elevated above the room ambient temperature. It is the purpose of this analysis to predict the extent of these temperature elevations.

I. Field Lens

It is assumed that the field lens consist of two parallel plane faces, each of Area A, which are each radiating into an infinite surroundings which has a temperature T_s. Further it is assumed that no heat will be lost due to conduction through the edges of the lens into the lens holder.

Using the Stefan-Boltzmann radiation law, $q = 2A\varepsilon\sigma(T^4 - T_s^4)$

Where, q is the power absorption by the lens (watts)

A is the area of each face (centimeter).

ε is the emissivity of each face.

σ is the Stefan - Boltzmann constant, $\sigma = 5.669 \times 10^{-12}$ watt-cm^{-2}-K^4

T is the Kelvin temperature of the lens.

T_s is the Kelvin temperature of the surroundings.

The steady state temperature of the lens may be evaluated.

For the field lens, the following values of the above quantities are appropriate:

q =	900 watts	ε =	.70
A =	320 cm^2	T_s =	430°K

Solving for the T, the steady temperature of the field lens is found to be 721°K.

II. Projection Lens

Although the preceeding assumptions would be appropriate for determining the steady state temperature of the projection lens, it should be pointed out that the power absorption by the projection lens will depend upon a total of three factors. They are:

a) Absorption of incident radiation from the source.

b) Absorption of radiation originating at the target and gas cap.

c) Absorption of radiation reflected from the target.

These three factors will be considered in turn.

a) Absorption of incident radiation from the source.

It was shown in the thermal loading analysis that a total of 600 watts of the incident power will be absorbed by the projection lens.

b) Absorption of radiation originating at the target and gas cap.

If hemispherical radiation is assumed for the gas cap and target area, the projection lens will have incident upon it a total fraction of this radiation which is equal to the ratio of the area of the lens to the area of a hemisphere which has radius equal to the distance from the target to lenses. This fraction, which may be referred to as the view factor for the lens, is given by the expression

$$f = \frac{\frac{1}{4}\pi D^2}{2\pi r^2} = \frac{D^2}{8r^2}$$ where D is the diameter of the projection lens and r is the distance from the lens to the target. The value of f is evaluated for D = 12" and r = 38.16" :

$$f = \frac{(12)^2}{8\,(38.16)^2} = .0125$$

According to data supplied by Forest Gowen of NASA/Ames, the total radiation from the gas cap will be 3,000 watts.

The target area will be at a temperature of approximately 4000°K, emissitivity ε = .85 and diameter of 4 inches. Under these conditions, the target will produce radiation of power 30.8 KW. The total radiation from gas cap and target will be approximately 34 KW, of which a fraction of .0125 or 4.3×10^2 watts will be incident upon the projection lens. If the absorbtivity of this lens is again assumed to be .065, the total power absorbed will be of the order of 30 watts.

c. Absorption of reflected radiation.

The total radiation incident upon the target for 13 sources will be 87.1 KW. If it is assumed that .15 of this radiation will undergo hemispherical reflection, an amount of radiation equal to 163 watt will be reflected back through each projection lens. Again assuming an absorption of .065 at total power absorbed by each projection lens will be of the order of 20 watts.

The total power absorption by the projection lens resulting from the three (3) mechanisms sighted will be of the order of 650 watts.

Once again applying the Stefan-Boltzmann radiation law, the steady state lens temperature is:

$$T = \sqrt[4]{\frac{q}{2A\epsilon\sigma} + \frac{T_1^4 + T_2^4}{2}}$$

where T_1 is the Kelvin temperature of the surroundings outside of the tank, $T_1 = 300°$ K and T_2 is the Kelvin temperature within the chamber, $T_2 = 425°$ K.

The area of one side of the lens is 7.1×10^2 cm^2 and the emissivity is as before $\epsilon = .7$.

Solving the above equation, the steady state temperature of the projection lens is found to be 610° K.

SPECTROLAB

DEVELOPMENT MEMORANDUM NO. 272-97

SUBJECT : Filtering Study - NAS2-1620

WRITTEN BY: Noel Bowman
DATE : 11 March 1964
JOB NUMBER: 6002-13

GRAPH I.

Combination of UV Reflector and AEM Filter

1. The dip at point (a) is caused by the failure of the UV reflector to extend far enough into the visible. The high reflectance zone for the UV reflector extends from 2658 Å to 3450 Å. A more extended range by use of other configurations and materials may be possible, but also may necessitate more layers with attendant problems in production and durability.

2. Point (b) shows the cut-off point of the filter to be at about 7000 Å . It should be a simple matter to shorten this cut-off.

GRAPH II.

This is a graph of a filter which can be made without undue difficulty. The dip at point (a) is not as deep as (a) in Graph I because the filter design gives better visible reflectance on the short wavelength side than the AEM design. However, the high secondary reflectance maximums in the I.R. are unavoidable without added sophistication as depicted with Graph III.

GRAPH III.

This graph shows what can be done with the filter shown on Graph II with considerable computer work. To achieve this result would take extensive development. The main problems in filter design is to reduce the secondary reflectance maximum in the I.R. without developing a large dip at point (a) in this graph.

The following are some notes about using mirrors in various angles of incidence:

These mirrors can be designed for use in angles from 0 to 30 degrees from normal without substantial change in the configuration. However, from 30 to 45 degrees, dips will appear and the cut-off slopes will lengthen and shift towards longer wavelengths.

Above 45 degrees polarization effects cause large splitting in the cut-off configuration. It would be strongly advisable not to use these mirrors at angles greater than 45 degrees of incidence. It would be extremely difficult, if not impossible, to design a filter to work effectively at angles much greater than 45 degrees.

Noel Bowman

NB:pm

Noel Bowman